IMMUNOSENSORS USING METALLIC NANOPARTICLE-BASED SIGNAL ENHANCEMENT FOR BACTERIAL DETECTION AND TUBERCULOSIS DIAGNOSIS

By

Yun Wang

A DISSERTATION

Submitted to
Michigan State University
in partial fulfillment of the requirements
for the degree of

Biosystems Engineering – Doctor of Philosophy

2014

ABSTRACT

IMMUNOSENSORS USING METALLIC NANOPARTICLE-BASED SIGNAL ENHANCEMENT FOR BACTERIAL DETECTION AND TUBERCULOSIS DIAGNOSIS

By

Yun Wang

Escherichia coli O157:H7 is one of the main foodborne/waterborne bacterial pathogens that can cause human illnesses with threat to public health. To control the spread of the contaminated food/water and minimize the harm to public health, rapid and sensitive detection methods need to be implemented. However, standard culture method requires two to four days to obtain results. The application of nanomaterials has drawn interest in the biosensor research to develop timely and low cost detection systems. Because of their unique characteristics, nanoparticles have been used to enhance biosensor sensitivity by increasing the target molecule capture efficiency or by amplifying detection signals. In this dissertation research, nanoparticle-based biosensors were designed for the rapid detection of *E. coli* O157:H7 in broth. Magnetic nanoparticles (MNPs) were conjugated with monoclonal antibodies to separate target *E. coli* O157:H7 cells from samples. Gold nanoparticles (AuNPs) conjugated with polyclonal antibodies were then introduced to the MNP-target complexes to form MNP-target-AuNP. By measuring the amount of gold nanoparticles through an electrochemical method, the presence and the amount of the target bacteria were determined. Based on this biosensor using AuNPs as labels for signal amplification, a tri-nano electrochemical immunosensor was developed by using three nanoparticles for the rapid detection. The gold nanoparticles (AuNPs) were conjugated with lead

sulfide (PbS) nanoparticles as electrochemical reporters via oligonucleotide linkage. AuNPs were also functionalized with polyclonal anti-*E. coli* O157:H7 antibodies in order to bind the target bacterial cells which were captured and separated from the sample by antibody-functionalized MNPs. Because each AuNP was linked to multiple PbS nanoparticles, each binding event to the target resulted in substantial amplification. The signal of PbS was measured on screen-printed carbon electrode (SPCE) by square wave anodic stripping voltammetry (SWASV). Results showed that the biosensor could detect *E. coli* O157:H7 in the range of 10^1 to 10^6 colony forming units per milliliter (cfu/ml) with a signal-to-noise ratio ranging from 2.77 to 4.31. With sample preparation being minimized, results were obtained within 1 h from sample processing to final readout. Tuberculosis (TB) is considered as one of the most widely spread infectious diseases, with estimated 8.8 million new cases and 2 million deaths annually. The biosensor developed in this dissertation research was also applied for TB diagnosis. Gold nanoparticles with anti-IFN-γ antibody were conjugated to oligonucleotides terminated with cadmium sulfide (CdS) nanoparticles. At the same time, AuNPs were conjugated with anti-IP-10 antibody and oligonucleotides terminated with PbS nanoparticles. Therefore, the electrochemical signals of cadmium and lead indicated IFN-γ and IP-10, respectively. By introducing MNPs with antibodies to IFN-γ or IP-10 and AuNP conjugates, IFN-γ and IP-10 were detected separately in buffer and simultaneously in both buffer and plasma. The results showed that IFN-γ in the range of 0.01 IU/ml to 10 IU/ml and IP-10 in the range of 0.01 ng/ml to 100 ng/ml were detected in 1 h. Due to its rapidity, high sensitivity and multiplex detection capability, this tri-nanobiosensor has potential applications in public health, biodefense, and food/water safety monitoring.

ACKNOWLEDGEMENTS

I sincerely thank everyone who has supported and contributed to this research. I would like to especially thank Dr. Evangelyn Alocilja, my advisor, for her guidance on this research. Throughout my doctoral study, her support and encouragement has been absolutely crucial to my graduate career and my growth as a scientist. She has been a friend and given me a lot of helpful suggestions. I am also very grateful for having an exceptional advisory committee and wish to thank Dr. Shantanu Chakrabartty, Dr. John Gerlach and Dr. Renfu Lu. I have learnt a lot from their advices on my research. I would like to thank Dr. Gerald Mazurek at CDC for his support on the Tuberculosis detection research. I would also like to thank A-CAPPP program for providing fund for my research.

I would also like to extend my sincerest gratitude to my friends and family for all their support and encouragement during my Ph.D pursuit, in particular my parents who are constant source of support. I would have never made it this far alone. Everything I have accomplished has been a combination of the support from all those in my life.

Yun Wang

TABLE OF CONTENTS

LIST OF TABLES ix

LIST OF FIGURES xi

Chapter 1 : Introduction 1
1.1 Hypothesis 3
1.2 Objectives 3
1.3 Innovations 4

Chapter 2 : Literature review 5
2.1 Pathogenic bacterial target: *Escherichia coli* O157:H7 5
2.2 Related research on *E. coli* O157:H7 detection 6
2.2.1 Enzyme-linked immunosorbent assay (ELISA) 7
2.2.2 Immunomagnetic separation 8
2.2.3 Polymerase chain reaction (PCR) 9
2.2.4 Biosensors 11
2.3 Tuberculosis (TB) 12
2.4 Related research on TB diagnosis 13
2.4.1 Tuberculin skin test 13
2.4.2 Interferon-gamma release assays (IGRAs) 14
2.4.3 Diagnostic microbiology 15
2.4.4 Chest radiograph 15
2.5 Cytokine biomarkers for disease diagnosis 15
2.5.1 Interferon-gamma (IFN-γ) 18
2.5.1.1 Diseases diagnosis by IFN-γ biomarker 19
2.5.1.2 Detection methods for IFN-γ 20
2.5.2 C-X-C motif chemokine 10 (CXCL10) 23
2.5.2.1 Diseases diagnosis by IP-10 biomarker 23
2.5.2.2 Detection methods for IP-10 24
2.5.3 Other cytokines and chemokines 26
2.5.3.1 Diseases diagnosis 27
2.5.3.2 Detection methods 29
2.6 Nanoparticle based biosensors 31
2.6.1 Gold nanoparticles 32
2.6.2 Bio-barcode biosensors 34
2.6.3 Nanotracers 36
2.7 Conclusions and outlook 37

Chapter 3 : Gold nanoparticle-labeled biosensor for detection of *E. coli* O157:H7 39
3.1 Introduction 39
3.2 Materials and methods 40
3.2.1 Reagents and materials 40
3.2.2 Bacterial culture 41

3.2.3 Apparatus 41
3.2.4 Synthesis of nanoparticles 42
3.2.5 Functionalization of nanoparticles 43
3.2.6 Detection of target pathogenic bacteria 44
3.2.7 Electrochemical measurement 46
3.3 Results and discussion 46
3.3.1 Magnetic separation of target *E. coli* O157:H7 46
3.3.2 AuNP-labeled biosensor for detection 48
3.4 Conclusion 52

Chapter 4 : PbS nanotracer-labeled biosensor for detection of *E. coli* O157:H7 53
4.1 Introduction 53
4.2 Materials and methods 54
4.2.1 Reagents and materials 54
4.2.2 Bacterial culture 56
4.2.3 Apparatus 56
4.2.4 Synthesis of nanoparticles 57
4.2.5 Functionalization of nanoparticles 59
4.2.6 Detection of target pathogenic bacteria 60
4.2.7 Electrochemical measurement 62
4.2.8 Specificity Test 62
4.3 Results and discussion 63
4.3.1 Functionalization of nanoparticles 63
4.3.2 PbS-labeled biosensor for detection 68
4.3.3 Specificity test 72
4.4 Conclusion 73

Chapter 5 : Nanotracer-labeled biosensor for single cytokine detection 75
5.1 Introduction 75
5.2 Materials and methods 77
5.2.1 Reagents and materials 77
5.2.2 Cytokine dilutions 79
5.2.3 Apparatus 79
5.2.4 Synthesis of nanoparticles 79
5.2.5 Functionalization of nanoparticles 81
5.2.6 Detection of the targets 82
5.2.7 Electrochemical measurement 83
5.3 Results and discussion 84
5.3.1 Characterization of nanoparticles 84
5.3.2 Biosensor detection 89
5.4 Conclusion 94

Chapter 6 : Multiplex biosensor for detection of IFN-γ and IP-10 cytokines 96
6.1 Introduction 96
6.2 Materials and methods 97
6.2.1 Reagents and materials 97
6.2.2 Cytokine dilutions and human plasma 98

6.2.3 Apparatus 99
6.2.4 Synthesis of nanoparticles 99
6.2.5 Functionalization of nanoparticles 101
6.2.6 Effect of IFN-γ and IP-10 concentration 102
6.2.7 Electrochemical measurement 104
6.3 Results and discussion 104
6.3.1 Electrochemical characterization of nanotracers 104
6.3.2 Functionalization of nanoparticles 106
6.3.3 IFN-γ and IP-10 detection 106
6.3.4 Effect of IFN-γ and IP-10 concentration 109
6.4 Conclusion 114

Chapter 7 : Conclusion and future work 116

APPENDIX 121

REFERENCES 204

LIST OF TABLES

Table 1-1. Research contribution of this dissertation project to the literature. 4

Table 3-1. Statistical analysis comparing samples and blank (*t* test) for AuNP-labeled biosensor. 52

Table 4-1. Statistical analysis comparing bacterial samples and blank for PbS-labeled biosensor. 71

Table 5-1**.** Statistical analysis comparing samples and blank for IFN-γ detection in single cytokine detection. 93

Table 5-2. Statistical analysis comparing samples and blank for IP-10 detection in single cytokine detection. 94

Table A-1. Differential pulse voltammetry data for Figure 3-5. 122

Table A-2. Differential pulse voltammetry data for Figure 3-6. 126

Table A-3. Data for Figure 3-7. Normalized signals. 129

Table A-4. Data for Figure 4-4d. Current peaks for three tubes. 130

Table A-5. Square wave voltammetry data for Figure 4-5a. 131

Table A-6. Data for Figure 4-5b. 138

Table A-7. Data for Figure 4-6. 139

Table A-8. Square wave voltammetry data for Figure 5-5a. 140

Table A-9. Square wave voltammetry data for Figure 5-5b. 146

Table A-10. Data for Figure 5-6a. 152

Table A-11. Data for Figure 5-6b. 153

Table A-12. Data for Figure 5-6b insert. 154

Table A-13. Square wave voltammetry data for Figure 6-2a. 155

Table A-14. Square wave voltammetry data for Figure 6-2b. 161

Table A-15. Square wave voltammetry data for Figure 6-2c. 167

Table A-16. Square wave voltammetry data for Figure 6-3a. 173

Table A-17. Square wave voltammetry data for Figure 6-3b. 179

Table A-18. Square wave voltammetry data for Figure 6-3c. 185

Table A-19. Data for Figure 6-4a. 192

Table A-20. Data for Figure 6-4b 193

Table A-21. Square wave voltammetry data for Figure 6-5. 194

Table A-22. Data for Figure 6-6a. 201

Table A-23. Data for Figure 6-6b. 202

Table A-24. Data for Figure 6-7. 203

LIST OF FIGURES

Figure 2-1. IFN-γ and IP-10 responses to specific *M. tuberculosis* antigens. Unit of y-axis is pg/ml (Adapted from Kellar et al., 2011). 18

Figure 2-2. Bio-barcode biosensor assay: (a) nanoparticle preparation; (b) DNA detection (Adapted and modified from Nam et al., 2004). 35

Figure 2-3. Nanotracer biosensor for DNA detection (Adapted and modified from Zhang et al., 2010). 37

Figure 3-1. Schematic of the AuNP functionalization. Gold nanoparticles were firstly modified with protein A. Then the antibody was conjugated onto the AuNPs through the linkage of protein A. At last, BSA was added to block the uncoated surface. 44

Figure 3-2. Schematic of the AuNP-labeled biosensor for *E. coli* O157:H7 detection. Target cells in a sample were captured by MNP-mAb conjugates and separated by a magnet. Then the cells were labeled with AuNPs. The MNP-mAb-cell-pAb-AuNP complexes were transferred onto a SPCE chip connected to a potentiostat for electrochemical measurement. 45

Figure 3-3. TEM image of polyaniline (PANI) coated magnetic nanoparticles. 47

Figure 3-4. Schematic of the conjugation of PANI-coated MNP and antibody. The MNP coated with PANI conjugated to antibody through the interaction between the negatively charged Fc fragment of the antibody and the positively charged PANI. 48

Figure 3-5. Differential pulse voltammetric sensorgram of the AuNPs. The sensorgrams of AuNPs in 100 μl 1 M HCl and a blank (100 μl 1 M HCl) are presented. AuNPs show a current peak at 0.3 V. 49

Figure 3-6. Sensorgrams of AuNP-labeled biosensor for *E. coli* O157:H7 detection. Peak current for AuNPs at ~0.3V increases with increasing cell concentration. 50

Figure 3-7. Peak current vs. cell concentration of the AuNP-labeled biosensor for *E. coli* O157:H7 detection. The signal shows a linear relationship between 10^1 to 10^6 cfu/ml. 51

Figure 4-1. Synthesis of PbS nanoparticles with mercaptoacetic acid. 58

Figure 4-2. Schematic of the PbS-labeled biosensor for the detection of *E. coli* O157: H7. The target cell in a sample was captured by the MNP-mAb and separated by a simple magnet. Then the target cell was labeled with pAb-AuNP-PbS. The MNP-mAb-*E. coli*-pAb-AuNP-PbS complex was transferred onto a screen-printed carbon electrode (SPCE) chip connected to a potentiostat. PbS nanoparticles were dissolved and deposited onto the SPCE chip for electrochemical measurement. 61

Figure 4-3. TEM image of (a) AuNPs and (b) PbS nanoparticles. (c) Determination of the amount of polyclonal antibody for the preparation of pAb-AuNP-PbS. Each tube contained AuNP (pH 9.2) and varying amount of polyclonal antibody: 0, 4, 8, 12, 16, and 20 μg/ml (left to right). Third tube from left (8 μg/ml) is red in color but shows some aggregates. Fourth (12 μg/ml) to sixth tubes from left are red in color and show no aggregates..... 64

Figure 4-4. Verification of the formation of pAb-AuNP-PbS conjugates: (a) before centrifugation; (b) tubes with supernatant after centrifugation; (c) tubes with precipitate after centrifugation; (d) current peak of lead in the supernatant after centrifugation. Tube 1: PbS nanoparticles only; Tube 2: PbS nanoparticles mixed with EDC and NHS only; Tube 3: PbS nanoparticles mixed EDC, NHS and pAb-AuNP- oligonucleotides. 67

Figure 4-5. Sensorgram and signal vs. concentration. (a) Typical sensorgram of square wave voltammetry (bacterial concentration is at 10^4 cfu/ml); (b) relationship between current peak and bacterial concentration. (Insert: relationship between peak current and concentration of blank, 10^0, 10^3 and 10^6 cfu/ml. The units of x- and y-axis are the same as Figure 4-5b.)..... 69

Figure 4-6. Box plot of the *E. coli* O157:H7 detection using the PbS nanotracer-based biosensor. 72

Figure 4-7. Specificity test results of the biosensor with four non-target bacteria: *E. coli* O55:H7, *E. coli* C3000, *S. enteritidis* and *B. anthracis*. Positive control (*E. coli* O157:H7), negative control (no pAb-AuNP-PbS added to the sample), and blank (no bacteria) are also presented.. 73

Figure 5-1. Schematic of the NT-labeled biosensor for IFN-γ detection. The target in a sample was captured by MNP-cAbs and separated by a magnet. Then the target was labeled with dAb-AuNP-CdS. The MNP-cAb-target-dAb-AuNP-CdS complexes were transferred onto a SPCE chip connected to a potentiostat. The CdS nanoparticles were dissolved and deposited onto the electrodes on the SPCE chip for electrochemical measurement..... 83

Figure 5-2. TEM images of CdS nanoparticles. The CdS nanoparticles appear close to spherical shape with an average diameter of about 5 nm..... 85

Figure 5-3. UV/Vis spectra of: (a) AuNPs and dextrin, (b) CdS nanoparticles, (c) dAb-AuNP-oligo-CdS conjugates, (d) PbS nanoparticles and (e) dAb-AuNP-oligo-PbS conjugates..... 86

Figure 5-4. Determination of the amount of detection antibody for the preparation of dAb-AuNP-NT. (a) Anti-IFN-γ antibody: each tube contained AuNP (pH 9.2) and varying amount of antibody: 0, 2 and 10 μg/ml (left to right). The two left tubes are blue with aggregate. The third tube from left (10 μg/ml) is red in color but shows some aggregate. (b) Anti-IP-10 antibody: each tube contained AuNP (pH 9.2) and varying amount of antibody: 0, 8, 12, 16, 24 and 28 μg/ml (left to right). The sixth tube from left (28 μg/ml) is red in color with much less aggregate on the bottom of the tube compared to the others..... 88

Figure 5-5. Typical sensorgrams of using nanotracers-labeled biosensor for the detection of single cytokine: (a) sensorgram of IFN-γ detection (IFN-γ concentration: 0.1 IU/ml), and (b) sensorgram of IP-10 detection (IP-10 concentration: 10 ng/ml). For IFN-γ detection, a current

peak of cadmium appeared at -0.87 V in the square wave voltammetric stripping scan from -1.2 V to 0 V. A current peak of lead appeared at -0.67 V for the detection of IP-10. 90

Figure 5-6. Electrochemical measurement results of single cytokine detection in buffer solution: (a) relationship between the current peak and IFN-γ concentration, and (b) relationship between the current peak and IP-10 concentration (Insert: signal to noise number (SNN) at different IP-10 concentration). 92

Figure 6-1. Schematic of the NT-labeled biosensor for the multiple analyte detection of IP-10 and IFN-γ. Two kinds of MNPs, MNP-anti-IFN-γ and MNP-anti-IP-10, captured the two targets and separated them from a sample matrix when magnetic field was applied. Then, the targets were labeled with AuNP-NTs so that anti-IFN-γ-AuNP-oligo-CdS attached to IFN-γ and anti-IP-10-AuNP-oligo-PbS attached to IP-10. After magnetic separation, the NTs attached to the targets were dissolved in nitric acid and introduced to the surface of SPCEs for electrochemical measurement. 103

Figure 6-2. Typical sensorgram of square wave voltammetry for: (a) PbS alone, (b) CdS alone and (c) CdS and PbS. 105

Figure 6-3. Specificity test of the biosensor: (a) the detection of IFN-γ alone, (b) the detection of IP-10 alone, and (c) the detection of both the targets. In all experiments, MNP-anti-IFN-γ and MNP-anti-IP-10 conjugates were used for target separation, and anti-IP-10-AuNP-PbS and anti-IFN-γ-AuNP-CdS conjugates were introduced to the captured target/targets. 108

Figure 6-4. Relationship between peak current and target concentration of multiple cytokine detection in buffer solution. (a) Signals for IFN-γ at different concentration, and (b) signals for IP-10 at different concentration. 110

Figure 6-5. Typical sensorgrams of multiple cytokine detection in 10% plasma. For the detection of IFN-γ, the current peaks of cadmium at around -0.8 V increase with increasing IFN-γ concentration. For the detection of IP-10, the current peaks of lead at around -0.62 V increase with increasing IP-10 concentration. 112

Figure 6-6. Relationship between peak current and target concentration of multiple cytokine detection in 10% plasma. (a) Signals for IFN-γ at different concentration, and (b) signals for IP-10 at different concentration. 113

Figure 6-7. The calibration curves of peak current vs. target concentration of the multiple cytokine biosensor for the detection of IFN-γ and IP-10 in 10% plasma. *The unit of IFN-γ concentration is IU/ml, and the unit of IP-10 concentration is ng/ml. 114

Chapter 1 : Introduction

Escherichia coli O157:H7 is one of the Shiga toxin-producing foodborne/waterborne bacteria which cause human illness. Several multistate outbreaks of *E. coli* O157:H7 in the United States in recent years (CDC, 2013; CDC, 2012a; CDC, 2011a; CDC, 2009; CDC, 2007) indicated that it is a serious threat to public health. To effectively prevent the outbreaks, rapid and sensitive detection methods are needed to enable timely response to the bacterial contamination in food and water. Conventional standard plating method requires days to get results, which may delay the control of the spread of pathogens before indentifying the bacteria. Faster enzyme-linked immunosorbent assays (ELISA) are commonly used, but several hours are still needed. Polymerase chain reaction (PCR) is sensitive and specific, but the enrichment step is desired to obtain the sensitivity. In addition, multiple steps for handling the samples such as DNA extraction require trained personnel to operate. Based on this information, *E. coli* O157:H7 is chosen as the bacterial target in this research.

Tuberculosis (TB) is an air-transmitted infectious disease cause by bacterium called *Mycobacterium tuberculosis* with millions of estimated new cases annually, which is the second cause of death among the infectious diseases worldwide, only after HIV (WHO, 2011). Early diagnosis will greatly assist in the prevention of its spread and the treatment of infected individuals. Tuberculin skin test takes 48 to 72 hours to decide whether a person is infected. Another common method, blood test, which is also called as interferon-gamma release assays (IGRAs), may be affected by many factors (Kellar et al., 2011; Pai et al., 2008). Diagnostic microbiology takes around 24 h to confirm TB infection, and only laboratories with certain competence can provide the test services (American Thoracic Society, 2000). Chest radiograph

checks chest abnormalities along with skin test or blood test, but the accuracy of this method is not insured because the majority of pulmonary tuberculosis infections are clinically and radiographically unapparent (American Thoracic Society, 2000; Dannenberg, 1992). According to recent research (Ruhwald et al., 2007; Kellar et al., 2011), interferon gamma-induced protein 10 (IP-10) was released in a high level in blood in response to the *M. tuberculosis* antigens. Based on the IGRAs, IP-10 could be an adjunct biomarker to IFN-γ for better performance of the TB diagnosis. In order to develop a rapid and sensitive diagnostic method, IP-10 and IFN-γ cytokines are chosen as protein targets and TB biomarkers in this research for single analyte and multiple analyte detection.

This dissertation describes the development of electrochemical immunosensors based on nanoparticles for the detection of *E. coli* O157:H7 and the diagnosis of tuberculosis. Chapter 2 presents a review of the literature relevant to this research including current detection methods of *E. coli* O157:H7, diagnosis approaches of tuberculosis, disease biomarkers and their detection methods, and nanoparticle-based biosensors. Chapter 3 describes the development of an electrochemical immunosensor for *E. coli* O157:H7 detection using gold nanoparticles (AuNPs) for target labeling and signal generation. Chapter 4 describes nanotracers (NTs, nanoparticles of heavy metals)-conjugated gold nanoparticles for the bacterial detection based on the AuNP labeling. This biosensor was applied to detected IFN-γ and IP-10 separately, which is presented in Chapter 5. Chapter 6 describes the multiple analyte detection using the NT-based biosensor for the detection of IFN-γ and IP-10 simultaneously. Some discussion and the conclusion of this dissertation are addressed in Chapter 7, as well as recommendations for future work.

1.1 Hypothesis

The hypothesis of this research is that nanotracer (NT)-conjugated AuNPs can be used for sensitive and rapid detection of bacterial cell surface antigens and proteins.

1.2 Objectives

The overall goal of this research is to develop a sensitive and rapid detection method using nanoparticle-based immunosensor for bacterial detection and TB diagnosis. The nano-biosensor is based on antibody conjugated magnetic nanoparticles for target separation, gold nanoparticles for target labeling, nanotracers for signal amplification and electrochemical measurement for signal acquisition. According to the overall goal, the detailed objectives are:

1. To develop an AuNP-labeled biosensor (design 1) for bacterial detection. To demonstrate that the basic MNP-target-AuNP system is feasible, the biosensor with magnetic separation and only AuNP label is used for detecting the bacterial target.

2. To modify the gold nanoparticles with both antibody and NT-terminated oligonucleotides (oligos).

3. To use an NT-labeled biosensor (design 2) to detect *E. coli* O157:H7 and determine the main parameters of the biosensor such as sensitivity.

4. To demonstrate that the NT-labeled biosensor can detect cytokines (IFN-γ or IP-10, separately) and determine the main parameters such as the sensitivity of the cytokine detection.

5. To demonstrate that the NT-labeled biosensor can detect both cytokines (IFN-γ and IP-10) at the same time (multiple analyte detection) and determine the main parameters of the biosensor such as sensitivity.

1.3 Innovations

The key novelty of this research lies in the employment of NTs in immunosensor for pathogenic bacterial detection and multiple cytokine detection for TB diagnosis. So far, there has been no report on using nanotracer amplification in immunosensor. The advantage of using the immunosensor for the detection is to minimize the manipulation of samples. For bacterial detection, there is no need for pretreatment such as DNA extraction. For cytokine detection, the immunosensor enables the direct detection of the cytokines. The advantage of using NTs in the biosensor is signal amplification with short detection time and low cost. The detection system is sensitive, rapid, low cost, and simple to manipulate. A summary of the presented research is listed in Table 1-1, and a comparison with the current literature illustrates the novelty and scientific contribution (Zhang et al., 2010; Ding et al., 2009; Nam et al., 2004; Hill and Mirkin 2006; Jenison et al., 2001; Bonham et al., 2013)

Table 1-1. Research contribution of this dissertation project to the literature.

Subject	References		
Multiple analyte detection	This work	Zhang et al., 2010	Jenison et al., 2001
Signal amplification using nanotracers in biobarcode-based biosensor	This work	Zhang et al., 2010	Ding et al., 2009
Gold nanoparticle functionalization with antibodies and oligonucleotides	This work	Hill and Mirkin 2006	
Biosensor for the detection of IP-10	This work	Bonham et al., 2013	
IFN-γ and IP-10 multiplex detection in buffer and plasma using biosensors	This work		
Direct detection of *E. coli* O157:H7 cell using nanotracer signal amplification	This work		

Chapter 2 : Literature review

2.1 Pathogenic bacterial target: *Escherichia coli* O157:H7

Escherichia coli O157:H7 (abbreviated as *E. coli* O157:H7) is one of the major foodborne and biodefense bacterial agents. It was firstly identified as a pathogen in 1982 when there were 47 infection cases in two hemorrhagic colitis outbreaks (Santos Mendonça et al., 2012). It belongs to *E. coli* species, which is a gram-negative, rod-shaped bacterium. The "O" is designated by the somatic (cell wall) antigen, and the "H" refers to the flagella antigen (Santos Mendonça et al., 2012). Though most stains of *E. coli* are harmless, the O157:H7 is among the strains which cause disease by producing Shiga toxin (Kudva et al., 1997). It is also referred as one of the enterohemorrhagic *Escherichia coli* (EHEC) which is a defined subset of Shiga toxin-producing *E. coli* (STEC; Griffin and Tauxe, 1991).

The Shiga toxin-producing *E. coli* (STEC) have been isolated from ruminant and nonruminant animals such as cattle, goats, sheep, deer, poultry, dogs and elk, but most of STEC serotypes are nonpathogenic and asymptomatic to animals except several serotypes which cause disease in pig and calves (Kudva et al., 1997). *E. coli* O157:H7 was reported only in cattle, sheep and deer (Kudva et al., 1997). The clinical manifestation of EHEC-caused disease in human can progress from hemorrhagic colitis to hemolytic-uremic syndrome or thrombotic thrombocytopenic purpura (Griffin and Tauxe, 1991; Kudva et al., 1997). The ability of EHEC to attach to intestinal epithelial cells and colonize the human gut greatly contributes to them causing disease in human (Welinder-Olsson and Kaijser, 2005).

Food products contaminated during cultivation or handling, such as raw or cooked poultry and meat, dairy products and fresh vegetables are the major sources of human infections. Direct

contact with infected farm or companion animals or their faeces is another way of the transmission of *E. coli* O157:H7 (Locking et al., 2001, Schets et al., 2005). Contaminated water is one infection source as well (Schets et al., 2005, Chalmers et al., 2000). The pathogen is also transmitted from one person to another. There were many outbreaks which endangered public health caused by *E. coli* O157:H7 in recent years in the United States. A nationwide outbreak of *E. coli* O157:H7 which came from spinach caused 205 confirmed illnesses and three deaths in 2006 (FDA, 2007). In 2007, frozen ground beef contaminated with *E. coli* O157:H7 caused 40 infection cases in eight states and 21.7 million pounds of meat products were recalled (CDC, 2007). In 2009, 72 human infections have been reported from 30 states which were associated with raw prepackaged cookie dough (CDC, 2009). Moreover, 60 persons from 10 states were infected in 2011. Romaine lettuce was the likely the source of this outbreak (CDC, 2011a). There were other two outbreakds happened in 2011 with smaller impact (CDC, 2011b; CDC 2011c). In 2012, 33 persons from 5 states infected with *E. coli* O157:H7 were reported, linked to organic spinach and spring mix blend (CDC, 2012a). Most recently, 33 individuals from 4 states in U.S. were infected with the outbreak strain of *E. coli* O157:H7, and ready-to-eat salads were the likely sources of this outbreak (CDC, 2013). In order to reduce the harm to public health, the methods of early detection, diagnosis and control of the spread are needed.

2.2 Related research on *E. coli* O157:H7 detection

The conventional culture plating method of detection is time consuming. It is based on the multiplication of bacteria in liquid media. Then the detection and identification of bacteria are carried on by transferring them to solid selective culture media and analyzing metabolic properties or serotyping (Ibenyassine et al., 2008). It usually takes two to four days to get the information on the pathogen contamination and concentration. In some cases, pre-enrichment is

required (Ibenyassine et al., 2008), which extended the detection time even more. In order to prevent an outbreak of *E. coli* O157:H7, early identification of the pathogen is critical for controlling the spread and avoiding human contact. More convenient, sensitive and rapid methods are desired. The major methods presently used are immunoassays and polymerase chain reaction (PCR). The immunoassays include enzyme-linked immunosorbent assay (ELISA) and methods based on immunomagnetic separation.

2.2.1 Enzyme-linked immunosorbent assay (ELISA)

ELISA is an immunochemical test involving enzymes, antibodies and antigens. It employs the catalytic ability of enzyme and immunological reactions between the antibodies and antigens. In most cases, the assay involves two antibodies, one of which captures a target antigen and the other is coupled with enzyme to bind the analyte (antibody-antigen complex). The signal is generated by catalytic reaction of the enzyme which modifies its substrate to elicit a chromogenic or fluorescent signal. Sandwich and competitive ELISA are two common forms of ELISA. Sandwich ELISA introduces a detection antibody (secondary antibody) binding to target antigens after the capture of target antigens. Usually, the secondary antibody is labeled with an enzyme. Competitive ELISA utilizes the principle of competitive immunoassay in which the weaker signal is generated for the higher concentration of antigen (Goldsby et al., 2003). Padhye and Doyle (1991) reported an ELISA for the detection of *E. coli* O157:H7 in food. The procedure took 20 h from the enrichment of samples to detection assay. The sensitivity of the assay was 0.2 to 0.9 cell per gram of food for beef and dairy products. Johnson et al. (1995) used ELISA to detect *E. coli* O157:H7 in meat and investigated the specificity of the method. In recent years, other techniques have been incorporated with ELISA for more rapid and sensitive detection. By employing Russell's viper venom factor X activator (RVV-XA) as the enzyme

label in a standard sandwich immunoassay, a microsphere coagulation ELISA was reported which could detect 10^3 per ml *E. coli* O157:H7 within 3 h (Strachan and Ogden, 2000). Park et al. (2012) developed an immunostrip on immuno-chromatographic membrane based on chemiluminescent ELISA method. *E. coli* O157:H7 in the range of 1.1×10^3-1.1×10^7 colony forming unit per milliliter (cfu/ml) was detected within 16 min. Moreover, a microsystem using ELISA method which comprised immunomagnetic extraction chip, retention and horseradish peroxidase (HRP) chip and fluorescence detection chip was designed and fabricated to detect *E. coli* O157:H7 in soil samples (Sen et al., 2011). The limit of detection of this microsystem is 10^6 cfu/ml. Compared to the culture plating method, ELISA lessens the detection time. However, traditional ELISA method still takes at least several hours, and the sensitivity and specificity needs to be improved.

2.2.2 Immunomagnetic separation

Immunomagnetic separation is not a complete procedure of detection but a method of separating the target from the sample matrix, which can be coupled with various detection methods (Dudak and Boyaci, 2008). The immunomagnetic separation method employs antibody-coated magnetic beads to capture the target bacteria and remove the bacteria from the solution. The target bacteria are concentrated and components which may interfere with the analysis are removed (Dudak and Boyaci, 2008). This separation method is very useful for detecting target bacteria in food matrices. Setterington et al. (2011) studied antibody-conjugated magnetic nanoparticles for the extraction and concentration of microbial pathogens including *E. coli* O157:H7. This procedure required only 35 min without enrichment steps and could be combined with detection method following the separation. A method of detecting *E. coli* in water samples

by using antibody-coated paramagnetic beads and quantum dot-labeled secondary antibodies was described (Dudak and Boyaci, 2008), and the lowest concentration of the bacteria detected was 8.9×10^{1} cfu/ml within 2 h. Decory et al. (2005) reported using immunomagnetic beads for *E. coli* O157:H7 capture and sulforhodamine B-containing liposome nanovesicles for fluorescent signals. It took 8 h to detection 1 cfu/ml of the bacteria in various aqueous matrices. Moreover, an ELISA-based method integrated with an immuno-magnetic separation was reported (Cho and Irudayaraj, 2013) to detect 3 cells/ml of *E. coli* O157:H7 in 2 h. In this method, gold nanoparticles (AuNPs) were conjugated with various antibody components to form a network which bound to the cells and allowed HRP-labeled antibodies to bind to the network complex and enhanced the signal. There are many other detection methods involving immunomagnetic separation (Yang et al., 2013; Zhu et al., 2011; Tu et al., 2011; Laczka et al., 2011; Varshney et al., 2007; DeCory et al., 2005). Immonoassays have been developed to be sensitive methods for bacterial detection. The sensitivity and selectivity of the assays greatly depends on antibodies. In most cases, viable cells, which are the most concerned in food contamination, cannot be differentiated from dead cells.

2.2.3 Polymerase chain reaction (PCR)

Polymerase chain reaction (PCR) has been widely used for pathogenic detection. It is a technique of amplifying the target DNA. There are three main steps: denaturation, annealing and extension. For identifying the DNA of bacteria, usually the extraction of DNA from the cells is required. Ibenyassine et al. (2008) reported a PCR procedure for the detection of *E. coli* O157:H7 in contaminated vegetables. It took 24 h to get the result, including enrichment. Bonetta et al. (2011) reported a PCR protocol for detecting multiple bacteria. They could detect 3 cfu/l *E. coli* O157:H7 in spiked surface water samples. This method included the enrichment of

samples. Multiplex PCR (m-PCR) is a technique to amplify multiplex targets by using several sets of primers specific to different targets in one tube, which enabled simultaneous identification of gene sequences. A study isolated *E. coli* O157:H7 from food samples of animal origin (meat and cheese) using immunomagnetic separation and detected virulence genes by m-PCR (Ertas et al., 2013). Because enrichment cultures were prepared from food samples before the magnetic separation and the DNA extraction was conducted following the isolation, this method took at least two days. Guan et al. (2013) also reported m-PCR for the detection of *E. coli* O157:H7 along with several foodborne pathogens. After overnight enrichment, 670 cfu/ml of *E. coli* O157:H7 could be detected in pork inoculated with the pathogens. Quantitative polymerase chain reaction (q-PCR, also called real-time PCR) which detects and quantifies targets is another PCR technique commonly used for *E. coli* O157:H7 detection. Bacteria from raw milk were concentrated by centrifugation coupled with chemical and enzymatic treatment, and then the DNA was extracted. The exacted DNA was quantified with a 5′ nuclease q-PCR assay, and 1 cfu/ml *E. coli* O157:H7 from a 10 ml sample was detected in less than 3 h (Paul et al., 2013). Viable but non-culturable (VBNC) *E. coli* O157:H7 on the surface of lettuce and spinach plants was detected by q-PCR combined with propidium monoazide (PMA) dye which covalently linked to DNA of dead bacteria and prevented the amplification of the DNA (Dinu and Bach, 2013). This assay had a detection limit of 10^3 cfu/g leaf. In recent years, many research have reported using PCR for the detection (Kumar et al., 2013; Delannoy et al., 2012; Elizaquivel et al., 2012; Yoshitomi et al., 2012; Miszczycha et al., 2012; Fedio et al., 2011; Bonetta et al., 2011; Haugum et al., 2011). Compared with culture plating method, PCR reduced the time for detection. Several studies compared PCR with ELISA (Alexandre et al., 2001; Fratamico and Strobaugh, 1998). According to the results, PCR is more sensitive and specific than ELISA.

However, it usually requires a pre-enrichment of samples to obtain the sensitivity (Bonetta et al., 2011; Moganedi et al., 2007). The general detection time is 24 h when enrichment is counted.

2.2.4 Biosensors

A biosensor is "a compact analytical device incorporating a biological or biologically-derived sensing element either integrated within or intimately associated with a physicochemical transducer" (Turner, 1996). Sensing element and transducer are the two most important components of a biosensor. The sensing element recognizes the specific target through bio-reactions such as antibody-antigen, enzyme-substrate and probe-DNA recognition. These bio-reactions generate some properties such as electric and optical signals which can be directly measured by transducers or can be converted into measurable quantities through some transducing materials. Because of their sensitivity, rapidity and low cost compared with some conventional methods and possible portability, biosensors are considered promising analytical devices for the detection of various targets. Many configurations of biosensors have been reported for the detection of *E. coli* O157:H7. According to sensing materials, there are immunosensors (Radke and Alocilja, 2005; Wang et al., 2010; Luo et al., 2010; Tan et al., 2011; Barreiros dos Santos et al., 2013), immunosensors with enzyme (Yang et al., 2004; Park et al., 2008; Linman et al., 2010; Li et al., 2012) and DNA sensors (Liu et al., 2008; Wang et al., 2009; Sun et al., 2009; Bahsi et al., 2009; Jiang et al., 2013; Anderson et al., 2013). For example, gold electrodes were modified by anti- *E. coli* antibodies via a self-assembled monolayer (SAM) of mercaptohexadecanoic acid, and the target bacteria were introduced to the electrode surface (Barreiros dos Santos et al., 2013). A detection limit of 2 cfu/ml was reported. Li et al. (2013) developed a sandwich electrochemical immunosensor which was constructed by fullerene (C_{60}), ferrocene (Fc) and thiolated chitosan (CHI–SH) composite nano-layer with Au-SiO_2

nanocomposites which were modified by antibody. The captured target *E. coli* O157:H7 cells were labeled with glucose oxidase (GOD) loaded Pt nanochains (PtNCs), and cyclic voltammetric (CV) measurement in glucose solution was performed to obtain the electrochemical signals. Fifteen cfu/ml *E. coli* O157:H7 could be detected with a detection time of about 1 h. Anderson et al. (2013) described a biosensor involved magnetic microparticles for separating target DNAs and gold nanoparticles (AuNPs) functionalized with various oligonucleotide reporters. Electrochemical signal was obtained from AuNPs and fluorescent signals were obtained through three different oligonucleotide reporters. The target at a concentration of 5 cfu/ml was detected using the electrochemical measurement and 5×10^4 cfu/ml was detected using the fluorescent reporters. Compared to conventional methods, biosensors report the results much faster, usually within hours. The detection limit of most reported biosensors is generally at the level of 10^2 cfu/ml. The sensitivity of the biosensors is under improvement since the bacterial infection could be caused by as low as 10 organisms (CAST, 1994).

2.3 Tuberculosis (TB)

Tuberculosis (TB) is considered as one of the most widely spread infectious diseases, with 8.8 million new cases and 2 million deaths annually as estimated by WHO (WHO, 2006). It is the second cause of death among the infectious diseases worldwide, only after HIV (WHO, 2011). The disease is caused by the bacillus *Mycobacterium tuberculosis*, and transmitted in the air from persons sick with pulmonary TB expel bacteria to other persons (WHO, 2011). Symptoms of the disease include fever, chills, flu-like symptoms, gastrointestinal symptoms,

weakness and fatigue at the early stage, while more severe symptoms are persistent cough, chest pain, breathing difficulty, weight loss and progressive shortness of breath.

TB diagnosis is critical not only because the disease is widely spread, but also because there are difficulties for preventing and curing the disease due to drug resistance and latent TB. The drug resistance which results in the failure of treatment has been a large concern since nearly 300,000 new cases of multidrug-resistant TB (MDR-TB) emerged annually (WHO, 2006). At the same time, the contact with persons with latent TB (no symptoms) causes infections. There are over 50 million people who are latently infected with MDR strains of TB, which shows the severity of the two problems combined. Besides these two, there are several other constrains worldwide for TB control. They are synergism between human immunodeficiency virus (HIV) and *M. tuberculosis* infection, inadequate diagnostic tools, long and arduous treatment regimens, ineffective vaccine, HIV pandemic and poverty (WHO, 2006). Facing the threat of TB, diagnostic methods with high sensitivity, rapidity and low cost will greatly help in control, which will ensure the early diagnosis, proper quarantine, early treatment and even the diagnosis of latent TB.

2.4 Related research on TB diagnosis

2.4.1 Tuberculin skin test

The conventional method of TB diagnosis is tuberculin skin test (TST). It has been used to diagnose tuberculosis (TB) and latent *Mycobacterium tuberculosis* infection for almost a century (Mazurek et al., 2007). It is based on the principle that mycobacterial antigens cause infiltration of antigen-specific lymphocytes and the elaboration of inflammatory cytokines (Anderson et al., 2000). The test is performed by injecting a small amount of tuberculin purified protein derivative (PPD), which is a mixture of proteins from *M. tuberculosis* culture, into epidermal layer of skin.

A person taking the test returns within 48 to 72 hours to be checked to assess cell-mediated hypersensitivity to *M. tuberculosis* antigens in order to decide whether the person is infected (Mazurek et al., 2007; CDC, 2012b). The test has the limitation that laboratory contamination, technician and sampling errors, and vaccination with live-attenuated virus can cause false-positive results (Mazurek et al., 2007; American Thoracic Society, 2000).

2.4.2 Interferon-gamma release assays (IGRAs)

Another method of TB diagnosis is blood test, which is also called as interferon-gamma release assays (IGRAs). It is useful for detecting both latent infection and overt disease (Kellar et al., 2011). Interferon-gamma (IFN-γ) is a 15.5 kDa protein (Dijksma et al., 2001). IGRAs detect IFN-γ release after the incubation of whole blood or peripheral blood mononuclear cells (PBMCs) with *M. tuberculosis* antigens such as early secretory antigenic target-6 (ESAT-6) and culture filtrate protein-10 (CFP-10), by using ELISA to measure differences in the concentration of IFN-γ or enzyme-linked immunosorbent spot (ELISPOT) assay to measure differences in the number of cells which produce IFN-γ (Kellar et al., 2011; Mazurek et al., 2007; Yilmaz et al., 2012). The basis of the test is that when T cells sensitized with tuberculosis antigens encounter mycobacteiral antigens, they produce IFN-γ at a high level (Anderson et al., 2000; Pai et al., 2004). This *in vitro* assay has been commercialized that two assays. The QuantiFERON-TB assay (Cellestic Limited, Carnegie, Victoria, Australia) and T-SPOT.TB assay (Oxford Immunotec, Oxford, UK) have been developed (Pai et al., 2004). The IGRAs are rapid since they can evaluate multiple antigens and assay parameters (Mazurek et al., 2007). The sensitivity of IGRAs is high in low TB-endemic countries, but the sensitivity is lower in high TB-endemic countries (Kellar et al., 2011; Pai et al., 2008). The lack of diagnostic standard with which to confirm the presence of latent infection also affects the sensitivity of IGRAs (Kellar et al., 2011).

2.4.3 Diagnostic microbiology

The microbiology tests are methods of detecting the presence of mycobacteria. It includes the detection, isolation and identification of mycobacteria (American Thoracic Society, 2000). A common method uses acid-fast bacilli (AFB) on a sputum smear or other specimen as an indication of TB disease (CDC, 2011d). It is an easy procedure to give the first evidence of the presence of mycobacteria (American Thoracic Society, 2000). The AFB in stained smears is examined microscopically. Culture of a sample is prepared to confirm the TB disease because the microscopy checks the AFBs which include some AFBs that are not *M. tuberculosis.* The growth of the mycobacteria takes 1-3 weeks in broth, while it takes 3-8 weeks on solid media (Morgan et al., 1983; American Thoracic Society, 2000). Only laboratories with certain competence can provide the test services (American Thoracic Society, 2000).

2.4.4 Chest radiograph

Chest radiograph is a method to check chest abnormalities. Lesion which appears in the lungs may suggest TB. This method is usually used with TST or blood test to determine whether it is a pulmonary TB in a person who is positive in the tests but has no symptoms of disease. However, the accuracy of this method is not insured because the majority of pulmonary tuberculosis infections are clinically and radiographically unapparent (American Thoracic Society, 2000; Dannenberg, 1992).

2.5 Cytokine biomarkers for disease diagnosis

Cytokines are protein molecules released by numerous cells (e.g. lymphocytes and macrophages), and they affect the behavior of other cells with receptors for them (Janeway et al., 2001). This group includes immunomodulators, growth factors, adipocytokines, extracellular

matrix (ECM) proteins and cytokine regulatory proteins (Huang et al., 2012). They play an important role in cell-to-cell communication and cellular signaling, activation, growth and differentiation (Chowdhury et al., 2009). They act as the mediators of inflammation in immune-system response to implanted grafts, cell communicating pathogen invasion and tumor growth and proliferation (Brunet, 2012; Huang et al., 2012). Their prominent role in many diseases is the basis of using them as biomarkers for disease diagnosis. The understanding of the role could also enable their potential therapeutic use in clinical conditions, either by direct use, blocking or indirect modulation of pathways (Chowdhury et al., 2009).

Chemokines are a special family of cytokines. They are small chemoattractant proteins that stimulate the migration and activation of various cells, including neutrophils, monocytes, lymphocytes, eosinophils, fibroblasts, and keratinocytes (Borish and Steinke, 2003; Janeway et al., 2001). They participate in immune response: recruiting and activating leukocytes and initiating wound healing (e.g. inflammatory chemokines). They also have the functions of homeostatic, lymphocyte trafficking, hematopoiesis, antigen sampling in secondary lymphoid tissue and immune surveillance (Borish and Steinke, 2003; Moser and Loetscher, 2001). There are four subfamilies of chemokines: C, CC, CX3C and CXC (Romagnani and Crescioli, 2012).

It is critical to evaluate cytokine expression levels in biomarker discovery and development process (Huang et al., 2012). Keller et al. reported that the measurement of multiple proinflammatory and anti-inflammatory cytokines, chemokines, and growth factors associated with *M. tuberculosis* antigen infection could improve TB diagnosis (Kellar et al., 2011). They found that using whole blood from patients stimulated with *M. tuberculosis* antigens greatly increased the release of cytokines such as IFN-γ, IL-2, Il-6, IL-8, IP-10, TNF-α and etc. IFN-gamma-inducible protein 10 (IP-10/CXCL10) is an 8.7 kDa protein secreted by cells such as

monocytes and endothelial cells in response to IFN-γ (Luster et al., 1985). Among the cytokines which respond to *M. tuberculosis* antigens infection, it was produced in nanogram amount, which clearly differentiated the samples from patients and the samples from controls as shown in Figure 2-1 (Kellar et al., 2011). Kellar et al. suggested IP-10 as one of promising indicators for TB diagnosis (Kellar et al., 2011). Ruhwald et al. also reported that IP-10 was released in a high level in response to the *M. tuberculosis* antigens (Ruhwald et al., 2008). The detection rate of assessing both IFN-γ and IP-10 is 90% compared to 83% and 81% for IP-10 or IFN-γ alone, respectively. Their results indicated that IP-10 could be an adjunct maker to IFN-γ for better performance of the TB diagnosis (Ruhwald et al., 2007; Kellar et al., 2011). Other studies also revealed that IP-10 could be a potential maker for TB diagnosis (Azzurri et al., 2005; Okamoto et al., 2005; Kabeer et al., 2010; Goletti et al., 2010). Therefore, IFN-γ and IP-10 as two important biomarkers are emphasized here, and other cytokines and chemokines are also introduced.

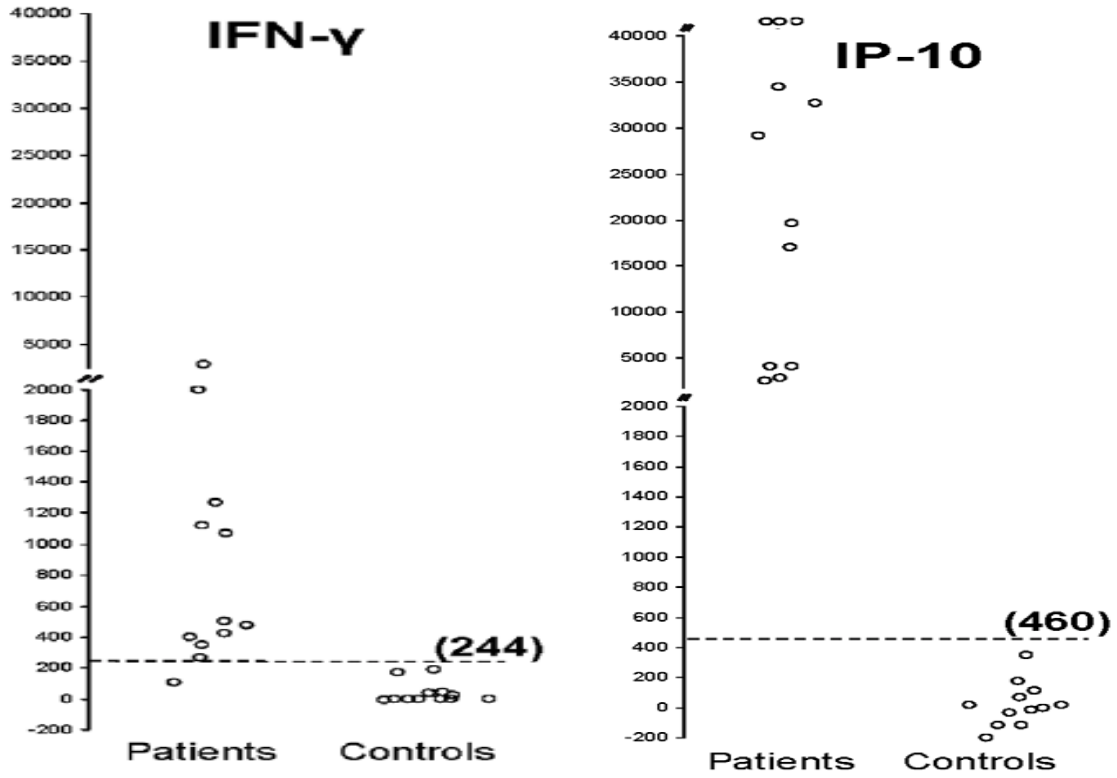

(a) (b)

Figure 2-1. IFN-γ and IP-10 responses to specific *M. tuberculosis* antigens. Unit of y-axis is pg/ml (Adapted from Kellar et al., 2011).

2.5.1 Interferon-gamma (IFN-γ)

The basis of collective designation of interferons (IFN) is their capacity to induce antiviral activity against a broad spectrum of mammalian viruses (Meager 2002; Stewart, 1979). There are type I (IFN-α and IFN-β) and II (IFN-γ) interferons. The classification is according to receptor specificity and sequence homology (Schroder et al., 2004). IFN-γ is encoded by a chromosomal locus different from type I IFNs (Schroder et al., 2004). It is primarily α-helical (Ealick et al., 1991; Dijksma et al., 2001). The structure includes two dimmers related by a noncrystallographic twofold axis in the asymmetric unit (Ealick et al., 1991). IFN-γ is secreted by various cells, such

as CD4+ T helper cell type 1 (Th1) lymphocytes, CD8+ cytotoxic lymphocytes, NK cells, B cells and professional antigen-presenting cells (Frucht et al., 2001; Janeway et al., 2001; Bach et al., 1997). The functions of IFN- γ include immune responses driven by Th1, induced regulatory T (Treg) cell activity to control natural immune system responses and cellular proliferation and apoptosis (Schroder et al., 2004; Brunet, 2012). It is an important cytokine responsible for cell mediated immunity.

2.5.1.1 Diseases diagnosis by IFN-γ biomarker

IFN-γ is associated with various diseases. Studies have revealed many diseases which could be indicated by the level of IFN-γ according to its functions and important role in immune responses.

IGRAs for IFN-γ TB diagnosis is a successful employment of IFN-γ biomarker. Besdies, Billman-Jacobe et al. reported that the IFN-γ is a biomarker to indicate the infection of Johne's disease (Billman-Jacobe et al. 1992). Assays for the detection of IFN-γ have been used for Johne's disease diagnosis in animals (Robbe-Austerman et al., 2006a and 2006b). One commonly used method of leprosy disease diagnosis is peripheral blood mononuclear cell (PBMC)-based IFN-γ release assays (Geluk et al., 2010). Geluk et al. analyzed several cytokines for their potential in leprosy diagnosis and concluded that IFN-γ based whole blood assay combined with IL-12 is sensitive (Geluk et al., 2010). Qari et al. reported that IFN-γ in patients with sickle cell disease significant increased (Qari et al., 2012), which indicated that IFN-γ could be used as a biomarker for the diagnosis of sickle cell disease. Moreover, IFN-γ was associated with chronic graft-versus-host disease in children (Rozmus et al., 2011). IFN-γ is a biomarker for cancer diagnosis as well. Peripheral blood lymphocytes (PBL) of breast cancer patients and

healthy controls were analyzed, and IFN-γ was showed to correlate with the disease (Konjevic et al., 2011).

IFN-γ have been reported to associated with many other diseases such as malignant melanoma, renal cell carcinoma (Rudman et al., 2011), interstitial lung disease (Truchetet et al., 2011), oral lichen planus (Liu et al, 2009), non-small cell lung cancer (Borgia et al., 2009), chronic rhinosinusitis (Niederfuhr et al., 2008), Crohn's colitis (Ljung et al., 2007), relapsed multiple myeloma (Richardson et al., 2004), *Listeria monocytogenes* infection (Kim et al., 2001), Epstein-Barr virus infection (Imashuku et al., 1998) and chronic beryllium disease (Tinkle et al., 1997).

2.5.1.2 Detection methods for IFN-γ

Enzyme-linked immunosorbent assay (ELISA) is a commonly used method for IFN-γ detection. Berg reported a "one site" ELISA which used a single monoclonal antibody to capture the target and carried an enzyme-horseradish peroxidase. The assay could detect human IFN-γ at the concentration of <0.5 u/ml (Berg, 1994). Bouyon et al also reported a "one site" ELISA for the detection of recombinant human IFN-γ. The detection limit of this assay is 1.26 ng/ml (Bouyon et al., 2003). A sandwich ELISA was employed to detect IFN-γ with the detection limit of 6.9 ng/l (Borg et al., 2002). Robbe-Austerman et al. used ELISA for IFN-γ detection as well (Robbe-Austerman et al., 2006a and 2006b). In addition, as mentioned before, the commercialized IGRA, the QuantiFERON-TB assay (Cellestic Limited, Carnegie, Victoria, Australia) measures the concentration of IFN-γ using ELISA technique.

Enzyme-linked immunospot (ELISPOT) assays are based on ELISA. The difference is that ELISPOT measures release of cytokines from single cells instead of measuring the total amount of cytokines released from all cells in an ELISA assay (Cox et al., 2006). The method has been

reported for the detection of IFN-γ and IFN-γ secreting cells (Czerkinsky et al., 1988; Schmitte et al., 1997; Karlsson et al., 2003; Yang et al., 2012). T-SPOT.TB assay (Oxford Immunotec, Oxford, UK) is a commercialized IGRA based on ELISPOT (Pai et al., 2004)

Cytokine flow cytometry (CFC) is a method using anticytokine antibodies as markers in flow cytometry. The technique employs intracellular staining of cytokines (Maecker 2004). It is used for the detection of IFN-γ and IFN-γ secreting cells (Karlsson et al., 2003; Maecker et al., 2005; Maecker et al., 2008; Tilley and Menon, 2000).

IFN-γ has the ability to induce nitric oxide production in cells (Farrar and Schreiber 1993). Malu et al. reported a bioassay for mouse IFN-γ detection by measuring nitric oxide which is produced by macrophages following the induction of inducible nitric oxide synthase (iNOS) by IFN-γ. The assay could detect IFN-γ in the range of 0.03~0.25 U/ml (Malu et al., 2003).

Immunofluorescence is another approach for IFN-γ detection. A protocol based on the ability of IFN-γ to induce major histocompatibility (MHC) class II antigens (Ia antigens) was developed (Schreiber, 2001). The expression of Ia antigens by human or murine cells cultured with IFN-γ was tested and quantified by immunofluorescence and flow cytometry.

Other methods including “antiviral assays” (AVA) for measuring the IFN potency and “reporter gene assays” based on the cloning of IFN responsive genes are also introduced (Meager, 2002). Moreover, arrayed imaging reflectometry was reported for IFN-γ detection (Carter et al., 2011).

Several studies reported the detection of IFN-γ using biosensors. Dijksma et al. developed an electrochemical immunosensor. IFN- γ was adsorbed on a self-assembled monolayer (SAM) of cysteine or acetylcysteine on electropolished polycrystalline gold electrodes. The detection limit of this biosensor is 0.02 fg/ml (1 aM) with a dynamic range of 0-12 pg/ml (Dijksma et al.,

2001). Bart et al. described an immunosensor prepared by immobilizing anti-IFN-γ antibodies on a self-assembled monolayer (SAM) of acetylcysteine, deposited on polycrystalline gold. The signal was measured by a multi-frequency impedance method. The biosensor could detect IFN-γ in the range of 10^{-18} to 10^{-9} M (Bart et al., 2005). An optical thin film biosensor was developed to detect multiple cytokines including interleukin (IL)-6, IL1-β, and IFN-γ. IFN-γ at the concentration of 437 ng/l was detected in 40 min (Jenison et al., 2001). Moreover, Liu et al. reported an electrochemical DNA aptamer-based biosensor which could detect IFN- γ in the range of 0.06 nM to 10 nM (Liu et al., 2010). Min et al. also reported aptamer-based quartz crystal microbalance (QCM) biosensors (Min et al., 2008). In this study, the RNA-aptamer-based biosensor could detect 100 fM IFN- γ, and DNA-aptamer-based one could detect 1 pM in sodium phosphate buffer. Ten pM was detected by the DNA aptamer in fetal bovine serum. Tuleuova and Revzin described an aptamer based biosensor for IFN-γ detection as well (Tuleuova and Revzin, 2010). In addition, a surface plasmon resonance (SPR) biosensor was tested for the detection of IFN-γ (Stigter et al., 2005). The dextran-coated SPR sensor could detect 250 ng/ml IFN-γ in plasma. Whelan and Zare described a single-cell immunosensor which used human monocytic cell line U-937 to detect IFN-γ (Whelan and Zare, 2003). In summary, the detection limit of biosensor is comparable to ELISA which could detect 44 pg/ml of IFN-γ (Siawaya et al., 2008). However, biosensor with the ability of detecting multiple analytes at the same time will be more competitive for disease diagnosis than conventional ELISA, since the addition of adjunct biomarkers (other cytokines) to IFN-γ may improve the performance of diagnosis for some diseases (Ruhwald et al., 2007; Kellar et al., 2011).

2.5.2 C-X-C motif chemokine 10 (CXCL10)

CXCL10 is also known as interferon gamma-induced protein 10 (IP-10). It belongs to CXC chemokine subfamily. It is an 8.7 kDa protein secreted by cells such as monocytes and endothelial cells in response to IFN-γ (Luster et al., 1985). It plays a critical role in inflammation and chemotaxis (Romagnani and Crescioli, 2012). Therefore, one section is allotted to IP-10 as an example of important chemokines.

2.5.2.1 Diseases diagnosis by IP-10 biomarker

Besides mentioned as a potential biomarker for TB diagnosis, IP-10 was also reported to indicate human immunodeficiency virus (HIV) and cytomegalovirus (CMV, Kasprowicz et al., 2011). Interleukin (IL)-6, IL-8, IP-10, TNF-a, vascular endothelial growth factor (VEGF) and macrophage inflammatory protein (MIP)-3a increased in patients with nasopharyngeal carcinoma (NPC), a malignant neoplasm of the head and neck (Chang et al., 2011). The level of IP-10 changed during the IFN-α2b therapy for melanoma, indicating that IP-10 could be a biomarker for monitoring the treatment of melanoma (Yurkovetsky et al., 2007). Abu El-Asrar et al. reported that IP-10 might be involved in the pathogenesis of proliferative diabetic retinopathy (PDR) and proliferative vitreoretinopathy (PVR), which indicates that IP-10 is a potential biomarker for diagnosis of the diseases (Abu El-Asrar et al. 2006). It is reported that hodgkin lymphoma (HL) is associated with the secretion of cytokines including IP-10 (Ma et al., 2008). Dengue fever is a tropical diseases caused by the infection of dengue virus. The infection results in the increased expression of IP-10 (Martha Salgado et al., 2010). The measurement of IP-10 amount could be a potential indication of the infection. The infection of human cytomegalovirus (HCMV) causes significant morbidity in lung transplant recipients (LTRs). A study showed that increased IP-10 level was associated with the infection and might be used as reporter of the

infection (Weseslindtner et al., 2011). Thirty nine respiratory viruses were detected in patients by Sumino et al., associated with increased level of IP-10. The results implied that IP-10 might be used as a biomarker for respiratory viral infection (Sumino et al., 2010). Renal allograft injury secondary to subclinical and clinical tubulitis causes the allograft fibrosis and loss. Ho et al. indicated that IP-10 might be a useful supplementary noninvasive screening test for tubulitis in renal transplant patients (Ho et al., 2011). For studying the rhinovirus- and RS virus-induced acute exacerbation of childhood wheezing, IP-10 concentration was found to be significantly elevated in rhinovirus-induced wheezing compared with controls (Kato et al., 2011). Lokensgard et al. (2001) found that in response to nonproductive infection with herpes simplex virus, microglia produced considerable amount of IP-10. The results suggested that the chemokine has direct antiviral activity in neurons while it also helps in antiviral defense of the brain and the amplification of immune responses during neuroinflammation (Kato et al., 2001).

In addition, IP-10 was also reported as a potential biomarker for *Leptospira* infection (Lowanitchapat et al., 2010), acute kidney injury (Vaidya et al., 2008), severe acute respiratory syndrome (SARS)-coronavirus infection (Law et al., 2005), knee osteoarthritis (Saetan et al., 2011), cancers (Liu et al., 2011), urolithiasis (Suen et al., 2010), cerebral malaria (Armah et al., 2007), hepatitis C virus infection (Zeremski et al., 2007) and Epstein-Barr virus infection (Nakai et al., 2012).

2.5.2.2 Detection methods for IP-10

ELISA is a commonly used method for IP-10 detection. Takahata et al. mentioned approaches to detect IP-10, including ELISA (Takahata et al., 2003). They measured IP-10 in colostrum and sera using a sandwich ELISA. In this research, the expression of IP-10 in cellular components of human milk was measured by reverse transcription polymerase chain reaction

(RT-PCR), which determined IP-10 mRNA level. IP-10 expression in mammary gland tissues was determined by immunohistochemistry with immunohistochemical staining (Takahata et al., 2003). Caproni et al. also reported ELISA for IP-10 detection (Caproni et al., 2004).

Immunofluorescence is another major method. Chang et al. used Bio-Plex® Suspension Array System (Bio-Rad Laboratories, Hercules, CA) to determine the concentration of multiple cytokines including IP-10 (Chang et al., 2011). The system is a commercialized product based on beads with optical properties and conjugated with antibodies (e.g. immunofluorescence), which is used for the analysis of multiple proteins, peptides, and nucleic acids. Another commercialized product, xMAP technology (Luminex Corp.) which is based on a sandwich immunoassay and fluorescent beads was used for cytokine detection including IP-10 (Yurkovetsky et al., 2007). Aliberti et al. employed immunofluorescence for IP-10 detection as well (Aliberti et al., 2001).

IP-10 produced during a delayed-type hypersensitivity (DTH) reaction was detected using immunocytochemical staining (Kaplan et al., 1987). In another study on delayed cellular immune responses, IP-10 was detected by immunocytochemical detection in immunoperoxidase studies of formalin-fixed frozen skin sections with an affinity-purified rabbit anti-IP-10 antibody, and the expression of IP-10 was analyzed by Northern Blot (Gottlieb et al., 1988).

A multiplex-25 bead array cytokine assay was developed, which was able to detect IP-10 at the concentration of 3 pg/ml (Heijmans-Antonissen et al., 2006). The measurement was done by microbead-based flow cytometry system.

Exhaled breath condensate (EBC) analysis which assesses cytokines in the airways based on chemiluminescence was used for IP-10 detection (Matsunaga et al., 2009). Another chemiluminescence based assay was described by Sack et al. The chemiluminescence substrate system was coupled with membrane-bound antibody array (Sack et al. 2005).

There are limited reports on IP-10 detection using biosensors. Bonham et al. (2013) described an electrochemical biosensor for label free detection. The sensing element was a 21-residue polypeptide binding element derived from the naturally occurring receptor CXCR3. This polypeptide was covalently linked to a DNA strand which hybridized to an anchor DNA strand with a distal methylene blue redox reporter. The binding of IP-10 to the polypeptide reduced the electron transfer between the methylene blue and electrode, and resulted in change in current accordingly. The biosensor could detect ~60 pM of IP-10.

2.5.3 Other cytokines and chemokines

Cytokines derived from antigen-presenting cells (APCs) especially affect the cellular infiltrate and damage to resident tissue characteristic of inflammation (Borish and Steinke, 2003). Examples of the production of these cytokines are: 1) the processing of antigens by APCs and then presenting to T-helper lymphocytes; 2) the triggering of producing cytokines through the innate immune system by monocytes: this class of cytokines includes tumor necrosis factor (TNF), and several interleukin (IL) molecules (e.g. IL-2, IL-4, IL-5, IL-6, IL-7, IL-10, IL-12 and IL-15; Borish and Steinke, 2003); and 3) the secreting by macrophages in response to pathogens: these cytokines include interleukin-1 (IL-1), interleukin-6 (IL-6), interleukin-12 (IL-12), TNF-α and chemokine interleukin-8 (IL-8; Janeway et al., 2001). Tumor necrosis factors mainly have effect on antitumor immune responses, cachexia in chronic infections, vascular leakage and toxic shock (Borish and Steinke, 2003; Tracey et al., 1987; Beutler and Cerami, 1989). Interleukins (ILs) are “molecules secreted by, and acting on, leukocytes” (Janeway et al., 2001). They have the functions of activating T lymphocytes (IL-1), mediating T-cell activation, growth, and differentiation (IL-6), activating and inducing proliferation, cytotoxicity, cytokine production of NK cells (IL-12 and IL-15), stimulating B-cell growth and differentiation (IL-15), and activating

cytotoxic immunity (IL-2, IL-4, IL-5, IL-6, IL-7, IL-10, IL-12, and IL-15; Borish and Steinke, 2003). These are important cytokines for disease diagnosis. Besides TNFs and ILs, other cytokines for disease diagnosis are also introduced in this section.

2.5.3.1 Diseases diagnosis

IL-2 was associated with chronic graft-versus-host disease in children as well as IFN-γ and IL-4 (Rozmus et al., 2011). IL-2 was indicated as a potential biomarker for the differentiation, classification and improved understanding of the pathogenesis of interstitial lung disease (Beirne et al., 2009). IL-2 was also reported as a biomarker to preterm birth (Matoba et al., 2009), coronary artery disease (Alber et al., 2006), relapsed multiple myeloma (Richardson et al., 2004), chronic beryllium disease (Tinkle et al., 1997), hepatocellular carcinomas (Ikeguchi et al., 2005), lung diseases such as cystic fibrosis and chronic obstructive pulmonary disease (Eickmeier et al., 2010), colorectal cancer (Burgdorf et al., 2009), prostate cancer (Christensen et al., 2009), asthma (Brasier et al., 2008) and colonic schistosomiasis (Hamed et al., 2011).

In a study of the rhinovirus- and respiratory syncytial (RS) virus-induced acute exacerbation of childhood wheezing, IL-5 was found to be significantly elevated in the rhinovirus induced wheezing compared with RS virus induced wheezing (Kato et al., 2011). IL-5 may be used as a biomarker in the determination of the viral infection. IL-5 was also a potential biomarker of interstitial lung disease (Beirne et al., 2009), preterm birth (Matoba et al., 2009), chronic rhinosinusitis (Niederfuhr et al., 2008), colorectal cancer (Burgdorf et al., 2009) and asthma (Brasier et al., 2008).

Monokine-induced by IFN-c (MIG) can be detected as one of the reporters of human immunodeficiency virus (HIV) and cytomegalovirus (CMV), besides TB (Kasprowicz et al., 2011).

Besides IP-10, interleukin (IL)-6, IL-8, TNF-a, vascular endothelial growth factor (VEGF), and macrophage inflammatory protein (MIP)-3a level increases in patients with nasopharyngeal carcinoma (NPC), which indicates the illness (Chang et al., 2011).

In order to diagnose complex regional pain syndrome type 1 (CRPS1), also known as reflex sympathetic dystrophy (RSD), Heijmans-Antonissen et al. suggested that IL-6, IL-8, TNF-α, monocyte chemoattractant protein (MCP)-1, macrophage inflammatory protein (MIP)-1β, IL-10, and IL-12 could be used as biomarkers (Heijmans-Antonissen et al., 2006).

Yurkovetsky et al. found that IL-1α, IL-1h, IL-6, IL-8, IL-12p40, IL-13, granulocyte colony-stimulating factor, MCP-1, MIP-1α, MIP-1h, IFN-α, TNF-α, epidermal growth factor, VEGF, and TNF receptor II in serum were found to be significantly higher in patients with resected high-risk melanoma compared with healthy controls (Yurkovetsky et al. 2007). They also found the changes of the level of cytokines during the treatment of the disease. Their results indicated that assessing the biomarkers is useful for detecting melanoma and monitoring the therapy of melanoma patients.

MCP-1 and stromal cell-derived factor 1 (SDF-1) are two cytokines participating in the pathogenesis of proliferative diabetic retinopathy (PDR) and proliferative vitreoretinopathy (PVR). They might be potential biomarkers for the diseases as well as IP-10 (Abu El-Asrar et al. 2006).

IL-12 was reported to enhance the sensitivity of leprosy disease diagnosis, combined with IFN-γ based whole blood assay (Geluk et al., 2010).

Hodgkin lymphoma (HL) is associated with cytokines including fractalkine, Interleukin 1 receptor, type II (IL1R2), IL-25, IP-10, migration inhibitory factor (MIF), Chemokine (C-C motif) ligand 5 (CCL5, also called RANTES), and thymus and activation regulated

chemokine(TARC). Among these cytokines, the level of IL1R2, MIF, and TARC was significantly elevated in patient plasma compared with healthy controls, which implied their potential as biomarkers for HL diagnosis.

MIP-1α, RANTES and MCP-1 have been also reported to be associated with severe acute respiratory syndrome (SARS)-coronavirus infection (Law et al., 2005).

MCP-1/CCL2 was a potential biomarker for prostatic growth dysregulation and benign prostatic hyperplasia as reported (Fujita et al., 2010).

A study indicated that IL-18 is increased in the brains of Alzheimer's disease patients (Ojala et al., 2009).

1L-8, MIP-I beta, platelet-derived growth factor bb (PDGFbb), IL-I ra, Fas ligand (Fas-L), sTNF-RI, and sTNF-R2 may be potential biomarkers in predicting mortality in cerebral malaria (Armah et al., 2007).

IL-6, IL-15, IL-8, IL-13, IL-1 alpha, IL-1 beta showed potential as biomarkers for Chronic Fatigue Syndrome (CFS), reported by Fletcher et al. (2009).

2.5.3.2 Detection methods

ELISA is commonly used for cytokine detection. Tumor necrosis factor (TNF)-α, interleukin (IL)-12 and IL-18 were detected using ELISA, as reported by Takahata et al. (Takahata et al., 2001 and 2003). The detection limit is 5 pg/ml, 2 pg/ml and 12.5 pg/ml, respectively. Caproni et al. detected IL-4, IFN-γ, IL-13, eotaxin, macrophage inflammatory protein (MIP)-1α, thymus and activation regulated chemokine (TARC) and IP-10 using ELISA (Caproni et al., 2004). O'Connor et al. developed an assay for multiple cytokines detection based on ELISA, which analyzed the samples on multiple proinflammatory cytokine ELISA kits (O'Connor et al., 2004).

Immunofluorescence assays are used for cytokine detection, including chemokine detection. Interleukin (IL)-2, IL-4, IL-6, IL-8, IL-10, Tumor necrosis factors (TNF)-α and chemokine (C-C motif) ligand 5 (CCL5 or RANTES) were detected using Bio-Plex® Suspension Array System (Bio-Rad Laboratories, Hercules, CA), reported by Chang et al. (2011). Multiple cytokines including chemokines could be detected use xMAP technology (Luminex Corp.), reported by Yurkovetsky et al. (2007). Macrophage inflammatory protein (MIP)-2 and MIP-1α were detected using immunofluorescence (Aliberti et al., 2001).

Exhaled breath condensate (EBC) analysis could detect IL-4, IL-17, TNF-α, RANTES (or CCL5), MIP-1α, MIP-1β, IL-8 and TGF-β, as reported by Matsunaga et al. (2009). The chemiluminescence substrate system coupled with membrane-bound antibody array mentioned before was used for the detection of 80 cytokines including chemokines (Sack et al. 2005).

Biosensors are reported for cytokine detection. A bioluminescence based biosensor was developed for the detection of TNFα (Gross and Piwnica-Worms, 2005). The detection of 1 ng/ml TNFα was reported. In another study, TNFα detection was performed using a microspot fluorescence immunoassay on photonic crystal surfaces by Cunningham (2010). The lowest concentration of TNFα detected was 1.6 pg/ml. In addition, Ganesh et al. reported a fluorescence sandwich immunosensor for the detection of TNFα (Ganesh et al., 2008). Chou et al. described a sandwich type immunoassay based surface plasmon resonance (SPR) biosensors for the detection of IL-6 with the detection limit of 1.3 ng/ml (Chou et al., 2010). The immobilization of DNA and protein on arrayed electrodes for the potential simultaneous detection of BRCA1 gene and IL-12 was reported by Harper et al. (2007). An optical thin film biosensor was employed for the detection of multiple cytokines. Four ng/l for IL-6, 31 ng/l for IL1-β, and 437 ng/l for IFN-γ were reported as the detection limits (Jenison et al., 2001). Moreover, a label-free

electrochemical impedance biosensor was described for the detection of IL-12 with a detection limit of < 100fM (La Belle et al., 2007). Dou et al. reported an electrochemical immunosensor for the detection of human IL10, which could detect the target from 0.001 ng/ml to 50 ng/ml (Dou et al., 2012). Additionally, IL-6, IL-8 (Chemokine), IL-10 and TNF-α were detected using a magnetic lab-on-a-chip biosensor, which incorporated magnetic sample preparation and detection by embedded GMR-type magnetoresistive sensors (Schotter et al., 2009). Vega et al reported a surface plasmon resonance biosensor for observing the receptor/ligand interaction of CXCR4/CXCL12 chemokines (Vega et al., 2011). A biochemically modified field effect transistor (BioFET) sensor using antibody fragment molecules was developed for minimally invasive detection of MIG (or CXCL9) as an early warning system in transplant rejection, as described by Eteshola et al. (2010). Fractalkine (CX3CL1) could be detected by using a surface plasmon resonance biosensor with its receptor (CX3CR1). The kinetics of the binding was measured (Fong et al., 2002). In addition, Krasnikova et al. used a biosensor for studying monocytic chemotactic protein-1 (MCP-1, Krasnikova et al., 2011).

2.6 Nanoparticle based biosensors

Nanoparticles with special optical, electrical, magnetic or catalytic properties have drawn the interest in their use in biotechnological systems, diagnosis systems and biological imaging systems. Because of their large surface-volume ratio, they have much more binding sites than larger particles. They are excellent for signal amplification for biosensors. Research showed that unfavorable lateral interactions between proteins attached to the nanoparticles which caused protein deactivation are reduced due to increasing curvature of nanosized materials compared to flat surfaces (Asuri et al., 2006). For example, magnetic nanoparticles have large surface area than magnetic particles in normal size. Therefore, there are more binding sites for biomolecules

such as antibodies for target capture. They provide enhanced capture capability when they are used for immunomagnetic separation. They are commonly applied in biosensors for separating targets (Zhang et al, 2010; Zhang et al., 2009; Setterington et al., 2011; Li et al., 2011; Anderson et al., 2013). At the same time, some nanoparticles have encoding capabilities from variable physical properties such as size, shape and composition. Therefore, they could be used for multiple analyte detection (Sanvicens et al., 2009).

2.6.1 Gold nanoparticles

Gold nanostructures create widespread interest for employing them in biosystems because of their characteristics such as surface plasmon resonance (SPR), the ease of bioconjugation and potential noncytotoxicity (Darbha et al., 2008). Gold nanoparticles (AuNPs) have the optical and electrical properties (e.g. electron beam contrast) and biocompatibility, which are widely used in detection and diagnostic technologies such as immunblotting, immunochromatography and flow cytometry. They are used for labeling target molecules especially biomolecules because of their biocompatibility and the capability of enhancing signals. They can interact with incoming visible or near-infrared spectroscopy (NIR) photons so that they are excellent substrates to detect molecules with surface-enhanced Raman scattering (SERS, Murphy et al., 2008). Moreover, they have been used in the detection of DNA, proteins, antibodies, glucose and toxic metal ions based on their aggregation (Murphy et al., 2008). The gold nanoparticles in spherical shape can be easily produced by chemically reducing gold salts (Busbee et al., 2003). Gold (III) chloride trihydrate and dextrin were used for the synthesis of gold nanoparticles under alkaline conditions (Anderson et al., 2011). As reported, gold nanoparticles have been used for signal amplification in biosensors. A quartz crystal microbalance (QCM) DNA biosensor using AuNPs as signal amplifier was developed for the detection of *Bacillus anthracis* (Hao et al., 2011). The target

DNA hybridized with a thiol DNA probe which was immobilized on the QCM gold surface, and then AuNPs conjugated with another thiol-DNA fragment which was complementary to the free end of the target DNA were introduced to the target. Therefore, the increased mass due to the hybridization of AuNP-probe to the target DNA resulted in the further decrease in resonance frequency of the QCM biosensor. Wang et al. (2013) reported an impedimetric electrochemical DNA biosensor which also used AuNPs as signal amplifiers. In their design, probe ssDNA were immobilized on a gold electrode as well as linked to AuNPs. The electrode and AuNPs were in close contact in the absence of target DNA, enabling a low electron transfer resistance. After the target DNA and the probe hybridized, a rigid duplex formed which caused a larger electron transfer resistance due to the increase in the distance between the electrode and AuNPs. The target DNA from 5 fM to 500 pM was detected. Jiao et al. (2013) also reported an electrochemical biosensor based on AuNP signal amplification recently. Aptamers which are a class of synthetic single-stranded DNA (ssDNA) or RNA oligonucleotides with target specificity were used as the sensing element to detect the protein target thrombin in this research. The binding of the target to the aptamers resulted in the release of AuNPs and a decrease in chronocoulometric signal. Using the optical properties of AuNPs, Gnedenko et al. (2013) amplified the signal of a surface plasmon resonance biosensor by approximately 30-fold compared to the biosensor without AuNPs. A sandwich structure of antibody-target-AuNP (conjugated with a secondary antibody) formed to provide the sensitivity. Various designs of biosensors based on AuNP signal amplification has been reported in recent years (Xu et al., 2013; He et al., 2013; Fan et al., 2012; Thiruppathiraja et al., 2011; Ahn et al., 2011; Hall et al., 2011).

2.6.2 Bio-barcode biosensors

Bio-barcode assay is a DNA amplification method based on oligonucleotide-modified particles. The assay provides the PCR-like sensitivity for detection without the need for enzymatic amplification (Nam et al., 2004). Gold nanoparticles were modified with DNA probes (pDNAs) complementary to the target DNA (tDNA) and oligonucleotides complementary (cbDNAs) to barcode oligonucleotides (bDNAs). Magnetic microparticles (MMPs) were modified with oligonucleotides which are complementary to the target DNA and recognize a different region of the target (different from the region that DNA probes on gold nanoparticles recognize), shown in Figure 2-2a (Nam et al., 2004). The typical bio-barcode assay and the detection process are explained in Figure 2-2b (Nam et al., 2004). Modified MMPs were added to the detection samples for hybridization with target single-stranded DNA. Then modified gold nanoparticles were introduced. After hybridization, magnetic field pulled the MMPs to the field to separated reacted and unreacted components. The barcode DNAs were released at the end and assessed by scanometric method which is a chip-based measurement using silver enhancement. The whole assay is usually 3 to 4 h (Nam et al., 2004). many studies applied the concept of bio-barcode for the detection of nucleic acid targets, proteins and pathogen bacteria (Thaxton et al., 2005; Tang et al., 2007; Hill et al., 2007).

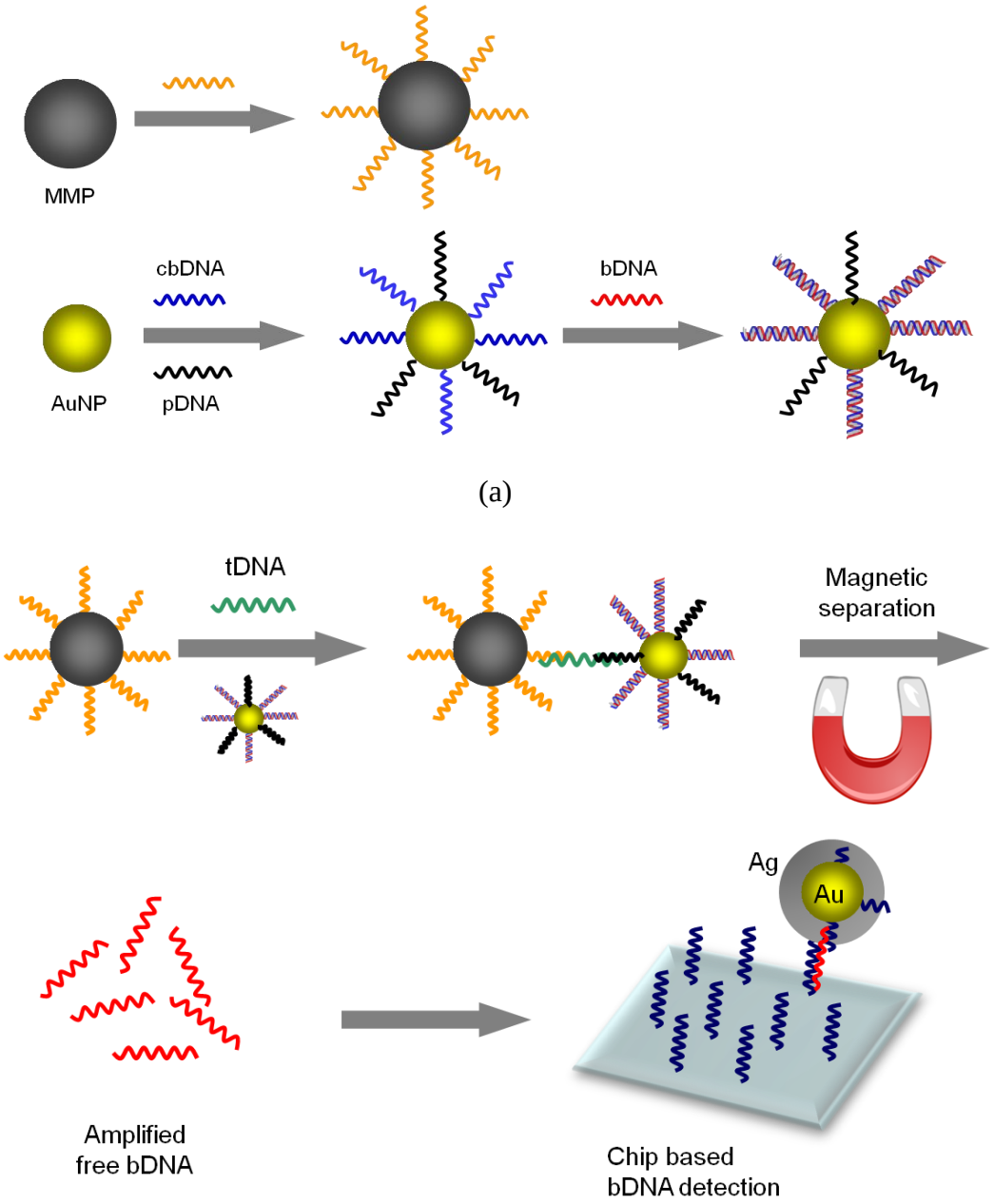

Figure 2-2. Bio-barcode biosensor assay: (a) nanoparticle preparation; (b) DNA detection (Adapted and modified from Nam et al., 2004).

2.6.3 Nanotracers

The bio-barcode assay requires the release of barcode DNAs, microarray-based immobilization of oligonucleotides on a chip and silver enhancement for light scattering measurement, which cumulatively increase the detection time and the cost. Nanotracers (NTs) which are nanoparticles of heavy metals were reported for the detection of multiple targets, and they showed the ability of enhancing signals for electrochemical measurement (Zhang et al., 2010; Wang et al., 2003). Some studies investigated the utilization of NTs' encoding capabilities. Ding et al. and Zhang et al. attached NTs to the gold nanoparticles through the linkage of DNA, and conducted electrochemical measurement to obtain the signals for DNA detection, which required less time and cost but still kept the high sensitivity (Ding et al., 2009; Zhang et al., 2010). Figure 2-3 presents a biosensor using NTs for signal amplification (Zhang et al., 2010). Gold nanoparticles were conjugated with pDNA and bDNA terminated with NTs. The pDNA 1 hybridized with tDNA 1, and the pDNA 2 on AuNPs hybridized with tDNA 2. The NTs provided electrochemical signals for the detection. Therefore, the signals of two NTs encoded the detection of two different targets. By employing this biosensor, 0.5 ng/ml of the insertion element (Iel) gene of *Salmonella enteritidis* was detected using CdS NTs, and 50 pg/ml of the pagA gene of *Bacillus anthracis* using PbS NTs.

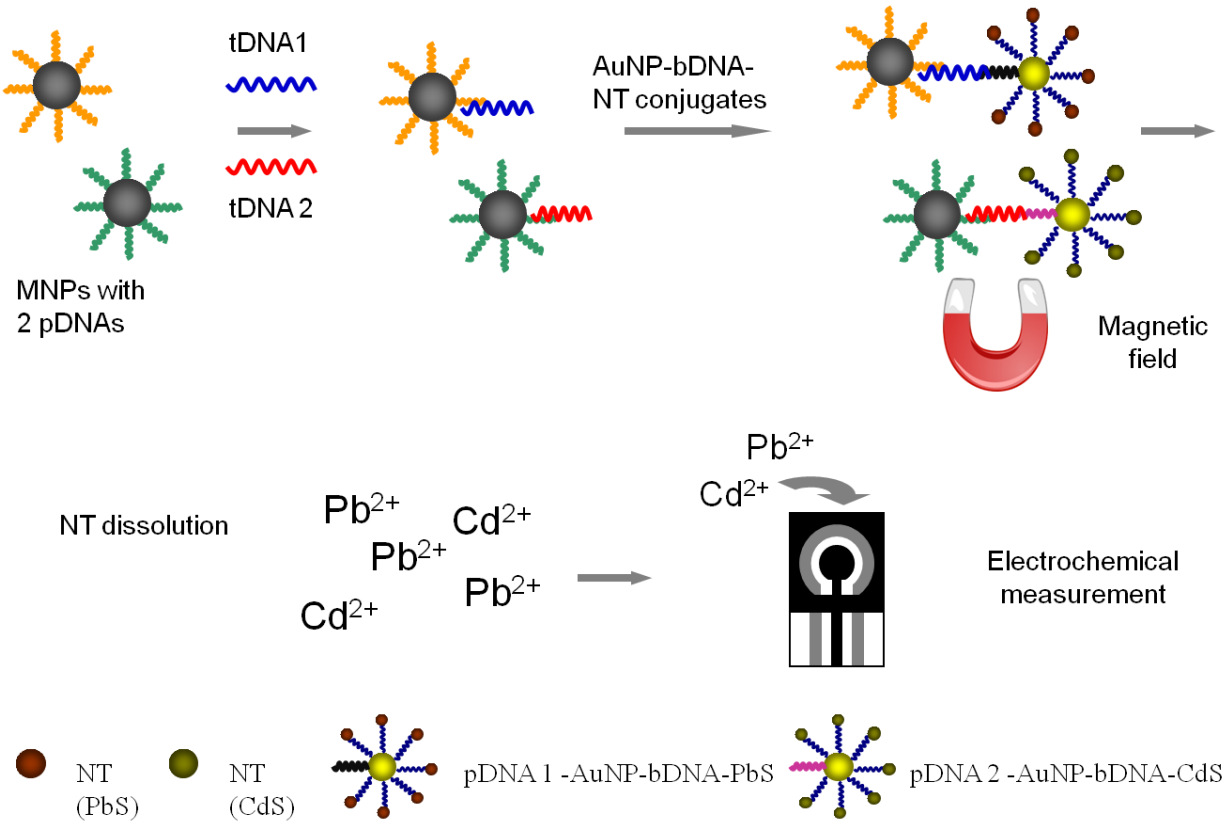

Figure 2-3. Nanotracer biosensor for DNA detection (Adapted and modified from Zhang et al., 2010).

2.7 Conclusions and outlook

Many technologies have been developed to identify the threat to public health. To detect the foodborne and waterborne pathogen *E. coli* O157: H7, ELISA, PCR and biosensors were investigated to provide more sensitive and rapid approaches compared to conventional culture plating methods. For diagnosing infectious diseases such as TB to enable timely and effective prevention and treatment, research has progressed in the aspects of clinical tests, biomarker recognition, latent TB identification and etc. However, methods which require easy manipulation and low cost with possible in-field test capabilities are still areas to explore. Biosensors show the

potential of achieving the goal. Introducing nanotechnology into biosensors further improves the sensitivity of biosensors due to the properties such as large surface to volume ratio, signal amplification and encoding abilities of nanomaterials. Currently, miniatured nano-sized transducers and biomolecule-functionalized nanomaterials for labeling have been employed to improve biosensor performance. DNA-based nano-biosensors still need multiple treatments of samples such as DNA extraction from bacteria. Immunosensors which rely on antigen-antibody recognition are easier to handle, though the specificity of immunosensors should be considered.

Metallic nanoparticles have the property of registering at certain potential during electrochemical measurement. Research on surface modification also enables them to conjugate with biomolecules. In addition, due to their large surface area for binding biomolecules, these particles are utilized in electrochemical biosensors. The synthesis, functionalization and signal generation methods of these nanoparticles need investigation when used in biosensing systems for sensitive, rapid, portable and multiplex detection.

Chapter 3 : Gold nanoparticle-labeled biosensor for detection of *E. coli* O157:H7

3.1 Introduction

The rapid detection of pathogenic bacteria is critical to public health, biodefense, and food/water safety. *Escherichia coli* O157:H7 is one of the major foodborne and biodefense bacterial agents. Because conventional culture plating methods for *E. coli* O157:H7 take two to four days to obtain results, the development of rapid detection methods is important. Biosensors are emerging technologies that have the potential for getting rapid results and that can be employed in the field. There are many configurations and approaches in the research and design stage, which include antibody-based systems (Luo et al., 2010; Radke and Alocilja, 2005; Setterington et al., 2011; Tan et al., 2011; Wang et al., 2010), enzyme-based detection (Linman et al., 2010; Park et al., 2008) and DNA-based sensors (Sun et al., 2009; Wang et al., 2009). In addition to speed, biosensors have the potential to generate highly sensitive results. This is especially critical as many bacterial infections could be caused by as low as 10 organisms (CAST, 1994).

The application of nanomaterials in biosensors has drawn interest to enhance sensor sensitivity either by increasing the capture efficiency of the target molecules or by utilizing the optical and electronic properties of the nanostructures to amplify signals. Magnetic nanoparticles were employed for separating targets for bacterial detection (Li et al., 2011; Setterington et al., 2011; Zhang et al., 2010). Gold nanoparticles were used for signal amplification (Hao et al., 2011; Zhang et al., 2010). Polymeric nanoparticles were also introduced for signal amplification (Jiang et al, 2011; Setterington and Alocilja, 2011). Electrochemical biosensors can be used for nanoparticle-based detection. The electrochemical measurement provides advantages such as low

detection limits, a wide linear response range, and good stability and reproducibility (Faridbod et al., 2011).

In this chapter, an electrochemical biosensor using antibody-modified nanoparticles for the detection of *E. coli* O157:H7 was developed. Two novel nanoparticles were utilized in the biosensor design: 1) polymer-coated magnetic nanoparticles (MNPs) to separate the target bacteria from the sample matrix and 2) carbohydrate-capped gold nanoparticles (AuNPs) to label the separated target by forming a sandwich structure and generate the signal. The signal of AuNPs for the corresponding target was measured by differential pulse voltammetry (DPV) on a screen printed carbon electrode (SPCE) chip. The biosensor enabled rapid pathogen detection in 45 min from sample preparation to final readout of results.

3.2 Materials and methods

3.2.1 Reagents and materials

Two kinds of nanoparticles were synthesized: magnetic nanoparticles (MNPs) and gold nanoparticles (AuNPs). Aniline, iron (III) oxide nanopowder, ammonium persulfate, methanol, and diethyl ether were used for the synthesis of the MNPs. Gold (III) chloride trihydrate (Aldrich, MO) and dextrin (Fluka, MO) were used for the synthesis of gold nanoparticles under alkaline conditions (Anderson et al., 2011).

Magnetic nanoparticles were functionalized with monoclonal anti-*E. coli* O157:H7 antibodies (mAbs) obtained from Meridian Life Science, Inc (Saco, ME). Gold nanoparticles were conjugated with polyclonal anti- *E. coli* O157:H7 antibodies (pAbs) from Meridian Life Science, Inc (Saco, ME). Protein A from *Staphylococcus aureus* was used as the linkage agent for AuNP and antibody conjugation.

Triton-X100, phosphate buffered saline (PBS), casein, bovine serum albumin (BSA) and sodium phosphate (dibasic and monobasic) were obtained from Sigma-Aldrich (St. Louis, MO). PBS buffer (0.01 M, pH 7.4), PBS buffer with 0.05% (w/v) Triton-X100, phosphate buffer (0.1 M sodium phosphate, pH 7.4), PBS buffer with 0.01% casein, PBS buffer with 0.1% (w/v) BSA were prepared with deionized water from Millipore Direct-Q system. PBS buffer and phosphate buffer were used in preparing nanoparticle-antibody (Ab) conjugates and in washing. PBS buffer with casein or BSA was used to block nanoparticle surface against nonspecific binding. PBS buffer with Triton-X100 was used for washing off unbound or nonspecifically bound reactants after capture.

3.2.2 Bacterial culture

Escherichia coli O157:H7 Sakai strain was obtained from the Nano-Biosensors Lab collection at Michigan State University. The colonies from frozen (stored at –70 ℃) culture were grown on trypticase soy agar (BD Biosciences, MD) plates. A single colony was isolated and inoculated in tryptic soy broth (BD Biosciences, MD) and grown overnight at 37 ℃. One milliliter of the liquid culture was transferred to another tube of tryptic soy broth and incubated overnight at 37 ℃. One milliliter of this liquid culture was transferred to a new tube of broth and incubated at 37 ℃ for 6 hr before each experiment. The serial dilutions of bacterial culture were prepared using 0.1% (w/v) peptone water (Fluka-Biochemika, Switzerland) before each experiment. Viable cells were enumerated by microbial plating on Sorbitol MacConkey agar (SMAC, BD Biosciences, MD).

3.2.3 Apparatus

Electrochemical measurement was performed with a potentiostat/galvanostat (263A, Princeton Applied Research, MA) with a software operating system (PowerSuite, Princeton

Applied Research, MA) on a computer connected to the potentiostat. The measurement was performed by introducing each sample onto a screen-printed carbon electrode (SPCE) chip (Gwent Inc. England). The SPCE chip consisted of a working electrode (carbon) and a counter and reference electrode (silver/silver chloride electrode).

3.2.4 Synthesis of nanoparticles

Polyaniline (PANI) coated magnetic nanoparticles were synthesized according to a published method (Setterington et al., 2011). Fifty milliliters of 1 M HCl, 10 ml of water and 0.4 ml of aniline monomer were mixed in a flask, and then 0.65 g of iron (III) oxide nanopowder were added to the solution to maintain a final γ-Fe_2O_3: aniline weight ratio of 1: 0.6. The mixture was put in a beaker filled with ice and sonicated for 1 h. The solution was stirred while it was still on ice. During the stirring, ammonium persulfate (1 g of ammonium persulfate in 20 ml deionized water) was added to the solution slowly for 30 min. The solution was stirred for another 1.5 h. After the reaction, the solution was filtered using 2.5 μm filter paper and washed with 20% methanol. Hydrochloric acid (1 M) was used to wash until the filtrate became clear, followed by washing with 10 ml 20% methanol. The filtrate was filtered again using a 1.2 μm filter paper. Twenty percent methanol solution was added to the filter. The HCl and methanol wash was repeated. The nanoparticles on the filter paper were left under a fume hood to dry for 24 h at room temperature and stored in a vacuum desiccator after drying.

Gold nanoparticles were synthesized under alkaline conditions following the approach published by Anderson et al (Anderson et al., 2011). Briefly, 20 ml of dextrin stock solution (25 g/l) and 20 ml of sterile water were mixed in a 50 ml sterile orange cap tube (disposable). Five milliliters of $HAuCl_4$ stock solution (8 g/ml) were then added, and the pH of the solution was

adjusted to 9 with sterile 10% (w/v) Na_2CO_3 solution. The final volume was brought to 50 ml with pH 9 water. The reaction was carried out by incubating the solution in a sterile flask in the dark at 50 ℃ with continuous shaking (100 rpm) for 6 h. A red solution was obtained at the end of the reaction. The final concentration of AuNP was 10 mg/ml.

3.2.5 Functionalization of nanoparticles

Magnetic nanoparticles were functionalized with a monoclonal antibody (mAb) to *E. coli* O157:H7 (Setterington et al., 2011). MNPs (2.5 mg) were suspended in 150 µl of 0.1M phosphate buffer, and sonicated for 15 min. Monoclonal anti-*E. coli* O157:H7 antibody (2.5 mg/ml, 100 µl) was added to the suspension, and mixed on tube rotator for 5 min. Twenty five microliters of PBS buffer (0.1 M) were added. Then the conjugation was carried on for 55 min on the tube rotator. The MNPs were separated from the solution by magnetic separation, and blocked by adding 250 µl of 0.1 M tris buffer with 0.01% casein for 5 min incubation. This step was repeated three times, and the suspension was put on tube rotator for 1 h hybridization at the last time. Finally, the MNPs were magnetically separated and resuspended in 2.5 ml of 0.1M phosphate buffer. The MNP-mAb conjugate was stored at 4 ºC before use.

Gold nanoparticles were conjugated with a polyclonal antibody to *E. coli* O157:H7 (pAb) through the protein A linkage. Two hundred microliters of AuNPs were put into a 2 ml microcentrifuge tube and sonicated for 10 min. Then the suspension was centrifuged for 6 min at 13,000 rpm. The supernatant was removed after centrifugation. To modify the surface of the AuNPs, protein A (0.25 mg/ml) in PBS buffer was used to resuspend the AuNPs. The conjugation was conducted by rotating the mixture for 1 h. The modified AuNPs were separated from the suspension by centrifugation for 6 min at 13,000 rpm. The nanoparticles were washed by adding 200 µl of 0.01 PBS buffer and centrifuged. After removing the supernatant, 100 µl of

1 mg/ml antibody and 100 µl PBS buffer were added to the tube and mixed for 1 h by rotating. After separating the AuNP-antibody (AuNP-pAb) conjugates, 200 µl of PBS buffer with 0.1% (w/v) BSA were added to the tube. The mixture was rotated for 30 min. Finally, the AuNP-pAb conjugates were separated from the suspension by centrifugation, and the final suspension of the conjugates in PBS buffer was stored at 4 °C. The procedure of AuNP functionalization is shown in Figure 3-1.

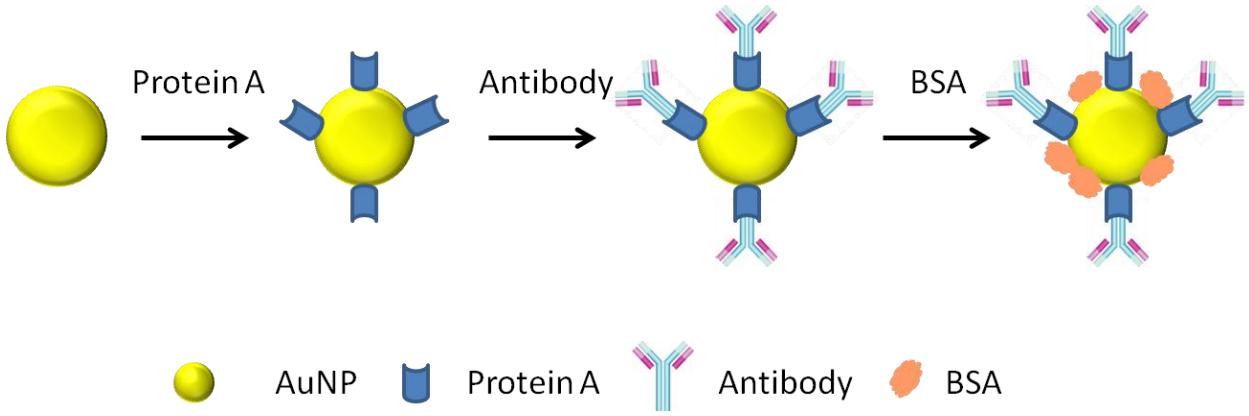

Figure 3-1. Schematic of the AuNP functionalization. Gold nanoparticles were firstly modified with protein A. Then the antibody was conjugated onto the AuNPs through the linkage of protein A. At last, BSA was added to block the uncoated surface.

3.2.6 Detection of target pathogenic bacteria

Detection of the target pathogen is presented in Figure 3-2. Blank control for the tests was peptone water in the same volume as the sample. Firstly, 400 µl of PBS buffer, 50 µl of cell dilution (or peptone water for the blank) and 50 µl of MNP-mAb conjugates were combined in a 2 ml sterile tube. After 15 min incubation, PBS buffer (55 µl, 0.01 M) with 0.1% BSA was added to the mixture as a blocking agent. Then, the MNP-*E. coli* complexes were magnetically separated from the solution and resuspended in 450 µl of PBS buffer. Secondly, the AuNP-pAb

conjugates were introduced to the system, followed by 15 min incubation. After washing the complexes once with 0.01 M PBS buffer, the complexes were resuspended in 500 µl of PBS buffer with 0.05% Triton-X100, and let stand for 3 min. Finally, the complexes were suspended in 500 µl of PBS buffer. One hundred microliters of the suspension were plated on SMAC for cell counting. The rest was magnetically separated from the supernatant (400 µl).

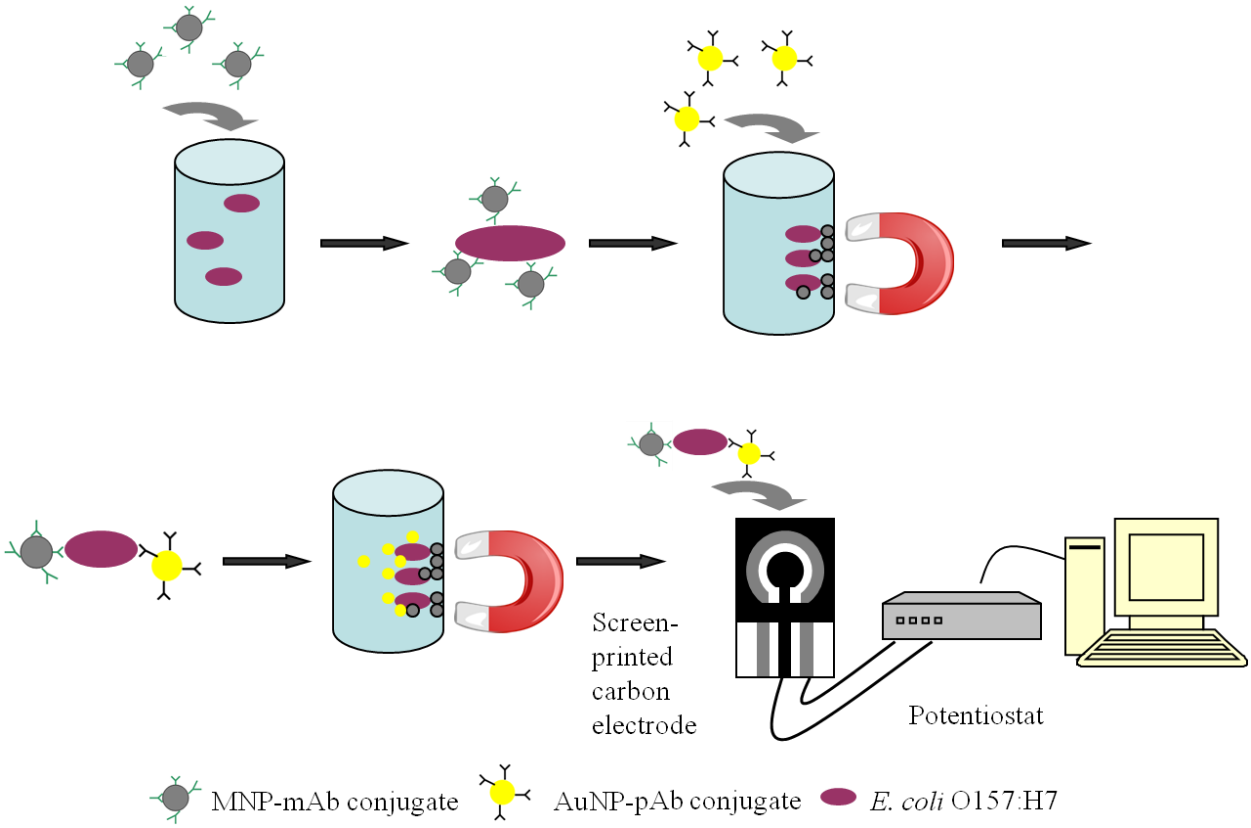

Figure 3-2. Schematic of the AuNP-labeled biosensor for *E. coli* O157:H7 detection. Target cells in a sample were captured by MNP-mAb conjugates and separated by a magnet. Then the cells were labeled with AuNPs. The MNP-mAb-cell-pAb-AuNP complexes were transferred onto a SPCE chip connected to a potentiostat for electrochemical measurement.

3.2.7 Electrochemical measurement

The target bacteria were detected by measuring the electrochemical signal of AuNPs. Each sample from section 3.2.6 (complexes magnetically separated from supernatant) was incubated for 5 min in 100 μl 1 M HCl and then introduced to the SPCE chip. An oxidation potential of 1.4 V vs. Ag/AgCl was applied to the working electrode. After oxidation, a differential pulse voltammetric (DPV) measurement was performed. The scan was conducted from 1.5 V to -1.5 V. The potential and currents were recorded. All measurements were performed at room temperature. Each sample was measured three times. At least three samples for each concentration of bacteria were tested.

3.3 Results and discussion

3.3.1 Magnetic separation of target *E. coli* O157:H7

The Fe_2O_3 nanoparticles were coated with PANI for direct immobilization of anti-*E. coli* O157:H7 antibody. Figure 3-3 presents the transmission electron microscope (TEM) image of the PANI-coated magnetic nanoparticles. Because the coating resulted in polymer layers in uneven thickness, the coated MNPs show diameters ranging from 50 to 100 nm. At the same time, there are some small particles which are uncoated Fe_2O_3 nanoparticle core shown in the image with the average diameter of 20 nm.

Electrostatic interaction has been used to modify the PANI-coated MNPs with antibody. The interaction between the negatively charged Fc fragment of antibody molecules and the positively charged PANI contributes to the conjugation (Pal and Alocilja, 2009). Figure 3-4 is the schematic of the interaction between the PANI-coated MNPs and the antibody.

The culture dilutions and the MNP-cell-AuNP samples (captured cells) were plated on SMAC for cell counting, and the MNP capture efficiency (CF) was calculated for each test using Equation 3-1 as shown below.

$$CF=(\log_{10} C_{cap} / \log_{10} C_{cul}) \times 100\% \quad (3\text{-}1)$$

Where C_{cap} is the number of captured cells obtained from plate counting and C_{cul} is the number of cells in culture from plate counting with the unit of cfu/ml. An average of 97.2% $\pm$ 2.86% was obtained, which indicated that the capture using MNPs was very efficient.

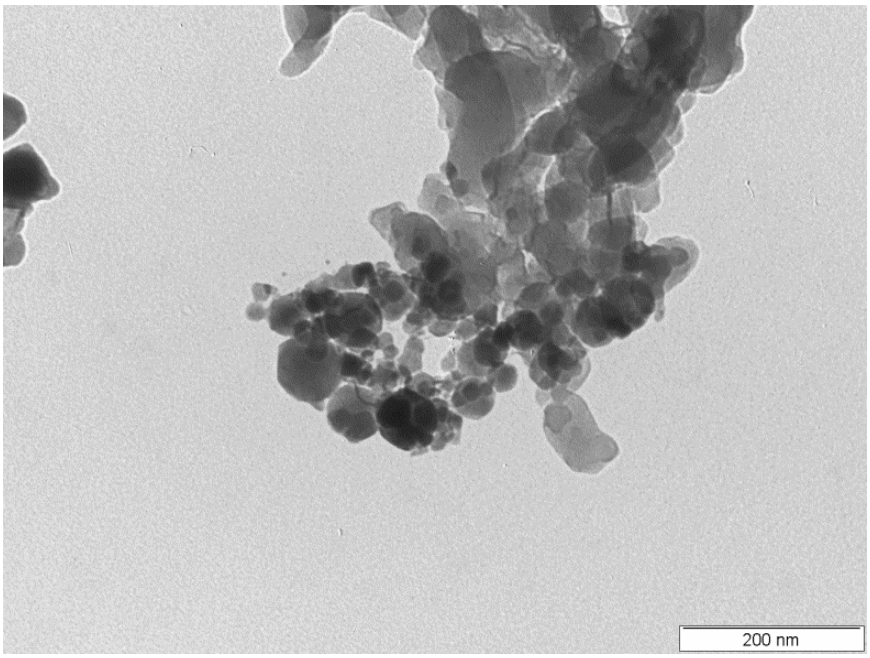

Figure 3-3. TEM image of polyaniline (PANI) coated magnetic nanoparticles.

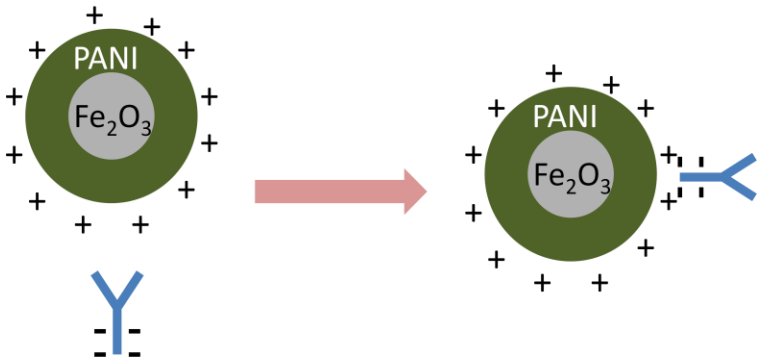

Figure 3-4. Schematic of the conjugation of PANI-coated MNP and antibody. The MNP coated with PANI conjugated to antibody through the interaction between the negatively charged Fc fragment of the antibody and the positively charged PANI.

3.3.2 AuNP-labeled biosensor for detection

Figure 3-5 shows a typical sensorgram of AuNPs in 100 µl 1 M HCl on SPCE. A control (blank) of only 100 µl 1 M HCl is also presented. It was found that from 1.5 V to 0 V, there were three current peaks shown during the DPV measurement. Compared the AuNP sensorgram with the blank, there are two peaks at potential higher than 0.6 V for both AuNP sample and the blank. Since reduction reaction happened during the DPV test, the incomplete peak shown in this voltammetry at around ~1.3 V and the peak at ~0.6 V may be resulted from the two-step four-electron reduction of O_2 to H_2O through H_2O_2 (Britto et al., 1999; El-Deab et al., 2003). For AuNP sample, the reduction of H_2O_2 to H_2O was hindered due to the possible bond between Au and peroxide (Rosca et al., 2013), and a smaller peak was observed at ~0.6 V. A potential at 1.4 V was applied to the working electrode to oxidize the AuNPs to gold ions before DPV. Therefore, the gold ion was reduced to Au during the DPV, which shows a peak at 0.3 V compared to the blank without AuNPs. According to this characteristic peak, samples with

bacterial cells which were labeled with AuNPs had the same peak during the DPV measurement. Figure 3-6 shows typical DPV sensorgrams for the detection of *E. coli* O157:H7 at different cell concentrations (10^2, 10^4, and 10^6 cfu/ml). The sensorgrams show curves similar to the sample with only AuNPs shown in Figure 3-5. For the analysis, peak current to the left (representing AuNPs) around 0.3 V was chosen for signal reporting. As shown in the sensorgrams, peak current for AuNPs increased with increasing cell concentration. Figure 3-6 confirms the formation of the MNP-cell-AuNP complex. The amount of target cells detected was proportional to the amount of AuNPs.

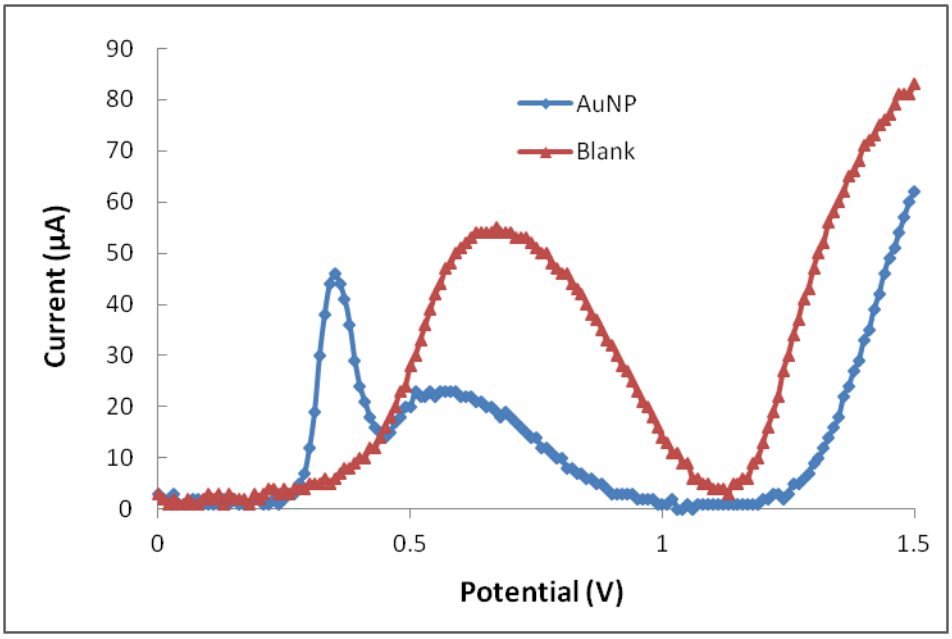

Figure 3-5. Differential pulse voltammetric sensorgram of the AuNPs. The sensorgrams of AuNPs in 100 µl 1 M HCl and a blank (100 µl 1 M HCl) are presented. AuNPs show a current peak at 0.3 V.

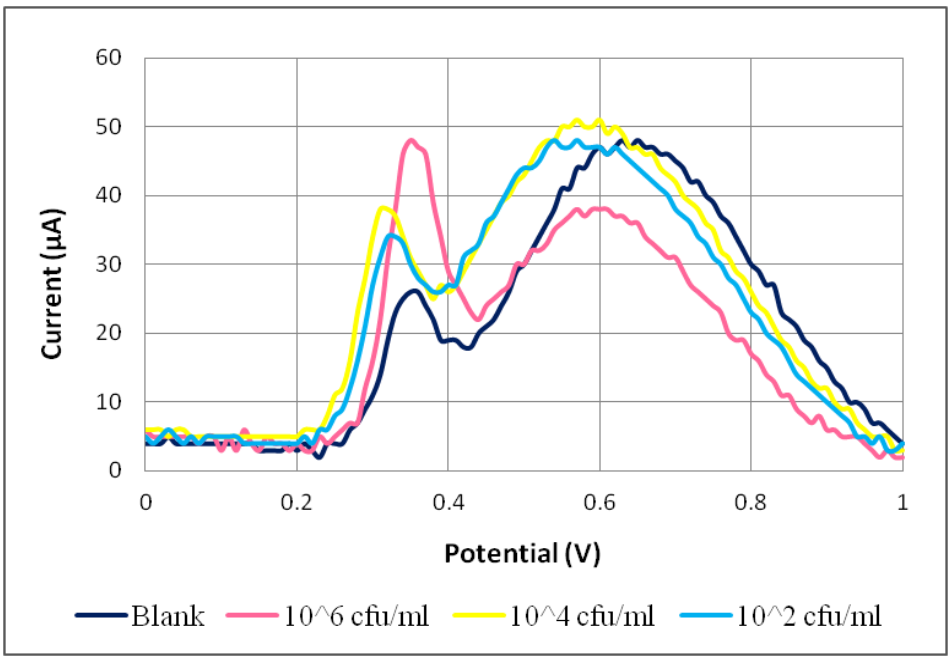

Figure 3-6. Sensorgrams of AuNP-labeled biosensor for *E. coli* O157:H7 detection. Peak current for AuNPs at ~0.3V increases with increasing cell concentration.

A linear relationship between signal to noise ratio (SNR) and cell concentration is shown in Figure 3-7, with an R^2 value of 0.953. The SNR was calculated as the peak current of AuNPs for each concentration divided by the peak current of the blank. The SNR for 10^1, 10^2, 10^3, 10^4, 10^5 and 10^6 cfu/ml are 1.28, 1.56, 1.69, 1.73, 2.12 and 2.36, respectively. A statistical analysis using *t* test was conducted and the results are presented in Table 3-1. As shown, cell concentration at 10^1 cfu/ml is not significantly different from the blank, with a P value of 0.0546 (which is close to critical value of P=0.05). The P value for other concentrations shows that the samples are significantly different from the blank. Therefore, the lowest cell concentration detected is 10^2 cfu/ml with strongly significance and 10^1 cfu/ml with weakly significance. These results verify

that MNP-mAb-cell-pAb-AuNP is an effective approach to highly sensitive detection. Furthermore, the antibody-antigen binding complex structure would provide an enhanced specificity to the detection. The specificity of the biosensor was tested by evaluating the mAb using western blot by Cloutier (Cloutier, 2012). Among the seventy five bacteria tested, including *E. coli* O157:H7 strains and non-*E. coli* O157:H7 bacteria, an inclusivity of 94% and an exclusivity of 69% was obtained (Cloutier, 2012). The inclusivity was calculated as the number of positive tests identified by the antibody divided by the actual total positive test number, while the exclusivity was calculated as the negative tests identified divided by the actual total negative test number.

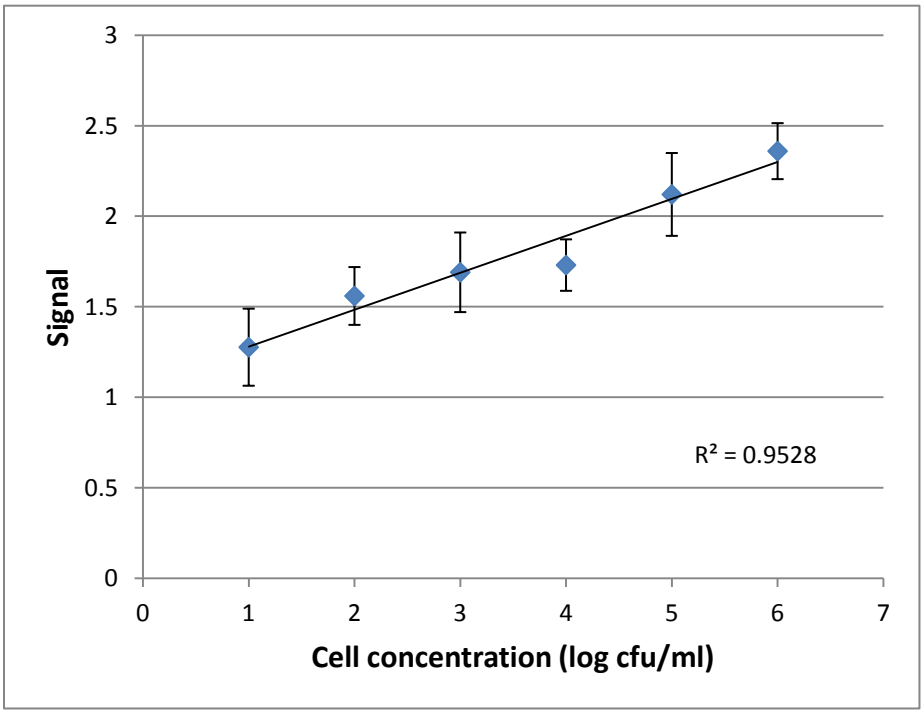

Figure 3-7. Peak current vs. cell concentration of the AuNP-labeled biosensor for *E. coli* O157:H7 detection. The signal shows a linear relationship between 10^1 to 10^6 cfu/ml.

Table 3-1. Statistical analysis comparing samples and blank (*t* test) for AuNP-labeled biosensor.

Concentration (cfu/ml)	10^1	10^2	10^3	10^4	10^5	10^6
P value[a]	0.0546	0.0212	0.0044	0.0054	0.0079	0.0007

[a] P value was calculated by a one-tailed paired *t* test. The critical value, P=0.05.

3.4 Conclusion

A gold nanoparticle-labeled biosensor has been developed for the sensitive and rapid detection of *E. coli* O157: H7. The lower limit of detection is at 10^2 cfu/ml with a dynamic range of 10^2 to 10^6 colony forming units per milliliter (cfu/ml) within 45 min. Furthermore, sample preparation requires minimal effort. This biosensor has the potential of being used for in-field detection of bacterial contamination in food products (e.g. ground beef, vegetables, and juices) and water systems as it is simple to use and quick to results. The biosensor is also a promising technology for point-of-care screening of diseases and environmental determination of harmful biological agents. Based on the detection using AuNP-label, further signal amplification will be available by employing the biomolecule-attachment property of the AuNPs.

Chapter 4 : PbS nanotracer-labeled biosensor for detection of *E. coli* O157:H7

4.1 Introduction

Nanomaterials have been utilized in sensing technologies due to their large surface-to-volume ratio and their optical, electrical, magnetic and catalytic properties (Sanvicens et al., 2009; Claussen et al., 2012). Biosensors for rapid and sensitive detection have involved the use of nanostructures, including nanoparticles, in various forms. With the current development of nanofabrication technologies, conductive nanostructures are used for enhanced transducing such as one dimensional or scalable nanoelectrode arrays (Claussen et al., 2012; Triroj et al., 2011; Liu et al., 2009; Singh et al., 2012). Moreover, magnetic nanoparticles are commonly used for separating target analyte from its sample matrix (Setterington et al., 2011; Li et al., 2011). Another major application of nanomaterials is signal amplification (Joung et al., 2008; Jiang et al., 2011; Zhang et al., 2010; Hao et al., 2011; Wang and Alocilja, 2012).

There are many studies on signal amplification using nanomaterials. For example, a bio-barcode assay by Nam et al. involved a DNA amplification method based on oligonucleotide-modified gold nanoparticles for signal amplification and magnetic microparticles for separation. The assay provided PCR-like sensitivity for detection without the need for enzymatic amplification (Nam et al., 2004). The whole assay took 3 to 4 h (Nam et al., 2004). The concept of bio-barcode was employed for the detection of nucleic acid targets, proteins and pathogenic bacteria (Thaxton et al., 2005; Tang et al., 2007; Hill et al., 2007). Instead of the release of barcode DNAs and chip-based silver enhancement light scattering measurement used in bio-barcode assays, nanotracers (NTs), nanoparticles of heavy metals, were attached to the gold nanoparticles (AuNPs) through the linkage of single-strand DNA, and electrochemical

measurement was conducted to obtain the signal for double-strand DNA detection (Zhang et al., 2010; Ding et al., 2009; Wang et al., 2003). This approach required less time and cost than bio-barcode assays but still kept the high sensitivity.

In this chapter, an immunosensor consisting of three nanoparticles is described. Signal amplification was conducted through lead sulfide (PbS) nanoparticles which were conjugated to AuNPs via oligonucleotide linkage. The detection was based on antibody-antigen recognition, which is a simplified approach for bacterial detection because there is no DNA extraction required. At the same time, the detection time was lessened compared to bio-barcode assays. The three kinds of nanoparticles used in this biosensor design were: 1) magnetic nanoparticles (MNPs) to separate the target bacteria from the sample matrix; 2) gold nanoparticles (AuNPs) to label the separated target by forming a sandwich structure with the magnetic nanoparticle; and 3) PbS nanoparticles which were linked to AuNPs, to generate the electrochemical signal. The attachment of a single AuNP to the target carried multiple PbS nanoparticles to the final MNP-target-AuNP-PbS complex. *Escherichia coli* O157:H7 was chosen as the target in this chapter because it is a life-threatening pathogen causing diseases from a low infective dose. In addition, because the bacteria can be monitored during the detection by plating methods, this target is suitable for the proof of concept. Compared to conventional culture plating methods which take two to four days to obtain results, the immunosensor can detect the target in less than one hour from sample processing to final readout with comparable sensitivity.

4.2 Materials and methods

4.2.1 Reagents and materials

Three kinds of nanoparticles were synthesized: magnetic nanoparticles (MNPs), gold nanoparticles (AuNPs) and lead sulfide (PbS) nanoparticles. Aniline, iron (III) oxide

nanopowder, ammonium persulfate, methanol, and diethyl ether were used for the synthesis of the MNPs. Gold (III) chloride trihydrate (Aldrich, MO) and dextrin (Fluka, MO) were used for the synthesis of gold nanoparticles under alkaline conditions (Anderson et al., 2011). Sodium sulfide, 3-mercaptoacetic acid, and lead nitrate were used for the synthesis of PbS nanoparticles. Both monoclonal and polyclonal anti-*E. coli* O157:H7 antibodies were obtained from Meridian Life Science, Inc. (Saco, ME).

MNPs were functionalized with a monoclonal anti-*E. coli* O157:H7 antibody (mAb) while AuNPs were conjugated with a polyclonal anti-*E. coli* O157:H7 antibody (pAb). An oligonucleotide sequence (5'-GTC AGT CAG TCA GTC AGT CA-3') with 3' thiol modifier and 5' amino modifier was employed as a linker between AuNPs and PbS nanoparticles, which was purchased from Integrated DNA Technologies Inc. (Coralville, IA). 1,4-Dithio-dl-threitol (DTT) was used for the cleavage of oxidized thiolated oligonucleotides. Nap-5 column (GE Healthcare, NJ) was used for the purification of oligonucleotides from DTT solution. 1-Ethyl-3-[3-dimethylaminopropyl] carbodiimide hydrochloride (EDC) and N-hydroxysuccinimide (NHS) were used for the linkage of carboxylic groups on PbS nanoparticles and amine groups on oligonucleotides bound to AuNPs. These reagents were purchased from Sigma (St. Louis, MO). Bismuth standard stock solution (10,000 ppm) was purchased from Ricca Chemical Company (Arlington, TX). Acetate buffer solution (0.1 M, pH 4.5) with 1 mg/l bismuth was used for electrochemical measurement.

Triton-X100, phosphate buffered saline (PBS), casein, bovine serum albumin (BSA) and sodium phosphate (dibasic and monobasic) were obtained from Sigma-Aldrich (St. Louis, MO). PBS buffer (0.01 M, pH 7.4), PBS buffer (0.01 M, pH 7.4) with 0.05% (w/v) Triton-X100, phosphate buffer (0.1 M sodium phosphate, pH 7.4), 0.1 M tris buffer with 0.01% casein, PBS

buffer (0.01 M, pH 7.4) with 0.1% (w/v) BSA, assay buffer (0.562 g Na_2HPO_4, 0.125g NaH_2PO_4, 4.383g NaCl and 0.5g BSA in 500 ml water; Hill and Mirkin, 2006) were prepared with deionized water from Millipore Direct-Q system.

4.2.2 Bacterial culture

E. coli O157:H7 Sakai strain was obtained from the Nano-Biosensors Lab collection at Michigan State University. The colonies from frozen (stored at –70 ℃) culture were grown on trypticase soy agar (BD Biosciences, MD) plates. A single colony was isolated and inoculated in tryptic soy broth (BD Biosciences, MD) and grown overnight at 37 ℃. One milliliter of the liquid culture was transferred to another tube of tryptic soy broth and incubated overnight at 37 ℃. One milliliter of this liquid culture was transferred to a new tube of broth and incubated at 37 ℃ for 6 h before each experiment. Tenfold serial dilutions of the bacterial culture, from 10^0 to 10^6 colony forming units per milliliter (cfu/ml), were prepared using 0.1% (w/v) peptone water (Fluka-Biochemika, Switzerland) before each experiment. Viable cells were enumerated by microbial plating on MacConkey agar with sorbitol (SMAC, BD Biosciences, MD).

4.2.3 Apparatus

Electrochemical measurement was performed using a potentiostat/galvanostat (263A, Princeton Applied Research, MA) with the software operating system (PowerSuite, Princeton Applied Research, MA) on a computer connected to the potentiostat. The measurement was performed by introducing each sample onto a screen-printed carbon electrode (SPCE) chip (Gwent Inc. England). The SPCE chip consisted of a working electrode (carbon) and a counter and reference electrode (silver/silver chloride electrode). One hundred microliters of each sample were introduced to the working electrode area on the SPCE chip.

4.2.4 Synthesis of nanoparticles

Polyaniline (PANI) coated magnetic nanoparticles were synthesized according to published methods (Setterington et al., 2011). Briefly, 50 µl of 1 M HCl, 10 ml of water and 0.4 ml of aniline monomer were mixed in a flask, and then 0.65 g of iron (III) oxide nanopowder was added to the solution to maintain a final γ-Fe_2O_3: aniline weight ratio of 1: 0.6. The mixture was put in a beaker filled with ice and sonicated for 1 h. The solution was stirred while it was still on ice. During the stirring, ammonium persulfate (1 g of ammonium persulfate in 20 ml deionized water) was added to the solution slowly for 30 min. The solution was stirred for another 1.5 h. After the reaction, the solution was filtered using 2.5 µm filter paper and washed with 20% methanol. Hydrochloric acid (1 M) was used to wash until the filtrate was clear, followed by washing with 10 ml of 20% methanol. The filtrate was filtered again using a 1.2 µm filter paper. Twenty percent methanol solution was added to the filter. The HCl and methanol wash was repeated. The nanoparticles on the filter paper were left under the fume hood to dry for 24 h at room temperature and then stored in a vacuum desiccator ready to use.

Gold nanoparticles were synthesized under alkaline conditions following the approach published by Anderson et al. (2011). Briefly, 20 ml of dextrin stock solution (25 g/l) and 20 ml of sterile water were mixed in a 50 ml sterile orange cap tube (disposable). Five milliliters of $HAuCl_4$ stock solution (0.4 g/50 ml) were then added, and the pH of the solution was adjusted to 9 with sterile 10% (w/v) Na_2CO_3 solution. The final volume was brought to 50 ml with pH 9 water. The $HAuCl_4$ concentration in the reaction was 2 mM (for $HAuCl_4 \cdot 3H_2O$ = 0.04g/50 ml). The reaction was carried out by incubating the solution in a sterile flask in the dark at 50 ℃ with

continuous shaking (100 rpm) for 6 h. A red solution was obtained at the end of the reaction. The pH of AuNP colloidal was adjusted to 9.2 before use.

Lead sulfide nanoparticles were synthesized by using published procedures (Zhang et al., 2010; Zhu et al., 2009). Mercaptoacetic acid (9.22 µl) was mixed with 50 ml of 0.4 mM $Pb(NO_3)_2$, and the pH of the solution was adjusted to 7 with 1 M NaOH. After bubbling the solution with nitrogen (oxygen free) for 30 min, 40 ml of Na_2S (1.34 mM) were added dropwise to the solution. Then the solution was continuously bubbled with nitrogen for 24 h. The mercaptoacetic acid was used as thiol stabilizer for the aqueous synthesis of thiol-capped PbS nanoparticles. The reaction is presented as Figure 4-1:

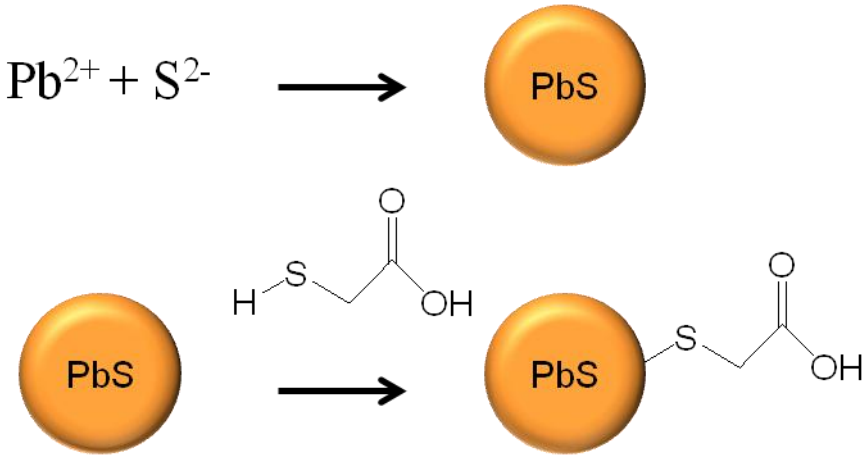

Figure 4-1. Synthesis of PbS nanoparticles with mercaptoacetic acid.

The size of AuNPs and PbS nanoparticles was measured using a zetasizer (Nano ZS, Malvern, UK) at room temperature. One milliliter of nanoparticle colloidal in a 2.5 ml disposable polystyrene cuvette (GmbH & Co. KG) was used for the measurement. The zeta-potential of AuNPs was also measured using the zetasizer (Nano ZS, Malvern, UK). Transmission electron

microscopy (TEM) and UV/Vis (NanoDrop, Thermo Fisher Scientific, DE) were also used to characterize the nanoparticles.

4.2.5 Functionalization of nanoparticles

Magnetic nanoparticles (MNPs) were functionalized with the monoclonal antibody (mAb) to *E. coli* O157:H7 (Setterington et al., 2011). Magnetic nanoparticles (2.5 mg) were suspended in 150 µl of 0.1 M phosphate buffer, and sonicated for 15 min. Monoclonal anti-*E. coli* O157:H7 antibody (2.5 mg/ml, 100 µl) was added to the suspension, and mixed on a tube rotator for 5 min. Twenty five microliters of PBS buffer (0.1 M) were added. Then the conjugation was carried on for 55 min on the tube rotator. The MNPs were separated from the solution by magnetic separation, and blocked by adding 250 µl of 0.1M tris buffer with 0.01% casein with 5 min incubation. This step was repeated three times. The third suspension in tris-casein buffer was put on the tube rotator for 60 min. Finally, the MNPs were magnetically separated and resuspended in 2.5 ml of 0.1M phosphate buffer. The MNP-mAb conjugate was stored at 4 ºC before use.

Gold nanoparticles were conjugated with the polyclonal antibody (pAb) to *E. coli* O157:H7 and PbS-terminated oligonucleotides (pAb-AuNP-PbS). To determine the suitable amount of antibody, 4-20 µg (in 4 µg increments) of antibodies were added to 1 ml AuNP (pH 9.2) and incubated for 30 min. Optimized antibody concentration was determined by monitoring the color change visually. From the shifting of color after adding 100 µl of 2 M NaCl (Hill and Mirkin, 2006; Greg, 2007), it was determined that the optimal amount was 10 µg. Based on this result, 10 µg of antibody were added to 1 ml AuNP and the solution was allowed to incubate for 30 min before conjugating with PbS nanoparticles.

The modification of AuNPs with oligonucleotides followed the procedure published by Hill and Mirkin (2006), and the conjugation of PbS nanoparticles to AuNPs followed the procedure

published by Zhang et al. (2010). Briefly, 25 µl of 200 µM thiolated oligonucleotides were mixed with 25 µl of 0.2 M DTT solution and then purified using a Nap-5 column. The oligonucleotides were added to the pAb-AuNP conjugates, and a serial salt addition was conducted for 3 h. After washing away the excess reagents, EDC and NHS were added to form the linkage between PbS nanoparticles and oligonucleotides on AuNPs. The pAb-AuNP-PbS conjugates were ready to use after washing. The attachment of PbS to AuNPs was confirmed by monitoring the electrochemical response. In this experiment, three tubes were used: tube 1 contained PbS nanoparticles only; tube 2 contained PbS nanoparticles mixed with EDC and NHS; and tube 3 contained PbS nanoparticles mixed with EDC and NHS and AuNPs (AuNPs conjugated with antibody and oligonucleotides). Tube 2 and tube 3 went through the same procedure of preparing pAb-AuNP-PbS (as shown above). Then all three tubes were centrifuged at 13,000 rpm for 15 min. The electrochemical response of lead in solution was measured using the potentiostat.

4.2.6 Detection of target pathogenic bacteria

A schematic of the detection of the target pathogen is presented in Figure 4-2. Blank for the tests was peptone water in the same volume as the sample containing the target pathogen. Firstly, 400 µl of PBS buffer, 50 µl of cell dilution and 50 µl of MNP-mAb conjugates were combined in a 2 ml sterile tube. After 15 min incubation, PBS buffer (55 µl, 0.01 M) with 0.1% BSA was added to the mixture as a blocking agent and incubated for 5 min. Then, the MNP-mAb-*E. coli* complexes were magnetically separated from the solution and resuspended in 450 µl assay buffer. Secondly, the pAb-AuNP-PbS (50 µl) conjugates were introduced to the system, followed by 15 min incubation. After washing the MNP-mAb-*E. coli*-pAb-AuNP-PbS complex once with 0.01 M PBS buffer, the complex was resuspended in 500 µl of PBS buffer with 0.05% Triton-

X100, and allowed to stand for 3 min. After magnetic separation, the complex was suspended in 500 µl of PBS buffer. One hundred microliters of the suspension were plated on SMAC for cell counting. The rest of the suspension was magnetically separated from the supernatant. At the same time, the cell culture (100 µl) was plated on SMAC for cell counting. Therefore, the bacterial growth during the detection time was counted when calculating capture efficiency.

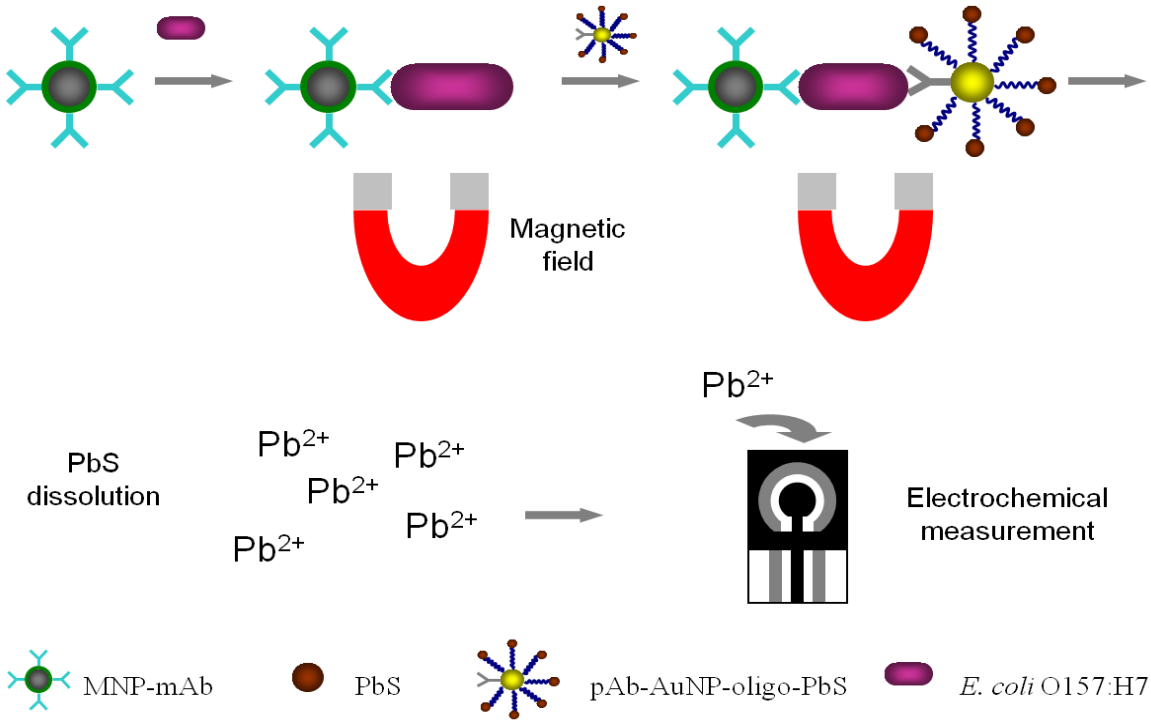

Figure 4-2. Schematic of the PbS-labeled biosensor for the detection of *E. coli* O157: H7. The target cell in a sample was captured by the MNP-mAb and separated by a simple magnet. Then the target cell was labeled with pAb-AuNP-PbS. The MNP-mAb-*E. coli*-pAb-AuNP-PbS complex was transferred onto a screen-printed carbon electrode (SPCE) chip connected to a potentiostat. PbS nanoparticles were dissolved and deposited onto the SPCE chip for electrochemical measurement.

4.2.7 Electrochemical measurement

Twenty microliters of HNO_3 (0.8 M) were added to each sample from section 4.2.6 (complexes magnetically separated from supernatant) and incubated for 10 min. Then, 180 µl of 1 mg/l bismuth in acetate buffer (Zhang et al., 2010) were added. One hundred microliters of the suspension were introduced to the SPCE chip. Ten minute deposition of -1.2 V vs. Ag/AgCl was applied to the working electrode, followed by a square wave voltammetric measurement from -1.2 V to 0.0 V (Zhang et al., 2010; Wang et al., 2000). All measurements were performed at room temperature. Each sample was measured three times. At least three samples for each concentration of bacteria were tested.

4.2.8 Specificity Test

The specificity of the biosensor was tested with non-target bacteria, including *E. coli* O55:H7 (8.5×10^3 cfu/ml), *E. coli* C3000 (6.3×10^1 cfu/ml), *Salmonella enteritidis* (3.1×10^3 cfu/ml) and *Bacillus anthracis*. The same procedure for the detection of *E. coli* O157:H7 (1.2×10^3 cfu/ml) were used in the test, except that one of the non-target bacteria was used in each sample instead of *E. coli* O157:H7. Blank and negative control samples were also tested, and they were not exposed to any bacteria. Assay buffer was added to the negative control samples instead of pAb-AuNP-PbS conjugates. Blank samples were the same as those for the detection of *E. coli* O157:H7. Three replicates for each bacterium were conducted, and the electrochemical signals were measured, following the same method in the previous section.

4.3 Results and discussion

4.3.1 Functionalization of nanoparticles

A TEM image of AuNPs is presented in Figure 4-3a from which an average diameter of 16 nm was observed. PbS nanoparticles were also characterized by TEM, as shown in Figure 4-3b. An average diameter of 7 nm was observed for PbS nanoparticles. PbS nanoparticles with smaller size than AuNPs were synthesized in order to enable the attachment of multiple PbS nanoparticles. PbS nanoparticles were attached to AuNPs through the oligonucleotide linkage (oligo-PbS). As shown in Figure 4-2, the AuNPs were conjugated with both antibodies and PbS-terminated oligonucleotides. The protein A linkage is not suitable for this purpose since the protein will occupy the binding sites for oligonucleotides. The challenge was to attach the antibodies to the AuNPs but provide enough space for the attachment of the oligonucleotides. Therefore, the suitable amount of the antibody was determined. The amount of antibody was evaluated by adding 2 M NaCl to the AuNP-antibody conjugation following the method by Greg (2007). The AuNPs in colloidal are negatively charged, with a zeta-potential of -29.7 mV. When particles approach each other, there is an energy barrier between them to overcome charge repulsion and to aggregate (Greg, 2007). When NaCl was added, it masked the negative charge on uncoated or partially coated particles and breached the barrier (Greg, 2007). A zeta-potential of uncoated AuNPs was obainted as -9.58 mV after adding NaCl, which indicated the decrease in negative charges on particles. The shift of color according to the different amount of antibody is shown in Figure 4-3c. From left to right, the tubes contained antibody in the amount of 0 μg/ml (blank), 4 μg/ml, 8 μg/ml, 12 μg/ml, 16 μg/ml, and 20 μg/ml, respectively. The tube with 8 μg/ml antibody starts to turn red, but shows some aggregates. The tubes with 12~20 μg/ml antibody have red color with no aggregates. These indicate that the optimized amount of antibody to keep

colloidal stability and still provide binding sites for the oligonucleotides is between 8 and 12 µg/ml. Ten micrograms of antibody per milliliter of AuNPs was used for the succeeding experiments.

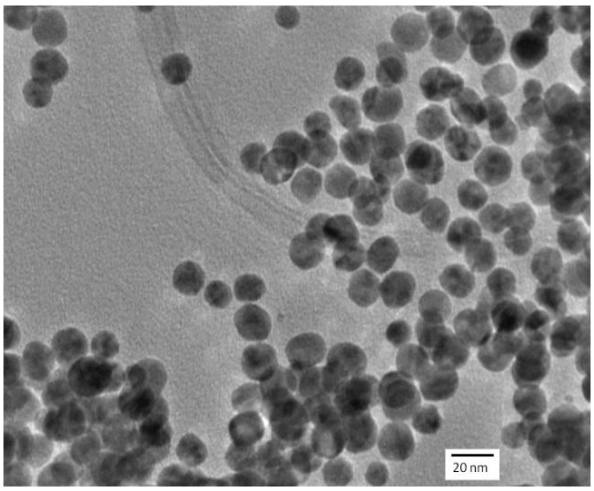

(a)

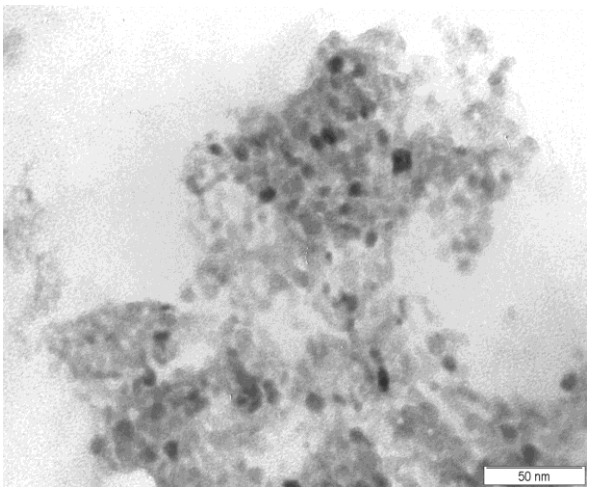

(b)

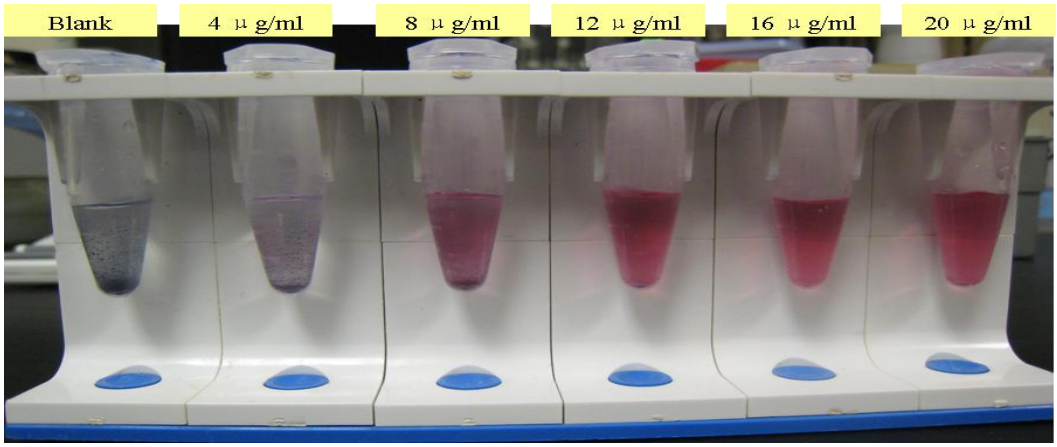

(c)

Figure 4-3. TEM image of (a) AuNPs and (b) PbS nanoparticles. (c) Determination of the amount of polyclonal antibody for the preparation of pAb-AuNP-PbS. Each tube contained AuNP (pH 9.2) and varying amount of polyclonal antibody: 0, 4, 8, 12, 16, and 20 µg/ml (left to right). Third tube from left (8 µg/ml) is red in color but shows some aggregates. Fourth (12 µg/ml) to sixth tubes from left are red in color and show no aggregates.

Thiolated oligonucleotides form self-assembled monolayer on AuNP surface. PbS nanoparticles were attached to AuNPs through the crosslinking of carboxylic group on PbS and the amine group on the 5' end of the oligonucleotides. PbS attachment to AuNPs was verified by measuring the electrochemical response. Figure 4-4 shows the electrochemical signal comparison of three tubes which were processed differently. Tube 1 contained PbS nanoparticles only. Tube 2 contained PbS nanoparticles mixed with only EDC and NHS. Tube 3 contained PbS nanoparticles mixed with EDC, NHS and AuNPs (conjugated with antibody and oligonucleotides). Tube 2 and tube 3 went through the same procedure for preparing pAb-AuNP-PbS (section 4.2.5). Then all three tubes were centrifuged at 13,000 rpm for 15 min and the supernatant was measured for lead electrochemical response. Figure 4-4a shows the color of the three tubes before centrifugation. The three tubes in Figure 4-4b are supernatant after centrifugation, while the precipitate tubes after centrifugation are shown in Figure 4-4c. The color of tube 1 in Figure 4-4b is very similar to the color of tube 1 in Figure 4-4a. Tube 1 in Figure 4-4c shows a bit brown precipitate. This indicates that most of the PbS nanoparticles remained in solution during centrifugation. This is expected as PbS nanoparticles are very small (~7 nm) and hence would remain in solution during centrifugation. The color of tube 2 in Figure 4-4b is slightly lighter than the color of tube 2 in Figure 4-4a. Tube 2 in Figure 4-4c shows a small black precipitate as well. The black precipitate could be a result of the EDC/NHS coating on the PbS nanoparticle surface. Yet, most of the PbS remained in solution. Despite the EDC/NHS coating, the size of the PbS nanoparticles is still small and could not be precipitated during centrifugation. The color of tube 3 in Figure 4-4b is almost clear, vastly different from the color of tube 3 in Figure 4-4a. This could indicate that the PbS nanoparticles have been removed

from the supernatant. Tube 3 in Figure 4-4c shows a lot of red precipitate. The color of the precipitate is that of AuNPs. Figure 4-4d shows the results of the electrochemical measurement of the supernatant in the three tubes (the supernatant in Figure 4-4b). Tube 1 has the highest signal indicating PbS in the solution. Although tube 2 has a slightly lower signal than tube 1, it is still a high signal. Tube 3 has the lowest signal indicating that PbS has been removed from the solution. The removal could only happen if the conjugate pAb-AuNP-PbS formed. This result is consistent with the color observations in Figure 4-4b and precipitate in Figure 4-4c. Blank is 10 µl of HNO_3 (0.8 M) and 90 µl of 1 mg/l bismuth in acetate buffer. At the same time, the signal of PbS in solution indicated that excessive amount of PbS nanoparticles were used during the PbS and AuNP conjugation, which ensured the enough binding of PbS to each AuNP.

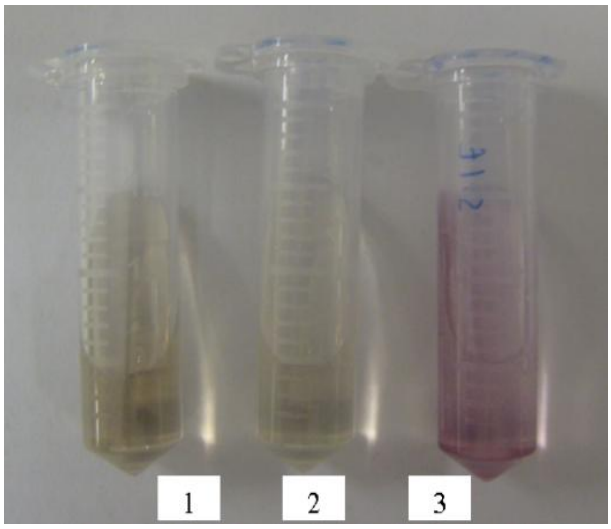

(a)

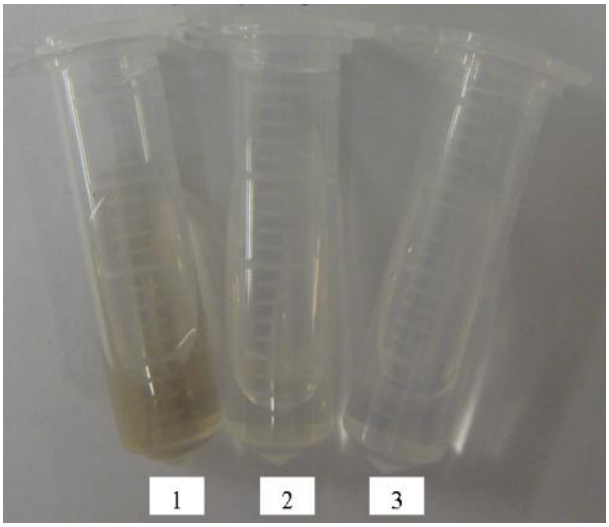

(b)

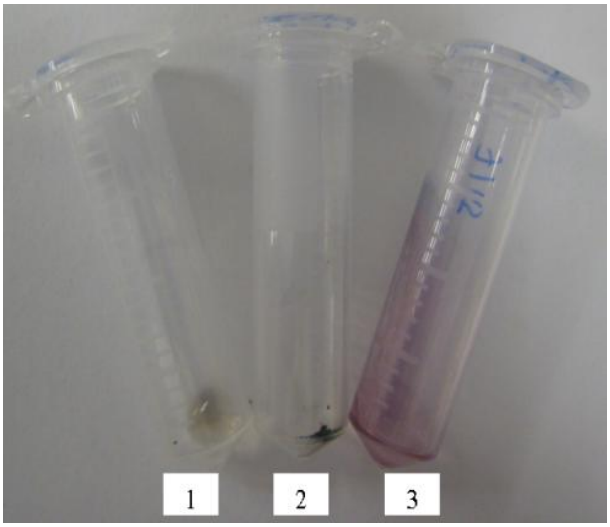

(c)

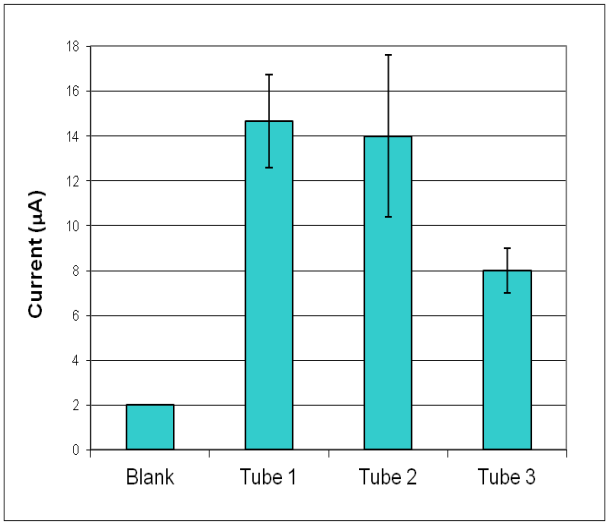

(d)

Figure 4-4. Verification of the formation of pAb-AuNP-PbS conjugates: (a) before centrifugation; (b) tubes with supernatant after centrifugation; (c) tubes with precipitate after centrifugation; (d) current peak of lead in the supernatant after centrifugation. Tube 1: PbS nanoparticles only; Tube 2: PbS nanoparticles mixed with EDC and NHS only; Tube 3: PbS nanoparticles mixed EDC, NHS and pAb-AuNP- oligonucleotides.

4.3.2 PbS-labeled biosensor for detection

The capture efficiency (CF) of using MNP-mAb conjugates were calculated according to the microbial plating, by comparing the enumeration of cells in bacterial culture with cells captured by MNPs as shown in the following Equation 4-1:

$$CF=(\log_{10} C_{cap} / \log_{10} C_{cul}) \times 100\% \quad (4\text{-}1)$$

Where C_{cap} is the number of captured cells obtained from plate counting and C_{cul} is the number of cells in culture from plate counting with the unit of cfu/ml. An average of 94.96% ± 2.26% was obtained, indicating that the target bacteria were captured and separated with high efficiency.

After magnetic separation using MNPs, the target bacteria were labeled with pAb-AuNP-PbS through the binding of the pAb on AuNPs to the antigen surface of the target bacteria. Figure 4-5a is a typical sensorgram of the square wave scan from -1.2 V to 0.0 V for the bacterial detection. Lead signal using bismuth-coated electrode was measured, which was prepared by depositing bismuth and lead onto the electrode at the same time (Zhang et al., 2010; Wang et al., 2000). No signal (current peak) was observed for the blank. For the samples with bacteria, labeling the captured bacteria with pAb-AuNP-PbS resulted in the appearance of a peak at ~ -0.7 V which is for lead. This current peak was used as the detection signal.

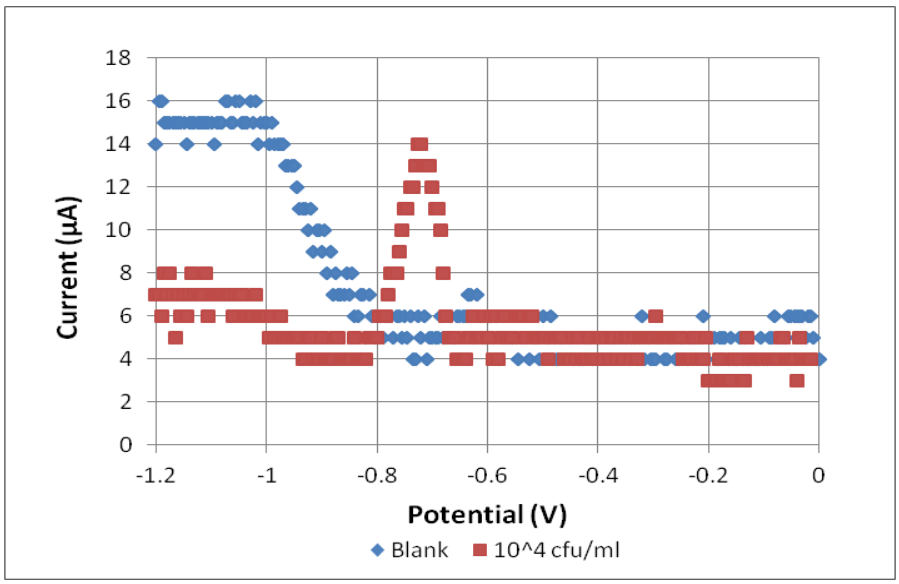

(a)

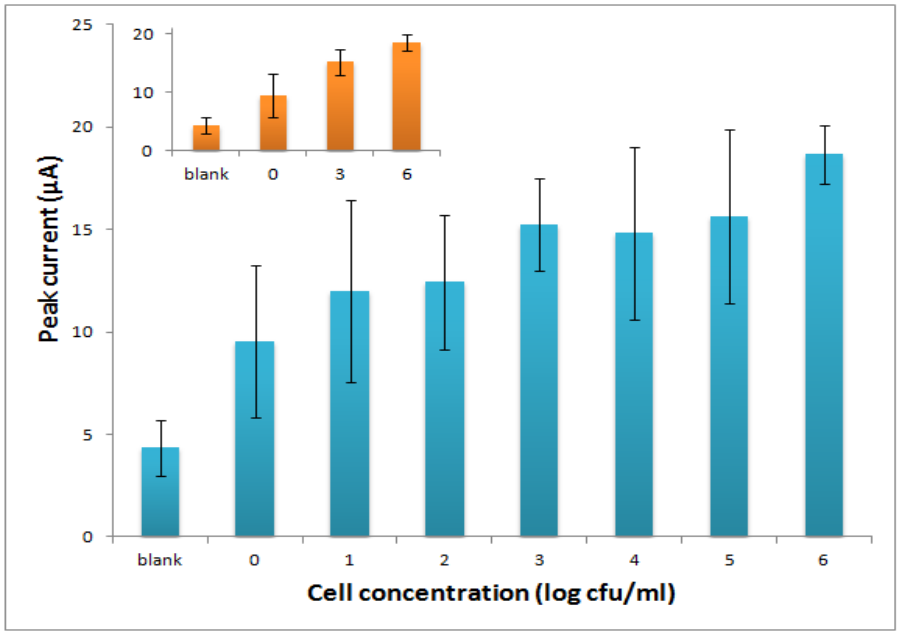

(b)

Figure 4-5. Sensorgram and signal vs. concentration. (a) Typical sensorgram of square wave voltammetry (bacterial concentration is at 10^4 cfu/ml); (b) relationship between current peak and bacterial concentration. (Insert: relationship between peak current and concentration of blank, 10^0, 10^3 and 10^6 cfu/ml. The units of x- and y-axis are the same as Figure 4-5b.)

Figure 4-5b presents the relationship between the peak current for Pb^{2+} at various bacterial concentrations (blank, 10^0~10^6 cfu/ml). The peak current increased with increasing bacterial concentration. The signal to noise ratio (S/N) at each bacterial concentration was calculated by dividing the average peak current of bacterial samples by the average peak current of the blank at the same potential. The lowest concentration (10^0 cfu/ml) detected has the signal to noise ratio of 2.20, and that for the highest concentration (10^6 cfu/ml) is 4.31. A statistical analysis using *t* test was conducted and the results are presented in Table 4-1. As shown, cell concentration at 10^0 cfu/ml is significantly higher than the blank, with a P value of 0.01 (critical value, P=0.05). The P value for the other concentrations shows that the various concentrations are also significantly different from the blank. In another evaluation, comparing the signals of bacterial samples to the average signal of blank samples plus three times the standard deviation (Blank Avg. + 3×S. D. which is considered as the limit of detection), as shown in Table 4-1, we found that 10^0 cfu/ml has small overlap with the Blank Avg. + 3×S. D. Therefore, the lowest detectable cell concentration is 10^1 cfu/ml, which is comparable to other detection methods (Yang et al., 2004; Tan et al., 2011; Wang et al., 2010; Wang and Alocilja, in press). A box plot is presented in Figure 4-6, with a central rectangle which expands from the first quartile to the third quartile and "whiskers" above and below the box which show the locations of the minimum and maximum. Interquartile range (IR) is: 1.00, 4.33, 7.08, 4.33, 2.17, 4.33, 3.00 and 1.00 for blank, 10^0, 10^1, 10^2, 10^3, 10^4, 10^5 and 10^6, respectively. There are no outliers, when data points which are three times of IR (3×IR) above the third quartile or 3×IR below the first quartile are considered as outliers. These results indicate that the tri-nano biosensor design results in a sensitive detection

system. It is noted that we tested samples from different batches of bacteria culture and on different days to determine the detection capability under possible in-field conditions, the variations between each data point were expected. From Figure 4-5b, the differentiation between concentrations different at one log is not obvious in this verification stage. However, it was observed that the signals between blank, 10^0, 10^3 and 10^6 can be differentiated as shown in Figure 4-5b insert. Compared to the AuNP-labeled biosensor, larger variations between each data point may due to the involvement of PbS nanoparticles. The attachment of AuNP to target may be affected by adding PbS nanoparticles. However, PbS nanotracer-labled biosensor can detect a lower concentration of the target.

Table 4-1. Statistical analysis comparing bacterial samples and blank for PbS-labeled biosensor.

Concentration (cfu/ml)	*0*	10^0	10^1	10^2	10^3	10^4	10^5	10^6
Average Current Peak (μA)	4.3	9.5	12.0	12.4	15.2	14.8	15.7	18.7
Standard Deviation (μA)	1.36	3.72	4.42	3.29	2.27	4.21	4.24	1.41
S/N	N/A	2.20	2.77	2.87	3.51	3.42	3.62	4.31
Blank Avg. + 3×S. D.	8.42							
P value[a]	N/A	0.01	0.003	2×10^{-4}	2×10^{-7}	5×10^{-4}	7×10^{-6}	5×10^{-8}

[a] P value was calculated by a one-tailed paired *t* test. The critical value, P=0.05.

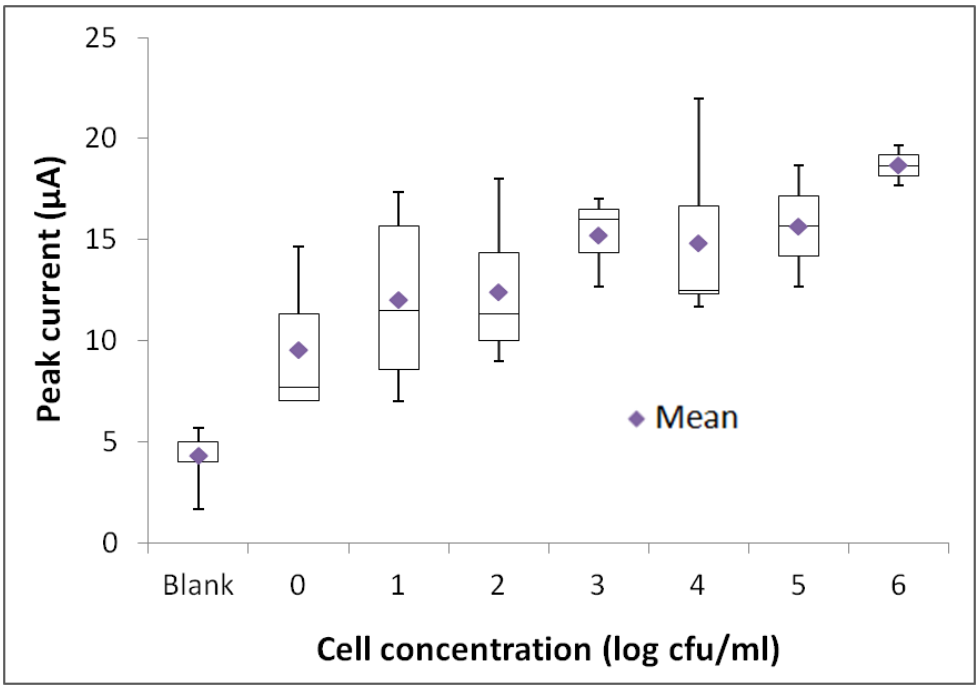

Figure 4-6. Box plot of the *E. coli* O157:H7 detection using the PbS nanotracer-based biosensor.

4.3.3 Specificity test

The specificity of the biosensor is shown in Figure 4-6. Samples detected on the same day were presented in this figure. It is noticed that the signals for negative control samples (no pAb-AuNP-PbS added) and blank samples were 6.0 ±1 and 5.7 ±1.2 μA, respectively. Because the only difference between these two sets of samples was that whether the pAb-AuNP-PbS conjugates were added to the system, the very close signals indicate that the non-specific binding of pAb-AuNP-PbS to the MNPs was minimized in the system. The signals for the non-target bacteria *E. coli* O55:H7, *E. coli* C3000, *S. enteritidis* and *B. anthracis* were significantly smaller than the signal of *E. coli* O157:H7 (critical value, P=0.05), indicating that they didn't interfere with the detection of *E. coli* O157:H7 and the biosensor is specific to the target.

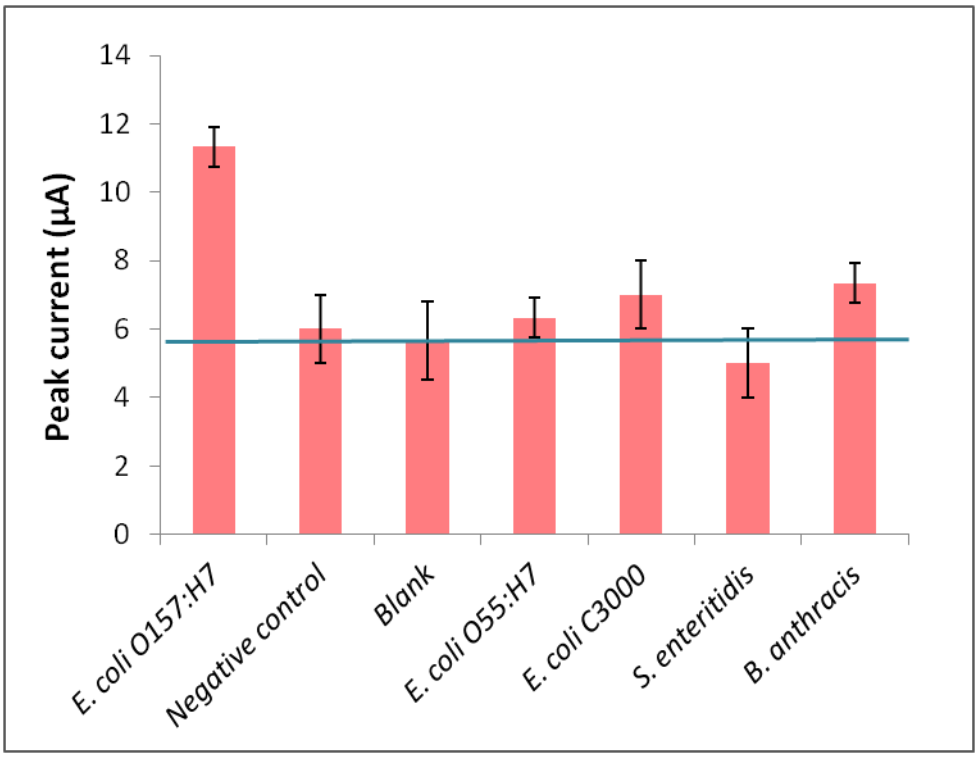

Figure 4-7. Specificity test results of the biosensor with four non-target bacteria: *E. coli* O55:H7, *E. coli* C3000, *S. enteritidis* and *B. anthracis*. Positive control (*E. coli* O157:H7), negative control (no pAb-AuNP-PbS added to the sample), and blank (no bacteria) are also presented.

4.4 Conclusion

A biosensor based on three nanoparticle assembly was developed for the sensitive and rapid detection of *E. coli* O157: H7. Monoclonal antibody (mAb) was used to functionalize MNPs which were used to magnetically separate target bacterial cells from the sample. PbS nanoparticles and polyclonal antibody (pAb) were conjugated to AuNPs. By attaching multiple PbS nanoparticles to each AuNP through the oligonucleotide linkage, there were multiple reporters for each AuNP bound to the target. Lead signal was obtained at ~-0.7 V on the square wave voltammetric sensorgram. The biosensor can detect *E. coli* O157:H7 in the range of 10^1 to

10^6 cfu/ml within 1 h with minimal sample preparation. The lowest concentration (10^1 cfu/ml) detected had a signal to noise ratio of 2.77, and that for the highest concentration (10^6 cfu/ml) is 4.31. The signals of the samples were significantly higher than the signals of the blank ($p<0.05$). The high signal to noise ratio indicates the robustness of the system. Overall, these results show that the tri-nano biosensor is highly sensitive and robust, paving the way for practical relevance in field-based detection of threat agents. This biosensor therefore is potentially useful in public health, biodefense, and food/water safety applications.

Chapter 5 : Nanotracer-labeled biosensor for single cytokine detection

5.1 Introduction

Interferon-gamma (IFN-γ) is an important cytokine responsible for cell mediated immunity. It is a 15.5 kDa protein with primarily α-helical structure (Ealick et al., 1991; Dijksma et al., 2001). It is secreted by various cells, such as CD4+ T helper cell type 1 (Th1) lymphocytes, CD8+ cytotoxic lymphocytes, NK cells, B cells and professional antigen-presenting cells (Frucht et al., 2001; Janeway et al., 2001; Bach et al., 1997). Its main functions include immune responses driven by Th1, induced regulatory T (Treg) cell activity to control natural immune system responses and cellular proliferation and apoptosis (Schroder et al., 2004; Brunet, 2012). CXC motif chemokine 10 (CXCL10) is also known as interferon gamma-induced protein 10 (IP-10). It belongs to CXC chemokine subfamily. It is a protein secreted by cells such as monocytes and endothelial cells in response to IFN-γ (Luster et al., 1985). It plays a critical role in inflammation and chemotaxis (Romagnani and Crescioli, 2012). Kellar et al. suggested IP-10 as one of promising indicators for tuberculosis (TB) diagnosis (Kellar et al., 2011).

Enzyme-linked immunosorbent assay (ELISA) and enzyme-linked immunospot (ELISPOT) are commonly used methods for IFN-γ detection (Berg, 1994; Czerkinsky et al., 1988; Bouyon et al., 2003; Pai et al., 2004). A commercialized assay, QuantiFERON-TB assay (Cellestic Limited, Carnegie, Victoria, Australia) has been developed based on ELISA, and T-SPOT.TB assay (Oxford Immunotec, Oxford, UK) is a commercialized interferon-gamma release assay (IGRA) based on ELISPOT. Cytokine flow cytometry (CFC, Karlsson et al., 2003; Maecker et al., 2005), immunofluorescence (Schreiber, 2001) and arrayed imaging reflectometry (Carter et al., 2011) were also reported for the detection of IFN-γ. Enzyme-linked immunosorbent assay (ELISA) is

also the commonly used method for IP-10 detection (Takahata et al., 2003; Caproni et al., 2004). Immunohistochemical staining (Takahata et al., 2003), Northern Blot (Gottlieb et al., 1988), immunofluorescence (Chang et al., 2011; Yurkovetsky et al., 2007; Aliberti et al., 2001), and chemiluminescence based assays (Matsunaga et al., 2009; Sack et al. 2005) were reported for IP-10 detection as well. In these methods, IP-10 in the concentration of pg/ml level was detected. However, these methods require several hours to get results (e.g. ELISA) or complicated manipulation (e.g. RT-PCR).

Several studies reported the detection of IFN-γ using biosensors. Dijksma et al. developed an electrochemical immunosensor which could detect 0.02 fg/ml (1 aM) with a dynamic range of 0-12 pg/ml (Dijksma et al., 2001). Bart et al. described an immunosensor prepared by immobilizing anti-IFN-γ antibodies on a self-assembled monolayer (SAM) of acetylcysteine, deposited on polycrystalline gold (Bart et al., 2005). Several aptamer-based biosensors were also reported (Liu et al., 2010; Min et al., 2008; Tuleuova and Revzin, 2010). In addition, a dextran-coated surface plasmon resonance (SPR) biosensor was tested for detection of IFN-γ, which could detect 250 ng/ml IFN-γ in plasma (Stigter et al., 2005). There are not many reports on biosensors for IP-10 detection. Bonham et al., (2013) recently reported an electrochemical biosensor which could detect ~60 pM of IP-10. Biosensors enable the important roles of the cytokines in immune response to be potentially employed in rapid disease diagnosis.

In this chapter, a sensitive electrochemical immunosensor was developed for the detection of cytokines as the basis of future disease diagnosis. IFN-γ and IP-10 was detected separately. Magnetic nanoparticles, gold nanoparticles and nanotracers which are nanoparticles of heavy metals (e.g. PbS and CdS nanoparticles) were involved in this immunosensor. Magnetic nanoparticles (MNP) conjugated with anti-IFN-γ capture antibody were employed to separate the

target from a sample. Gold nanoparticles (AuNPs) which were functionalized with anti-IFN-γ detection antibody and conjugated with cadmium sulfide (CdS) nanoparticle-terminated oligonucleotides (oligo) were used to label the captured IFN-γ. The electrochemical signal of cadmium was obtained as the signal of the biosensor. The binding of one AuNP to the target through the antibody-antigen reaction resulted in the labeling of the target with multiple CdS nanoparticles. This design of the biosensor was also applied for the detection of IP-10 by using PbS nanoparticles instead of CdS nanoparticles and anti-IP-10 antibodies instead of anti- IFN-γ antibodies. The biosensor required no sample preparation, and the detection took only 1 h.

5.2 Materials and methods

5.2.1 Reagents and materials

Aniline, iron (III) oxide nanopowder, ammonium persulfate, methanol, and diethyl ether were used for the synthesis of the MNPs. Gold (III) chloride trihydrate (Aldrich, MO) and dextrin (Fluka, MO) were used for the synthesis of gold nanoparticles under alkaline conditions (Anderson et al., 2011). Sodium sulfide, 3-mercaptoacetic acid, and cadmium chloride were used for the synthesis of CdS nanoparticles. Instead of cadmium chloride, lead nitrate was used for the synthesis of PbS nanoparticles

MNPs were functionalized with a purified mouse anti-human IFN-γ (capture antibody, cAb) obtained from BD Pharmingen™ (#551221, San Diego, CA). AuNPs were conjugated with a purified mouse anti-human IFN-γ (detection antibody, dAb) obtained from BD Pharmingen™ (#554549, San Diego, CA). For IP-10 detection, MNPs were functionalized with a purified mouse anti-human IP-10 antibody (capture antibody, cAb) obtained from BD Pharmingen™ (#555046, San Diego, CA). AuNPs were conjugated with a Mouse Anti-Human IP-10 antibody

(detection antibody, dAb) obtained from BD Pharmingen^{TM} (#624084, San Diego, CA). An oligonucleotide (sequence 5'-AAA AAA AAA AAA AAA AAA AA-3') with 3' thiol modifier and 5' amino modifier was employed as a linker between AuNPs and CdS/PbS nanoparticles, which was purchased from Integrated DNA Technologies Inc. (Coralville, IA). 1,4-Dithio-dl-threitol (DTT) was used for the cleavage of oxidized thiolated oligonucleotides. Nap-5 column (GE Healthcare, Piscataway, NJ) was used for the purification of oligonucleotides from DTT solution. 1-Ethyl-3-[3-dimethylaminopropyl] carbodiimide hydrochloride (EDC) and N-hydroxysuccinimide (NHS) were used for the linkage of carboxylic groups on CdS/PbS nanoparticles and amine groups on oligonucleotides. These reagents were purchased from Sigma (St. Louis, MO). Bismuth standard stock solution (10,000 ppm) was purchased from Ricca Chemical Company (Arlington, TX). Acetate buffer solution (0.1 M, pH 4.5) with 1 mg/l bismuth was used for electrochemical measurement.

Phosphate buffered saline (PBS), casein, bovine serum albumin (BSA) and sodium phosphate (dibasic and monobasic) and all other reagents (unless otherwise noted) were obtained from Sigma-Aldrich (St. Louis, MO). PBS buffer (0.01 M, pH 7.4), phosphate buffer (0.1 M sodium phosphate, pH 7.4), 0.1 M tris buffer with 0.01% casein, PBS buffer with 0.1% (w/v) BSA, assay buffer (0.562 g Na_2HPO_4, 0.125g NaH_2PO_4, 4.383g NaCl and 0.5g BSA in 500 ml water; Hill and Mirkin, 2006) were prepared with deionized water from Millipore Direct-Q system. PBS buffer and phosphate buffer were used in preparing nanoparticle-antibody conjugates and in washing. Buffers with casein or BSA were used to block nanoparticle surface against nonspecific binding. Assay buffer was used for keeping pH during reactions and washing off unbound or nonspecifically bound reactants.

5.2.2 Cytokine dilutions

Lyophilized Human IFN-γ Standard was obtained from Cellestis (Valencia, CA). The serial dilutions of IFN-γ were prepared using sterile deionized water before experiments. Lyophilized recombinant human IP-10 was obtained from BD Pharmingen^{TM} (#551130, San Diego, CA). The serial dilutions of IP-10 were prepared using sterile deionized water before experiments.

5.2.3 Apparatus

Electrochemical measurement was performed with a potentiostat/galvanostat (263A, Princeton Applied Research, MA) with a software operating system (PowerSuite, Princeton Applied Research, MA) on a computer connected to the potentiostat. The measurement was performed by introducing each sample onto a screen-printed carbon electrode (SPCE) chip (Gwent Inc. England). The SPCE chip consisted of a working electrode (carbon) and a counter and reference electrode (silver/silver chloride electrode). One hundred microliters of each sample were introduced to the electrode area on the SPCE chip.

5.2.4 Synthesis of nanoparticles

Polyaniline (PANI) coated magnetic nanoparticles were synthesized according to published methods (Setterington et al., 2011). Briefly, 50 µl of 1 M HCl, 10 ml of water and 0.4 ml of aniline monomer were mixed in a flask, and then 0.65 g of iron (III) oxide nanopowder was added to the solution to maintain a final γ-Fe_2O_3: aniline weight ratio of 1: 0.6. The mixture was put in a beaker filled with ice and sonicated for 1 h. The solution was stirred while it was still on ice. During the stirring, ammonium persulfate (1 g of ammonium persulfate in 20 ml deionized water) was added to the solution slowly for 30 min. The solution was stirred for another 1.5 h. After the reaction, the solution was filtered using 2.5 µm filter paper and washed with 20%

methanol. Hydrochloric acid (1 M) was used to wash until the filtrate was clear, followed by washing with 10 ml of 20% methanol. The filtrate was filtered again using a 1.2 μm filter paper. Twenty percent methanol solution was added to the filter. The HCl and methanol wash was repeated. The nanoparticles on the filter paper were left under the fume hood to dry for 24 h at room temperature and then stored in a vacuum desiccator ready to use.

Gold nanoparticles were synthesized under alkaline conditions following the approach published by Anderson et al (2011). Briefly, 20 ml of dextrin stock solution (25 g/l) and 20 ml of sterile water were mixed in a 50 ml sterile orange cap tube (disposable). Five milliliters of $HAuCl_4$ stock solution (0.4 g/50 ml) were then added, and the pH of the solution was adjusted to 9 with sterile 10% (w/v) Na_2CO_3 solution. The final volume was brought to 50 ml with pH9 water. The $HAuCl_4$ concentration in the reaction was 2 mM (for $HAuCl_4 \cdot 3H_2O$ = 0.04g/50 ml). The reaction was carried out by incubating the solution in a sterile flask in the dark at 50 ℃ with continuous shaking (100 rpm) for 6 h. A red solution was obtained at the end of the reaction. The pH of AuNP colloidal was adjusted to 9.2 before use.

Cadmium sulfide (CdS) nanoparticles were synthesized by using published procedures (Zhang et al., 2010; Ding et al., 2009; Jie et al., 2007). Mercaptoacetic acid (2 μl) was mixed with 100 ml of 1 mM $CdCl_2$, and the pH of the solution was adjusted to 11 with 1 M NaOH. After bubbling the solution with nitrogen (oxygen free) for 30 min, 50 ml of Na_2S (1.34 mM) were added dropwise to the solution. Then the solution was continuously bubbled with nitrogen for 24 h. Lead sulfide nanoparticles were synthesized by using published procedures (Zhang et al., 2010; Zhu et al., 2004). Mercaptoacetic acid (9.22 μl) was mixed with 50 ml of 0.4 mM $Pb(NO_3)_2$, and the pH of the solution was adjusted to 7 with 1 M NaOH. After bubbling the

solution with nitrogen (oxygen free) for 30 min, 40 ml of Na_2S (1.34 mM) were added dropwise to the solution. Then the solution was continuously bubbled with nitrogen for 24 h. Transmission electron microscopy (TEM) and UV/Vis (NanoDrop, Thermo Fisher Scientific, DE) were used to characterize the nanoparticles.

5.2.5 Functionalization of nanoparticles

Magnetic nanoparticles were functionalized with the capture antibody (cAb) to IFN-γ. MNPs (2.5 mg) were suspended in 150 µl of 0.1 M phosphate buffer, and sonicated for 15 min. The capture antibody (1.0 mg/ml, 100 µl) was added to the suspension, and mixed on tube rotator for 5 min. Twenty five microliters of PBS buffer (0.1 M) were added. Then the conjugation was carried on for 55 min on the tube rotator. The MNPs were separated from the solution by magnetic separation, and blocked by adding 250 µl of 0.1M tris buffer with 0.01% casein with 5 min incubation. This step was repeated three times. The third suspension in tris-casein buffer was put on the tube rotator for 60 min. Finally, the MNPs were magnetically separated and resuspended in 2.5 ml of 0.1M phosphate buffer. The MNP-cAb conjugate was stored at 4 °C before use. For IP-10 detection, MNPs were functionalized with the capture antibody to IP-10. The capture antibody (1.0 mg/ml, 100 µl) was added to the MNP suspension in 150 µl of 0.1 M phosphate buffer. The rest steps were the same as preparing the MNPs with capture antibody to IFN-γ.

Gold nanoparticles were conjugated with the detection antibody (dAb) to IFN-γ/IP-10 and CdS/PbS-terminated oligonucleotides (oligos). To determine suitable amount of anti-IFN-γ detection antibody, 2 µg to 10 µg of the antibody were added to 1 ml AuNP colloidal (pH 9.2) and mixed for 30 min on a tube rotator. For anti-IP-10 antibody, 8 µg to 28 µg of anti-IP-10 detection antibody were added to 1 ml AuNPs. From the shifting of color after adding 100 µl of

2 M NaCl (Hill and Mirkin, 2006; Greg, 2007), it is determined that the optimal amount was 10 μg for the anti-IFN-γ antibody and 20 μg for the anti-IP-10 antibody. Antibodies in the optimal amount were added to 1 ml AuNPs to prepare AuNP-dAb conjugates, and AuNP-anti-IFN-γ and AuNP-anti-IP-10 were obtained. The modification of AuNPs with oligonucleotides followed the procedure published by Hill and Mirkin (2006), and the conjugation of NTs (CdS or PbS nanoparticles) to AuNPs followed the procedure published by Zhang et al (2010). Briefly, 25 μl of 200 μM thiolated oligonucleotides were mixed with 25 μl of 0.2 M DTT solution and then purified using a Nap-5 column. The oligonucleotides were added to the AuNP-dAb conjugates, and a serial salt addition was conducted for 3 h. After washing away the excess reagents, EDC and NHS were added to form the linkage between CdS/PbS and oligonucleotides on AuNPs. The dAb-AuNP-oligo-NT (PbS/CdS) conjugates were ready to use after washing.

5.2.6 Detection of the targets

The detection of the targets is presented in Figure 5-1, using IFN-γ as an example. When detecting IP-10, dAb-AuNP-oligo-PbS was used instead of dAb-AuNP-oligo-CdS. Blanks (negative controls) for the tests were water in the same volume as the sample containing the targets. Firstly, 100 μl PBS buffer, 100 μl IFN-γ or IP-10 dilution and 25 μl of MNP-cAb (anti-IFN-γ or anti-IP-10 cAb) conjugates were combined in a 2 ml sterile tube. After 20 min mixing on tube rotator, 50 μl of 0.01 M PBS buffer with 0.1% BSA were added to the mixture as a blocking agent with another 5 min reaction. Then, the MNP-target complexes were magnetically separated from the solution and resuspended in 200 μl of assay buffer. Secondly, 25 μl of AuNP-dAb-NT (CdS/PbS) conjugates were introduced to the system, and put on tube rotator for 20 min. After magnetically separation, the complexes were washed once with assay buffer.

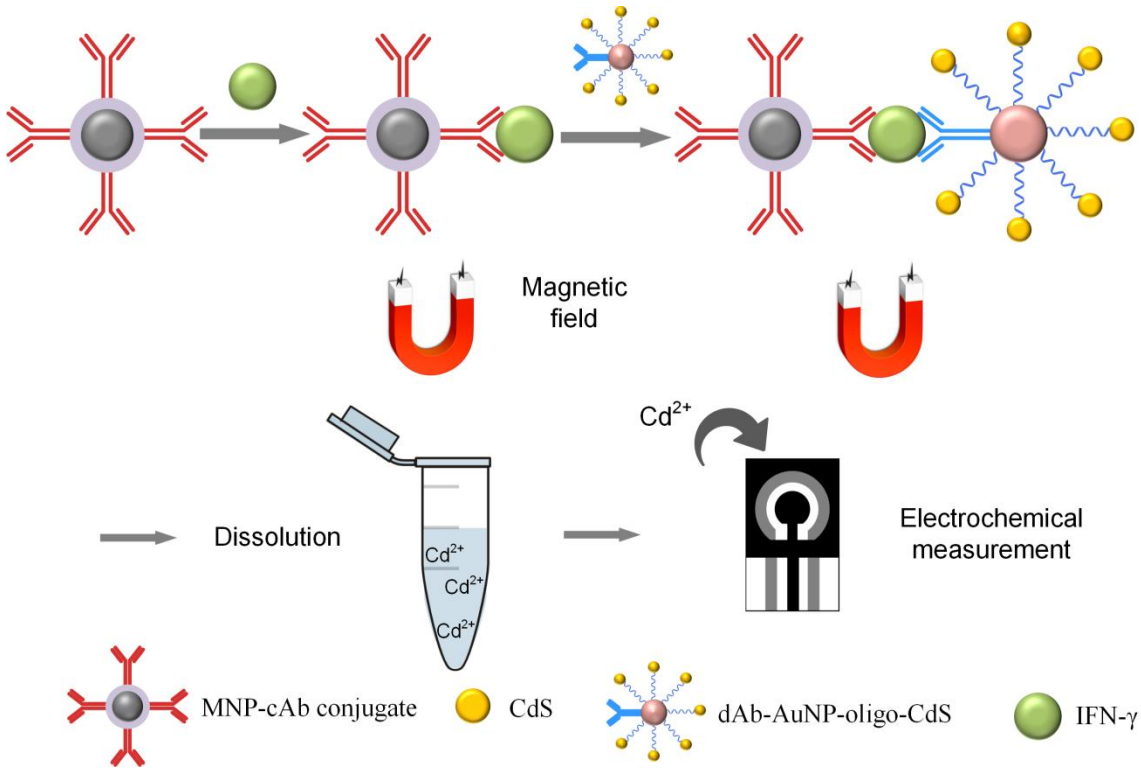

Figure 5-1. Schematic of the NT-labeled biosensor for IFN-γ detection. The target in a sample was captured by MNP-cAbs and separated by a magnet. Then the target was labeled with dAb-AuNP-CdS. The MNP-cAb-target-dAb-AuNP-CdS complexes were transferred onto a SPCE chip connected to a potentiostat. The CdS nanoparticles were dissolved and deposited onto the electrodes on the SPCE chip for electrochemical measurement.

5.2.7 Electrochemical measurement

Ten microliters of HNO_3 (0.8 M) were added to each sample from section 5.2.6 (complexes magnetically separated from supernatant) and incubated for 10 min. Then, 90 µl of 1 mg/l bismuth in acetate buffer were added, and the 100 µl of suspension were introduced to the SPCE chip. Ten minute deposition of -1.2 V vs. Ag/AgCl was applied to the working electrode, followed by a square wave voltammetric measurement from -1.2 V to 0.0 V (Zhang et al., 2010;

Wang et al., 2000). All measurements were performed at room temperature. Each sample was measured three times. At least three samples for each concentration of IFN-γ/IP-10 were tested.

5.3 Results and discussion

5.3.1 Characterization of nanoparticles

A TEM image of CdS nanoparticles is shown in Figure 5-2. The TEM images of AuNPs and PbS nanoparticles have been presented in Chapter 4. The gold nanoparticles are in spherical shape with an average diameter of 16 nm, measured from the TEM image. The PbS nanoparticles have an average diameter of 7 nm. The CdS nanoparticles appear close to spherical shape with an average diameter of 5 nm.

The nanoparticles were also observed with UV/Vis spectra. Figure 5-3a shows an absorbance of AuNPs (colloidal obtained after synthesis) at 520 nm (the red curve on the top). It is noted the spectrum of dextrin (the black curve on the bottom) is also shown in Figure 5-3a with an absorbance peak at 290 nm. The UV/Vis absorption spectrum of CdS nanoparticles is presented in Figure 5-3b. The absorption appears in a band range of 220 nm to 500 nm, and the spectrum exhibits a well defined absorption peak at 228 nm. The absorption peaks of CdS are blue-shifted compared to the absorption peak of bulk CdS at 512 nm (Bai et al., 2009). The UV/vis spectrum of dAb-AuNP-oligo-CdS conjugates was also carried out at room temperature, which is presented in Figure 5-3c. The spectrum in black curve with a higher peak at 228 nm is the absorption spectrum of CdS nanoparticles only, and the spectrum in red curve below is the absorption spectrum of the conjugates. It is observed that there are two peaks in the spectrum of the dAb-AuNP-oligo-CdS conjugates, one at 228 nm and the other at 260 nm. The peak at 228 nm is consistent with CdS nanoparticle absorption peak, and the one at 260 nm is the peak for oligonucleotides (Gerstein, 2001). The presence of the two peaks verified that CdS and

oligonucleotides were attached to AuNP. It is noticed that the absorption peak of AuNP no longer exists in Figure 5-3c. The absence of AuNP peak was resulted from the increase of the size of the gold nanoparticles due to the conjugation, which caused the change in the absorption. The UV/vis spectrum of PbS nanoparticles and dAb-AuNP-oligo-PbS conjugates are shown in Figure 5-3d and 5-3e, respectively. Lead sulfide nanoparticles have an absorption peak at 226 nm while it shows the absorption in a band range of 225 to 550 nm, which also shows the blue shifting of the absorption edge due to the decreasing particle size (Xu et al., 2003). The same peak at 226 nm was also found for dAb-AuNP-oligo-PbS conjugates, which verifies the existence of PbS in the conjugates. The same peak at 260 nm is also presented, which indicates the attachment of oligonucleotides.

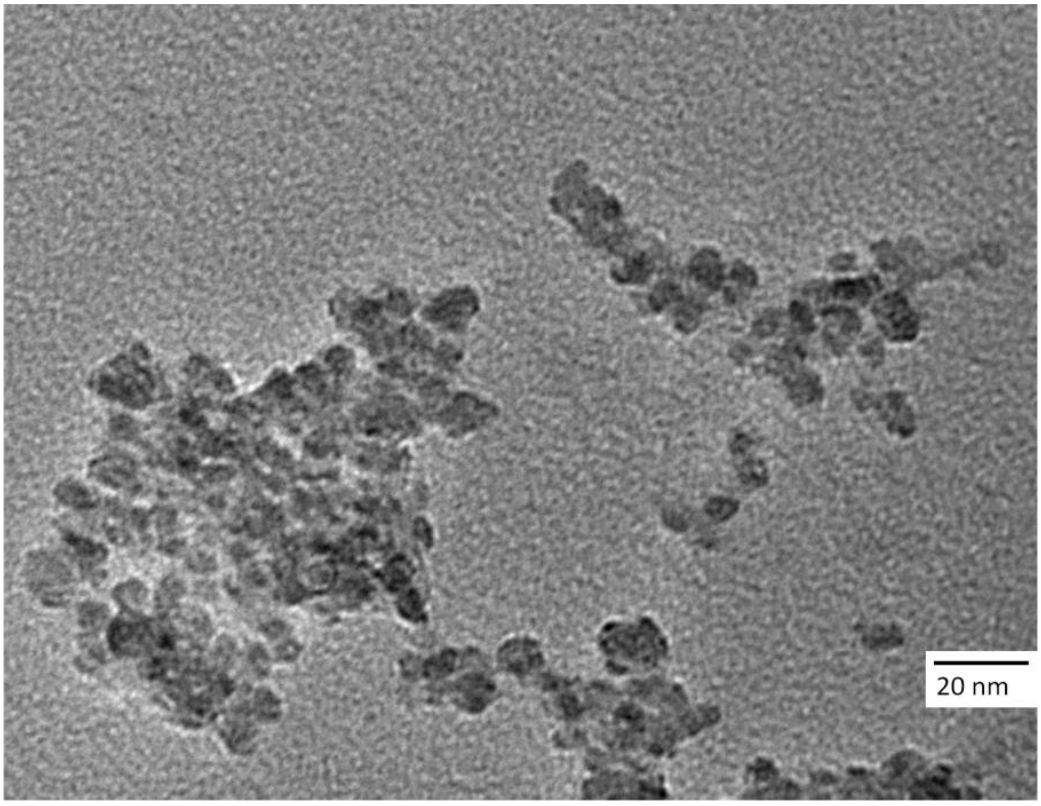

Figure 5-2. TEM images of CdS nanoparticles. The CdS nanoparticles appear close to spherical shape with an average diameter of about 5 nm.

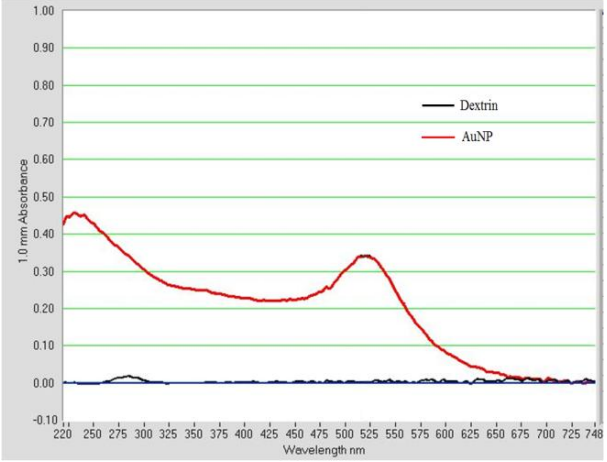

(a)

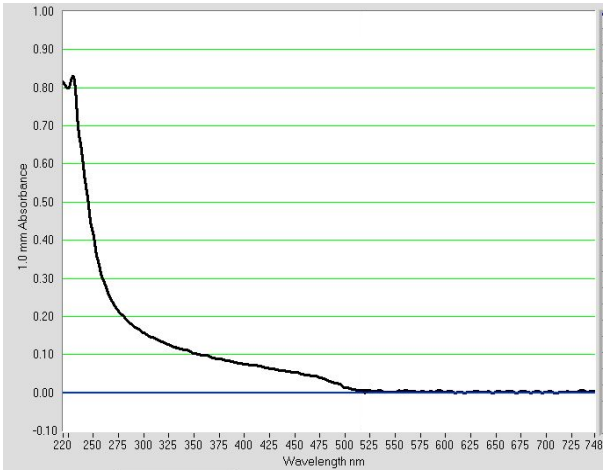

(b)

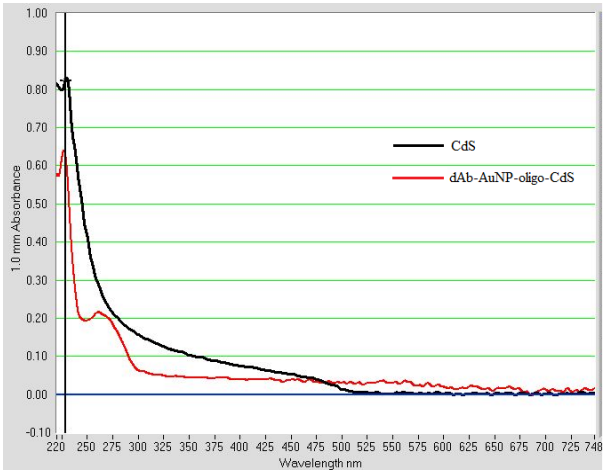

(c)

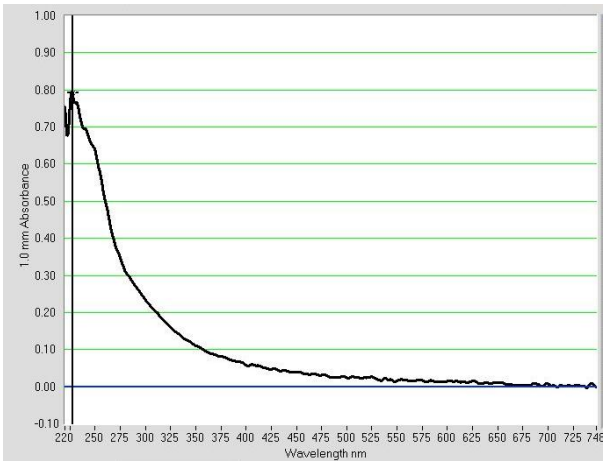

(d)

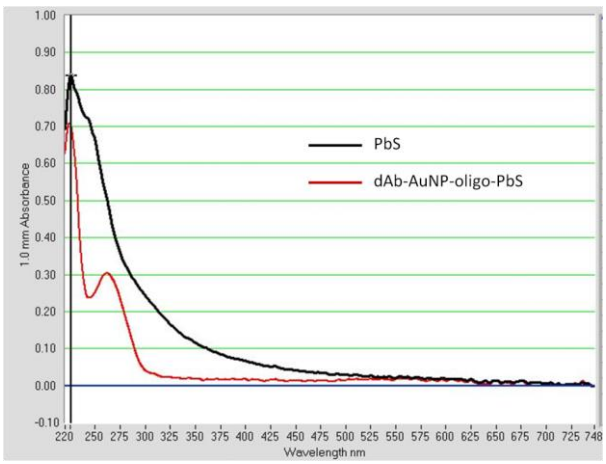

(e)

Figure 5-3. UV/Vis spectra of: (a) AuNPs and dextrin, (b) CdS nanoparticles, (c) dAb-AuNP-oligo-CdS conjugates, (d) PbS nanoparticles and (e) dAb-AuNP-oligo-PbS conjugates.

The attachment of dAb to AuNPs were verified by adding NaCl to the AuNP-dAb conjugates and observing the color change (Hill and Mirkin, 2006; Greg, 2007). The uncoated AuNPs form clusters after adding the salt, and the color of the colloidal changes to blue because of the increase of the particle size. However, those coated with antibody stay in red color. For anti-IFN-γ dAb conjugation, three tubes of AuNPs with different concentration of dAb after 30 min conjugation (Figure 5-4a) were observed after adding NaCl. The tubes contained antibody in the amount of 0 μg/ml (blank), 2 μg/ml, and 10 μg/ml, respectively. The blank tube showed blue with aggregate. The tube with 2 μg/ml antibody was blue, but showed less aggregate than the blank. The tubes with 10 μg/ml antibody had purple color with some aggregate. It is indicated that dAb was attached to AuNPs which helped to stabilized the colloidal after adding the salt. Therefore, the AuNPs coated with dAb didn't aggregate and remined in red color. According to the color change and aggregation, it was determined that 10 μg/ml is a suitable concentration of antibody, which ensures that the AuNPs were functionalized with antibody and there were still space on the AuNP surface for oligonucleotides to bind. The same experiment was conducted to determine the suitable amount of anti-IP-10 dAb, and the tubes after adding NaCl are shown in Figure 5-4b. Tubes from the left to the right are 0 μg/ml (blank), 8 μg/ml, 12 μg/ml, 16 μg/ml, 24 μg/ml and 28 μg/ml. The tube with 28 μg/ml antibody has much less aggregates than the other tubes. There is no obvious difference between 16 and 24 μg/ml. Both show red color with some aggregates. Therefore, the suitable amount of antibody is within the range of 16 to 24 μg/ml. Based on the observation, 20 μg/ml was determined as a suitable amount of the antibody.

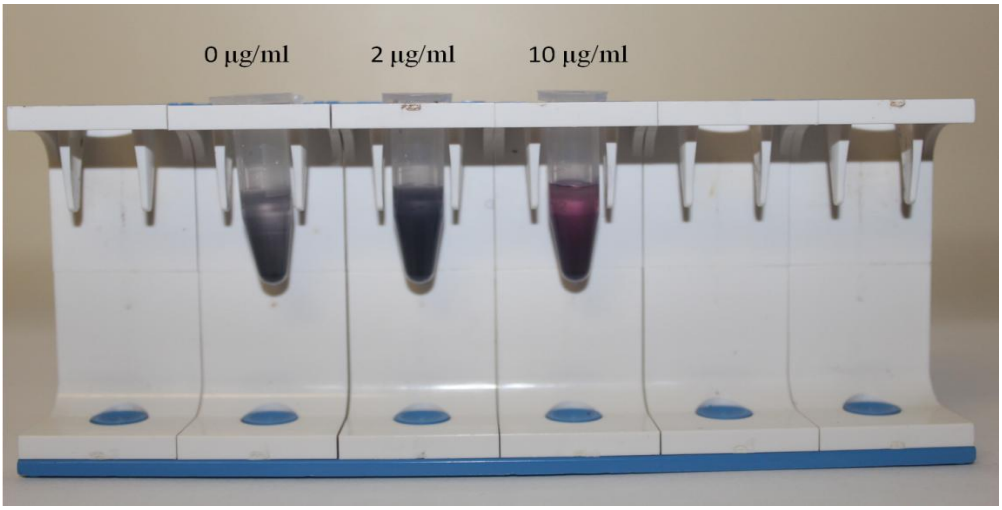

(a)

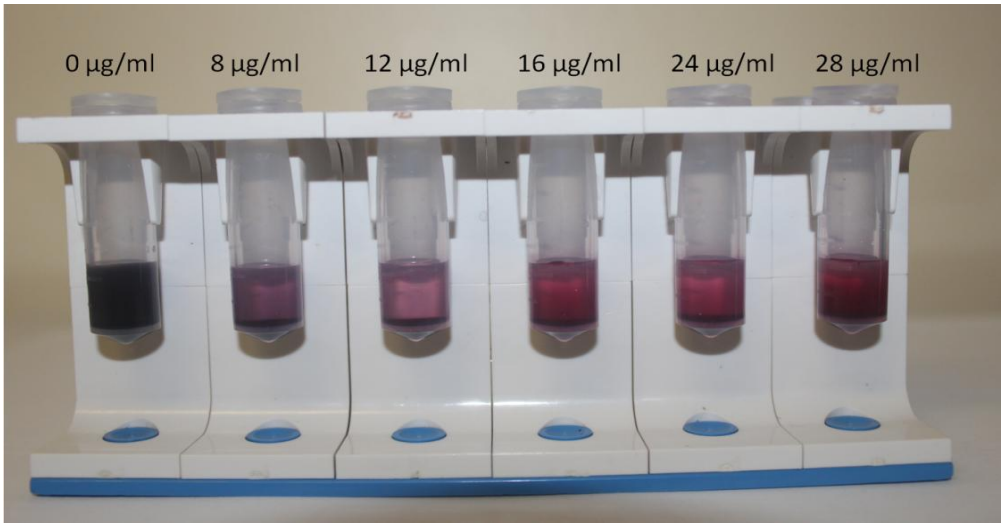

(b)

Figure 5-4. Determination of the amount of detection antibody for the preparation of dAb-AuNP-NT. (a) Anti-IFN-γ antibody: each tube contained AuNP (pH 9.2) and varying amount of antibody: 0, 2 and 10 µg/ml (left to right). The two left tubes are blue with aggregate. The third tube from left (10 µg/ml) is red in color but shows some aggregate. (b) Anti-IP-10 antibody: each tube contained AuNP (pH 9.2) and varying amount of antibody: 0, 8, 12, 16, 24 and 28 µg/ml (left to right). The sixth tube from left (28 µg/ml) is red in color with much less aggregate on the bottom of the tube compared to the others.

5.3.2 Biosensor detection

After the capture of target IFN-γ or IP-10, dAb-AuNP-oligo-CdS or dAb-AuNP-oligo-PbS conjugates were introduced to the MNP-target complexes. The dAb-AuNP-oligo-CdS/PbS conjugates labeled the target proteins through antibody-antigen reaction. Therefore, CdS or PbS nanoparticles would present when there was the binding event of AuNPs to the targets. The signal of the biosensor was obtained by electrochemical measurement. After depositing bismuth and cadmium/lead at the same time at -1.2 V vs. Ag/AgCl for 10 min, a square wave voltammetric stripping scan from -1.2 V to 0 V was conducted on a SPCE chip. According to the literature (Zhang et al., 2010), the current peak of cadmium appears at ~ -0.87 V and it is also observed in the sensorgram as shown in Figure 5-5a when 0.1 IU/ml of IFN-γ presented in a sample. The magnitude of peak current at -0.87 V was used to indicate cadmium signal. No current peak was observed for the blank. For the blank, the magnitude of current at -0.87 V was used to calculate the signals. For lead, the current peak appeared at around -0.67 V. The magnitude of peak current at -0.67 V was used to indicate lead signal. No current peak was observed for the blank. For the blank, the magnitude of current at -0.67 V was used to calculate the signals. A typical sensorgram is presented in Figure 5-5b, and the detection of 10 ng/ml IP-10 is shown.

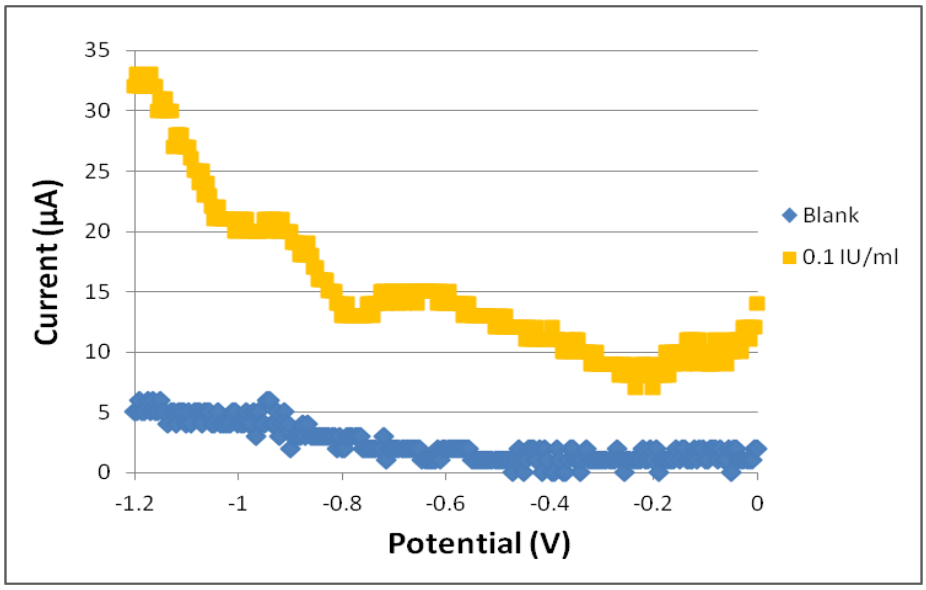

(a)

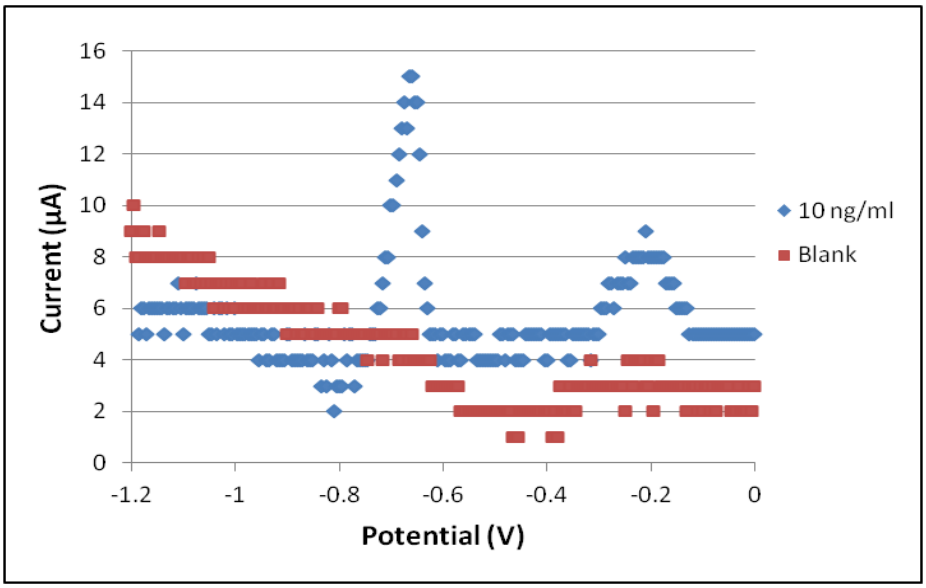

(b)

Figure 5-5. Typical sensorgrams of using nanotracers-labeled biosensor for the detection of single cytokine: (a) sensorgram of IFN-γ detection (IFN-γ concentration: 0.1 IU/ml), and (b) sensorgram of IP-10 detection (IP-10 concentration: 10 ng/ml). For IFN-γ detection, a current peak of cadmium appeared at -0.87 V in the square wave voltammetric stripping scan from -1.2 V to 0 V. A current peak of lead appeared at -0.67 V for the detection of IP-10.

In order to evaluate the sensitivity and detection range of the biosensor, a serial dilution of IFN-γ was detected using the biosensor. Figure 5-6a shows the relationship between the current peak of cadmium and various IFN-γ concentrations (blank, 0.01 IU/ml to 10 IU/ml). It is observed that the current peak of cadmium for samples with IFN-γ are differentiated from the current at the same potential for the blanks, noted that the current magnitude at -0.87 was used as the signal of the blank. The signal increased with increasing target concentration, except the highest concentration of 10 IU/ml. At 10 IU/ml, signal lower than the expected (signals increase with increasing concentration) was observed due to the hook effect in immunological tests which caused the non-equilibrium status because of high antigen concentration (Gatto-Menking et al., 1995). The results for IP-10 detection are presented in Figure 5-6b, which shows the relationship between the current peaks and various IP-10 concentrations (blank, 1 pg/ml to 100 ng/ml). Compared to the results of IFN-γ detection, the variation of signals is larger, which may be attributed to the instability of PbS nanoparticles compared to CdS nanoparticles. It was found during the experiments that the CdS nanoparticles were stable under room temperature for at least 6 months, but PbS nanoparticles were easily oxidized and precipitated from the colloidal in a couple of days. Therefore, during the preparation of the AuNP-NT conjugates and the detection, some PbS nanoparticles might be oxidized and resulted in the inconsistency between the signals obtained with different samples and on different days. If the experiments on different days were taken in account, the variation was greatly decreased as shown in Figure 5-6b insert. Here, the results are presented in signal to noise number (SNN) which is calculated by subtracting current magnitude at -0.67 V for blank obtained during the experiment on each day from the current magnitude for samples obtained the same day.

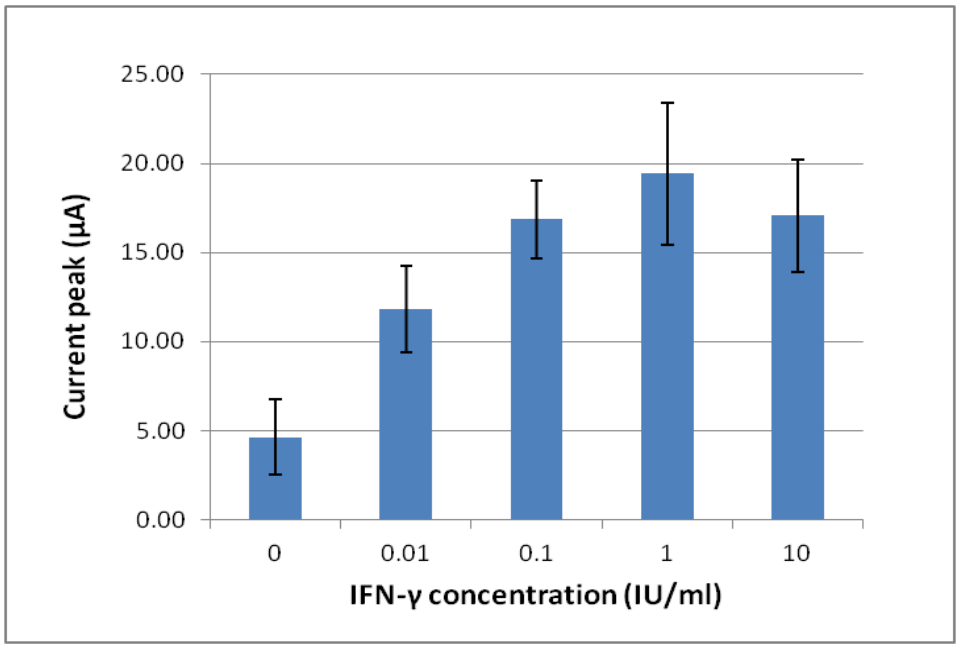

(a)

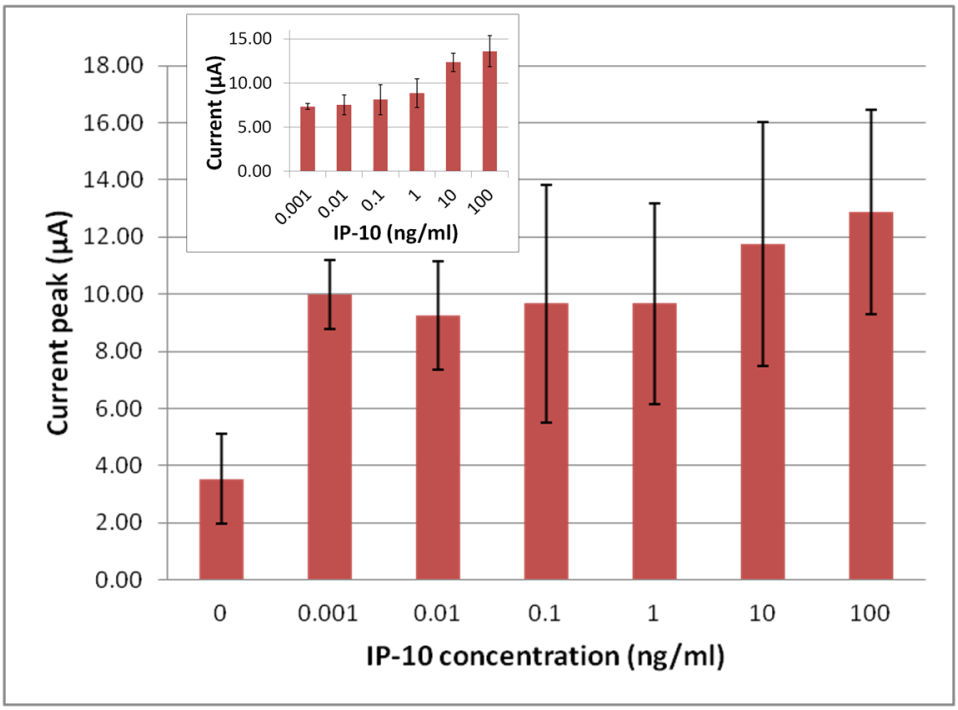

(b)

Figure 5-6. Electrochemical measurement results of single cytokine detection in buffer solution: (a) relationship between the current peak and IFN-γ concentration, and (b) relationship between the current peak and IP-10 concentration (Insert: signal to noise number (SNN) at different IP-10 concentration).

A statistical analysis including *t* test for IFN-γ detection was conducted and the results are presented in Table 5-1. The average signal and standard deviation for each concentration is shown. Signal to noise ratio (S/N) is calculated as dividing the average signal for each concentration by the signal for blank, which results in the S/N of 2.55 for 0.01 IU/ml, 3.64 for 0.1 IU/ml, 4.19 for 1 IU/ml and 3.68 for 10 IU/ml. By comparing the signal of each IFN-γ concentration to the average signal of blank samples plus three times of standard deviation (Blank Avg. + 3×S. D.), it is found that 0.01 IU/ml has a small overlap with the Blank Avg. + 3×S. D. However, the detection of other concentrations is obvious. In another evaluation, signals for all concentrations are significantly different from the blank as shown by P value ($P<0.05$). Therefore, the detection limit of this biosensor is 0.01 IU/ml according to the P value. International units/ml (IU/ml) reported here can be converted to pg/ml as 1 IU/ml=40 pg/ml (Kellar et al., 2011). Compared with other methods, this biosensor can sensitively detect the target IFN-γ with a detection time of 1 h.

Table 5-1**.** Statistical analysis comparing samples and blank for IFN-γ detection in single cytokine detection.

Concentration (IU/ml)	*0*	*0.01*	*0.1*	*1*	*10*
Average Current Peak (μA)	4.63	11.81	16.87	19.42	17.06
Standard Deviation (μA)	2.10	2.41	2.19	3.96	3.15
S/N	N/A	2.55	3.64	4.19	3.68
Blank Avg. + 3×S. D.	10.94				
P value[a]	N/A	8.87E-06	1.33E-07	1.06E-06	2.30E-07

[a] P value was calculated by a one-tailed paired *t* test. The critical value, P=0.05.

The statistical analysis including *t* test was also conducted for IP-10 detection, and the results are presented in Table 5-2. By comparing the signal of each IP-10 concentration to the average signal of blank samples plus three times of standard deviation (Blank Avg. + 3×S. D.) as in Table 5-2, it is found that 0.01 ng/ml has a small overlap with the Blank Avg. + 3×S. D, but the detection of other concentrations is obvious. Shown by P value, signals for all concentrations are significantly different from the blank. Therefore, the detection limit of this biosensor is 1 pg/ml. The sensitivity of IP-10 detection is also comparable with other methods with a detection time of 1 h.

Table 5-2. Statistical analysis comparing samples and blank for IP-10 detection in single cytokine detection.

Concentration (ng/ml)	*0*	*0.001*	*0.01*	*0.1*	*1*	*10*	*100*
Average Current Peak (μA)	3.53	10.00	9.24	9.67	9.67	11.75	12.89
Standard Deviation (μA)	1.58	1.20	1.89	4.17	3.50	4.26	3.58
SNN	N/A	7.33	7.78	8.11	8.83	11.50	13.33
Blank Avg.+3×S. D.	8.27						
P value[a]	N/A	9.05E-06	9.28E-07	0.016487	0.000125	0.000397	1.25E-05

[a] P value was calculated by a one-tailed paired *t* test. The critical value, P=0.05.

5.4 Conclusion

An electrochemical biosensor based on nanoparticle conjugates was developed for single cytokine detection. Magnetic nanoparticles and gold nanoparticles functionalized with antibodies bound to a target cytokine through the antibody-antigen biorecognition. Magnetic nanoparticles captured and separated the target from a sample, and gold nanoparticles labeled the target, which

formed a sandwich structure. Because the gold nanoparticles were also conjugated with CdS or PbS nanoparticle-terminated oligonucleotides, signal amplification was achieved due to the binding of multiple CdS/PbS nanoparticles to one AuNP through oligonucleotide linkage. For IFN-γ detection, the electrochemical signal of CdS nanoparticles were measured using a potentiostat, and a current peak at ~-0.87 V for cadmium during a squarewave voltammetry scan was obtained. A detectable range of 0.01 IU/ml to 10 IU/ml was obtained with a detection limit of 0.01 IU/ml. Meanwhile, the IP-10 detection took 1 h with a detectable concentration of 1 pg/ml. The biosensor required less time than other technologies but achieved comparable sensitivity.

Chapter 6 : Multiplex biosensor for detection of IFN-γ and IP-10 cytokines

6.1 Introduction

Tuberculosis (TB) is considered as one of the most widely spread infectious diseases which threaten the public health. The diagnosis of TB includes methods such as tuberculin skin test (TST), blood test which is also called as interferon-gamma release assays (IGRAs), microbiology tests and chest radiograph. Kellar et al. (2011), Ruhwald et al. (2007) and several other studies (Azzurri et al., 2005; Okamoto et al., 2005; Kabeer et al., 2010; Goletti et al., 2010) reported that besides IFN-γ which was used as a biomarker for TB diagnosis in IGRAs, IFN-gamma-inducible protein 10 (IP-10/CXCL10) was also produced in a high level when infected with TB. Therefore, IP-10 was suggested as an adjunct biomarker for TB diagnosis.

In this chapter, a biosensor for the detection of IFN-γ and IP-10 was developed for potential TB diagnosis. This new rapid and sensitive approach for multiplex cytokine detection combines magnetic separation and signal amplification based on nanoparticles. Using the biosensor, the two biomarkers for TB can be detected in one sample simultaneously. This was achieved by using magnetic nanoparticles (MNPs) functionalized with antibodies to IFN-γ and IP-10 for target separation first. Then gold nanoparticles (AuNPs) conjugated with nanotracers (NTs) and antibodies were utilized to label the targets and provide electrochemical signals. The nanotracers are two kinds of nanoparticles: lead sulfide (PbS) and cadmium sulfide (CdS). They were conjugated with AuNPs through the linkage of oligonucleotides. There were two types of AuNP conjugates: one was functionalized with antibody to IFN-γ and CdS-terminated oligonucleotides and the other was functionalized with antibody to IP-10 and PbS-terminated oligonucleotides. Therefore, the electrochemical signal of cadmium would report the detection of IFN-γ and that of

lead would represent the existence of IP-10. The electrochemical signals were measured using potentiostat on a screen-printed carbon electrode (SPCE). It took 1 h from the sample to final signal read-out. IFN-γ and IP-10 in buffer and in plasma were tested.

6.2 Materials and methods

6.2.1 Reagents and materials

Aniline, iron (III) oxide nanopowder, ammonium persulfate, methanol, and diethyl ether were used for the synthesis of the MNPs. Gold (III) chloride trihydrate (Aldrich, MO) and dextrin (Fluka, MO) were used for the synthesis of gold nanoparticles under alkaline conditions (Anderson et al., 2011). Sodium sulfide, 3-mercaptoacetic acid, and cadmium chloride were used for the synthesis of CdS nanoparticles. Sodium sulfide, 3-mercaptoacetic acid, and lead nitrate were used for the synthesis of PbS nanoparticles.

Antibodies conjugated with MNPs (capture antibody, cAb) were purified mouse anti-human IFN-γ (#551221) and purified mouse anti-human IP-10 antibody (#555046) obtained from BD Pharmingen^{TM} (San Diego, CA). Detection antibodies (dAb) conjugated with AuNPs were purified mouse anti-human IFN-γ (#554549) and mouse anti-human IP-10 antibody (#624084) obtained from BD Pharmingen^{TM} (San Diego, CA). An oligonucleotide (sequence 5'-AAA AAA AAA AAA AAA AAA AA-3') with 3' thiol modifier and 5' amino modifier was employed as a linker between AuNPs and NTs, which was purchased from Integrated DNA Technologies Inc. (Coralville, IA). 1,4-Dithio-dl-threitol (DTT) was used for the cleavage of oxidized thiolated oligonucleotides. Nap-5 column (GE Healthcare, Piscataway, NJ) was used for purifying oligonucleotides from DTT solution. 1-Ethyl-3-[3-dimethylaminopropyl] carbodiimide hydrochloride (EDC) and N-hydroxysuccinimide (NHS) were used for the linkage

of carboxylic groups on NTs and amine groups on oligonucleotides. These reagents were purchased from Sigma (St. Louis, MO). Bismuth standard stock solution (10,000 ppm) was purchased from Ricca Chemical Company (Arlington, TX). Acetate buffer solution (0.1 M, pH 4.5) with 1 mg/l bismuth was used for electrochemical measurement.

Phosphate buffered saline (PBS), casein, bovine serum albumin (BSA) and sodium phosphate (dibasic and monobasic) and all other reagents (unless otherwise noted) were obtained from Sigma-Aldrich (St. Louis, MO). PBS buffer (0.01 M, pH 7.4), phosphate buffer (0.1 M sodium phosphate, pH 7.4), 0.1 M tris buffer with 0.01% casein, PBS buffer with 0.1% (w/v) BSA, assay buffer (0.562 g Na_2HPO_4, 0.125g NaH_2PO_4, 4.383g NaCl and 0.5g BSA in 500 ml water; Hill and Mirkin, 2006) were prepared with deionized water from Millipore Direct-Q system. PBS buffer and phosphate buffer were used in preparing nanoparticle-antibody conjugates and in washing. Buffers with casein or BSA were used to block nanoparticle surface against nonspecific binding. Assay buffer was used for keeping pH during reactions and washing off unbound or nonspecifically bound reactants.

6.2.2 Cytokine dilutions and human plasma

Lyophilized Human IFN-γ Standard was obtained from Cellestis (Valencia, CA). Lyophilized recombinant human IP-10 was obtained from BD Pharmingen^{TM} (#551130, San Diego, CA). The serial dilutions of IFN-γ or IP-10 were prepared using sterile deionized water before experiments. For the detection of the two cytokines in buffer, the dilutions in water were used directly. For the detection in plasma, IFN-γ and IP-10 were spiked in 10% plasma (plasma incubated with Nil as described below). The plasma was provided by Centers for Disease Control and Prevention (CDC). Blood was collected and divided into different tubes, followed

by overnight incubation at 37 ℃ with saline (Nil). Then plasma was collected and divided into aliquots. Ten percent plasma was prepared at the beginning of the detection with PBS buffer.

6.2.3 Apparatus

Electrochemical measurement was performed with a potentiostat/galvanostat (263A, Princeton Applied Research, MA) with a software operating system (PowerSuite, Princeton Applied Research, MA) on a computer connected to the potentiostat. The measurement was performed by introducing each sample onto a screen-printed carbon electrode (SPCE) chip (Gwent Inc. England). The SPCE chip consisted of a working electrode (carbon) and a counter and reference electrode (silver/silver chloride electrode). One hundred microliters of each sample were introduced to the electrode area on the SPCE chip.

6.2.4 Synthesis of nanoparticles

Polyaniline (PANI) coated magnetic nanoparticles were synthesized according to published methods (Setterington et al., 2011). Briefly, 50 µl of 1 M HCl, 10 ml of water and 0.4 ml of aniline monomer were mixed in a flask, and then 0.65 g of iron (III) oxide nanopowder was added to the solution to maintain a final γ-Fe_2O_3: aniline weight ratio of 1: 0.6. The mixture was put in a beaker filled with ice and sonicated for 1 h. The solution was stirred while it was still on ice. During the stirring, ammonium persulfate (1 g of ammonium persulfate in 20 ml deionized water) was added to the solution slowly for 30 min. The solution was stirred for another 1.5 h. After the reaction, the solution was filtered using 2.5 µm filter paper and washed with 20% methanol. Hydrochloric acid (1 M) was used to wash until the filtrate was clear, followed by washing with 10 ml of 20% methanol. The filtrate was filtered again using a 1.2 µm filter paper. Twenty percent methanol solution was added to the filter. The HCl and methanol wash was

repeated. The nanoparticles on the filter paper were left under the fume hood to dry for 24 h at room temperature and then stored in a vacuum desiccator ready to use.

Gold nanoparticles were synthesized under alkaline conditions following the approach published by Anderson et al (2011). Briefly, 20 ml of dextrin stock solution (25 g/l) and 20 ml of sterile water were mixed in a 50 ml sterile orange cap tube (disposable). Five milliliters of $HAuCl_4$ stock solution (0.4 g/50 ml) were then added, and the pH of the solution was adjusted to 9 with sterile 10% (w/v) Na_2CO_3 solution. The final volume was brought to 50 ml with pH 9 water. The $HAuCl_4$ concentration in the reaction was 2 mM (for $HAuCl_4 \cdot 3H_2O$ = 0.04g/50 ml). The reaction was carried out by incubating the solution in a sterile flask in the dark at 50 ℃ with continuous shaking (100 rpm) for 6 h. A red solution was obtained at the end of the reaction. The pH of AuNP colloidal was adjusted to 9.2 before use.

Cadmium sulfide (CdS) nanoparticles were synthesized by using published procedures (Zhang et al., 2010; Ding et al., 2009; Jie et al., 2007) with some modifications. Mercaptoacetic acid (2 µl) was mixed with 100 ml of 1 mM $CdCl_2$, and the pH of the solution was adjusted to 11 with 1 M NaOH. After bubbling the solution with nitrogen (oxygen free) for 30 min, 50 ml of Na_2S (1.34 mM) were added dropwise to the solution. Then the solution was continuously bubbled with nitrogen for 24 h. Lead sulfide nanoparticles were synthesized by similar procedures (Zhang et al., 2010; Zhu et al., 2004). Mercaptoacetic acid (9.22 µl) was mixed with 50 ml of 0.4 mM $Pb(NO_3)_2$, and the pH of the solution was adjusted to 7 with 1 M NaOH. After bubbling the solution with nitrogen (oxygen free) for 30 min, 40 ml of Na_2S (1.34 mM) were added dropwise to the solution. Transmission electron microscopy (TEM) and UV/Vis (NanoDrop, Thermo Fisher Scientific, DE) were used to characterize the nanoparticles.

6.2.5 Functionalization of nanoparticles

Two kinds of MNPs were prepared by functionalizing them with the capture antibody (cAb) to IFN-γ or IP-10, respectively. Taking the example of preparing MNPs-cAb for capturing IFN-γ, MNPs (2.5 mg) were suspended in 150 μl of 0.1 M phosphate buffer, and sonicated for 15 min. The anti-IFN-γ antibody (1.0 mg/ml, 100 μl) was added to the suspension, and mixed on tube rotator for 5 min. Twenty five microliters of PBS buffer (0.1 M) were added. Then the conjugation was carried on for 55 min on the tube rotator. The MNPs were separated from the solution by magnetic separation, and blocked by adding 250 μl of 0.1M tris buffer with 0.01% casein with 5 min incubation. This step was repeated three times. The third suspension in tris-casein buffer was put on the tube rotator for 60 min. Finally, the MNPs were magnetically separated and resuspended in 2.5 ml of 0.1M phosphate buffer. The MNP-cAb conjugate was stored at 4 ℃ before use. MNP-cAb conjugates for capturing IP-10 were prepared in the same way except that anti-IP-10 capture antibody was used instead.

Gold nanoparticles were conjugated with the anti-IFN-γ detection antibody (dAb) and CdS-terminated oligonucleotides (oligos), or the anti-IP-10 dAb and PbS-terminated oligonucleotides (oligos). Therefore, AuNPs with CdS would bind to IFN-γ, and AuNPs with PbS would bind to IP-10. To determine a suitable amount of antibody, different amount of antibody was added to 1 ml AuNP solution (pH 9.2) and mixed for 30 min on a tube rotator as mentioned in Chapter 5. From the shifting of color after adding 100 μl of 2 M NaCl (Hill and Mirkin, 2006; Greg, 2007), the optimal amount was 10 μg for anti-IFN-γ and 20 μg for anti-IP-10 antibody. The modification of AuNPs with oligonucleotides followed the procedure published by Hill and Mirkin (2006), and the conjugation of NTs to AuNPs followed the procedure published by Zhang et al. (2010). Briefly, 25 μl of 200 μM thiolated oligonucleotides were mixed with 25 μl

of 0.2 M DTT solution and then purified using a Nap-5 column. The oligonucleotides were added to the AuNP-dAb conjugates, and a serial salt addition was conducted for 3 h. After washing away the excess reagents, EDC and NHS were added to form the linkage between NTs and oligonucleotides on AuNPs. At the last, CdS nanoparticles were attached to AuNPs with anti-IFN-γ dAb (anti-IFN-γ-AuNP-oligo-CdS), and PbS nanoparticles were attached to AuNPs with anti-IP-10 dAb (anti-IP-10-AuNP-oligo-PbS). The dAb-AuNP-oligo-NT (Cds/PbS) conjugates were ready to use after washing.

6.2.6 Effect of IFN-γ and IP-10 concentration

The biosensor was used to detect IFN-γ and IP-10 in buffer and in 10% plasma. The detection of the target is presented in Figure 6-1. For the tests in buffer, blank was water in the same volume as the samples containing the targets. Firstly, 200 µl PBS buffer, 100 µl IFN-γ dilution, 100 µl IP-10 dilution, 25 µl of MNP-anti-IFN-γ and 25 µl MNP-anti-IP-10 were combined in a 2 ml sterile tube. After 20 min mixing on tube rotator, 100 µl of 0.01 M PBS buffer with 0.1% BSA were added to the mixture as a blocking agent with another 5 min reaction. Then, the MNP-IFN-γ and MNP-IP-10 complexes were magnetically separated from the solution and resuspended in 200 µl of assay buffer. Secondly, 25 µl of anti-IFN-γ-AuNP-oligo-CdS conjugates and 25 µl of anti-IP-10-AuNP-oligo-PbS were introduced to the system, and put on tube rotator for 20 min. After magnetically separation, the complexes were washed once with assay buffer. For the tests in 10% plasma, 20 µl of plasma (plasma incubated with nil) were diluted to 200 µl with PBS buffer and used as the blank. IFN-γ and IP-10 were spiked into the 10% plasma to get a serial dilution of the two targets.

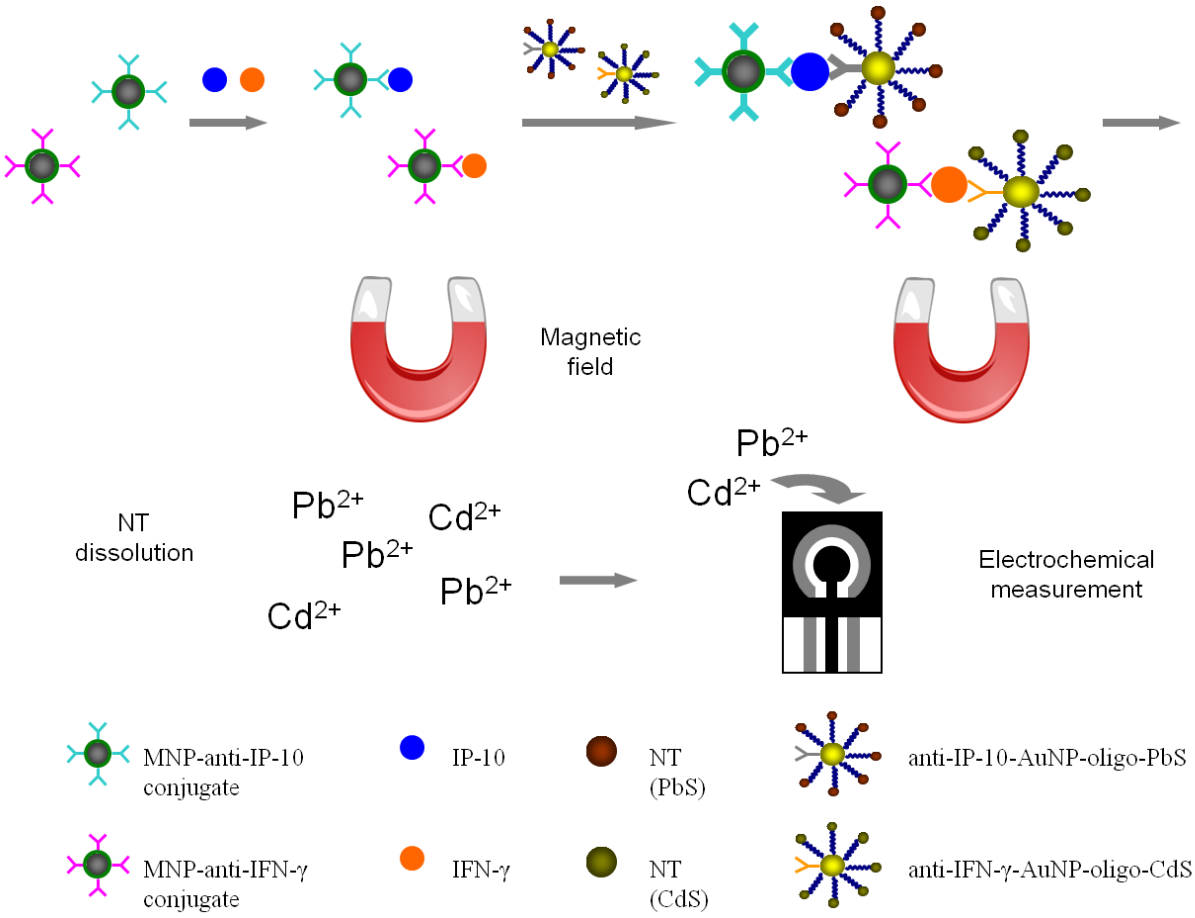

Figure 6-1. Schematic of the NT-labeled biosensor for the multiple analyte detection of IP-10 and IFN-γ. Two kinds of MNPs, MNP-anti-IFN-γ and MNP-anti-IP-10, captured the two targets and separated them from a sample matrix when magnetic field was applied. Then, the targets were labeled with AuNP-NTs so that anti-IFN-γ-AuNP-oligo-CdS attached to IFN-γ and anti-IP-10-AuNP-oligo-PbS attached to IP-10. After magnetic separation, the NTs attached to the targets were dissolved in nitric acid and introduced to the surface of SPCEs for electrochemical measurement.

6.2.7 Electrochemical measurement

Ten microliters of HNO_3 (0.8 M) were added to MNP-targets-AuNP-NT complexes obtained after final magnetic separation in each tube from section 6.2.6 and incubated for 10 min. Then, 90 µl of 1 mg/l bismuth in acetate buffer were added, and the suspension (100 µl) was introduced to the SPCE chip. Ten minute deposition of -1.2 V vs. Ag/AgCl was applied to the working electrode, followed by a square wave voltammetric measurement from -1.2 V to 0.0 V (Zhang et al., 2010; Wang et al., 2000). All measurements were performed at room temperature. Each sample was measured three times. At least three replicates were tested for each sample or blank.

6.3 Results and discussion

6.3.1 Electrochemical characterization of nanotracers

The multiple analyte detection was based on the use of PbS and CdS as the signal amplifiers for IP-10 and IFN-γ, respectively. In order to measure the signals of lead and cadmium at same time during one voltammetry measurement, the two nanoparticles should have separated current peaks. As presented here, the signal of lead or cadmium was measured alone as Figure 6-2a and 6-2b, respectively. The signals of both lead and cadmium were measured at the same time in Figure 6-2c. The control is AuNP-oligo conjugates, which indicated that AuNP-oligo conjugates did not interfere with lead or cadmium signals. The current peak of lead appeared at ~-0.67 V, and cadmium showed a peak at ~-0.87 V. The lead and cadmium showed two peaks in Figure 6-2c, which indicates that the two nanotracers were deposited at the same time, and their signals could be measured by the same voltammetry. According to the results, PbS and CdS are able to be used as amplifiers for multiple analyte detection.

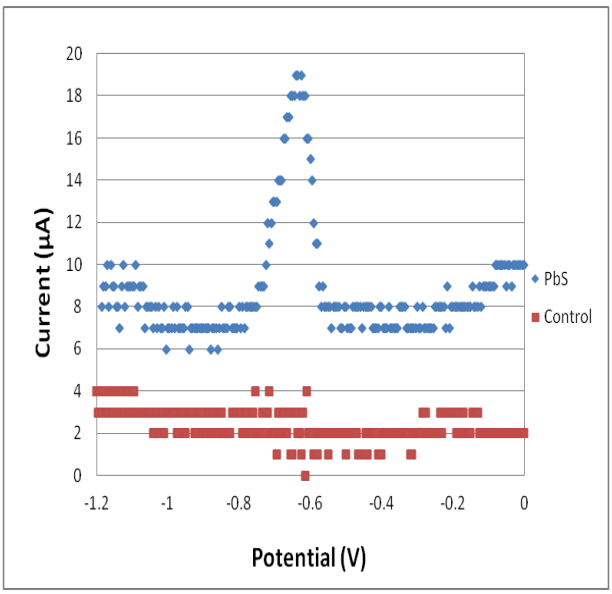

(a)

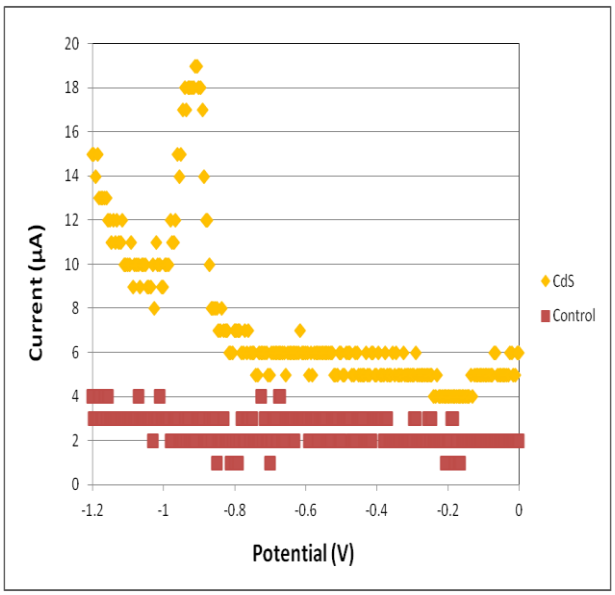

(b)

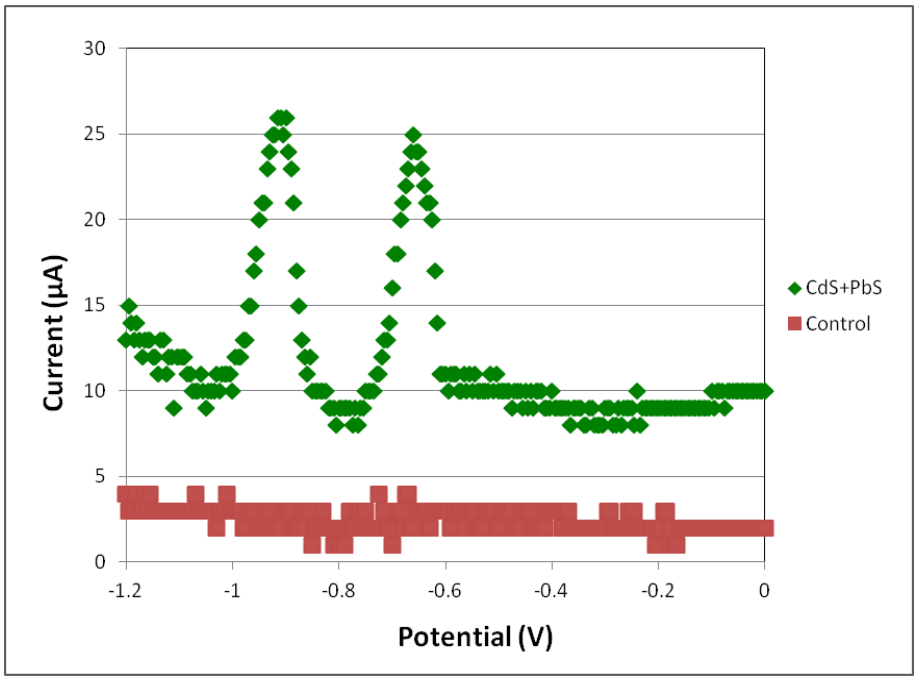

(c)

Figure 6-2. Typical sensorgram of square wave voltammetry for: (a) PbS alone, (b) CdS alone and (c) CdS and PbS.

6.3.2 Functionalization of nanoparticles

The detail of nanoparticle functionalization was provided in Chapter 5. Magnetic nanoparticles functionalized with capture antibodies to IFN-γ or IP-10 were prepared separately. The attachment of antibodies to MNPs was based on the electrostatic interaction. The dAb-AuNP-oligo-NT conjugates were prepared by firstly attaching dAb to AuNPs surface. The amount of dAb was controlled to ensure both enough antibody for binding target antigens and the attachment of oligonucleotides. Twenty micrograms of anti-IP-10 dAb and 10 μg of anti-IFN-γ dAb were found to be suitable amount conjugated to 1 ml of AuNPs. Cadmium sulfide and lead sulfide nanoparticles were attached to AuNPs through the linkage of oligonucleotides which formed self-assembled monolayer on AuNPs and bond to NTs through the reaction between carboxylic group on NTs and the amine group on the 5' end of the oligonucleotides. EDC and NHS were involved in crosslinking the carboxylic group and amine group.

6.3.3 IFN-γ and IP-10 detection

Through the use of AuNP-NT conjugates, target concentration could be determined by electrochemical measurement using SPCE chips and a potentiostat. Serially diluted samples with both IFN-γ and IP-10 were mixed with 25 μl of MNP-anti-IFN-γ and 25 μl of MNP-anti-IP-10 for target capture and magnetic separation. Then, the MNP-target complexes were mixed with 25 μl of anti-IP-10-AuNP-PbS and 25 μl of anti-IFN-γ-AuNP-CdS conjugates. Therefore, AuNPs which carried PbS nanoparticles bond to MNP-IP-10 complexes, and AuNPs which carried CdS nanoparticles bond to MNP-IFN-γ complexes. The two sets of sandwich-structured complexes were the final "products" acquired after the second magnetic separation as shown in Figure 6-1. The NTs (CdS and PbS) were released in nitric acid from the complexes, and the signals for the NTs were measured on SPCE chips. During the square wave voltammetric scan, two peaks

registered for lead and cadmium respectively. Therefore, the peak of lead could be associated to IP-10, and the peak of cadmium could be associated IFN-γ. Figure 6-3a and 6-3b shows the detection of IFN-γ and IP-10 alone, and also verifies the specificity of the biosensor. The procedures were the same as the detection of both targets in one sample, except that only one target presented. A control (blank) without any of the targets was also detected, and no peaks obtained in the square wave voltammetric scan. When there was only IFN-γ, a current peak of 17 μA at -0.8 V appears in Figure 6-3a, and there is no peak around -0.67 V. When only IP-10 presented in the sample, a current peak of 22 μA at -0.62 V appears in Figure 6-3b, and there is no peak around -0.87 V. Meantime, the sample with both the targets shows two current peaks at -0.87 V and -0.65 V, presented in Figure 6-3c which is also a typical sensorgram for the multiplex detection. It is noted that the current peaks shift. However, the shift does not affect the appearance of individual peak for cadmium and lead in the figure. The shift will be explained in the next section.

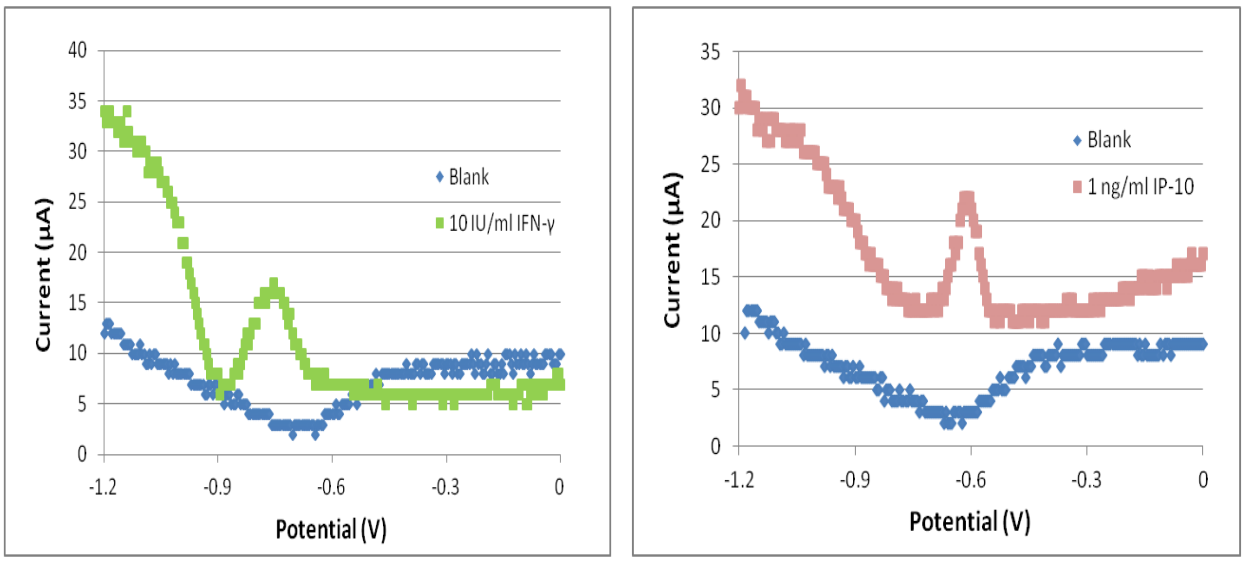

(a) (b)

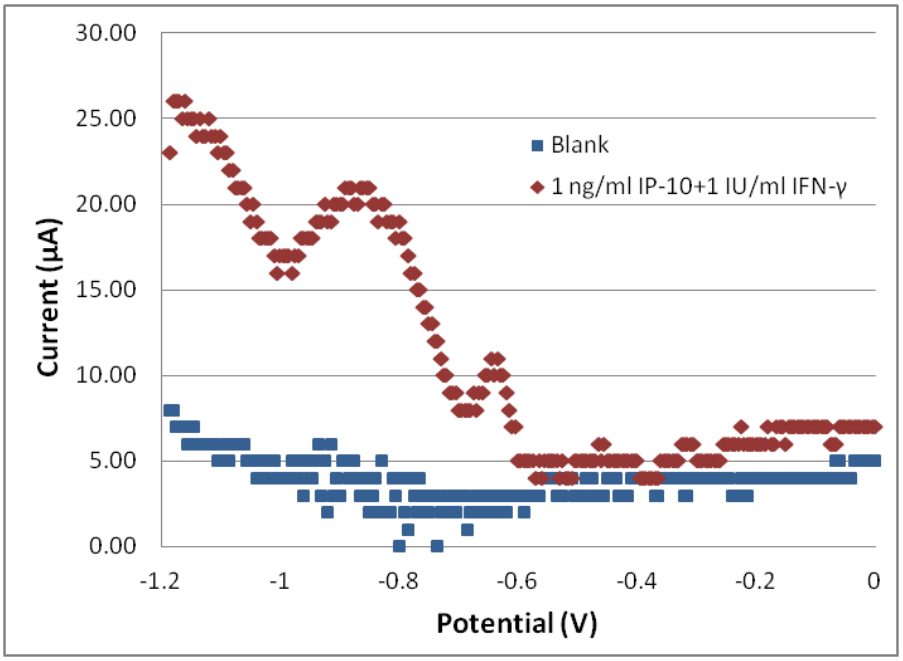

(c)

Figure 6-3. Specificity test of the biosensor: (a) the detection of IFN-γ alone, (b) the detection of IP-10 alone, and (c) the detection of both the targets. In all experiments, MNP-anti-IFN-γ and MNP-anti-IP-10 conjugates were used for target separation, and anti-IP-10-AuNP-PbS and anti-IFN-γ-AuNP-CdS conjugates were introduced to the captured target/targets.

6.3.4 Effect of IFN-γ and IP-10 concentration

The detection of single target (IFN-γ or IP-10) in buffer was described in Chapter 5. The experimental results indicated that IP-10 in the range of 1 pg/ml to 100 ng/ml can be detected. Meanwhile, IFN-γ in the range of 0.01 IU/ml to 10 IU/ml can be detected in 1 h. In the detectable range, the signals of NTs increased with increasing target concentration except IFN-γ at 10 IU/ml which resulted in a lower signal due to hook effect (Gatto-Menking et al., 1995).

By using the multiplex biosensor in this chapter, both IFN-γ and IP-10 were detected at the same time in one sample. As shown in Figure 6-3c, two current peaks were obtained which represent the amount of IFN-γ (cadmium peak) and IP-10 (lead peak) at around -0.87 V and -0.67 V, respectively. Firstly, the mixture of IFN-γ and IP-10 at different concentration in buffer solution was detected. The current peak for each target is presented in one diagram shown in Figure 6-4, as Figure 6-4a shows the signals for IFN-γ and Figure 6-4b shows that for IP-10. The average current peak for IFN-γ at 0 IU/ml (blank), 0.01 IU/ml, 0.1 IU/ml, 1 IU/ml and 10 IU/ml is 5 μA, 13.8 μA, 17.2 μA, 19.5 μA and 18.4 μA, respectively. Compared to single target detection results in the last chapter, where the current peak for 0 IU/ml (blank), 0.01 IU/ml, 0.1 IU/ml, 1 IU/ml and 10 IU/ml is 4.6 μA, 11.8 μA, 16.9 μA, 19.4 μA and 17.1 μA, respectively, the signals obtained in multiplex detection are consistent with the single target detection. As shown in Figure 6-4a, at the highest concentration, the results were also affected by hook effect. For the multiplex detection, the average current peak for IP-10 at 0 ng/ml (blank), 0.01 ng/ml, 0.1 ng/ml, 1 ng/ml, 10 ng/ml and 100 ng/ml is 4.3 μA, 13.9 μA, 15 μA, 15.6 μA, 16.1 μA and 14.4 μA. While detecting IP-10 alone, the average current is 3.53 μA, 10.00 μA, 9.24 μA, 9.67 μA, 9.67 μA, 11.75 μA and 12.89 μA for the different concentrations, respectively. Though for

the multiplex and single detection of IP-10, the signals are slightly different, they are following the same trend within the same current range.

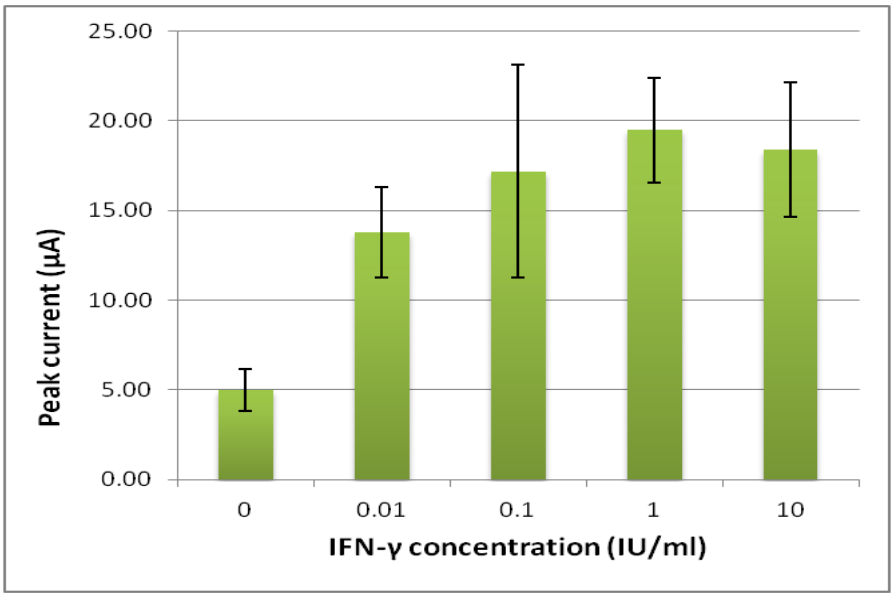

(a)

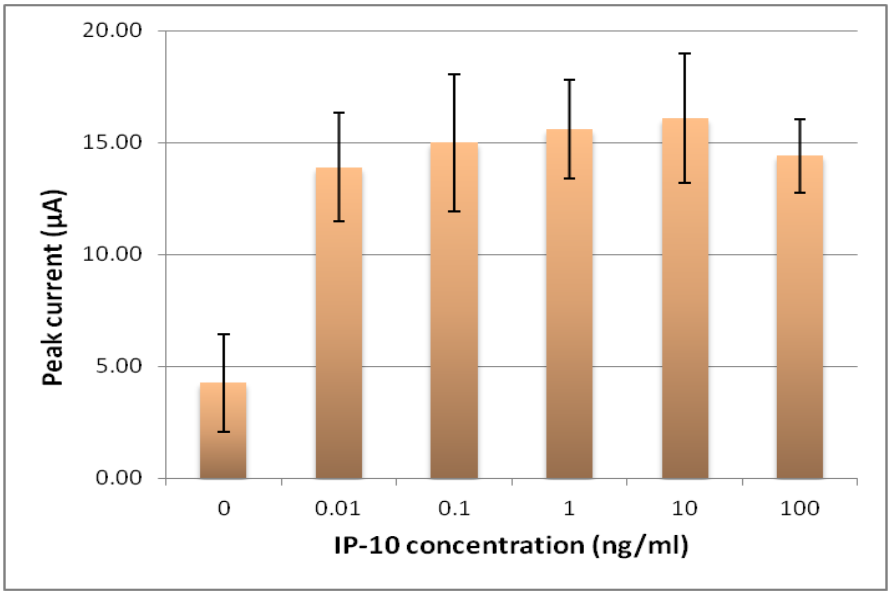

(b)

Figure 6-4. Relationship between peak current and target concentration of multiple cytokine detection in buffer solution. (a) Signals for IFN-γ at different concentration, and (b) signals for IP-10 at different concentration.

The multiplex biosensor was also tested in samples with 10% plasma. Plasma diluted in PBS buffer was spiked with both IFN-γ and IP-10. Magnetic nanoparticles functionalized with anti-IFN-γ and anti-IP-10 cAb were added to the samples, and they captured and separated the corresponding targets from the sample matrix when applying magnetic field. Then, AuNP-PbS labeled IP-10, and AuNP-CdS labeled IFN-γ. The electrochemical measurement procedure was optimized to provide more stable signal in this detection: 10 µl of assay buffer was added to each sample before deposition. It was observed that adding assay buffer could balance the pH in the solution and avoid too-fast deposition of lead onto the working electrode at the beginning of the deposition which prevented the further deposition. For the detection of IFN-γ, the current peaks of cadmium at around -0.8 V increase with increasing IFN-γ concentration, as shown in the typical sensorgrams in Figure 6-5. The current peaks of lead at around -0.62 V represent the signals for the detection of IP-10, and they also increase when IP-10 concentration increases. It is noticed that the current peaks shift. Reasons contributing to this shift could be: 1) the change of the reference potential on Ag/AgCl electrode with the flows of the current, since two-electrode system was used to simplify the measurement, 2) the difference between different SPCE chips, and 3) the difference in the coverage area of the electrodes between each sample when introduced solution to the SPCE surface. Figure 6-6a shows the relationship between the current peak of cadmium and the concentration of IFN-γ. Figure 6-6b shows the relationship between the current peak of lead and the concentration of IP-10. A *t* test was conducted, and the results reveal that the signals for samples with targets are significantly different from the blanks ($p<0.05$). There is a noticeable higher average signal for the blanks in the detection of IP-10, compared to the detection in buffer. The reason might be that the blanks, which were plasma incubated with nil, contained IP-10. This also explains the higher signals for samples with IP-10 obtained for the

detection in plasma compared to the detection in buffer, noted that targets were spiked in 10% plasma incubated in Nil. On the other hand, IFN-γ signal for the blanks was similar to that obtained in the detection in buffer. Therefore, IFN-γ signals remained in the same range as in the detection in buffer. Figure 6-7 shows linear relationship between the signals for cadmium and lead with the logarithmic concentration of IFN-γ and IP-10, with R^2 values of 0.9505 and 0.9624, respectively.

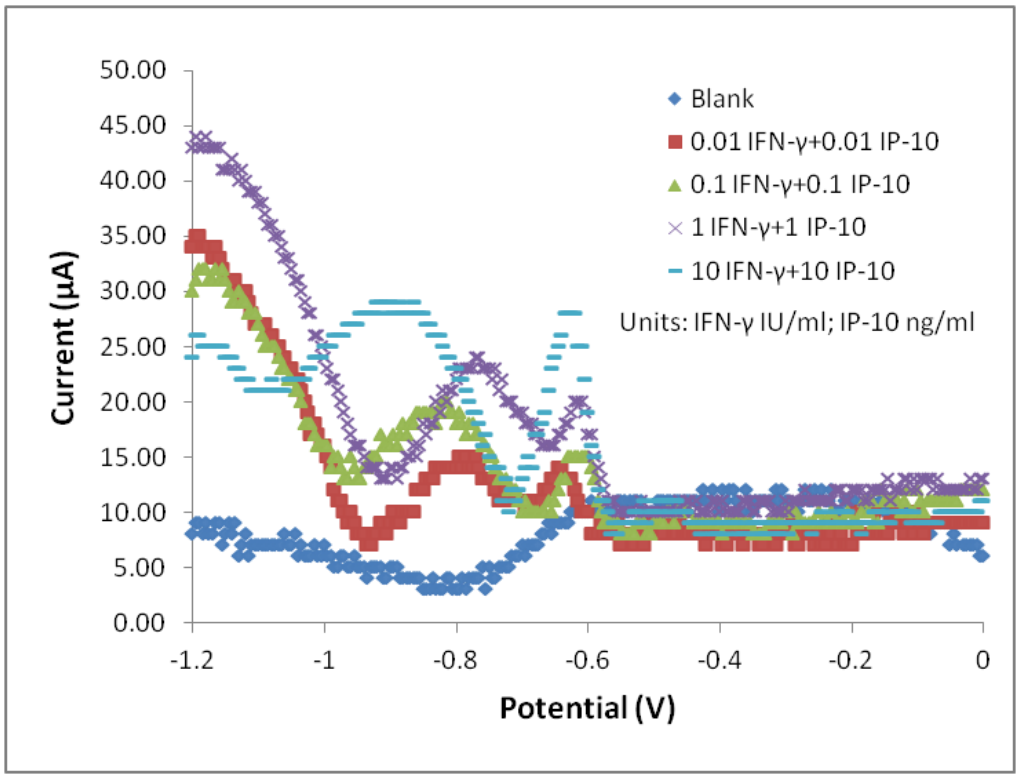

Figure 6-5. Typical sensorgrams of multiple cytokine detection in 10% plasma. For the detection of IFN-γ, the current peaks of cadmium at around -0.8 V increase with increasing IFN-γ concentration. For the detection of IP-10, the current peaks of lead at around -0.62 V increase with increasing IP-10 concentration.

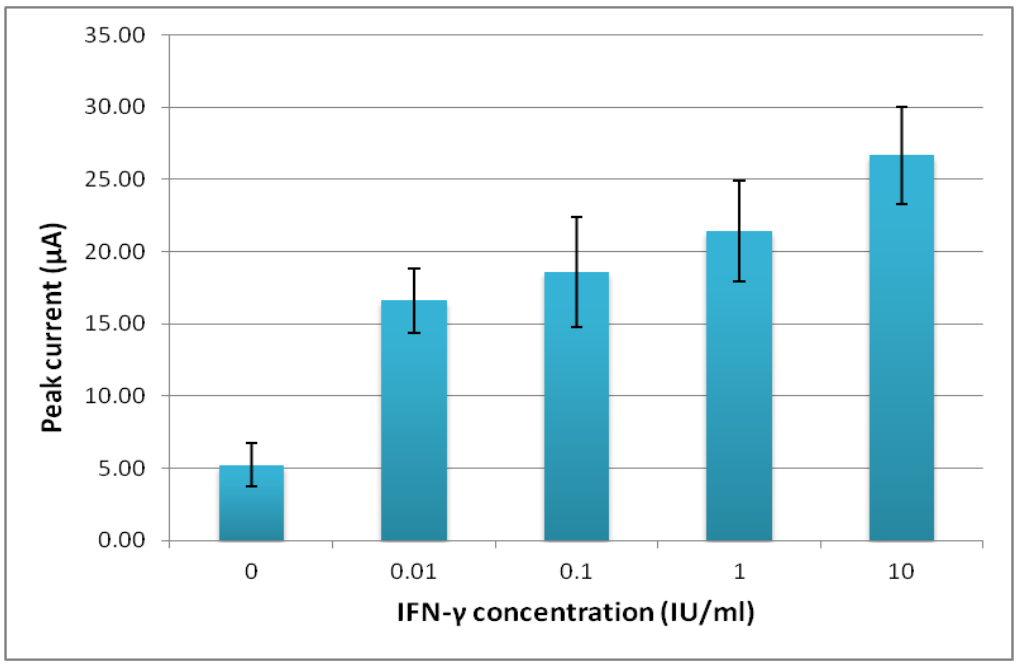

(a)

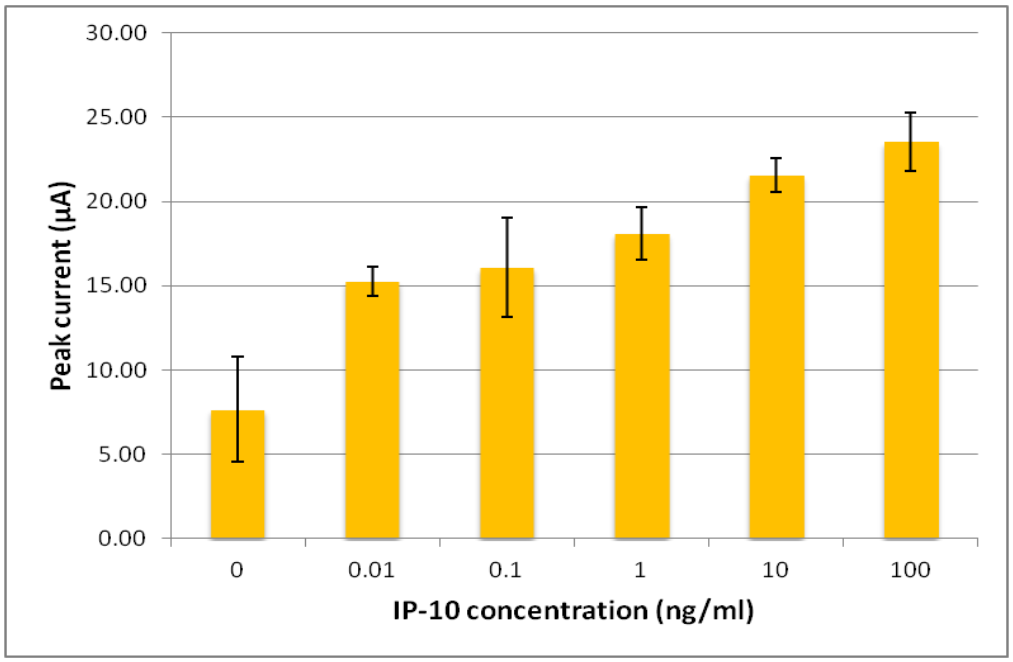

(b)

Figure 6-6. Relationship between peak current and target concentration of multiple cytokine detection in 10% plasma. (a) Signals for IFN-γ at different concentration, and (b) signals for IP-10 at different concentration.

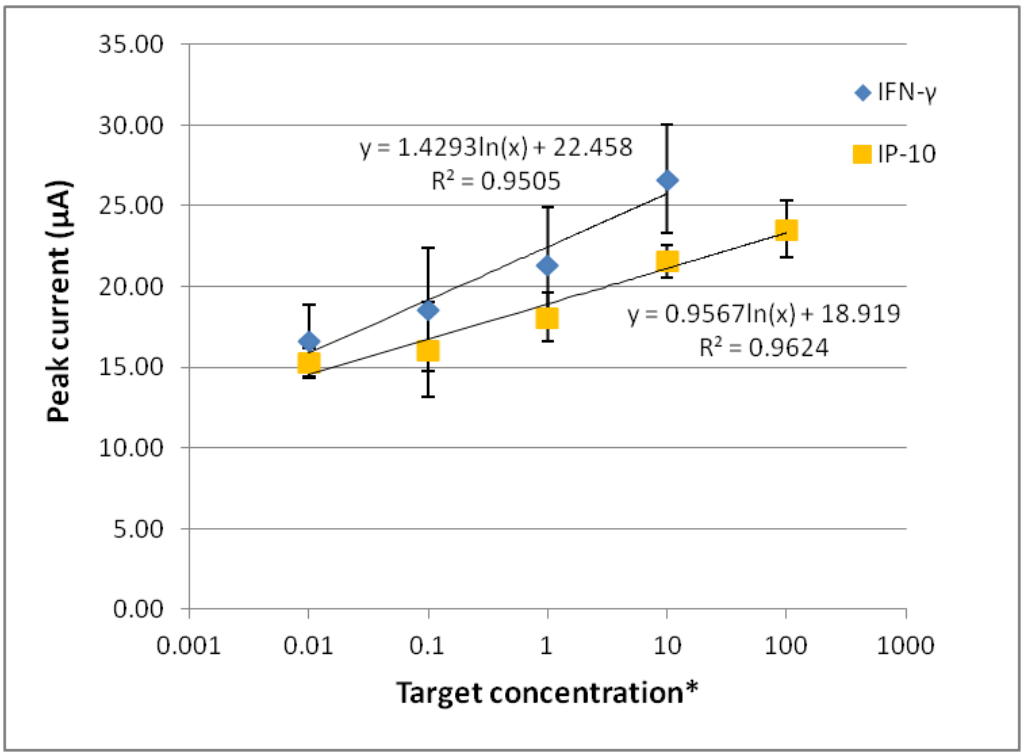

Figure 6-7. The calibration curves of peak current vs. target concentration of the multiple cytokine biosensor for the detection of IFN-γ and IP-10 in 10% plasma. *The unit of IFN-γ concentration is IU/ml, and the unit of IP-10 concentration is ng/ml.

6.4 Conclusion

A multiplex biosensor was developed for the detection of two cytokines: IFN-γ and IP-10 which are potential biomarkers for TB diagnosis. The biosensor employed two sets of MNPs with anti-IFN-γ and anti-IP-10 antibodies and two sets of AuNPs with different antibodies. Therefore, both IFN-γ and IP-10 in one sample can be separated from the sample matrix and labeled. Gold nanoparticles were also conjugated with NT-terminated oligonucleotides where CdS nanoparticles were attached to anti-IFN-γ-AuNPs conjugates and PbS nanoparticles were attached to anti-IP-10-AuNPs. Therefore, the signal of cadmium obtained in electrochemical

measurement was correlated to the concentration of IFN-γ, and the signal of lead indicated the concentration of IP-10. Using this biosensor to detect IFN-γ and IP-10 in buffer and 10% plasma, it is found that the electrochemical signals increased with increasing target concentration. Interferon-gamma in the range of 0.01 IU/ml (0.4 pg/ml) to 10 IU/ml (400 pg/ml) and IP-10 in 0.01 ng/ml to 100 ng/ml were detected. The results also showed that the biosensor has a good specificity. This biosensor has the potential in multiplex detection of cytokines for disease diagnosis.

Chapter 7 : Conclusion and future work

The research presented in Chapter 3 to 6 described the design and development of electrochemical immunosensors based on nanoparticles for target separation and signal amplification. *Escherichia coli* O157:H7 and two cytokines as potential biomarkers for tuberculosis (TB) diagnosis were detected using the immunosensors with high sensitivity. Compared to conventional culture plating method for *E. coli* identification which needs days for results, the detection using the immunosensors developed in this research only take 1 h from samples to final readout. For TB diagnosis, the immunosensor presented in Chapter 5 and 6 enables the multiple analyte detection. Therefore, two biomarkers IFN-γ and IP-10 can be detected at the same time to potentially improve the efficiency and accuracy of the diagnosis.

Two designs of immunosensors for *E. coli* detection were developed. In design 1, the target bacteria were separated from samples by using polyaniline (PANI)-coated magnetic nanoparticles (MNPs) conjugated with monoclonal antibody (mAb). After magnetic separation, bacteria cells captured by MNPs were labeled with gold nanoparticles (AuNPs) functionalized with polyclonal antibody (pAb). The electrochemical measurement was conducted to report the signal of AuNPs, which further indicated the existence and concentration of *E. coli* O157:H7 due to the labeling resulted from the antibody-antigen recognition. A detection limit of 10^2 colony forming units per milliliter (cfu/ml) of bacteria with a detection range of 10^2 to 10^6 cfu/ml was obtained using this design. Ten colony forming units per milliliter (cfu/ml) of bacteria were detected with weakly significance compared to the blank. The signal to noise ratio was calculated as 1.28 for the lowest concentration and 2.36 for the highest concentration.

Based on design 1, a new approach (design 2) with further signal amplification was investigated to improve the performance of the immunosensor with higher signal to noise ratio. In this design, AuNPs were not only conjugated with antibodies but also linked to multiple PbS nanoparticles through oligonucleotides. The functionalization of the AuNPs were optimized by choosing suitable antibody concentration, and the amplification by adding PbS nanoparticles was estimated by calculating the number of PbS nanoparticles bound to each AuNP in Chapter 4. Using this immunosensor, the target bacterial cells captured and separated by MNPs were labeled by pAb-AuNP-PbS conjugates instead of pAb-AuNP. The electrochemical signal of lead was measured to reflect the existence and concentration of the target. An improvement of signal to noise ratio was observed using the PbS amplification, and a detection range of 10^1 to 10^6 cfu/ml was obtained using this design.

In addition to bacterial target detection, design 2 biosensor was applied for identifying protein targets. Since IFN-γ and IP-10 are two important cytokines in immune responses and potential biomarkers for TB diagnosis, they were chosen as the targets, expanding the application of the biosensor to disease diagnosis. Magnetic nanoparticles modified with anti-IFN-γ or anti-IP-10 capture antibody (cAb) were used to separate the targets from the samples. Gold nanoparticles functionalized with anti-IFN-γ detection antibody (dAb) were also conjugated with CdS nanoparticle-terminated oligonucleotides. At the same time, anti-IP-10-AuNP-PbS conjugates were prepared. The two targets were detected separately with high sensitivity using this biosensor. Compared to TB blood test (interferon-gamma release assays) which are based on enzyme-linked immunosorbent assay (ELISA) and enzyme-linked immunosorbent spot (ELISPOT), the detection time was reduced to 1 h with comparable sensitivity using the immunosensor.

Involving IP-10 as an adjunct biomarker can improve the TB diagnosis. Since the electrochemical signals of lead and cadmium do not interfere with each other, the multiple analyte detection can be achieved using the two kinds of AuNPs functionalized with different antibody and PbS/CdS nanoparticles. A multiplex immunosensor was developed based on the detection of single cytokine. In the multiplex sensing system, MNPs for capturing IFN-γ and IP-10 were introduced to samples in buffer solution and plasma with both IFN-γ and IP-10. Then two kinds of AuNPs were used to label their targets. In one square wave voltammetry scanning, the electrochemical signals of both lead and cadmium were measured and analyzed for the detection of IP-10 and IFN-γ, respectively. It was verified that there was no cross-reaction between the detection of two targets in one sample, and a high sensitivity was achieved in both buffer solution and 10% plasma samples. This multiple analyte detection method provides a rapid and sensitive approach without the requirement of sample pretreatment and long time signal acquisition.

Future work is required to further improve the sensitivity of the immunosensor especially the differentiation between different concentrations of targets. The TB diagnosis is based on the different level of cytokines released in response to the infection, so the larger difference of signals at different concentration will provide more accurate diagnosis. This could be improved by exploring the better control of the number of nanotracers (NTs, PbS and CdS nanoparticles) conjugated to AuNPs to reduce the variation between different batches of AuNP-NT conjugates. Moreover, the optimization of electrochemical measurement such as restrained sample area on screen printed carbon electrode (SPCE) chips to minimize the effect of different area the sample spread on the electrodes, the stirring during the measurement and three electrode electrochemical

measurement system will help improving the system. The cost and complication of the optimization need to be considered.

Stability of the nanoparticles is another aspect to improve the biosensor for future practical application. The stable nanoparticles and nanoparticle conjugates with easy storage requirement and long shelf life will be important for using the biosensor in expanded detection application. Not only can the conjugates be prepared in a large batch to minimize the variation between batches, but also the transportation of the conjugates for in-field detection will be benefitted from the stability.

For future biosensor development towards the market, systematic validation on difference concentrations for multiplex detection and verification with unknown samples can be performed. Additionally, shelf life of the sensing elements and more simplified procedures to use should be considered.

The development of portable devices will greatly increase the practical applications of the biosensor. There have been several commercialized hand-held potentiostats available in market. These hand-held potentiostats can perform the same electrochemical measurement as the desktop potentiostats used in this research. Using the hand-held devices, the bacteria pathogens or diseases can be identified in a more timely manner.

Besides the aspects mentioned above, investigation of easy regeneration of the sensing materials would reduce the detection cost, and new nanomaterials can be involved in the system for detecting more than two analytes.

In summary, this research demonstrated the viability of nanotracers in immunosensors for the detection of bacterial target and protein targets. The immunosensors developed in this research can detect single or multiple targets with high sensitivity and rapidity. The

immunosensors provide promising approaches to food/water safety assurance and disease diagnosis.

APPENDIX

APPENDIX A: DATA

A.1 CHAPTER 3 DATA

Table A-1. Differential pulse voltammetry data for Figure 3-5.

Blank		Gold nanoparticle (AuNP)	
Potential (V)	Current (μA)	Potential (V)	Current (μA)
1.5	83	1.5	62
1.49	81	1.49	60
1.48	81	1.48	57
1.47	81	1.47	54
1.46	79	1.46	51
1.45	77	1.45	49
1.44	76	1.44	46
1.43	75	1.43	42
1.42	73	1.42	39
1.41	72	1.41	35
1.4	71	1.4	33
1.39	68	1.39	29
1.38	66	1.38	27
1.37	65	1.37	24
1.36	62	1.36	22
1.35	60	1.35	18
1.34	58	1.34	16
1.33	56	1.33	14
1.32	52	1.32	12
1.31	50	1.31	10
1.3	47	1.3	9
1.29	43	1.29	7
1.28	41	1.28	6
1.27	37	1.27	5
1.26	34	1.26	5
1.25	30	1.25	3
1.24	27	1.24	2
1.23	22	1.23	3
1.22	19	1.22	3
1.21	16	1.21	2
1.2	13	1.2	2
1.19	10	1.19	1
1.18	9	1.18	1
1.17	6	1.17	1
1.16	6	1.16	1

Table A-1 (cont'd).

1.15	5	1.15	1
1.14	5	1.14	1
1.13	3	1.13	1
1.12	4	1.12	1
1.11	4	1.11	1
1.1	4	1.1	1
1.09	5	1.09	1
1.08	5	1.08	1
1.07	6	1.07	1
1.06	6	1.06	0
1.05	9	1.05	1
1.04	9	1.04	0
1.03	11	1.03	0
1.02	11	1.02	2
1.01	13	1.01	1
1	14	1	1
0.99	16	0.99	1
0.98	18	0.98	2
0.97	20	0.97	2
0.96	21	0.96	2
0.95	23	0.95	2
0.94	25	0.94	3
0.93	27	0.93	3
0.92	28	0.92	3
0.91	30	0.91	3
0.9	32	0.9	3
0.89	33	0.89	4
0.88	35	0.88	5
0.87	37	0.87	5
0.86	38	0.86	6
0.85	40	0.85	6
0.84	42	0.84	7
0.83	43	0.83	7
0.82	44	0.82	8
0.81	46	0.81	8
0.8	46	0.8	10
0.79	47	0.79	10
0.78	48	0.78	11
0.77	50	0.77	12
0.76	50	0.76	12
0.75	51	0.75	14
0.74	52	0.74	14
0.73	53	0.73	15

Table A-1 (cont'd).

0.72	53	0.72	16
0.71	53	0.71	17
0.7	54	0.7	18
0.69	54	0.69	19
0.68	54	0.68	18
0.67	55	0.67	19
0.66	54	0.66	20
0.65	54	0.65	20
0.64	54	0.64	21
0.63	54	0.63	21
0.62	53	0.62	22
0.61	52	0.61	22
0.6	51	0.6	22
0.59	50	0.59	23
0.58	48	0.58	23
0.57	47	0.57	23
0.56	44	0.56	23
0.55	42	0.55	22
0.54	39	0.54	23
0.53	36	0.53	22
0.52	33	0.52	22
0.51	30	0.51	23
0.5	28	0.5	20
0.49	24	0.49	20
0.48	23	0.48	18
0.47	20	0.47	17
0.46	18	0.46	15
0.45	16	0.45	14
0.44	14	0.44	15
0.43	12	0.43	16
0.42	12	0.42	18
0.41	10	0.41	21
0.4	10	0.4	24
0.39	9	0.39	29
0.38	8	0.38	36
0.37	8	0.37	41
0.36	7	0.36	44
0.35	6	0.35	46
0.34	5	0.34	44
0.33	6	0.33	38
0.32	5	0.32	30
0.31	5	0.31	19
0.3	5	0.3	12

Table A-1 (cont'd).

0.29	4	0.29	7
0.28	4	0.28	5
0.27	4	0.27	3
0.26	3	0.26	3
0.25	4	0.25	2
0.24	3	0.24	1
0.23	4	0.23	2
0.22	4	0.22	1
0.21	3	0.21	1
0.2	2	0.2	2
0.19	3	0.19	2
0.18	1	0.18	1
0.17	2	0.17	1
0.16	2	0.16	1
0.15	2	0.15	2
0.14	3	0.14	1
0.13	1	0.13	2
0.12	3	0.12	1
0.11	2	0.11	1
0.1	3	0.1	1
0.09	2	0.09	1
0.08	1	0.08	2
0.07	1	0.07	2
0.06	2	0.06	1
0.05	1	0.05	1
0.04	1	0.04	1
0.03	2	0.03	3
0.02	1	0.02	2
0.01	2	0.01	2
0	3	0	3

Table A-2. Differential pulse voltammetry data for Figure 3-6.

Blank		10^6 cfu/ml		10^4 cfu/ml		10^2 cfu/ml	
Potential (V)	Current (μA)	Potential (V)	Current (μA)	Potential (V)	Current (μA)	Potential (V)	Current (μA)
1	4	1	2	1	3	1	4
0.99	5	0.99	2	0.99	3	0.99	3
0.98	6	0.98	3	0.98	5	0.98	3
0.97	7	0.97	2	0.97	5	0.97	5
0.96	7	0.96	3	0.96	5	0.96	4
0.95	9	0.95	4	0.95	6	0.95	5
0.94	10	0.94	5	0.94	7	0.94	5
0.93	10	0.93	5	0.93	9	0.93	7
0.92	12	0.92	5	0.92	9	0.92	8
0.91	13	0.91	6	0.91	10	0.91	9
0.9	15	0.9	6	0.9	12	0.9	10
0.89	16	0.89	8	0.89	12	0.89	11
0.88	18	0.88	7	0.88	13	0.88	12
0.87	19	0.87	8	0.87	15	0.87	13
0.86	21	0.86	9	0.86	16	0.86	14
0.85	22	0.85	11	0.85	18	0.85	16
0.84	23	0.84	11	0.84	19	0.84	18
0.83	27	0.83	13	0.83	21	0.83	19
0.82	27	0.82	14	0.82	23	0.82	20
0.81	29	0.81	16	0.81	24	0.81	22
0.8	30	0.8	17	0.8	26	0.8	23
0.79	32	0.79	19	0.79	28	0.79	25
0.78	34	0.78	19	0.78	29	0.78	27
0.77	36	0.77	20	0.77	31	0.77	28
0.76	37	0.76	23	0.76	32	0.76	30
0.75	39	0.75	24	0.75	35	0.75	31
0.74	40	0.74	25	0.74	36	0.74	33
0.73	42	0.73	26	0.73	38	0.73	34
0.72	42	0.72	27	0.72	39	0.72	36
0.71	44	0.71	29	0.71	40	0.71	37
0.7	45	0.7	31	0.7	42	0.7	38
0.69	46	0.69	31	0.69	43	0.69	40
0.68	46	0.68	32	0.68	44	0.68	41
0.67	47	0.67	33	0.67	46	0.67	42
0.66	47	0.66	34	0.66	46	0.66	43
0.65	48	0.65	36	0.65	47	0.65	44
0.64	47	0.64	36	0.64	47	0.64	45
0.63	48	0.63	37	0.63	49	0.63	46
0.62	47	0.62	37	0.62	50	0.62	47
0.61	46	0.61	38	0.61	49	0.61	46

Table A-2 (cont'd).

0.6	47	0.6	38	0.6	51	0.6	47
0.59	46	0.59	38	0.59	50	0.59	47
0.58	44	0.58	37	0.58	50	0.58	47
0.57	44	0.57	38	0.57	51	0.57	48
0.56	41	0.56	37	0.56	50	0.56	47
0.55	41	0.55	36	0.55	50	0.55	47
0.54	38	0.54	35	0.54	48	0.54	48
0.53	36	0.53	33	0.53	48	0.53	47
0.52	34	0.52	32	0.52	47	0.52	45
0.51	32	0.51	32	0.51	45	0.51	44
0.5	30	0.5	30	0.5	43	0.5	44
0.49	29	0.49	30	0.49	42	0.49	43
0.48	26	0.48	27	0.48	40	0.48	41
0.47	24	0.47	26	0.47	39	0.47	39
0.46	22	0.46	25	0.46	37	0.46	37
0.45	21	0.45	24	0.45	35	0.45	36
0.44	20	0.44	22	0.44	33	0.44	33
0.43	18	0.43	23	0.43	31	0.43	32
0.42	18	0.42	25	0.42	29	0.42	31
0.41	19	0.41	27	0.41	27	0.41	27
0.4	19	0.4	29	0.4	26	0.4	27
0.39	19	0.39	34	0.39	27	0.39	26
0.38	22	0.38	39	0.38	25	0.38	26
0.37	24	0.37	46	0.37	27	0.37	27
0.36	26	0.36	47	0.36	29	0.36	28
0.35	26	0.35	48	0.35	31	0.35	30
0.34	25	0.34	46	0.34	34	0.34	33
0.33	23	0.33	38	0.33	37	0.33	34
0.32	19	0.32	31	0.32	38	0.32	34
0.31	14	0.31	22	0.31	38	0.31	31
0.3	11	0.3	16	0.3	34	0.3	27
0.29	9	0.29	12	0.29	28	0.29	21
0.28	7	0.28	7	0.28	23	0.28	16
0.27	6	0.27	7	0.27	16	0.27	12
0.26	4	0.26	6	0.26	12	0.26	9
0.25	4	0.25	5	0.25	11	0.25	8
0.24	4	0.24	4	0.24	8	0.24	6
0.23	2	0.23	5	0.23	6	0.23	6
0.22	3	0.22	3	0.22	6	0.22	4
0.21	4	0.21	3	0.21	6	0.21	5
0.2	3	0.2	4	0.2	5	0.2	4
0.19	4	0.19	3	0.19	5	0.19	4
0.18	3	0.18	4	0.18	5	0.18	4

Table A-2 (cont'd).

0.17	3	0.17	4	0.17	5	0.17	4
0.16	3	0.16	5	0.16	5	0.16	4
0.15	3	0.15	3	0.15	5	0.15	4
0.14	4	0.14	4	0.14	5	0.14	4
0.13	4	0.13	6	0.13	5	0.13	4
0.12	4	0.12	3	0.12	5	0.12	5
0.11	4	0.11	5	0.11	5	0.11	5
0.1	4	0.1	3	0.1	5	0.1	5
0.09	4	0.09	5	0.09	5	0.09	5
0.08	4	0.08	5	0.08	5	0.08	5
0.07	4	0.07	4	0.07	5	0.07	4
0.06	4	0.06	5	0.06	5	0.06	5
0.05	4	0.05	5	0.05	6	0.05	4
0.04	4	0.04	5	0.04	6	0.04	5
0.03	5	0.03	5	0.03	5	0.03	6
0.02	4	0.02	5	0.02	6	0.02	5
0.01	4	0.01	5	0.01	6	0.01	4
0	4	0	6	0	6	0	5

Table A-3. Data for Figure 3-7. Normalized signals.

Cell concentration (cfu/ml)	Signal (signal to noise ratio)	Standard deviation
10^1	1.28	0.213
10^2	1.56	0.160
10^3	1.69	0.220
10^4	1.73	0.142
10^5	2.12	0.229
10^6	2.36	0.155

A.2 CHAPTER 4 DATA

Table A-4. Data for Figure 4-4d. Current peaks for three tubes.

Sample	Potential (V)	Current peak (μA)	Standard deviation (μA)
Blank	-0.69	2	0.0
Tube 1	-0.66	15	2.1
Tube 2	-0.68	14	3.6
Tube 3	-0.69	8	1.0

Table A-5. Square wave voltammetry data for Figure 4-5a.

Blank		10^4 cfu/ml bacteria	
Potential (V)	Current (μA)	Potential (V)	Current (μA)
-1.2	14	-1.2	6
-1.195	16	-1.195	7
-1.19	16	-1.19	7
-1.185	15	-1.185	7
-1.18	15	-1.18	7
-1.175	15	-1.175	6
-1.17	15	-1.17	8
-1.165	15	-1.165	7
-1.16	15	-1.16	8
-1.155	15	-1.155	7
-1.15	15	-1.15	5
-1.145	14	-1.145	7
-1.14	15	-1.14	6
-1.135	15	-1.135	7
-1.13	15	-1.13	6
-1.125	15	-1.125	7
-1.12	15	-1.12	8
-1.115	15	-1.115	7
-1.11	15	-1.11	7
-1.105	15	-1.105	7
-1.1	15	-1.1	7
-1.095	14	-1.095	8
-1.09	15	-1.09	6
-1.085	15	-1.085	7
-1.08	15	-1.08	7
-1.075	16	-1.075	7
-1.07	16	-1.07	7
-1.065	15	-1.065	7
-1.06	15	-1.06	7
-1.055	16	-1.055	7
-1.05	16	-1.05	7
-1.045	15	-1.045	6
-1.04	15	-1.04	7
-1.035	15	-1.035	7
-1.03	16	-1.03	7
-1.025	15	-1.025	6
-1.02	16	-1.02	6

Table A-5 (cont'd).

-1.015	14	-1.015	6
-1.01	15	-1.01	6
-1.005	15	-1.005	7
-1	15	-1	6
-0.995	14	-0.995	6
-0.99	15	-0.99	6
-0.985	14	-0.985	6
-0.98	14	-0.98	5
-0.975	14	-0.975	6
-0.97	14	-0.97	5
-0.965	13	-0.965	5
-0.96	13	-0.96	6
-0.955	13	-0.955	5
-0.95	13	-0.95	5
-0.945	12	-0.945	5
-0.94	11	-0.94	5
-0.935	11	-0.935	5
-0.93	11	-0.93	5
-0.925	10	-0.925	5
-0.92	11	-0.92	4
-0.915	9	-0.915	4
-0.91	10	-0.91	5
-0.905	10	-0.905	5
-0.9	9	-0.9	4
-0.895	10	-0.895	4
-0.89	8	-0.89	4
-0.885	9	-0.885	5
-0.88	7	-0.88	4
-0.875	8	-0.875	4
-0.87	7	-0.87	4
-0.865	7	-0.865	4
-0.86	7	-0.86	5
-0.855	8	-0.855	5
-0.85	7	-0.85	4
-0.845	8	-0.845	4
-0.84	6	-0.84	4
-0.835	6	-0.835	4
-0.83	7	-0.83	4
-0.825	7	-0.825	5

Table A-5 (cont'd).

-0.82	5	-0.82	4
-0.815	7	-0.815	4
-0.81	6	-0.81	4
-0.805	5	-0.805	4
-0.8	5	-0.8	5
-0.795	6	-0.795	5
-0.79	5	-0.79	5
-0.785	6	-0.785	5
-0.78	6	-0.78	6
-0.775	6	-0.775	6
-0.77	5	-0.77	6
-0.765	6	-0.765	7
-0.76	6	-0.76	8
-0.755	5	-0.755	8
-0.75	6	-0.75	8
-0.745	5	-0.745	9
-0.74	6	-0.74	10
-0.735	4	-0.735	11
-0.73	4	-0.73	11
-0.725	6	-0.725	12
-0.72	5	-0.72	12
-0.715	6	-0.715	13
-0.71	4	-0.71	14
-0.705	5	-0.705	14
-0.7	5	-0.7	13
-0.695	5	-0.695	13
-0.69	5	-0.69	13
-0.685	6	-0.685	12
-0.68	5	-0.68	11
-0.675	5	-0.675	11
-0.67	6	-0.67	10
-0.665	5	-0.665	8
-0.66	5	-0.66	6
-0.655	6	-0.655	5
-0.65	6	-0.65	5
-0.645	6	-0.645	5
-0.64	6	-0.64	4
-0.635	7	-0.635	4
-0.63	7	-0.63	4

Table A-5 (cont'd).

-0.625	5	-0.625	4
-0.62	7	-0.62	5
-0.615	6	-0.615	5
-0.61	5	-0.61	6
-0.605	5	-0.605	5
-0.6	6	-0.6	5
-0.595	6	-0.595	5
-0.59	5	-0.59	6
-0.585	6	-0.585	5
-0.58	4	-0.58	6
-0.575	5	-0.575	4
-0.57	5	-0.57	6
-0.565	5	-0.565	4
-0.56	5	-0.56	5
-0.555	5	-0.555	6
-0.55	5	-0.55	5
-0.545	4	-0.545	5
-0.54	5	-0.54	5
-0.535	5	-0.535	6
-0.53	5	-0.53	6
-0.525	4	-0.525	6
-0.52	5	-0.52	6
-0.515	5	-0.515	5
-0.51	5	-0.51	6
-0.505	4	-0.505	6
-0.5	6	-0.5	5
-0.495	5	-0.495	5
-0.49	5	-0.49	5
-0.485	6	-0.485	5
-0.48	5	-0.48	5
-0.475	4	-0.475	4
-0.47	5	-0.47	5
-0.465	5	-0.465	5
-0.46	5	-0.46	5
-0.455	5	-0.455	5
-0.45	5	-0.45	5
-0.445	4	-0.445	4
-0.44	5	-0.44	4
-0.435	4	-0.435	4

Table A-5 (cont'd).

-0.43	4	-0.43	5
-0.425	5	-0.425	4
-0.42	5	-0.42	5
-0.415	5	-0.415	4
-0.41	4	-0.41	4
-0.405	5	-0.405	4
-0.4	5	-0.4	5
-0.395	5	-0.395	4
-0.39	5	-0.39	4
-0.385	5	-0.385	5
-0.38	5	-0.38	5
-0.375	5	-0.375	4
-0.37	5	-0.37	5
-0.365	5	-0.365	4
-0.36	5	-0.36	5
-0.355	5	-0.355	5
-0.35	5	-0.35	4
-0.345	4	-0.345	5
-0.34	5	-0.34	4
-0.335	5	-0.335	5
-0.33	4	-0.33	5
-0.325	5	-0.325	4
-0.32	6	-0.32	5
-0.315	4	-0.315	4
-0.31	5	-0.31	5
-0.305	4	-0.305	5
-0.3	4	-0.3	5
-0.295	4	-0.295	5
-0.29	5	-0.29	5
-0.285	5	-0.285	5
-0.28	4	-0.28	6
-0.275	4	-0.275	5
-0.27	5	-0.27	5
-0.265	5	-0.265	5
-0.26	4	-0.26	5
-0.255	4	-0.255	5
-0.25	5	-0.25	5
-0.245	5	-0.245	5
-0.24	4	-0.24	5

Table A-5 (cont'd).

-0.235	5	-0.235	5
-0.23	5	-0.23	4
-0.225	5	-0.225	4
-0.22	5	-0.22	4
-0.215	5	-0.215	4
-0.21	6	-0.21	5
-0.205	4	-0.205	4
-0.2	5	-0.2	4
-0.195	5	-0.195	4
-0.19	5	-0.19	5
-0.185	4	-0.185	3
-0.18	5	-0.18	3
-0.175	5	-0.175	3
-0.17	5	-0.17	3
-0.165	4	-0.165	4
-0.16	5	-0.16	3
-0.155	4	-0.155	3
-0.15	4	-0.15	3
-0.145	5	-0.145	3
-0.14	4	-0.14	4
-0.135	5	-0.135	4
-0.13	4	-0.13	4
-0.125	4	-0.125	3
-0.12	4	-0.12	3
-0.115	4	-0.115	5
-0.11	4	-0.11	4
-0.105	5	-0.105	4
-0.1	4	-0.1	4
-0.095	4	-0.095	4
-0.09	5	-0.09	4
-0.085	5	-0.085	4
-0.08	6	-0.08	4
-0.075	5	-0.075	4
-0.07	5	-0.07	4
-0.065	5	-0.065	4
-0.06	5	-0.06	4
-0.055	6	-0.055	5
-0.05	6	-0.05	5
-0.045	6	-0.045	4

Table A-5 (cont'd).

-0.04	6	-0.04	4
-0.035	6	-0.035	4
-0.03	6	-0.03	4
-0.025	5	-0.025	3
-0.02	6	-0.02	5
-0.015	6	-0.015	4
-0.01	5	-0.01	4
-0.005	4	-0.005	4
0	4	0	4

Table A-6. Data for Figure 4-5b.

Concentration (cfu/ml)	Peak current (μA)	Standard deviation (μA)
0 (blank)	4.3	1.36
10^0	9.5	3.72
10^1	12.0	4.42
10^2	12.4	3.29
10^3	15.2	2.27
10^4	14.8	4.21
10^5	15.7	4.24
10^6	18.7	1.41

Table A-7. Data for Figure 4-6.

Sample	Peak current (μA)	Standard deviation (μA)
E. coli O157:H7	11.3	0.58
Negative control	6.0	1.00
Blank	5.7	1.15
E. coli O55:H7	6.3	0.58
E. coli C3000	7.0	1.00
*S. enteritidi*s	5.0	1.00
B. anthracis	7.3	0.58

A.3 CHAPTER 5 DATA

Table A-8. Square wave voltammetry data for Figure 5-5a.

Blank		0.1 IU/ml IFN-γ	
Potential (V)	Current (μA)	Potential (V)	Current (μA)
-1.2	5	-1.2	32
-1.195	5	-1.195	33
-1.19	6	-1.19	32
-1.185	5	-1.185	32
-1.18	5	-1.18	32
-1.175	6	-1.175	32
-1.17	5	-1.17	33
-1.165	6	-1.165	32
-1.16	5	-1.16	32
-1.155	5	-1.155	30
-1.15	6	-1.15	31
-1.145	5	-1.145	30
-1.14	5	-1.14	31
-1.135	4	-1.135	30
-1.13	5	-1.13	30
-1.125	5	-1.125	27
-1.12	4	-1.12	28
-1.115	5	-1.115	28
-1.11	5	-1.11	28
-1.105	5	-1.105	27
-1.1	4	-1.1	27
-1.095	5	-1.095	27
-1.09	4	-1.09	26
-1.085	5	-1.085	25
-1.08	5	-1.08	25
-1.075	5	-1.075	24
-1.07	4	-1.07	25
-1.065	5	-1.065	23
-1.06	5	-1.06	24
-1.055	5	-1.055	23
-1.05	4	-1.05	22
-1.045	4	-1.045	21
-1.04	5	-1.04	22
-1.035	4	-1.035	21
-1.03	4	-1.03	21
-1.025	4	-1.025	21
-1.02	4	-1.02	21
-1.015	4	-1.015	21
-1.01	5	-1.01	21

Table A-8 (cont'd).

-1.005	5	-1.005	20
-1	4	-1	20
-0.995	4	-0.995	21
-0.99	4	-0.99	21
-0.985	5	-0.985	21
-0.98	4	-0.98	20
-0.975	4	-0.975	20
-0.97	5	-0.97	20
-0.965	3	-0.965	20
-0.96	5	-0.96	20
-0.955	4	-0.955	20
-0.95	4	-0.95	21
-0.945	6	-0.945	21
-0.94	6	-0.94	20
-0.935	4	-0.935	21
-0.93	4	-0.93	21
-0.925	5	-0.925	20
-0.92	3	-0.92	20
-0.915	4	-0.915	21
-0.91	5	-0.91	20
-0.905	4	-0.905	20
-0.9	2	-0.9	20
-0.895	3	-0.895	19
-0.89	3	-0.89	19
-0.885	3	-0.885	19
-0.88	3	-0.88	18
-0.875	4	-0.875	18
-0.87	3	-0.87	18
-0.865	4	-0.865	19
-0.86	3	-0.86	18
-0.855	3	-0.855	17
-0.85	3	-0.85	17
-0.845	3	-0.845	16
-0.84	3	-0.84	16
-0.835	3	-0.835	16
-0.83	3	-0.83	16
-0.825	3	-0.825	15
-0.82	3	-0.82	15
-0.815	3	-0.815	15
-0.81	2	-0.81	14
-0.805	3	-0.805	14
-0.8	2	-0.8	13
-0.795	2	-0.795	13

Table A-8 (cont'd).

-0.79	3	-0.79	14
-0.785	3	-0.785	13
-0.78	3	-0.78	13
-0.775	3	-0.775	13
-0.77	3	-0.77	13
-0.765	3	-0.765	13
-0.76	2	-0.76	13
-0.755	2	-0.755	13
-0.75	2	-0.75	14
-0.745	2	-0.745	14
-0.74	2	-0.74	13
-0.735	2	-0.735	14
-0.73	2	-0.73	14
-0.725	2	-0.725	15
-0.72	3	-0.72	15
-0.715	1	-0.715	14
-0.71	2	-0.71	14
-0.705	2	-0.705	15
-0.7	2	-0.7	15
-0.695	2	-0.695	15
-0.69	2	-0.69	14
-0.685	2	-0.685	15
-0.68	2	-0.68	14
-0.675	2	-0.675	15
-0.67	2	-0.67	15
-0.665	2	-0.665	15
-0.66	2	-0.66	15
-0.655	2	-0.655	14
-0.65	2	-0.65	15
-0.645	1	-0.645	15
-0.64	1	-0.64	15
-0.635	1	-0.635	15
-0.63	1	-0.63	15
-0.625	1	-0.625	15
-0.62	1	-0.62	15
-0.615	2	-0.615	14
-0.61	1	-0.61	15
-0.605	2	-0.605	14
-0.6	2	-0.6	14
-0.595	2	-0.595	15
-0.59	2	-0.59	14
-0.585	2	-0.585	14
-0.58	2	-0.58	14

Table A-8 (cont'd).

-0.575	2	-0.575	14
-0.57	2	-0.57	14
-0.565	2	-0.565	13
-0.56	2	-0.56	14
-0.555	2	-0.555	14
-0.55	1	-0.55	13
-0.545	1	-0.545	13
-0.54	1	-0.54	13
-0.535	1	-0.535	13
-0.53	1	-0.53	13
-0.525	1	-0.525	13
-0.52	1	-0.52	13
-0.515	1	-0.515	13
-0.51	1	-0.51	13
-0.505	1	-0.505	12
-0.5	1	-0.5	12
-0.495	1	-0.495	13
-0.49	1	-0.49	12
-0.485	1	-0.485	13
-0.48	1	-0.48	12
-0.475	1	-0.475	12
-0.47	0	-0.47	12
-0.465	1	-0.465	12
-0.46	2	-0.46	12
-0.455	1	-0.455	12
-0.45	0	-0.45	12
-0.445	1	-0.445	11
-0.44	2	-0.44	12
-0.435	2	-0.435	11
-0.43	2	-0.43	11
-0.425	1	-0.425	12
-0.42	2	-0.42	11
-0.415	0	-0.415	11
-0.41	2	-0.41	11
-0.405	1	-0.405	11
-0.4	-1	-0.4	11
-0.395	0	-0.395	12
-0.39	0	-0.39	11
-0.385	2	-0.385	11
-0.38	1	-0.38	11
-0.375	0	-0.375	10
-0.37	0	-0.37	10
-0.365	1	-0.365	11

Table A-8 (cont'd).

-0.36	2	-0.36	10
-0.355	2	-0.355	10
-0.35	1	-0.35	11
-0.345	1	-0.345	11
-0.34	0	-0.34	10
-0.335	1	-0.335	10
-0.33	2	-0.33	10
-0.325	1	-0.325	10
-0.32	1	-0.32	9
-0.315	1	-0.315	9
-0.31	1	-0.31	10
-0.305	1	-0.305	9
-0.3	1	-0.3	9
-0.295	1	-0.295	9
-0.29	1	-0.29	9
-0.285	1	-0.285	9
-0.28	1	-0.28	9
-0.275	1	-0.275	9
-0.27	2	-0.27	9
-0.265	1	-0.265	8
-0.26	1	-0.26	9
-0.255	0	-0.255	9
-0.25	1	-0.25	8
-0.245	1	-0.245	8
-0.24	1	-0.24	9
-0.235	1	-0.235	7
-0.23	1	-0.23	8
-0.225	1	-0.225	8
-0.22	2	-0.22	9
-0.215	1	-0.215	9
-0.21	1	-0.21	8
-0.205	2	-0.205	9
-0.2	1	-0.2	7
-0.195	2	-0.195	8
-0.19	0	-0.19	8
-0.185	1	-0.185	9
-0.18	1	-0.18	8
-0.175	1	-0.175	10
-0.17	1	-0.17	8
-0.165	1	-0.165	10
-0.16	1	-0.16	9
-0.155	2	-0.155	10
-0.15	1	-0.15	10

Table A-8 (cont'd).

-0.145	2	-0.145	10
-0.14	2	-0.14	9
-0.135	1	-0.135	11
-0.13	1	-0.13	11
-0.125	1	-0.125	10
-0.12	2	-0.12	11
-0.115	1	-0.115	9
-0.11	2	-0.11	11
-0.105	2	-0.105	10
-0.1	1	-0.1	10
-0.095	1	-0.095	9
-0.09	2	-0.09	9
-0.085	2	-0.085	9
-0.08	2	-0.08	11
-0.075	1	-0.075	10
-0.07	2	-0.07	10
-0.065	1	-0.065	10
-0.06	1	-0.06	9
-0.055	2	-0.055	11
-0.05	0	-0.05	10
-0.045	2	-0.045	10
-0.04	2	-0.04	11
-0.035	1	-0.035	11
-0.03	1	-0.03	10
-0.025	1	-0.025	12
-0.02	1	-0.02	12
-0.015	1	-0.015	11
-0.01	1	-0.01	12
-0.005	2	-0.005	12
0	2	0	14

Table A-9. Square wave voltammetry data for Figure 5-5b.

Blank		10 ng/ml IP-10	
Potential (V)	Current (μA)	Potential (V)	Current (μA)
-1.2	9	-1.2	5
-1.195	10	-1.195	6
-1.19	8	-1.19	6
-1.185	8	-1.185	5
-1.18	9	-1.18	6
-1.175	9	-1.175	6
-1.17	8	-1.17	6
-1.165	8	-1.165	6
-1.16	8	-1.16	6
-1.155	8	-1.155	6
-1.15	8	-1.15	5
-1.145	9	-1.145	6
-1.14	8	-1.14	6
-1.135	8	-1.135	6
-1.13	8	-1.13	6
-1.125	8	-1.125	7
-1.12	8	-1.12	6
-1.115	8	-1.115	5
-1.11	8	-1.11	6
-1.105	8	-1.105	6
-1.1	8	-1.1	6
-1.095	7	-1.095	6
-1.09	8	-1.09	7
-1.085	8	-1.085	6
-1.08	7	-1.08	6
-1.075	7	-1.075	6
-1.07	8	-1.07	6
-1.065	7	-1.065	5
-1.06	8	-1.06	5
-1.055	7	-1.055	6
-1.05	8	-1.05	5
-1.045	7	-1.045	6
-1.04	6	-1.04	6
-1.035	7	-1.035	5
-1.03	7	-1.03	6
-1.025	7	-1.025	5
-1.02	6	-1.02	5
-1.015	7	-1.015	6
-1.01	6	-1.01	5
-1.005	7	-1.005	5
-1	6	-1	5

Table A-9 (cont'd).

-0.995	7	-0.995	5
-0.99	7	-0.99	5
-0.985	7	-0.985	5
-0.98	6	-0.98	5
-0.975	6	-0.975	5
-0.97	7	-0.97	4
-0.965	6	-0.965	5
-0.96	6	-0.96	5
-0.955	6	-0.955	4
-0.95	6	-0.95	4
-0.945	7	-0.945	5
-0.94	6	-0.94	5
-0.935	6	-0.935	4
-0.93	7	-0.93	4
-0.925	6	-0.925	4
-0.92	6	-0.92	4
-0.915	7	-0.915	5
-0.91	6	-0.91	5
-0.905	6	-0.905	4
-0.9	5	-0.9	4
-0.895	6	-0.895	4
-0.89	6	-0.89	4
-0.885	6	-0.885	4
-0.88	5	-0.88	5
-0.875	6	-0.875	4
-0.87	5	-0.87	4
-0.865	5	-0.865	4
-0.86	6	-0.86	5
-0.855	6	-0.855	5
-0.85	5	-0.85	3
-0.845	5	-0.845	4
-0.84	6	-0.84	3
-0.835	5	-0.835	5
-0.83	5	-0.83	4
-0.825	5	-0.825	2
-0.82	5	-0.82	3
-0.815	5	-0.815	3
-0.81	5	-0.81	3
-0.805	5	-0.805	5
-0.8	6	-0.8	4
-0.795	6	-0.795	5
-0.79	5	-0.79	5
-0.785	5	-0.785	3

Table A-9 (cont'd).

-0.78	5	-0.78	4
-0.775	5	-0.775	4
-0.77	5	-0.77	4
-0.765	5	-0.765	4
-0.76	5	-0.76	4
-0.755	5	-0.755	5
-0.75	5	-0.75	5
-0.745	4	-0.745	5
-0.74	5	-0.74	6
-0.735	5	-0.735	6
-0.73	5	-0.73	7
-0.725	5	-0.725	8
-0.72	5	-0.72	8
-0.715	4	-0.715	10
-0.71	5	-0.71	10
-0.705	5	-0.705	11
-0.7	5	-0.7	12
-0.695	5	-0.695	13
-0.69	5	-0.69	14
-0.685	4	-0.685	13
-0.68	4	-0.68	15
-0.675	5	-0.675	15
-0.67	5	-0.67	14
-0.665	4	-0.665	14
-0.66	5	-0.66	12
-0.655	4	-0.655	9
-0.65	4	-0.65	7
-0.645	4	-0.645	6
-0.64	4	-0.64	5
-0.635	4	-0.635	5
-0.63	4	-0.63	5
-0.625	4	-0.625	4
-0.62	3	-0.62	5
-0.615	3	-0.615	5
-0.61	3	-0.61	4
-0.605	3	-0.605	4
-0.6	3	-0.6	4
-0.595	3	-0.595	5
-0.59	3	-0.59	5
-0.585	3	-0.585	4
-0.58	3	-0.58	4
-0.575	3	-0.575	5
-0.57	3	-0.57	5

Table A-9 (cont'd).

-0.565	2	-0.565	5
-0.56	2	-0.56	5
-0.555	2	-0.555	5
-0.55	2	-0.55	4
-0.545	2	-0.545	4
-0.54	2	-0.54	4
-0.535	2	-0.535	4
-0.53	2	-0.53	4
-0.525	2	-0.525	4
-0.52	2	-0.52	4
-0.515	2	-0.515	4
-0.51	2	-0.51	4
-0.505	2	-0.505	5
-0.5	2	-0.5	5
-0.495	2	-0.495	4
-0.49	2	-0.49	5
-0.485	2	-0.485	5
-0.48	2	-0.48	5
-0.475	2	-0.475	4
-0.47	2	-0.47	4
-0.465	1	-0.465	4
-0.46	1	-0.46	4
-0.455	1	-0.455	5
-0.45	2	-0.45	5
-0.445	2	-0.445	5
-0.44	2	-0.44	5
-0.435	2	-0.435	5
-0.43	2	-0.43	5
-0.425	2	-0.425	5
-0.42	2	-0.42	4
-0.415	2	-0.415	4
-0.41	2	-0.41	5
-0.405	2	-0.405	5
-0.4	2	-0.4	5
-0.395	2	-0.395	5
-0.39	1	-0.39	5
-0.385	2	-0.385	5
-0.38	1	-0.38	5
-0.375	3	-0.375	4
-0.37	2	-0.37	4
-0.365	2	-0.365	5
-0.36	2	-0.36	5
-0.355	3	-0.355	5

Table A-9 (cont'd).

-0.35	2	-0.35	5
-0.345	2	-0.345	5
-0.34	3	-0.34	5
-0.335	3	-0.335	5
-0.33	3	-0.33	4
-0.325	3	-0.325	5
-0.32	3	-0.32	5
-0.315	4	-0.315	5
-0.31	3	-0.31	6
-0.305	3	-0.305	6
-0.3	3	-0.3	6
-0.295	3	-0.295	7
-0.29	3	-0.29	7
-0.285	3	-0.285	6
-0.28	3	-0.28	7
-0.275	3	-0.275	7
-0.27	3	-0.27	7
-0.265	3	-0.265	8
-0.26	3	-0.26	7
-0.255	3	-0.255	7
-0.25	2	-0.25	8
-0.245	4	-0.245	8
-0.24	4	-0.24	8
-0.235	3	-0.235	8
-0.23	4	-0.23	8
-0.225	4	-0.225	9
-0.22	4	-0.22	8
-0.215	4	-0.215	8
-0.21	3	-0.21	8
-0.205	3	-0.205	8
-0.2	4	-0.2	8
-0.195	2	-0.195	8
-0.19	4	-0.19	8
-0.185	4	-0.185	7
-0.18	3	-0.18	7
-0.175	3	-0.175	7
-0.17	3	-0.17	7
-0.165	3	-0.165	6
-0.16	3	-0.16	6
-0.155	3	-0.155	6
-0.15	3	-0.15	6
-0.145	3	-0.145	6
-0.14	3	-0.14	5

Table A-9 (cont'd).

-0.135	3	-0.135	5
-0.13	2	-0.13	5
-0.125	3	-0.125	5
-0.12	3	-0.12	5
-0.115	3	-0.115	5
-0.11	2	-0.11	5
-0.105	3	-0.105	5
-0.1	2	-0.1	5
-0.095	3	-0.095	5
-0.09	3	-0.09	5
-0.085	2	-0.085	5
-0.08	3	-0.08	5
-0.075	2	-0.075	5
-0.07	3	-0.07	5
-0.065	3	-0.065	5
-0.06	3	-0.06	5
-0.055	3	-0.055	5
-0.05	3	-0.05	5
-0.045	2	-0.045	5
-0.04	2	-0.04	5
-0.035	2	-0.035	5
-0.03	3	-0.03	5
-0.025	2	-0.025	5
-0.02	2	-0.02	5
-0.015	2	-0.015	5
-0.01	3	-0.01	5
-0.005	2	-0.005	6
0	3	0	5

Table A-10. Data for Figure 5-6a.

Concentration (IU/ml)	Peak current (μA)	Standard deviation (μA)
0	4.6	2.10
0.01	11.8	2.41
0.1	16.9	2.19
1	19.4	3.96
10	17.1	3.15

Table A-11. Data for Figure 5-6b.

Concentration (ng/ml)	Peak current (μA)	Standard deviation (μA)
0	3.5	1.58
0.001	10.0	1.20
0.01	9.2	1.89
0.1	9.7	4.17
1	9.7	3.50
10	11.8	4.26
100	12.9	3.58

Table A-12. Data for Figure 5-6b insert.

Concentration (ng/ml)	Current (μA, peak current-blank)	Standard deviation (μA)
0.001	7.33	0.33
0.01	7.52	1.12
0.1	8.11	1.71
1	8.83	1.64
10	12.33	1.05
100	13.60	1.75

A.4 CHAPTER 6 DATA

Table A-13. Square wave voltammetry data for Figure 6-2a.

Control		PbS	
Potential (V)	Current (μA)	Potential (V)	Current (μA)
-1.2	4	-1.2	8
-1.195	3	-1.195	9
-1.19	4	-1.19	9
-1.185	3	-1.185	10
-1.18	4	-1.18	8
-1.175	3	-1.175	10
-1.17	3	-1.17	9
-1.165	3	-1.165	9
-1.16	4	-1.16	8
-1.155	3	-1.155	8
-1.15	4	-1.15	7
-1.145	3	-1.145	9
-1.14	4	-1.14	10
-1.135	3	-1.135	8
-1.13	4	-1.13	9
-1.125	3	-1.125	9
-1.12	3	-1.12	9
-1.115	4	-1.115	9
-1.11	3	-1.11	9
-1.105	3	-1.105	10
-1.1	3	-1.1	8
-1.095	4	-1.095	9
-1.09	3	-1.09	9
-1.085	3	-1.085	9
-1.08	3	-1.08	7
-1.075	3	-1.075	8
-1.07	3	-1.07	8
-1.065	3	-1.065	8
-1.06	3	-1.06	8
-1.055	3	-1.055	7
-1.05	3	-1.05	8
-1.045	3	-1.045	7
-1.04	2	-1.04	8
-1.035	3	-1.035	7
-1.03	3	-1.03	7
-1.025	2	-1.025	8
-1.02	3	-1.02	6
-1.015	3	-1.015	7

Table A-13 (cont'd).

-1.01	2	-1.01	7
-1.005	3	-1.005	7
-1	3	-1	8
-0.995	3	-0.995	7
-0.99	3	-0.99	8
-0.985	3	-0.985	7
-0.98	3	-0.98	7
-0.975	2	-0.975	7
-0.97	2	-0.97	7
-0.965	3	-0.965	8
-0.96	3	-0.96	8
-0.955	2	-0.955	6
-0.95	2	-0.95	7
-0.945	3	-0.945	7
-0.94	3	-0.94	7
-0.935	3	-0.935	7
-0.93	3	-0.93	7
-0.925	2	-0.925	7
-0.92	2	-0.92	7
-0.915	3	-0.915	7
-0.91	3	-0.91	7
-0.905	3	-0.905	7
-0.9	2	-0.9	7
-0.895	2	-0.895	6
-0.89	2	-0.89	7
-0.885	3	-0.885	7
-0.88	2	-0.88	7
-0.875	3	-0.875	6
-0.87	2	-0.87	7
-0.865	2	-0.865	8
-0.86	2	-0.86	7
-0.855	3	-0.855	7
-0.85	3	-0.85	7
-0.845	2	-0.845	8
-0.84	2	-0.84	8
-0.835	2	-0.835	7
-0.83	2	-0.83	7
-0.825	2	-0.825	7
-0.82	3	-0.82	7
-0.815	3	-0.815	8
-0.81	3	-0.81	7
-0.805	3	-0.805	8
-0.8	3	-0.8	7

Table A-13 (cont'd).

-0.795	3	-0.795	8
-0.79	2	-0.79	8
-0.785	2	-0.785	8
-0.78	3	-0.78	8
-0.775	2	-0.775	8
-0.77	2	-0.77	8
-0.765	2	-0.765	8
-0.76	3	-0.76	9
-0.755	4	-0.755	9
-0.75	2	-0.75	9
-0.745	2	-0.745	9
-0.74	2	-0.74	10
-0.735	3	-0.735	12
-0.73	2	-0.73	11
-0.725	3	-0.725	12
-0.72	3	-0.72	13
-0.715	4	-0.715	13
-0.71	2	-0.71	13
-0.705	2	-0.705	14
-0.7	2	-0.7	14
-0.695	1	-0.695	14
-0.69	3	-0.69	16
-0.685	2	-0.685	16
-0.68	2	-0.68	17
-0.675	3	-0.675	17
-0.67	2	-0.67	18
-0.665	2	-0.665	18
-0.66	3	-0.66	18
-0.655	1	-0.655	19
-0.65	1	-0.65	19
-0.645	3	-0.645	18
-0.64	3	-0.64	19
-0.635	2	-0.635	18
-0.63	2	-0.63	18
-0.625	1	-0.625	16
-0.62	3	-0.62	16
-0.615	0	-0.615	15
-0.61	4	-0.61	14
-0.605	2	-0.605	12
-0.6	2	-0.6	11
-0.595	2	-0.595	11
-0.59	1	-0.59	9
-0.585	1	-0.585	8

Table A-13 (cont'd).

-0.58	1	-0.58	9
-0.575	2	-0.575	8
-0.57	2	-0.57	8
-0.565	2	-0.565	8
-0.56	2	-0.56	8
-0.555	2	-0.555	7
-0.55	1	-0.55	8
-0.545	2	-0.545	8
-0.54	2	-0.54	8
-0.535	2	-0.535	8
-0.53	2	-0.53	7
-0.525	2	-0.525	7
-0.52	2	-0.52	8
-0.515	2	-0.515	8
-0.51	2	-0.51	7
-0.505	2	-0.505	7
-0.5	1	-0.5	7
-0.495	2	-0.495	8
-0.49	2	-0.49	8
-0.485	2	-0.485	8
-0.48	2	-0.48	8
-0.475	2	-0.475	8
-0.47	2	-0.47	7
-0.465	1	-0.465	8
-0.46	1	-0.46	8
-0.455	1	-0.455	8
-0.45	1	-0.45	8
-0.445	2	-0.445	8
-0.44	1	-0.44	7
-0.435	2	-0.435	7
-0.43	2	-0.43	7
-0.425	2	-0.425	7
-0.42	2	-0.42	8
-0.415	2	-0.415	8
-0.41	1	-0.41	7
-0.405	1	-0.405	7
-0.4	1	-0.4	7
-0.395	2	-0.395	8
-0.39	2	-0.39	7
-0.385	2	-0.385	7
-0.38	2	-0.38	7
-0.375	2	-0.375	7
-0.37	2	-0.37	7

Table A-13 (cont'd).

-0.365	2	-0.365	8
-0.36	2	-0.36	8
-0.355	2	-0.355	8
-0.35	2	-0.35	8
-0.345	2	-0.345	7
-0.34	2	-0.34	7
-0.335	2	-0.335	7
-0.33	2	-0.33	7
-0.325	2	-0.325	7
-0.32	1	-0.32	7
-0.315	1	-0.315	8
-0.31	2	-0.31	7
-0.305	2	-0.305	7
-0.3	2	-0.3	8
-0.295	2	-0.295	7
-0.29	2	-0.29	7
-0.285	3	-0.285	7
-0.28	3	-0.28	7
-0.275	3	-0.275	7
-0.27	2	-0.27	7
-0.265	2	-0.265	8
-0.26	2	-0.26	8
-0.255	2	-0.255	8
-0.25	2	-0.25	8
-0.245	2	-0.245	8
-0.24	2	-0.24	8
-0.235	3	-0.235	7
-0.23	2	-0.23	9
-0.225	3	-0.225	7
-0.22	3	-0.22	8
-0.215	3	-0.215	8
-0.21	3	-0.21	8
-0.205	3	-0.205	8
-0.2	3	-0.2	8
-0.195	3	-0.195	8
-0.19	2	-0.19	8
-0.185	3	-0.185	8
-0.18	2	-0.18	8
-0.175	2	-0.175	8
-0.17	3	-0.17	8
-0.165	2	-0.165	8
-0.16	2	-0.16	9
-0.155	2	-0.155	8

Table A-13 (cont'd).

-0.15	2	-0.15	8
-0.145	3	-0.145	8
-0.14	3	-0.14	9
-0.135	3	-0.135	8
-0.13	3	-0.13	9
-0.125	2	-0.125	9
-0.12	2	-0.12	9
-0.115	2	-0.115	9
-0.11	2	-0.11	9
-0.105	2	-0.105	9
-0.1	2	-0.1	9
-0.095	2	-0.095	10
-0.09	2	-0.09	10
-0.085	2	-0.085	10
-0.08	2	-0.08	10
-0.075	2	-0.075	10
-0.07	2	-0.07	10
-0.065	2	-0.065	9
-0.06	2	-0.06	10
-0.055	2	-0.055	10
-0.05	2	-0.05	9
-0.045	2	-0.045	10
-0.04	2	-0.04	10
-0.035	2	-0.035	10
-0.03	2	-0.03	10
-0.025	2	-0.025	10
-0.02	2	-0.02	10
-0.015	2	-0.015	10
-0.01	2	-0.01	10
-0.005	2	-0.005	9
0	2	0	10

Table A-14. Square wave voltammetry data for Figure 6-2b.

Control		CdS	
Potential (V)	Current (μA)	Potential (V)	Current (μA)
-1.2	4	-1.2	15
-1.195	3	-1.195	15
-1.19	3	-1.19	14
-1.185	3	-1.185	15
-1.18	4	-1.18	13
-1.175	3	-1.175	13
-1.17	3	-1.17	13
-1.165	4	-1.165	13
-1.16	3	-1.16	13
-1.155	4	-1.155	12
-1.15	3	-1.15	12
-1.145	3	-1.145	11
-1.14	3	-1.14	12
-1.135	3	-1.135	11
-1.13	3	-1.13	12
-1.125	3	-1.125	11
-1.12	3	-1.12	11
-1.115	3	-1.115	12
-1.11	3	-1.11	10
-1.105	3	-1.105	10
-1.1	3	-1.1	10
-1.095	3	-1.095	10
-1.09	3	-1.09	11
-1.085	3	-1.085	9
-1.08	3	-1.08	10
-1.075	3	-1.075	10
-1.07	4	-1.07	10
-1.065	3	-1.065	9
-1.06	3	-1.06	10
-1.055	3	-1.055	10
-1.05	3	-1.05	10
-1.045	3	-1.045	9
-1.04	3	-1.04	9
-1.035	3	-1.035	9
-1.03	2	-1.03	10
-1.025	3	-1.025	8
-1.02	3	-1.02	11
-1.015	3	-1.015	10
-1.01	4	-1.01	10
-1.005	3	-1.005	9
-1	3	-1	9

Table A-14 (cont'd).

-0.995	3	-0.995	10
-0.99	3	-0.99	10
-0.985	3	-0.985	10
-0.98	2	-0.98	12
-0.975	2	-0.975	11
-0.97	3	-0.97	11
-0.965	3	-0.965	12
-0.96	3	-0.96	15
-0.955	2	-0.955	14
-0.95	2	-0.95	15
-0.945	2	-0.945	17
-0.94	3	-0.94	18
-0.935	2	-0.935	17
-0.93	3	-0.93	18
-0.925	2	-0.925	18
-0.92	2	-0.92	18
-0.915	2	-0.915	18
-0.91	2	-0.91	19
-0.905	3	-0.905	19
-0.9	3	-0.9	18
-0.895	3	-0.895	18
-0.89	3	-0.89	17
-0.885	2	-0.885	14
-0.88	2	-0.88	12
-0.875	2	-0.875	12
-0.87	3	-0.87	10
-0.865	2	-0.865	8
-0.86	3	-0.86	8
-0.855	3	-0.855	8
-0.85	1	-0.85	8
-0.845	2	-0.845	7
-0.84	2	-0.84	7
-0.835	2	-0.835	8
-0.83	3	-0.83	7
-0.825	2	-0.825	7
-0.82	2	-0.82	7
-0.815	2	-0.815	6
-0.81	1	-0.81	6
-0.805	2	-0.805	6
-0.8	1	-0.8	7
-0.795	2	-0.795	7
-0.79	1	-0.79	7
-0.785	2	-0.785	7

Table A-14 (cont'd).

-0.78	3	-0.78	6
-0.775	2	-0.775	6
-0.77	2	-0.77	7
-0.765	3	-0.765	6
-0.76	3	-0.76	7
-0.755	2	-0.755	6
-0.75	3	-0.75	6
-0.745	2	-0.745	6
-0.74	2	-0.74	5
-0.735	2	-0.735	5
-0.73	2	-0.73	6
-0.725	4	-0.725	6
-0.72	2	-0.72	6
-0.715	3	-0.715	6
-0.71	2	-0.71	6
-0.705	2	-0.705	5
-0.7	1	-0.7	5
-0.695	2	-0.695	6
-0.69	3	-0.69	6
-0.685	3	-0.685	6
-0.68	2	-0.68	6
-0.675	4	-0.675	6
-0.67	4	-0.67	6
-0.665	2	-0.665	6
-0.66	2	-0.66	6
-0.655	3	-0.655	5
-0.65	3	-0.65	6
-0.645	3	-0.645	6
-0.64	3	-0.64	6
-0.635	3	-0.635	6
-0.63	2	-0.63	6
-0.625	3	-0.625	6
-0.62	3	-0.62	6
-0.615	3	-0.615	7
-0.61	3	-0.61	6
-0.605	3	-0.605	6
-0.6	3	-0.6	6
-0.595	3	-0.595	6
-0.59	2	-0.59	5
-0.585	3	-0.585	6
-0.58	3	-0.58	5
-0.575	3	-0.575	6
-0.57	3	-0.57	6

Table A-14 (cont'd).

-0.565	2	-0.565	6
-0.56	3	-0.56	6
-0.555	3	-0.555	6
-0.55	3	-0.55	6
-0.545	3	-0.545	6
-0.54	2	-0.54	6
-0.535	2	-0.535	6
-0.53	2	-0.53	6
-0.525	3	-0.525	6
-0.52	3	-0.52	5
-0.515	3	-0.515	5
-0.51	3	-0.51	5
-0.505	2	-0.505	6
-0.5	2	-0.5	6
-0.495	3	-0.495	5
-0.49	3	-0.49	5
-0.485	3	-0.485	6
-0.48	3	-0.48	6
-0.475	3	-0.475	6
-0.47	2	-0.47	5
-0.465	2	-0.465	5
-0.46	2	-0.46	6
-0.455	3	-0.455	6
-0.45	3	-0.45	5
-0.445	3	-0.445	5
-0.44	3	-0.44	5
-0.435	2	-0.435	5
-0.43	2	-0.43	6
-0.425	2	-0.425	5
-0.42	2	-0.42	5
-0.415	2	-0.415	6
-0.41	3	-0.41	6
-0.405	3	-0.405	5
-0.4	3	-0.4	5
-0.395	3	-0.395	6
-0.39	3	-0.39	5
-0.385	3	-0.385	5
-0.38	2	-0.38	5
-0.375	3	-0.375	6
-0.37	3	-0.37	5
-0.365	2	-0.365	5
-0.36	2	-0.36	5
-0.355	2	-0.355	6

Table A-14 (cont'd).

-0.35	2	-0.35	5
-0.345	2	-0.345	6
-0.34	2	-0.34	5
-0.335	2	-0.335	5
-0.33	2	-0.33	5
-0.325	2	-0.325	6
-0.32	2	-0.32	5
-0.315	2	-0.315	5
-0.31	2	-0.31	5
-0.305	2	-0.305	5
-0.3	2	-0.3	5
-0.295	3	-0.295	5
-0.29	3	-0.29	6
-0.285	2	-0.285	5
-0.28	2	-0.28	5
-0.275	2	-0.275	5
-0.27	2	-0.27	5
-0.265	2	-0.265	5
-0.26	2	-0.26	5
-0.255	3	-0.255	5
-0.25	2	-0.25	5
-0.245	3	-0.245	5
-0.24	2	-0.24	4
-0.235	2	-0.235	4
-0.23	2	-0.23	5
-0.225	2	-0.225	4
-0.22	2	-0.22	4
-0.215	2	-0.215	4
-0.21	2	-0.21	4
-0.205	1	-0.205	4
-0.2	2	-0.2	4
-0.195	2	-0.195	4
-0.19	3	-0.19	4
-0.185	3	-0.185	4
-0.18	1	-0.18	4
-0.175	2	-0.175	4
-0.17	1	-0.17	4
-0.165	1	-0.165	4
-0.16	2	-0.16	4
-0.155	2	-0.155	4
-0.15	2	-0.15	4
-0.145	2	-0.145	4
-0.14	2	-0.14	4

Table A-14 (cont'd).

-0.135	2	-0.135	5
-0.13	2	-0.13	4
-0.125	2	-0.125	5
-0.12	2	-0.12	5
-0.115	2	-0.115	5
-0.11	2	-0.11	5
-0.105	2	-0.105	5
-0.1	2	-0.1	5
-0.095	2	-0.095	5
-0.09	2	-0.09	5
-0.085	2	-0.085	5
-0.08	2	-0.08	5
-0.075	2	-0.075	5
-0.07	2	-0.07	6
-0.065	2	-0.065	6
-0.06	2	-0.06	5
-0.055	2	-0.055	5
-0.05	2	-0.05	5
-0.045	2	-0.045	5
-0.04	2	-0.04	5
-0.035	2	-0.035	5
-0.03	2	-0.03	5
-0.025	2	-0.025	6
-0.02	2	-0.02	6
-0.015	2	-0.015	5
-0.01	2	-0.01	5
-0.005	2	-0.005	6
0	2	0	6

Table A-15. Square wave voltammetry data for Figure 6-2c.

Control		PbS+CdS	
Potential (V)	Current (μA)	Potential (V)	Current (μA)
-1.2	4	-1.2	13
-1.195	3	-1.195	15
-1.19	3	-1.19	14
-1.185	3	-1.185	13
-1.18	4	-1.18	14
-1.175	3	-1.175	13
-1.17	3	-1.17	12
-1.165	4	-1.165	13
-1.16	3	-1.16	13
-1.155	4	-1.155	13
-1.15	3	-1.15	12
-1.145	3	-1.145	12
-1.14	3	-1.14	11
-1.135	3	-1.135	13
-1.13	3	-1.13	13
-1.125	3	-1.125	11
-1.12	3	-1.12	12
-1.115	3	-1.115	12
-1.11	3	-1.11	9
-1.105	3	-1.105	12
-1.1	3	-1.1	12
-1.095	3	-1.095	12
-1.09	3	-1.09	12
-1.085	3	-1.085	11
-1.08	3	-1.08	11
-1.075	3	-1.075	10
-1.07	4	-1.07	10
-1.065	3	-1.065	10
-1.06	3	-1.06	11
-1.055	3	-1.055	10
-1.05	3	-1.05	9
-1.045	3	-1.045	10
-1.04	3	-1.04	10
-1.035	3	-1.035	10
-1.03	2	-1.03	11
-1.025	3	-1.025	10
-1.02	3	-1.02	11
-1.015	3	-1.015	11
-1.01	4	-1.01	11
-1.005	3	-1.005	11
-1	3	-1	10

Table A-15 (cont'd).

-0.995	3	-0.995	12
-0.99	3	-0.99	12
-0.985	3	-0.985	12
-0.98	2	-0.98	13
-0.975	2	-0.975	13
-0.97	3	-0.97	15
-0.965	3	-0.965	15
-0.96	3	-0.96	17
-0.955	2	-0.955	18
-0.95	2	-0.95	20
-0.945	2	-0.945	21
-0.94	3	-0.94	21
-0.935	2	-0.935	23
-0.93	3	-0.93	24
-0.925	2	-0.925	25
-0.92	2	-0.92	25
-0.915	2	-0.915	26
-0.91	2	-0.91	26
-0.905	3	-0.905	25
-0.9	3	-0.9	26
-0.895	3	-0.895	24
-0.89	3	-0.89	23
-0.885	2	-0.885	21
-0.88	2	-0.88	17
-0.875	2	-0.875	15
-0.87	3	-0.87	13
-0.865	2	-0.865	12
-0.86	3	-0.86	11
-0.855	3	-0.855	12
-0.85	1	-0.85	10
-0.845	2	-0.845	10
-0.84	2	-0.84	10
-0.835	2	-0.835	10
-0.83	3	-0.83	10
-0.825	2	-0.825	10
-0.82	2	-0.82	9
-0.815	2	-0.815	9
-0.81	1	-0.81	9
-0.805	2	-0.805	8
-0.8	1	-0.8	9
-0.795	2	-0.795	9
-0.79	1	-0.79	9
-0.785	2	-0.785	9

Table A-15 (cont'd).

-0.78	3	-0.78	9
-0.775	2	-0.775	8
-0.77	2	-0.77	9
-0.765	3	-0.765	8
-0.76	3	-0.76	9
-0.755	2	-0.755	9
-0.75	3	-0.75	10
-0.745	2	-0.745	10
-0.74	2	-0.74	10
-0.735	2	-0.735	10
-0.73	2	-0.73	11
-0.725	4	-0.725	11
-0.72	2	-0.72	12
-0.715	3	-0.715	13
-0.71	2	-0.71	13
-0.705	2	-0.705	14
-0.7	1	-0.7	16
-0.695	2	-0.695	18
-0.69	3	-0.69	18
-0.685	3	-0.685	20
-0.68	2	-0.68	21
-0.675	4	-0.675	22
-0.67	4	-0.67	23
-0.665	2	-0.665	24
-0.66	2	-0.66	25
-0.655	3	-0.655	24
-0.65	3	-0.65	24
-0.645	3	-0.645	23
-0.64	3	-0.64	22
-0.635	3	-0.635	21
-0.63	2	-0.63	21
-0.625	3	-0.625	20
-0.62	3	-0.62	17
-0.615	3	-0.615	14
-0.61	3	-0.61	11
-0.605	3	-0.605	11
-0.6	3	-0.6	11
-0.595	3	-0.595	10
-0.59	2	-0.59	11
-0.585	3	-0.585	11
-0.58	3	-0.58	11
-0.575	3	-0.575	10
-0.57	3	-0.57	10

Table A-15 (cont'd).

-0.565	2	-0.565	11
-0.56	3	-0.56	10
-0.555	3	-0.555	11
-0.55	3	-0.55	10
-0.545	3	-0.545	11
-0.54	2	-0.54	10
-0.535	2	-0.535	10
-0.53	2	-0.53	10
-0.525	3	-0.525	10
-0.52	3	-0.52	10
-0.515	3	-0.515	11
-0.51	3	-0.51	10
-0.505	2	-0.505	11
-0.5	2	-0.5	10
-0.495	3	-0.495	10
-0.49	3	-0.49	10
-0.485	3	-0.485	10
-0.48	3	-0.48	10
-0.475	3	-0.475	9
-0.47	2	-0.47	10
-0.465	2	-0.465	10
-0.46	2	-0.46	10
-0.455	3	-0.455	9
-0.45	3	-0.45	10
-0.445	3	-0.445	9
-0.44	3	-0.44	10
-0.435	2	-0.435	9
-0.43	2	-0.43	10
-0.425	2	-0.425	10
-0.42	2	-0.42	10
-0.415	2	-0.415	9
-0.41	3	-0.41	9
-0.405	3	-0.405	9
-0.4	3	-0.4	10
-0.395	3	-0.395	9
-0.39	3	-0.39	9
-0.385	3	-0.385	9
-0.38	2	-0.38	9
-0.375	3	-0.375	9
-0.37	3	-0.37	9
-0.365	2	-0.365	8
-0.36	2	-0.36	9
-0.355	2	-0.355	9

Table A-15 (cont'd).

-0.35	2	-0.35	9
-0.345	2	-0.345	9
-0.34	2	-0.34	8
-0.335	2	-0.335	8
-0.33	2	-0.33	9
-0.325	2	-0.325	9
-0.32	2	-0.32	8
-0.315	2	-0.315	8
-0.31	2	-0.31	8
-0.305	2	-0.305	8
-0.3	2	-0.3	9
-0.295	3	-0.295	9
-0.29	3	-0.29	9
-0.285	2	-0.285	8
-0.28	2	-0.28	8
-0.275	2	-0.275	9
-0.27	2	-0.27	8
-0.265	2	-0.265	9
-0.26	2	-0.26	9
-0.255	3	-0.255	9
-0.25	2	-0.25	9
-0.245	3	-0.245	8
-0.24	2	-0.24	10
-0.235	2	-0.235	8
-0.23	2	-0.23	9
-0.225	2	-0.225	9
-0.22	2	-0.22	9
-0.215	2	-0.215	9
-0.21	2	-0.21	9
-0.205	1	-0.205	9
-0.2	2	-0.2	9
-0.195	2	-0.195	9
-0.19	3	-0.19	9
-0.185	3	-0.185	9
-0.18	1	-0.18	9
-0.175	2	-0.175	9
-0.17	1	-0.17	9
-0.165	1	-0.165	9
-0.16	2	-0.16	9
-0.155	2	-0.155	9
-0.15	2	-0.15	9
-0.145	2	-0.145	9
-0.14	2	-0.14	9

Table A-15 (cont'd).

-0.135	2	-0.135	9
-0.13	2	-0.13	9
-0.125	2	-0.125	9
-0.12	2	-0.12	9
-0.115	2	-0.115	9
-0.11	2	-0.11	9
-0.105	2	-0.105	9
-0.1	2	-0.1	10
-0.095	2	-0.095	9
-0.09	2	-0.09	10
-0.085	2	-0.085	10
-0.08	2	-0.08	10
-0.075	2	-0.075	9
-0.07	2	-0.07	10
-0.065	2	-0.065	10
-0.06	2	-0.06	10
-0.055	2	-0.055	10
-0.05	2	-0.05	10
-0.045	2	-0.045	10
-0.04	2	-0.04	10
-0.035	2	-0.035	10
-0.03	2	-0.03	10
-0.025	2	-0.025	10
-0.02	2	-0.02	10
-0.015	2	-0.015	10
-0.01	2	-0.01	10
-0.005	2	-0.005	10
0	2	0	10

Table A-16. Square wave voltammetry data for Figure 6-3a.

Blank		10 IU/ml IFN-γ	
Potential (V)	Current (μA)	Potential (V)	Current (μA)
-1.2	12	-1.2	34
-1.195	13	-1.195	33
-1.19	13	-1.19	34
-1.185	13	-1.185	34
-1.18	12	-1.18	33
-1.175	12	-1.175	33
-1.17	12	-1.17	33
-1.165	12	-1.165	32
-1.16	12	-1.16	33
-1.155	12	-1.155	33
-1.15	11	-1.15	31
-1.145	11	-1.145	32
-1.14	11	-1.14	34
-1.135	11	-1.135	32
-1.13	11	-1.13	31
-1.125	10	-1.125	31
-1.12	10	-1.12	31
-1.115	10	-1.115	30
-1.11	10	-1.11	31
-1.105	11	-1.105	31
-1.1	10	-1.1	31
-1.095	10	-1.095	30
-1.09	9	-1.09	30
-1.085	9	-1.085	28
-1.08	10	-1.08	29
-1.075	9	-1.075	29
-1.07	10	-1.07	29
-1.065	10	-1.065	28
-1.06	9	-1.06	29
-1.055	9	-1.055	28
-1.05	9	-1.05	27
-1.045	9	-1.045	27
-1.04	9	-1.04	27
-1.035	9	-1.035	26
-1.03	8	-1.03	26
-1.025	9	-1.025	25
-1.02	8	-1.02	25
-1.015	9	-1.015	24
-1.01	8	-1.01	23
-1.005	8	-1.005	23
-1	8	-1	23

Table A-16 (cont'd).

-0.995	8	-0.995	21
-0.99	8	-0.99	21
-0.985	8	-0.985	19
-0.98	8	-0.98	19
-0.975	8	-0.975	18
-0.97	7	-0.97	17
-0.965	7	-0.965	16
-0.96	7	-0.96	15
-0.955	7	-0.955	14
-0.95	7	-0.95	13
-0.945	7	-0.945	12
-0.94	7	-0.94	11
-0.935	6	-0.935	11
-0.93	6	-0.93	10
-0.925	7	-0.925	9
-0.92	7	-0.92	8
-0.915	6	-0.915	8
-0.91	7	-0.91	8
-0.905	7	-0.905	8
-0.9	6	-0.9	8
-0.895	6	-0.895	6
-0.89	6	-0.89	7
-0.885	5	-0.885	7
-0.88	6	-0.88	7
-0.875	6	-0.875	7
-0.87	6	-0.87	7
-0.865	5	-0.865	7
-0.86	5	-0.86	8
-0.855	5	-0.855	8
-0.85	6	-0.85	9
-0.845	6	-0.845	8
-0.84	5	-0.84	9
-0.835	5	-0.835	10
-0.83	5	-0.83	11
-0.825	5	-0.825	12
-0.82	4	-0.82	11
-0.815	4	-0.815	12
-0.81	4	-0.81	13
-0.805	4	-0.805	13
-0.8	4	-0.8	13
-0.795	4	-0.795	15
-0.79	4	-0.79	15
-0.785	4	-0.785	15

Table A-16 (cont'd).

-0.78	4	-0.78	16
-0.775	4	-0.775	15
-0.77	4	-0.77	16
-0.765	4	-0.765	16
-0.76	3	-0.76	16
-0.755	3	-0.755	17
-0.75	3	-0.75	16
-0.745	3	-0.745	16
-0.74	3	-0.74	16
-0.735	3	-0.735	16
-0.73	3	-0.73	15
-0.725	3	-0.725	15
-0.72	3	-0.72	14
-0.715	3	-0.715	13
-0.71	3	-0.71	14
-0.705	2	-0.705	12
-0.7	3	-0.7	11
-0.695	3	-0.695	11
-0.69	3	-0.69	11
-0.685	3	-0.685	10
-0.68	3	-0.68	10
-0.675	3	-0.675	9
-0.67	3	-0.67	9
-0.665	3	-0.665	8
-0.66	3	-0.66	8
-0.655	3	-0.655	8
-0.65	3	-0.65	8
-0.645	2	-0.645	7
-0.64	3	-0.64	8
-0.635	3	-0.635	7
-0.63	3	-0.63	7
-0.625	3	-0.625	7
-0.62	4	-0.62	8
-0.615	4	-0.615	7
-0.61	4	-0.61	7
-0.605	4	-0.605	7
-0.6	4	-0.6	7
-0.595	4	-0.595	7
-0.59	5	-0.59	7
-0.585	4	-0.585	7
-0.58	4	-0.58	7
-0.575	5	-0.575	7
-0.57	5	-0.57	7

Table A-16 (cont'd).

-0.565	5	-0.565	7
-0.56	5	-0.56	7
-0.555	5	-0.555	7
-0.55	6	-0.55	7
-0.545	6	-0.545	6
-0.54	6	-0.54	6
-0.535	5	-0.535	7
-0.53	6	-0.53	6
-0.525	7	-0.525	6
-0.52	6	-0.52	7
-0.515	6	-0.515	7
-0.51	6	-0.51	6
-0.505	7	-0.505	6
-0.5	7	-0.5	6
-0.495	7	-0.495	6
-0.49	7	-0.49	6
-0.485	8	-0.485	6
-0.48	7	-0.48	7
-0.475	7	-0.475	6
-0.47	8	-0.47	6
-0.465	8	-0.465	6
-0.46	8	-0.46	5
-0.455	8	-0.455	6
-0.45	8	-0.45	6
-0.445	8	-0.445	6
-0.44	8	-0.44	6
-0.435	8	-0.435	6
-0.43	8	-0.43	6
-0.425	8	-0.425	6
-0.42	8	-0.42	6
-0.415	8	-0.415	6
-0.41	8	-0.41	6
-0.405	9	-0.405	6
-0.4	8	-0.4	6
-0.395	8	-0.395	6
-0.39	8	-0.39	5
-0.385	8	-0.385	6
-0.38	9	-0.38	6
-0.375	9	-0.375	6
-0.37	8	-0.37	6
-0.365	9	-0.365	6
-0.36	9	-0.36	6
-0.355	8	-0.355	6

Table A-16 (cont'd).

-0.35	8	-0.35	6
-0.345	8	-0.345	6
-0.34	8	-0.34	6
-0.335	9	-0.335	6
-0.33	9	-0.33	6
-0.325	9	-0.325	6
-0.32	9	-0.32	6
-0.315	9	-0.315	6
-0.31	9	-0.31	5
-0.305	8	-0.305	6
-0.3	9	-0.3	6
-0.295	9	-0.295	6
-0.29	9	-0.29	6
-0.285	8	-0.285	6
-0.28	9	-0.28	5
-0.275	9	-0.275	6
-0.27	8	-0.27	6
-0.265	8	-0.265	6
-0.26	9	-0.26	6
-0.255	9	-0.255	6
-0.25	9	-0.25	6
-0.245	9	-0.245	6
-0.24	9	-0.24	6
-0.235	10	-0.235	6
-0.23	9	-0.23	6
-0.225	8	-0.225	6
-0.22	10	-0.22	6
-0.215	9	-0.215	6
-0.21	9	-0.21	6
-0.205	8	-0.205	6
-0.2	8	-0.2	6
-0.195	9	-0.195	6
-0.19	10	-0.19	6
-0.185	8	-0.185	7
-0.18	8	-0.18	7
-0.175	9	-0.175	7
-0.17	9	-0.17	7
-0.165	8	-0.165	6
-0.16	8	-0.16	6
-0.155	9	-0.155	6
-0.15	8	-0.15	6
-0.145	10	-0.145	6
-0.14	10	-0.14	6

Table A-16 (cont'd).

-0.135	10	-0.135	6
-0.13	9	-0.13	6
-0.125	8	-0.125	5
-0.12	10	-0.12	6
-0.115	9	-0.115	6
-0.11	9	-0.11	6
-0.105	10	-0.105	7
-0.1	9	-0.1	7
-0.095	9	-0.095	7
-0.09	10	-0.09	5
-0.085	9	-0.085	5
-0.08	8	-0.08	6
-0.075	9	-0.075	7
-0.07	10	-0.07	6
-0.065	9	-0.065	6
-0.06	9	-0.06	7
-0.055	9	-0.055	7
-0.05	9	-0.05	6
-0.045	9	-0.045	6
-0.04	10	-0.04	7
-0.035	10	-0.035	7
-0.03	10	-0.03	7
-0.025	10	-0.025	7
-0.02	9	-0.02	7
-0.015	9	-0.015	7
-0.01	9	-0.01	8
-0.005	10	-0.005	8
0	10	0	7

Table A-17. Square wave voltammetry data for Figure 6-3b.

Blank		1 ng/ml IP-10	
Potential (V)	Current (μA)	Potential (V)	Current (μA)
-1.2	10	-1.2	30
-1.195	12	-1.195	32
-1.19	12	-1.19	31
-1.185	12	-1.185	31
-1.18	12	-1.18	31
-1.175	12	-1.175	30
-1.17	12	-1.17	30
-1.165	11	-1.165	30
-1.16	11	-1.16	30
-1.155	11	-1.155	28
-1.15	11	-1.15	29
-1.145	11	-1.145	29
-1.14	10	-1.14	28
-1.135	11	-1.135	29
-1.13	11	-1.13	27
-1.125	11	-1.125	29
-1.12	10	-1.12	27
-1.115	10	-1.115	29
-1.11	9	-1.11	29
-1.105	9	-1.105	28
-1.1	10	-1.1	28
-1.095	9	-1.095	28
-1.09	9	-1.09	28
-1.085	9	-1.085	28
-1.08	9	-1.08	27
-1.075	9	-1.075	27
-1.07	9	-1.07	27
-1.065	9	-1.065	28
-1.06	9	-1.06	28
-1.055	9	-1.055	27
-1.05	8	-1.05	27
-1.045	9	-1.045	27
-1.04	8	-1.04	28
-1.035	8	-1.035	26
-1.03	8	-1.03	26
-1.025	8	-1.025	26
-1.02	8	-1.02	26
-1.015	8	-1.015	26
-1.01	8	-1.01	26
-1.005	8	-1.005	26
-1	8	-1	25

Table A-17 (cont'd).

-0.995	7	-0.995	25
-0.99	8	-0.99	25
-0.985	8	-0.985	25
-0.98	7	-0.98	25
-0.975	8	-0.975	24
-0.97	7	-0.97	23
-0.965	7	-0.965	23
-0.96	7	-0.96	23
-0.955	7	-0.955	23
-0.95	7	-0.95	23
-0.945	6	-0.945	22
-0.94	7	-0.94	23
-0.935	7	-0.935	22
-0.93	6	-0.93	21
-0.925	6	-0.925	21
-0.92	7	-0.92	21
-0.915	6	-0.915	21
-0.91	6	-0.91	20
-0.905	7	-0.905	20
-0.9	6	-0.9	20
-0.895	6	-0.895	19
-0.89	6	-0.89	18
-0.885	6	-0.885	18
-0.88	6	-0.88	18
-0.875	6	-0.875	17
-0.87	6	-0.87	17
-0.865	6	-0.865	16
-0.86	5	-0.86	17
-0.855	5	-0.855	16
-0.85	6	-0.85	16
-0.845	6	-0.845	16
-0.84	4	-0.84	16
-0.835	5	-0.835	15
-0.83	5	-0.83	15
-0.825	5	-0.825	15
-0.82	4	-0.82	14
-0.815	4	-0.815	14
-0.81	4	-0.81	14
-0.805	4	-0.805	13
-0.8	5	-0.8	14
-0.795	4	-0.795	13
-0.79	4	-0.79	14
-0.785	4	-0.785	13

Table A-17 (cont'd).

-0.78	4	-0.78	13
-0.775	5	-0.775	13
-0.77	4	-0.77	13
-0.765	4	-0.765	12
-0.76	4	-0.76	12
-0.755	4	-0.755	12
-0.75	3	-0.75	12
-0.745	4	-0.745	13
-0.74	4	-0.74	12
-0.735	3	-0.735	12
-0.73	3	-0.73	12
-0.725	3	-0.725	12
-0.72	3	-0.72	12
-0.715	3	-0.715	12
-0.71	3	-0.71	12
-0.705	3	-0.705	13
-0.7	3	-0.7	13
-0.695	3	-0.695	12
-0.69	3	-0.69	13
-0.685	2	-0.685	12
-0.68	3	-0.68	13
-0.675	2	-0.675	14
-0.67	2	-0.67	13
-0.665	2	-0.665	14
-0.66	3	-0.66	15
-0.655	3	-0.655	16
-0.65	3	-0.65	16
-0.645	3	-0.645	18
-0.64	2	-0.64	17
-0.635	3	-0.635	18
-0.63	3	-0.63	20
-0.625	3	-0.625	21
-0.62	3	-0.62	22
-0.615	3	-0.615	22
-0.61	3	-0.61	22
-0.605	3	-0.605	22
-0.6	3	-0.6	21
-0.595	4	-0.595	20
-0.59	4	-0.59	19
-0.585	4	-0.585	19
-0.58	4	-0.58	17
-0.575	4	-0.575	16
-0.57	4	-0.57	15

Table A-17 (cont'd).

-0.565	4	-0.565	14
-0.56	5	-0.56	13
-0.555	5	-0.555	12
-0.55	5	-0.55	12
-0.545	5	-0.545	12
-0.54	6	-0.54	11
-0.535	5	-0.535	12
-0.53	5	-0.53	12
-0.525	5	-0.525	11
-0.52	6	-0.52	12
-0.515	6	-0.515	12
-0.51	6	-0.51	12
-0.505	6	-0.505	12
-0.5	7	-0.5	12
-0.495	7	-0.495	11
-0.49	7	-0.49	11
-0.485	7	-0.485	11
-0.48	7	-0.48	11
-0.475	6	-0.475	11
-0.47	7	-0.47	12
-0.465	7	-0.465	12
-0.46	7	-0.46	12
-0.455	8	-0.455	12
-0.45	8	-0.45	11
-0.445	8	-0.445	12
-0.44	8	-0.44	12
-0.435	8	-0.435	12
-0.43	8	-0.43	12
-0.425	7	-0.425	12
-0.42	7	-0.42	11
-0.415	8	-0.415	12
-0.41	8	-0.41	11
-0.405	8	-0.405	12
-0.4	8	-0.4	12
-0.395	8	-0.395	12
-0.39	9	-0.39	12
-0.385	7	-0.385	12
-0.38	8	-0.38	12
-0.375	8	-0.375	12
-0.37	8	-0.37	12
-0.365	8	-0.365	12
-0.36	8	-0.36	12
-0.355	8	-0.355	13

Table A-17 (cont'd).

-0.35	8	-0.35	12
-0.345	8	-0.345	13
-0.34	8	-0.34	13
-0.335	8	-0.335	12
-0.33	9	-0.33	12
-0.325	9	-0.325	12
-0.32	9	-0.32	12
-0.315	8	-0.315	12
-0.31	8	-0.31	12
-0.305	8	-0.305	12
-0.3	8	-0.3	12
-0.295	8	-0.295	12
-0.29	8	-0.29	12
-0.285	8	-0.285	13
-0.28	8	-0.28	12
-0.275	8	-0.275	13
-0.27	9	-0.27	13
-0.265	9	-0.265	12
-0.26	9	-0.26	13
-0.255	9	-0.255	13
-0.25	9	-0.25	13
-0.245	9	-0.245	13
-0.24	9	-0.24	13
-0.235	9	-0.235	13
-0.23	9	-0.23	13
-0.225	9	-0.225	13
-0.22	9	-0.22	13
-0.215	9	-0.215	13
-0.21	9	-0.21	14
-0.205	9	-0.205	14
-0.2	9	-0.2	14
-0.195	9	-0.195	14
-0.19	9	-0.19	13
-0.185	8	-0.185	14
-0.18	9	-0.18	14
-0.175	8	-0.175	14
-0.17	8	-0.17	14
-0.165	9	-0.165	14
-0.16	8	-0.16	15
-0.155	8	-0.155	15
-0.15	8	-0.15	14
-0.145	8	-0.145	14
-0.14	8	-0.14	15

Table A-17 (cont'd).

-0.135	8	-0.135	14
-0.13	8	-0.13	14
-0.125	9	-0.125	14
-0.12	8	-0.12	14
-0.115	9	-0.115	15
-0.11	9	-0.11	15
-0.105	9	-0.105	15
-0.1	8	-0.1	15
-0.095	9	-0.095	14
-0.09	9	-0.09	15
-0.085	9	-0.085	15
-0.08	9	-0.08	15
-0.075	9	-0.075	15
-0.07	9	-0.07	16
-0.065	9	-0.065	15
-0.06	9	-0.06	15
-0.055	9	-0.055	15
-0.05	9	-0.05	16
-0.045	9	-0.045	15
-0.04	9	-0.04	15
-0.035	9	-0.035	16
-0.03	9	-0.03	17
-0.025	9	-0.025	16
-0.02	9	-0.02	16
-0.015	9	-0.015	16
-0.01	9	-0.01	16
-0.005	9	-0.005	16
0	9	0	17

Table A-18. Square wave voltammetry data for Figure 6-3c.

Blank		1 IU/ml IFN-γ + 1 ng/ml IP-10	
Potential (V)	Current (μA)	Potential (V)	Current (μA)
-1.2	8	-1.2	23
-1.195	8	-1.195	26
-1.19	7	-1.19	26
-1.185	7	-1.185	26
-1.18	7	-1.18	25
-1.175	7	-1.175	26
-1.17	6	-1.17	25
-1.165	7	-1.165	25
-1.16	7	-1.16	25
-1.155	6	-1.155	24
-1.15	6	-1.15	25
-1.145	6	-1.145	24
-1.14	6	-1.14	24
-1.135	6	-1.135	25
-1.13	6	-1.13	24
-1.125	6	-1.125	24
-1.12	5	-1.12	23
-1.115	5	-1.115	24
-1.11	5	-1.11	23
-1.105	6	-1.105	23
-1.1	5	-1.1	22
-1.095	6	-1.095	22
-1.09	6	-1.09	21
-1.085	6	-1.085	21
-1.08	6	-1.08	21
-1.075	6	-1.075	21
-1.07	5	-1.07	20
-1.065	5	-1.065	19
-1.06	5	-1.06	20
-1.055	4	-1.055	19
-1.05	5	-1.05	18
-1.045	5	-1.045	18
-1.04	4	-1.04	18
-1.035	5	-1.035	18
-1.03	5	-1.03	18
-1.025	5	-1.025	17
-1.02	4	-1.02	16

Table A-18 (cont'd).

-1.015	4	-1.015	17
-1.01	4	-1.01	17
-1.005	4	-1.005	17
-1	4	-1	17
-0.995	5	-0.995	16
-0.99	4	-0.99	17
-0.985	4	-0.985	17
-0.98	5	-0.98	18
-0.975	3	-0.975	18
-0.97	5	-0.97	18
-0.965	4	-0.965	18
-0.96	4	-0.96	18
-0.955	5	-0.955	19
-0.95	6	-0.95	19
-0.945	3	-0.945	19
-0.94	5	-0.94	20
-0.935	2	-0.935	19
-0.93	6	-0.93	19
-0.925	3	-0.925	20
-0.92	4	-0.92	20
-0.915	3	-0.915	20
-0.91	5	-0.91	20
-0.905	5	-0.905	21
-0.9	4	-0.9	21
-0.895	4	-0.895	21
-0.89	5	-0.89	20
-0.885	4	-0.885	20
-0.88	3	-0.88	21
-0.875	3	-0.875	21
-0.87	4	-0.87	21
-0.865	2	-0.865	21
-0.86	3	-0.86	20
-0.855	4	-0.855	20
-0.85	2	-0.85	19
-0.845	5	-0.845	20
-0.84	2	-0.84	20
-0.835	2	-0.835	19
-0.83	2	-0.83	19
-0.825	4	-0.825	19

Table A-18 (cont'd).

-0.82	3	-0.82	18
-0.815	0	-0.815	19
-0.81	4	-0.81	18
-0.805	2	-0.805	18
-0.8	1	-0.8	17
-0.795	4	-0.795	16
-0.79	3	-0.79	16
-0.785	2	-0.785	15
-0.78	4	-0.78	15
-0.775	3	-0.775	14
-0.77	2	-0.77	14
-0.765	2	-0.765	13
-0.76	3	-0.76	13
-0.755	3	-0.755	12
-0.75	0	-0.75	12
-0.745	2	-0.745	11
-0.74	2	-0.74	10
-0.735	3	-0.735	10
-0.73	3	-0.73	9
-0.725	2	-0.725	9
-0.72	2	-0.72	9
-0.715	3	-0.715	8
-0.71	3	-0.71	8
-0.705	3	-0.705	8
-0.7	1	-0.7	8
-0.695	2	-0.695	8
-0.69	2	-0.69	9
-0.685	3	-0.685	8
-0.68	3	-0.68	9
-0.675	2	-0.675	9
-0.67	3	-0.67	10
-0.665	3	-0.665	10
-0.66	2	-0.66	11
-0.655	3	-0.655	10
-0.65	2	-0.65	11
-0.645	2	-0.645	10
-0.64	3	-0.64	10
-0.635	2	-0.635	9
-0.63	3	-0.63	8

Table A-18 (cont'd).

-0.625	3	-0.625	7
-0.62	3	-0.62	7
-0.615	3	-0.615	5
-0.61	3	-0.61	5
-0.605	2	-0.605	5
-0.6	3	-0.6	5
-0.595	3	-0.595	5
-0.59	3	-0.59	5
-0.585	3	-0.585	4
-0.58	3	-0.58	5
-0.575	4	-0.575	4
-0.57	4	-0.57	5
-0.565	4	-0.565	5
-0.56	4	-0.56	5
-0.555	4	-0.555	5
-0.55	3	-0.55	5
-0.545	3	-0.545	4
-0.54	3	-0.54	5
-0.535	4	-0.535	4
-0.53	4	-0.53	4
-0.525	4	-0.525	4
-0.52	3	-0.52	5
-0.515	3	-0.515	5
-0.51	3	-0.51	5
-0.505	3	-0.505	5
-0.5	4	-0.5	5
-0.495	4	-0.495	5
-0.49	4	-0.49	5
-0.485	3	-0.485	5
-0.48	3	-0.48	6
-0.475	3	-0.475	5
-0.47	3	-0.47	6
-0.465	4	-0.465	5
-0.46	4	-0.46	5
-0.455	4	-0.455	5
-0.45	4	-0.45	5
-0.445	3	-0.445	5
-0.44	3	-0.44	5
-0.435	3	-0.435	5

Table A-18 (cont'd).

-0.43	3	-0.43	5
-0.425	4	-0.425	5
-0.42	4	-0.42	5
-0.415	4	-0.415	5
-0.41	4	-0.41	4
-0.405	4	-0.405	4
-0.4	4	-0.4	4
-0.395	4	-0.395	4
-0.39	4	-0.39	4
-0.385	3	-0.385	4
-0.38	3	-0.38	4
-0.375	4	-0.375	5
-0.37	4	-0.37	5
-0.365	4	-0.365	5
-0.36	4	-0.36	5
-0.355	4	-0.355	5
-0.35	4	-0.35	5
-0.345	4	-0.345	5
-0.34	4	-0.34	6
-0.335	3	-0.335	6
-0.33	3	-0.33	6
-0.325	4	-0.325	6
-0.32	4	-0.32	6
-0.315	4	-0.315	5
-0.31	4	-0.31	5
-0.305	4	-0.305	5
-0.3	4	-0.3	5
-0.295	4	-0.295	5
-0.29	4	-0.29	5
-0.285	4	-0.285	5
-0.28	4	-0.28	5
-0.275	4	-0.275	5
-0.27	4	-0.27	6
-0.265	4	-0.265	6
-0.26	4	-0.26	6
-0.255	3	-0.255	6
-0.25	3	-0.25	6
-0.245	3	-0.245	6
-0.24	4	-0.24	7

Table A-18 (cont'd).

-0.235	3	-0.235	6
-0.23	3	-0.23	6
-0.225	4	-0.225	6
-0.22	4	-0.22	6
-0.215	4	-0.215	6
-0.21	4	-0.21	6
-0.205	4	-0.205	6
-0.2	4	-0.2	6
-0.195	4	-0.195	7
-0.19	4	-0.19	6
-0.185	4	-0.185	6
-0.18	4	-0.18	7
-0.175	4	-0.175	7
-0.17	4	-0.17	7
-0.165	4	-0.165	6
-0.16	4	-0.16	7
-0.155	4	-0.155	7
-0.15	4	-0.15	7
-0.145	4	-0.145	7
-0.14	4	-0.14	7
-0.135	4	-0.135	7
-0.13	4	-0.13	7
-0.125	4	-0.125	7
-0.12	4	-0.12	7
-0.115	4	-0.115	7
-0.11	4	-0.11	7
-0.105	4	-0.105	7
-0.1	4	-0.1	7
-0.095	4	-0.095	7
-0.09	4	-0.09	6
-0.085	4	-0.085	6
-0.08	5	-0.08	6
-0.075	5	-0.075	7
-0.07	4	-0.07	7
-0.065	4	-0.065	7
-0.06	4	-0.06	7
-0.055	4	-0.055	7
-0.05	5	-0.05	7
-0.045	5	-0.045	7

Table A-18 (cont'd).

-0.04	5	-0.04	7
-0.035	5	-0.035	7
-0.03	5	-0.03	7
-0.025	5	-0.025	7
-0.02	5	-0.02	7
-0.015	5	-0.015	7
-0.01	5	-0.01	7
-0.005	5	-0.005	7
0	5	0	7

Table A-19. Data for Figure 6-4a.

IFN-γ (IU/ml)	Peak current (μA)	Standard deviation (μA)
0	5.0	1.17
0.01	13.8	2.51
0.1	17.2	5.96
1	19.5	2.91
10	18.4	3.75

Table A-20. Data for Figure 6-4b

IP-10 (ng/ml)	Peak current (μA)	Standard deviation (μA)
0	4.27	2.18
0.01	13.89	2.42
0.1	15.00	3.06
1	15.61	2.21
10	16.08	2.89
100	14.42	1.64

Table A-21. Square wave voltammetry data for Figure 6-5.

Blank		0.01 IU/ml IFNγ+0.01 ng/ml IP-10		0.1 IU/ml IFN-γ+0.1 ng/ml IP-10		1 IU/ml IFN-γ+1 ng/ml IP-10		10 IU/ml IFN-γ+10 ng/ml IP-10	
Potential (V)	Current (µA)	Potential (V)	Current (µA)	Potential (V)	Current (µA)	Potential (V)	Current (µA)	Potential (V)	Current (µA)
-1.2	8	-1.2	34	-1.2	30	-1.2	43	-1.2	24
-1.195	9	-1.195	35	-1.195	31	-1.195	44	-1.195	26
-1.19	9	-1.19	35	-1.19	32	-1.19	43	-1.19	26
-1.185	8	-1.185	34	-1.185	32	-1.185	43	-1.185	25
-1.18	9	-1.18	34	-1.18	32	-1.18	44	-1.18	25
-1.175	8	-1.175	34	-1.175	31	-1.175	43	-1.175	25
-1.17	8	-1.17	33	-1.17	31	-1.17	43	-1.17	25
-1.165	9	-1.165	34	-1.165	32	-1.165	43	-1.165	25
-1.16	9	-1.16	33	-1.16	31	-1.16	43	-1.16	25
-1.155	7	-1.155	32	-1.155	32	-1.155	41	-1.155	25
-1.15	8	-1.15	31	-1.15	31	-1.15	41	-1.15	24
-1.145	9	-1.145	31	-1.145	30	-1.145	41	-1.145	24
-1.14	8	-1.14	31	-1.14	29	-1.14	42	-1.14	24
-1.135	9	-1.135	31	-1.135	29	-1.135	41	-1.135	23
-1.13	6	-1.13	30	-1.13	30	-1.13	40	-1.13	23
-1.125	7	-1.125	29	-1.125	29	-1.125	41	-1.125	22
-1.12	8	-1.12	30	-1.12	29	-1.12	40	-1.12	22
-1.115	6	-1.115	29	-1.115	28	-1.115	39	-1.115	22
-1.11	7	-1.11	28	-1.11	28	-1.11	39	-1.11	21
-1.105	7	-1.105	27	-1.105	28	-1.105	39	-1.105	21
-1.1	7	-1.1	27	-1.1	27	-1.1	38	-1.1	21
-1.095	7	-1.095	27	-1.095	26	-1.095	38	-1.095	21
-1.09	7	-1.09	27	-1.09	25	-1.09	37	-1.09	21
-1.085	7	-1.085	26	-1.085	25	-1.085	36	-1.085	21
-1.08	7	-1.08	26	-1.08	25	-1.08	36	-1.08	22
-1.075	7	-1.075	25	-1.075	25	-1.075	35	-1.075	21
-1.07	7	-1.07	25	-1.07	24	-1.07	35	-1.07	21
-1.065	7	-1.065	24	-1.065	23	-1.065	34	-1.065	21
-1.06	8	-1.06	24	-1.06	23	-1.06	33	-1.06	21
-1.055	7	-1.055	23	-1.055	22	-1.055	33	-1.055	22
-1.05	7	-1.05	23	-1.05	22	-1.05	32	-1.05	22
-1.045	8	-1.045	22	-1.045	21	-1.045	31	-1.045	22
-1.04	6	-1.04	22	-1.04	21	-1.04	31	-1.04	22
-1.035	7	-1.035	21	-1.035	20	-1.035	30	-1.035	22

Table A-21 (cont'd).

-1.03	6	-1.03	20	-1.03	18	-1.03	29	-1.03	22
-1.025	6	-1.025	19	-1.025	18	-1.025	28	-1.025	23
-1.02	6	-1.02	17	-1.02	18	-1.02	28	-1.02	23
-1.015	7	-1.015	18	-1.015	17	-1.015	26	-1.015	24
-1.01	6	-1.01	17	-1.01	16	-1.01	26	-1.01	24
-1.005	6	-1.005	16	-1.005	16	-1.005	25	-1.005	24
-1	7	-1	16	-1	16	-1	24	-1	25
-0.995	6	-0.995	15	-0.995	16	-0.995	23	-0.995	25
-0.99	6	-0.99	14	-0.99	14	-0.99	22	-0.99	25
-0.985	5	-0.985	12	-0.985	15	-0.985	22	-0.985	26
-0.98	5	-0.98	11	-0.98	15	-0.98	21	-0.98	26
-0.975	6	-0.975	11	-0.975	14	-0.975	20	-0.975	26
-0.97	6	-0.97	10	-0.97	13	-0.97	19	-0.97	26
-0.965	5	-0.965	9	-0.965	13	-0.965	18	-0.965	27
-0.96	5	-0.96	10	-0.96	15	-0.96	17	-0.96	27
-0.955	6	-0.955	9	-0.955	14	-0.955	16	-0.955	27
-0.95	5	-0.95	8	-0.95	13	-0.95	16	-0.95	27
-0.945	5	-0.945	8	-0.945	13	-0.945	16	-0.945	28
-0.94	5	-0.94	8	-0.94	14	-0.94	15	-0.94	28
-0.935	4	-0.935	7	-0.935	14	-0.935	14	-0.935	28
-0.93	5	-0.93	7	-0.93	15	-0.93	14	-0.93	28
-0.925	5	-0.925	8	-0.925	15	-0.925	14	-0.925	28
-0.92	5	-0.92	8	-0.92	15	-0.92	14	-0.92	29
-0.915	5	-0.915	9	-0.915	17	-0.915	13	-0.915	29
-0.91	4	-0.91	9	-0.91	16	-0.91	13	-0.91	28
-0.905	4	-0.905	8	-0.905	16	-0.905	13	-0.905	29
-0.9	5	-0.9	9	-0.9	16	-0.9	14	-0.9	29
-0.895	5	-0.895	10	-0.895	17	-0.895	14	-0.895	28
-0.89	5	-0.89	9	-0.89	16	-0.89	13	-0.89	28
-0.885	4	-0.885	9	-0.885	17	-0.885	14	-0.885	29
-0.88	4	-0.88	10	-0.88	18	-0.88	14	-0.88	28
-0.875	4	-0.875	10	-0.875	17	-0.875	15	-0.875	28
-0.87	4	-0.87	10	-0.87	18	-0.87	15	-0.87	28
-0.865	4	-0.865	10	-0.865	18	-0.865	16	-0.865	29
-0.86	4	-0.86	12	-0.86	19	-0.86	15	-0.86	28
-0.855	4	-0.855	12	-0.855	19	-0.855	16	-0.855	28
-0.85	3	-0.85	12	-0.85	19	-0.85	18	-0.85	28
-0.845	3	-0.845	13	-0.845	19	-0.845	17	-0.845	27
-0.84	3	-0.84	13	-0.84	19	-0.84	18	-0.84	27

Table A-21 (cont'd).

-0.835	4	-0.835	13	-0.835	19	-0.835	18	-0.835	26
-0.83	3	-0.83	14	-0.83	18	-0.83	20	-0.83	26
-0.825	3	-0.825	14	-0.825	19	-0.825	19	-0.825	26
-0.82	3	-0.82	14	-0.82	20	-0.82	21	-0.82	25
-0.815	4	-0.815	14	-0.815	20	-0.815	20	-0.815	24
-0.81	4	-0.81	14	-0.81	19	-0.81	21	-0.81	24
-0.805	3	-0.805	14	-0.805	19	-0.805	21	-0.805	23
-0.8	3	-0.8	14	-0.8	18	-0.8	22	-0.8	23
-0.795	3	-0.795	15	-0.795	19	-0.795	23	-0.795	22
-0.79	4	-0.79	14	-0.79	18	-0.79	23	-0.79	22
-0.785	3	-0.785	15	-0.785	17	-0.785	23	-0.785	21
-0.78	4	-0.78	14	-0.78	18	-0.78	23	-0.78	20
-0.775	4	-0.775	14	-0.775	18	-0.775	23	-0.775	19
-0.77	4	-0.77	15	-0.77	17	-0.77	24	-0.77	19
-0.765	4	-0.765	14	-0.765	17	-0.765	24	-0.765	18
-0.76	5	-0.76	13	-0.76	16	-0.76	23	-0.76	16
-0.755	3	-0.755	13	-0.755	16	-0.755	23	-0.755	17
-0.75	5	-0.75	13	-0.75	15	-0.75	23	-0.75	15
-0.745	4	-0.745	13	-0.745	15	-0.745	22	-0.745	14
-0.74	4	-0.74	12	-0.74	14	-0.74	23	-0.74	14
-0.735	5	-0.735	11	-0.735	13	-0.735	21	-0.735	14
-0.73	5	-0.73	11	-0.73	13	-0.73	22	-0.73	11
-0.725	5	-0.725	12	-0.725	13	-0.725	20	-0.725	13
-0.72	5	-0.72	11	-0.72	12	-0.72	20	-0.72	10
-0.715	6	-0.715	11	-0.715	12	-0.715	20	-0.715	12
-0.71	6	-0.71	11	-0.71	12	-0.71	19	-0.71	11
-0.705	6	-0.705	11	-0.705	11	-0.705	19	-0.705	12
-0.7	7	-0.7	11	-0.7	10	-0.7	19	-0.7	13
-0.695	6	-0.695	10	-0.695	11	-0.695	18	-0.695	14
-0.69	7	-0.69	10	-0.69	10	-0.69	18	-0.69	15
-0.685	7	-0.685	11	-0.685	10	-0.685	18	-0.685	14
-0.68	7	-0.68	11	-0.68	10	-0.68	17	-0.68	17
-0.675	7	-0.675	11	-0.675	10	-0.675	17	-0.675	17
-0.67	8	-0.67	11	-0.67	10	-0.67	16	-0.67	18
-0.665	8	-0.665	12	-0.665	10	-0.665	16	-0.665	19
-0.66	9	-0.66	12	-0.66	11	-0.66	16	-0.66	21
-0.655	8	-0.655	13	-0.655	10	-0.655	16	-0.655	23
-0.65	9	-0.65	13	-0.65	11	-0.65	16	-0.65	24
-0.645	9	-0.645	14	-0.645	12	-0.645	17	-0.645	25

Table A-21 (cont'd).

-0.64	9	-0.64	14	-0.64	13	-0.64	17	-0.64	26
-0.635	9	-0.635	13	-0.635	13	-0.635	18	-0.635	28
-0.63	9	-0.63	13	-0.63	15	-0.63	18	-0.63	28
-0.625	10	-0.625	13	-0.625	15	-0.625	19	-0.625	28
-0.62	10	-0.62	12	-0.62	15	-0.62	20	-0.62	28
-0.615	10	-0.615	11	-0.615	15	-0.615	20	-0.615	25
-0.61	10	-0.61	10	-0.61	15	-0.61	20	-0.61	25
-0.605	10	-0.605	10	-0.605	15	-0.605	19	-0.605	22
-0.6	10	-0.6	10	-0.6	15	-0.6	17	-0.6	19
-0.595	11	-0.595	8	-0.595	14	-0.595	17	-0.595	16
-0.59	10	-0.59	8	-0.59	13	-0.59	15	-0.59	15
-0.585	10	-0.585	8	-0.585	11	-0.585	14	-0.585	12
-0.58	10	-0.58	9	-0.58	10	-0.58	13	-0.58	11
-0.575	10	-0.575	8	-0.575	9	-0.575	12	-0.575	11
-0.57	10	-0.57	8	-0.57	9	-0.57	11	-0.57	10
-0.565	10	-0.565	8	-0.565	9	-0.565	11	-0.565	8
-0.56	10	-0.56	8	-0.56	9	-0.56	11	-0.56	9
-0.555	11	-0.555	9	-0.555	9	-0.555	10	-0.555	8
-0.55	11	-0.55	7	-0.55	8	-0.55	10	-0.55	9
-0.545	11	-0.545	8	-0.545	8	-0.545	10	-0.545	9
-0.54	10	-0.54	8	-0.54	8	-0.54	10	-0.54	9
-0.535	11	-0.535	8	-0.535	8	-0.535	10	-0.535	9
-0.53	11	-0.53	7	-0.53	8	-0.53	10	-0.53	10
-0.525	11	-0.525	8	-0.525	9	-0.525	10	-0.525	10
-0.52	11	-0.52	8	-0.52	9	-0.52	11	-0.52	9
-0.515	10	-0.515	7	-0.515	9	-0.515	10	-0.515	11
-0.51	10	-0.51	8	-0.51	8	-0.51	10	-0.51	9
-0.505	10	-0.505	8	-0.505	8	-0.505	10	-0.505	10
-0.5	10	-0.5	9	-0.5	9	-0.5	10	-0.5	10
-0.495	11	-0.495	8	-0.495	9	-0.495	10	-0.495	11
-0.49	11	-0.49	8	-0.49	9	-0.49	10	-0.49	10
-0.485	11	-0.485	8	-0.485	9	-0.485	10	-0.485	11
-0.48	11	-0.48	9	-0.48	10	-0.48	10	-0.48	11
-0.475	11	-0.475	9	-0.475	10	-0.475	10	-0.475	10
-0.47	11	-0.47	8	-0.47	9	-0.47	10	-0.47	11
-0.465	11	-0.465	8	-0.465	10	-0.465	10	-0.465	11
-0.46	11	-0.46	9	-0.46	10	-0.46	11	-0.46	10
-0.455	11	-0.455	8	-0.455	10	-0.455	10	-0.455	10
-0.45	11	-0.45	8	-0.45	10	-0.45	11	-0.45	10

Table A-21 (cont'd).

-0.445	11	-0.445	8	-0.445	10	-0.445	11	-0.445	9
-0.44	11	-0.44	8	-0.44	9	-0.44	10	-0.44	9
-0.435	11	-0.435	8	-0.435	9	-0.435	11	-0.435	9
-0.43	11	-0.43	8	-0.43	9	-0.43	10	-0.43	8
-0.425	12	-0.425	8	-0.425	9	-0.425	10	-0.425	9
-0.42	11	-0.42	7	-0.42	9	-0.42	10	-0.42	9
-0.415	11	-0.415	8	-0.415	9	-0.415	10	-0.415	9
-0.41	12	-0.41	8	-0.41	9	-0.41	11	-0.41	8
-0.405	11	-0.405	8	-0.405	9	-0.405	11	-0.405	8
-0.4	10	-0.4	8	-0.4	9	-0.4	10	-0.4	9
-0.395	12	-0.395	7	-0.395	8	-0.395	11	-0.395	9
-0.39	11	-0.39	7	-0.39	9	-0.39	10	-0.39	8
-0.385	12	-0.385	8	-0.385	9	-0.385	10	-0.385	9
-0.38	12	-0.38	8	-0.38	9	-0.38	10	-0.38	9
-0.375	11	-0.375	8	-0.375	9	-0.375	10	-0.375	9
-0.37	10	-0.37	8	-0.37	9	-0.37	10	-0.37	8
-0.365	10	-0.365	7	-0.365	9	-0.365	11	-0.365	8
-0.36	12	-0.36	8	-0.36	9	-0.36	11	-0.36	9
-0.355	11	-0.355	8	-0.355	9	-0.355	11	-0.355	8
-0.35	10	-0.35	8	-0.35	8	-0.35	10	-0.35	9
-0.345	11	-0.345	8	-0.345	8	-0.345	10	-0.345	9
-0.34	11	-0.34	7	-0.34	8	-0.34	11	-0.34	9
-0.335	11	-0.335	7	-0.335	8	-0.335	11	-0.335	8
-0.33	11	-0.33	8	-0.33	8	-0.33	11	-0.33	8
-0.325	11	-0.325	8	-0.325	9	-0.325	11	-0.325	9
-0.32	11	-0.32	8	-0.32	9	-0.32	10	-0.32	9
-0.315	12	-0.315	7	-0.315	9	-0.315	10	-0.315	8
-0.31	11	-0.31	8	-0.31	9	-0.31	10	-0.31	8
-0.305	12	-0.305	8	-0.305	9	-0.305	10	-0.305	9
-0.3	11	-0.3	8	-0.3	10	-0.3	11	-0.3	9
-0.295	11	-0.295	8	-0.295	10	-0.295	10	-0.295	8
-0.29	10	-0.29	9	-0.29	8	-0.29	11	-0.29	9
-0.285	10	-0.285	7	-0.285	10	-0.285	11	-0.285	9
-0.28	10	-0.28	7	-0.28	9	-0.28	11	-0.28	9
-0.275	11	-0.275	8	-0.275	9	-0.275	11	-0.275	9
-0.27	12	-0.27	8	-0.27	9	-0.27	12	-0.27	9
-0.265	11	-0.265	8	-0.265	9	-0.265	11	-0.265	9
-0.26	11	-0.26	8	-0.26	9	-0.26	11	-0.26	8
-0.255	12	-0.255	7	-0.255	9	-0.255	11	-0.255	9

Table A-21 (cont'd).

-0.25	11	-0.25	8	-0.25	10	-0.25	11	-0.25	9
-0.245	12	-0.245	7	-0.245	9	-0.245	11	-0.245	10
-0.24	11	-0.24	7	-0.24	9	-0.24	11	-0.24	9
-0.235	11	-0.235	8	-0.235	9	-0.235	11	-0.235	9
-0.23	12	-0.23	8	-0.23	10	-0.23	11	-0.23	9
-0.225	10	-0.225	9	-0.225	9	-0.225	12	-0.225	10
-0.22	10	-0.22	7	-0.22	9	-0.22	12	-0.22	9
-0.215	10	-0.215	8	-0.215	9	-0.215	12	-0.215	9
-0.21	11	-0.21	7	-0.21	9	-0.21	11	-0.21	10
-0.205	11	-0.205	7	-0.205	10	-0.205	11	-0.205	10
-0.2	10	-0.2	7	-0.2	9	-0.2	12	-0.2	9
-0.195	11	-0.195	10	-0.195	9	-0.195	12	-0.195	9
-0.19	10	-0.19	8	-0.19	9	-0.19	12	-0.19	9
-0.185	10	-0.185	8	-0.185	10	-0.185	12	-0.185	8
-0.18	10	-0.18	8	-0.18	11	-0.18	11	-0.18	9
-0.175	11	-0.175	8	-0.175	10	-0.175	11	-0.175	9
-0.17	11	-0.17	8	-0.17	11	-0.17	12	-0.17	9
-0.165	10	-0.165	10	-0.165	9	-0.165	12	-0.165	10
-0.16	10	-0.16	8	-0.16	9	-0.16	12	-0.16	10
-0.155	11	-0.155	8	-0.155	12	-0.155	12	-0.155	10
-0.15	10	-0.15	8	-0.15	11	-0.15	12	-0.15	9
-0.145	11	-0.145	8	-0.145	11	-0.145	13	-0.145	9
-0.14	10	-0.14	9	-0.14	11	-0.14	11	-0.14	9
-0.135	10	-0.135	9	-0.135	11	-0.135	12	-0.135	10
-0.13	9	-0.13	10	-0.13	11	-0.13	12	-0.13	10
-0.125	10	-0.125	9	-0.125	10	-0.125	12	-0.125	10
-0.12	10	-0.12	8	-0.12	11	-0.12	13	-0.12	10
-0.115	10	-0.115	9	-0.115	12	-0.115	13	-0.115	10
-0.11	10	-0.11	9	-0.11	10	-0.11	12	-0.11	9
-0.105	10	-0.105	8	-0.105	10	-0.105	13	-0.105	10
-0.1	10	-0.1	10	-0.1	12	-0.1	12	-0.1	9
-0.095	9	-0.095	9	-0.095	11	-0.095	13	-0.095	9
-0.09	9	-0.09	8	-0.09	10	-0.09	13	-0.09	9
-0.085	9	-0.085	9	-0.085	11	-0.085	13	-0.085	9
-0.08	8	-0.08	9	-0.08	11	-0.08	13	-0.08	9
-0.075	9	-0.075	9	-0.075	11	-0.075	12	-0.075	9
-0.07	9	-0.07	9	-0.07	11	-0.07	13	-0.07	9
-0.065	9	-0.065	9	-0.065	11	-0.065	12	-0.065	10
-0.06	9	-0.06	9	-0.06	11	-0.06	12	-0.06	10

Table A-21 (cont'd).

-0.055	9	-0.055	9	-0.055	11	-0.055	12	-0.055	10
-0.05	7	-0.05	9	-0.05	11	-0.05	12	-0.05	10
-0.045	8	-0.045	9	-0.045	11	-0.045	12	-0.045	10
-0.04	7	-0.04	9	-0.04	11	-0.04	12	-0.04	10
-0.035	9	-0.035	9	-0.035	12	-0.035	12	-0.035	10
-0.03	7	-0.03	9	-0.03	12	-0.03	12	-0.03	10
-0.025	7	-0.025	9	-0.025	12	-0.025	12	-0.025	10
-0.02	7	-0.02	9	-0.02	12	-0.02	13	-0.02	10
-0.015	7	-0.015	9	-0.015	12	-0.015	12	-0.015	10
-0.01	7	-0.01	9	-0.01	12	-0.01	12	-0.01	10
-0.005	6	-0.005	9	-0.005	12	-0.005	13	-0.005	11
0	6	0	9	0	12	0	13	0	11

Table A-22. Data for Figure 6-6a.

IFN-γ (IU/ml)	Peak current (μA)	Standard deviation (μA)
0	5.2	1.50
0.01	16.6	2.25
0.1	18.6	3.81
1	21.4	3.49
10	26.7	3.34

Table A-23. Data for Figure 6-6b.

IP-10 (ng/ml)	Peak current (μA)	Standard deviation (μA)
0	7.7	3.13
0.01	15.3	0.88
0.1	16.1	2.95
1	18.1	1.54
10	21.6	1.00
100	23.5	1.75

Table A-24. Data for Figure 6-7.

IFN-γ (IU/ml)	Peak current (μA)	Standard deviation (μA)
0.01	16.6	2.25
0.1	18.6	3.81
1	21.4	3.49
10	26.7	3.34

IP-10 (ng/ml)	Peak current (μA)	Standard deviation (μA)
0.01	15.3	0.88
0.1	16.1	2.95
1	18.1	1.54
10	21.6	1.00
100	23.5	1.75

REFERENCES

REFERENCES

Abu El-Asrar, A. M., S. Struyf, D. Kangave, K. Geboes and J. Van Damme. 2006. Chemokines in proliferative diabetic retinopathy and proliferative vitreoretinopathy. *European cytokine network* 17(3): 155-165.

Ahn, J., T. H. Lee, T. Li, K. Heo, S. Hong, J. Ko, Y. Kim, Y. Shin and M. Kim. 2011. Electrical immunosensor based on a submicron-gap interdigitated electrode and gold enhancement. *Biosensors and Bioelectronics* 26(12): 4690-4696.

Alber, H., M. Frick, A. Suessenbacher, J. Doerler, M. Schirmer, E. Stocker, W. Dichtl, O. Pachinger and F. Weidinger. 2006. Effect of atorvastatin on circulating proinflammatory T-lymphocyte subsets and soluble CD40 ligand in patients with stable coronary artery disease - A randomized, placebo-controlled study. *American Heart Journal* 151(1): e1-139.e7.

Alexandre, M., V. Prado, M. Ulloa, C. Arellano and M. Rios. 2001. Detection of enterohemorrhagic *Escherichia coli* in meat foods using DNA probes, enzyme-linked immunosorbent assay and polymerase chain reaction. *Journal of Veterinary Medicine Series B-Infectious Diseases and Veterinary Public Health* 48(5): 321-330.

Aliberti, J. C. S., J. T. Souto, A. P. M. P. Marino, J. Lannes-Vieira, M. M. Teixeira, J. Farber, R. T. Gazzinelli and J. S. Silva. 2001. Modulation of Chemokine Production and Inflammatory Responses in Interferon-γ- and Tumor Necrosis Factor-R1-Deficient Mice during Trypanosoma cruzi Infection. *The American Journal of Pathology* 158(4): 1433-1440.

American Thoracic Society. 2000. Diagnostic Standards and Classification of Tuberculosis in Adults and Children. This official statement of the American Thoracic Society and the Centers for Disease Control and Prevention was adopted by the ATS Board of Directors, July 1999. This statement was endorsed by the Council of the Infectious Disease Society of America, September 1999. *American journal of respiratory and critical care medicine* 161(4 Pt 1): 1376-1395.

Andersen, P., M. Munk, J. Pollock and T. Doherty. 2000. Specific immune-based diagnosis of tuberculosis. *The Lancet* 356(9235): 1099-1104.

Anderson, M. J., E. Torres-Chavolla, B. A. Castro and E. C. Alocilja. 2011. One step alkaline synthesis of biocompatible gold nanoparticles using dextrin as capping agent. *Journal of Nanoparticle Research* 13(7): 2843-2851.

Anderson, M. J., H. R. Miller and E. C. Alocilja. 2013. PCR-less DNA co-polymerization detection of Shiga like toxin 1 (stx1) in *Escherichia coli* O157:H7. *Biosensors and Bioelectronics* 42(0): 581-585.

Armah, H. B., N. O. Wilson, B. Y. Sarfo, M. D. Powell, V. C. Bond, W. Anderson, A. A. Adjei, R. K. Gyasi, Y. Tettey, E. K. Wiredu, J. E. Tongren, V. Udhayakumar and J. K. Stiles. 2007.

Cerebrospinal fluid and serum biomarkers of cerebral malaria mortality in Ghanaian children. *Malaria Journal* 6147.

Asuri, P., S. Karajanagi, H. Yang, T. Yim, R. Kane and J. Dordick. 2006. Increasing protein stability through control of the nanoscale environment. *Langmuir* 22(13): 5833-5836.

Azzurri, A., O. Y. Sow, A. Amedei, B. Bah, S. Diallo, G. Peri, M. Benagiano, M. M. D'Elios, A. Mantovani and G. Del Prete. 2005. IFN-γ-inducible protein 10 and pentraxin 3 plasma levels are tools for monitoring inflammation and disease activity in Mycobacterium tuberculosis infection. *Microbes and Infection* 7(1): 1-8.

Bach, E., M. Aguet and R. Schreiber. 1997. The IFN gamma receptor: A paradigm for cytokine receptor signaling. *Annual Review of Immunology* 15563-&.

Bahsi, Z. B., A. Bueyukaksoy, S. M. Olmezcan, F. Simsek, M. H. Aslan and A. Y. Oral. 2009. A Novel Label-Free Optical Biosensor Using Synthetic Oligonucleotides from *E. coli* O157:H7: Elementary Sensitivity Tests. *Sensors* 9(6): 4890-4900.

Bai, H., Z. Zhang, Y. Guo and W. Jia. 2009. Biological Synthesis of Size-Controlled Cadmium Sulfide Nanoparticles Using Immobilized Rhodobacter sphaeroides. *Nanoscale Research Letters* 4(7): 717-723.

Barreiros dos Santos, M., J. P. Agusil, B. Prieto-Simón, C. Sporer, V. Teixeira and J. Samitier. 2013. Highly sensitive detection of pathogen *Escherichia coli* O157:H7 by electrochemical impedance spectroscopy. *Biosensors and Bioelectronics* 45(0): 174-180.

Bart, M., E. C. A. Stigter, H. R. Stapert, G. J. de Jong and W. P. van Bennekom. 2005. On the response of a label-free interferon-γ immunosensor utilizing electrochemical impedance spectroscopy. *Biosensors and Bioelectronics* 21(1): 49-59.

Beirne, P., P. Pantelidis, P. Charles, A. U. Wells, D. J. Abraham, C. P. Denton, K. I. Welsh, P. L. Shah, R. M. du Bois and P. Kelleher. 2009. Multiplex immune serum biomarker profiling in sarcoidosis and systemic sclerosis. *European Respiratory Journal* 34(6): 1376-1382.

Berg, K. 1994. Human Interferon-Gamma Quantified Via a Sensitive One-Site Monoclonal-Antibody in a Sandwich Elisa - a Peg Modification for Measurement in Serum. *Apmis* 102(1): 13-22.

Beutler, B. and A. Cerami. 1989. The Biology of Cachectin/tnf - a Primary Mediator of the Host Response. *Annual Review of Immunology* 7625-655.

Billmanjacobe, H., M. Carrigan, F. Cockram, L. Corner, I. Gill, J. Hill, T. Jessep, A. Milner and P. Wood. 1992. A Comparison of the Interferon-Gamma Assay with the Absorbed Elisa for the Diagnosis of Johnes Disease in Cattle. *Australian Veterinary Journal* 69(2): 25-28.

Bonetta, S., E. Borelli, S. Bonetta, O. Conio, F. Palumbo and E. Carraro. 2011. Development of a PCR protocol for the detection of *Escherichia coli* O157:H7 and Salmonella spp. in surface water. *Environmental monitoring and assessment* 177(1-4): 493-503.

Bonham, A. J., N. G. Paden, F. Ricci and K. W. Plaxco. 2013. Detection of IP-10 protein marker in undiluted blood serum via an electrochemical E-DNA scaffold sensor. *Analyst* 138(19): 5580-5583.

Borg, L., J. Kristiansen, J. Christensen, K. Jepsen and L. Poulsen. 2002. Evaluation of accuracy and uncertainty of ELISA assays for the determination of interleukin-4, interleukin-5, interferon-gamma and tumor necrosis factor-alpha. *Clinical Chemistry and Laboratory Medicine* 40(5): 509-519.

Borgia, J. A., S. Basu, L. P. Faber, A. W. Kim, J. S. Coon, K. A. Kaiser-Walters, C. Fhied, S. Thomas, O. Rouhi, W. H. Warren, P. Bonomi and M. J. Liptay. 2009. Establishment of a Multi-Analyte Serum Biomarker Panel to Identify Lymph Node Metastases in Non-small Cell Lung Cancer. *Journal of Thoracic Oncology* 4(3): 338-347.

Borish, L. C. and J. W. Steinke. 2003. 2. Cytokines and chemokines. *Journal of Allergy and Clinical Immunology* 111(2, Supplement 2): S460-S475.

Bouyon, R., H. Santana, E. Perez, N. Hernandez, G. Furrazola and M. Abrahantes. 2003. Development and validation of an enzyme-linked Immunosorbent assay (ELISA) for recombinant human gamma interferon. *Journal of Immunoassay & Immunochemistry* 24(1): 1-10.

Brasier, A. R., S. Victor, G. Boetticher, H. Ju, C. Lee, E. R. Bleecker, M. Castro, W. W. Busse and W. J. Calhoun. 2008. Molecular phenotyping of severe asthma using pattern recognition of bronchoalveolar lavage-derived cytokines. *Journal of Allergy and Clinical Immunology* 121(1): 30-37.

Britto, P. J., K. S. V. Santhanam, A. Rubio, J. A. Alonso and P. M. Ajayan. 1999. Improved Charge Transfer at Carbon Nanotube Electrodes. *Advanced Materials* 11(2): 154-157.

Brunet, M. 2012. Cytokines as predictive biomarkers of alloreactivity. *Clinica Chimica Acta* 413(17–18): 1354-1358.

Burgdorf, S. K., M. H. Claesson, H. J. Nielsen and J. Rosenberg. 2009. Changes in cytokine and biomarker blood levels in patients with colorectal cancer during dendritic cell-based vaccination. *Acta Oncologica* 48(8): 1157-1164.

Busbee, B., S. Obare and C. Murphy. 2003. An improved synthesis of high-aspect-ratio gold nanorods. *Advanced Materials* 15(5): 414-416.

Caproni, M., C. Cardinali, B. Giomi, E. Antiga, A. D'Agata, S. Walter and P. Fabbri. 2004. Serological detection of eotaxin, IL-4, IL-13, IFN-γ, MIP-1α, TARC and IP-10 in chronic autoimmune urticaria and chronic idiopathic urticaria. *Journal of dermatological science* 36(1): 57-59.

Carter, J. A., S. D. Mehta, M. V. Mungillo, C. C. Striemer and B. L. Miller. 2011. Analysis of inflammatory biomarkers by Arrayed Imaging Reflectometry. *Biosensors and Bioelectronics* 26(9): 3944-3948.

CAST- Council for Agricultural Science and Technology. 1994. Foodborne Pathogens: Risks and Consequences, Report No. 122.

CDC, 2013. Multistate Outbreak of Shiga toxin-producing *Escherichia coli* O157:H7 Infections Linked to Ready-to-Eat Salads. Available at: http://www.cdc.gov/ecoli/2013/O157H7-11-13/. Accessed 6 Januarary 2014.

CDC, 2012a. Multistate Outbreak of Shiga Toxin-producing *Escherichia coli* O157:H7 Infections Linked to Organic Spinach and Spring Mix Blend (Final Update). Available at: http://www.cdc.gov/ecoli/2012/O157H7-11-12/index.html. Accessed 3 October 2013.

CDC, 2012b. Testing for TB Infection. Available at: http://www.cdc.gov/tb/topic/testing/default.htm. Accessed 3 October 2013.

CDC, 2011a. Investigation Announcement: Multistate Outbreak of *E. coli* O157:H7 Infections Linked to Romaine Lettuce. Available at: http://www.cdc.gov/ecoli/2011/ecoliO157/romainelettuce/120711/. Accessed 3 October, 2013.

CDC, 2011b. Investigation Announcement: Multistate Outbreak of *E. coli* O157:H7 Infections Associated with Lebanon Bologna. Available at: http://www.cdc.gov/ecoli/2011/O157_0311/index.html. Accessed 6 January 2014.

CDC, 2011c. Investigation Update: Multistate Outbreak of *E. coli* O157:H7 Infections Associated with In-shell Hazelnuts. Available at: http://www.cdc.gov/ecoli/2011/hazelnuts0157/index.html. Accessed 6 January 2014.

CDC, 2011d. Diagnosis of Tuberculosis Disease. Available at: http://www.cdc.gov/tb/publications/factsheets/testing/diagnosis.htm. Accessed 3 October 2013.

CDC, 2009. Multistate Outbreak of *E. coli* O157:H7 Infections Linked to Eating Raw Refrigerated, Prepackaged Cookie Dough. Available at: http://www.cdc.gov/ecoli/2009/0630.html. Accessed 3 October 2013.

CDC, 2007. Multistate Outbreak of *E. coli* O157 Infections Linked to Topp's Brand Ground Beef Patties. Available at: http://www.cdc.gov/ecoli/2007/october/100207.html. Accessed 3 October 2013.

Chalmers, R., H. Aird and F. Bolton. 2000. Waterborne *Escherichia coli* O157. *Journal of applied microbiology* 88124S-132S.

Chang, K., Y. Chang, C. Wu, Y. Liu, M. Chen, N. Tsang, C. Hsu, Y. Chang and J. Yu. 2011. Multiplexed Immunobead-Based Profiling of Cytokine Markers for Detection of Nasopharyngeal Carcinoma and Prognosis of Patient Survival. *Head and Neck-Journal for the Sciences and Specialties of the Head and Neck* 33(6): 886-897.

Cho, I. and J. Irudayaraj. 2013. In-situ immuno-gold nanoparticle network ELISA biosensors for pathogen detection. *International journal of food microbiology* 164(1): 70-75.

Chou, T., C. Chuang and C. Wu. 2010. Quantification of Interleukin-6 in cell culture medium using surface plasmon resonance biosensors. *Cytokine* 51(1): 107-111.

Chowdhury, F., A. Williams and P. Johnson. 2009. Validation and comparison of two multiplex technologies, Luminex® and Mesoscale Discovery, for human cytokine profiling. *Journal of immunological methods* 340(1): 55-64.

Christensen, E., M. Pintilie, K. R. Evan, M. Lenarduzzi, C. Menard, C. N. Catton, E. P. Diamandis and R. G. Bristow. 2009. Longitudinal Cytokine Expression during IMRT for Prostate Cancer and Acute Treatment Toxicity. *Clinical Cancer Research* 15(17): 5576-5583.

Claussen, J. C., A. Kumar, D. B. Jaroch, M. H. Khawaja, A. B. Hibbard, D. M. Porterfield and T. S. Fisher. 2012. Nanostructuring Platinum Nanoparticles on Multilayered Graphene Petal Nanosheets for Electrochemical Biosensing. *Advanced Functional Materials* 22(16): 3399-3405.

Cloutier, B. C. 2012. Development of mitigation strategies toward preventative postures in food defense. PhD diss. United States -- Michigan: Michigan State University.

Cox, J. H., G. Ferrari and S. Janetzki. 2006. Measurement of cytokine release at the single cell level using the ELISPOT assay. *Methods* 38(4): 274-282.

Cunningham, B. T. 2010. Photonic Crystal Surfaces as a General Purpose Platform for Label-Free and Fluorescent Assays. *Jala* 15(2): 120-135.

Czerkinsky, C., G. Andersson, H. Ekre, L. Nilsson, L. Klareskog and Ö. Ouchterlony. 1988. Reverse ELISPOT assay for clonal analysis of cytokine production I. Enumeration of gamma-interferon-secreting cells. *Journal of immunological methods* 110(1): 29-36.

Dannenberg, A. M. 1992. Pathogenesis of pulmonary tuberculosis: host–parasite interactions, cell-mediated immunity, and delayed-type hypersensitivity In *Basic Principles in Tuberculosis, 3rd ed*, ed. D. Schlossberg, New York: Springer-Verlag.

Darbha, G. K., U. S. Rai, A. K. Singh and P. C. Ray. 2008. Gold-nanorod-based sensing of sequence specific HIV-1 virus DNA by using hyper-Rayleigh scattering spectroscopy RID F-8827-2011. *Chemistry-a European Journal* 14(13): 3896-3903.

DeCory, T., R. Durst, S. Zimmerman, L. Garringer, G. Paluca, H. DeCory and R. Montagna. 2005. Development of an immunomagnetic bead-immunoliposome fluorescence assay for rapid detection of *Escherichia coli* O157 : H7 in aqueous samples and comparison of the assay with a standard microbiological method. *Applied and Environmental Microbiology* 71(4): 1856-1864.

Delannoy, S., L. Beutin and P. Fach. 2012. Use of Clustered Regularly Interspaced Short Palindromic Repeat Sequence Polymorphisms for Specific Detection of Enterohemorrhagic *Escherichia coli* Strains of Serotypes O26:H11, O45:H2, O103:H2, O111:H8, O121:H19, O145:H28, and O157:H7 by Real-Time PCR. *Journal of clinical microbiology* 50(12): 4035-4040.

Dijksma, M., B. Kamp, J. Hoogvliet and W. van Bennekom. 2001. Development of an electrochemical immunosensor for direct detection of interferon-gamma at the attomolar level. *Analytical Chemistry* 73(5): 901-907.

Ding, C., Q. Zhang, J. Lin and S. Zhang. 2009. Electrochemical detection of DNA hybridization based on bio-bar code method. *Biosensors and Bioelectronics* 24(10): 3140-3143.

Dinu, L. and S. Bach. 2013. Detection of viable but non-culturable *Escherichia coli* O157:H7 from vegetable samples using quantitative PCR with propidium monoazide and immunological assays. *Food Control* 31(2): 268-273.

Dou, Y., S. J. Haswell, J. Greenman and J. Wadhawan. 2012. Voltammetric Immunoassay for the Detection of Protein Biomarkers. *Electroanalysis* 24(2): 264-272.

Dudak, F. C. and I. H. Boyaci. 2008. Enumeration of immunomagnetically captured *Escherichia coli* in water samples using quantum dot-labeled antibodies RID F-7342-2010. *Journal of Rapid Methods and Automation in Microbiology* 16(2): 122-131.

Ealick, S. E., W. J. Cook, S. Vijay-Kumar, M. Carson, T. L. Nagabhushan, P. P. Trotta and C. E. Bugg. 1991. Three-dimensional structure of recombinant human interferon-gamma. *Science (New York, N.Y.)* 252(5006): 698-702.

Eickmeier, O., M. Huebner, E. Herrmann, U. Zissler, M. Rosewich, P. C. Baer, R. Buhl, S. Schmitt-Grohe, S. Zielen and R. Schubert. 2010. Sputum biomarker profiles in cystic fibrosis (CF) and chronic obstructive pulmonary disease (COPD) and association between pulmonary function. *Cytokine* 50(2): 152-157.

El-Deab, M., T. Okajima and T. Ohsaka. 2003. Electrochemical reduction of oxygen on gold nanoparticle-electrodeposited glassy carbon electrodes. *Journal of the Electrochemical Society* 150(7): A851-A857.

Elizaquivel, P., G. Sanchez and R. Aznar. 2012. Application of propidium monoazide quantitative PCR for selective detection of live *Escherichia coli* O157:H7 in vegetables after inactivation by essential oils. *International journal of food microbiology* 159(2): 115-121.

Ertas, N., Z. Gonulalan, Y. Yildirim, F. Karadal, S. Abay and S. Al. 2013. Detection of *Escherichia coli* O157:H7 using immunomagnetic separation and mPCR in Turkish foods of animal origin. *Letters in applied microbiology* 57(4): 373-379.

Eteshola, E. 2010. Isolation of scFv fragments specific for monokine induced by interferon-gamma (MIG) using phage display. *Journal of immunological methods* 358(1–2): 104-110.

Fan, Q., J. Zhao, H. Li, L. Zhu and G. Li. 2012. Exonuclease III-based and gold nanoparticle-assisted DNA detection with dual signal amplification. *Biosensors and Bioelectronics* 33(1): 211-215.

Faridbod, F., V. K. Gupta and H. A. Zamani. 2011. Electrochemical Sensors and Biosensors. *International Journal of Electrochemistry* 2011: 1-2.

Farrar, M. and R. Schreiber. 1993. The Molecular Cell Biology of Interferon-Gamma and its Receptor. *Annual Review of Immunology* 11571-611.

FDA, 2007. FDA Finalizes Report on 2006 Spinach Outbreak. Available at: http://www.fda.gov/NewsEvents/Newsroom/PressAnnouncements/2007/ucm108873.htm. Accessed 8 December, 2013.

Fedio, W. M., K. C. Jinneman, K. J. Yoshitomi, R. Zapata, C. N. Wendakoon, P. Browning and S. D. Weagant. 2011. Detection of *E. coli* O157:H7 in raw ground beef by Pathatrix™ immunomagnetic-separation, real-time PCR and cultural methods. *International journal of food microbiology* 148(2): 87-92.

Fletcher, M. A., X. R. Zeng, Z. Barnes, S. Levis and N. G. Klimas. 2009. Plasma cytokines in women with chronic fatigue syndrome. *Journal of Translational Medicine* 796.

Fong, A., S. Alam, T. Imai, B. Haribabu and D. Patel. 2002. CX(3)CR1 tyrosine sulfation enhances fractalkine-induced cell adhesion. *Journal of Biological Chemistry* 277(22): 19418-19423.

Fratamico, P. and T. Strobaugh. 1998. Evaluation of an enzyme-linked immunosorbent assay, direct immunofluorescent filter technique, and multiplex polymerase chain reaction for detection of *Escherichia coli* O157 : H7 seeded in beef carcass wash water. *Journal of food protection* 61(8): 934-938.

Frucht, D., T. Fukao, C. Bogdan, H. Schindler, J. O'Shea and S. Koyasu. 2001. IFN-gamma-production by antigen-presenting cells: mechanisms emerge. *Trends in immunology* 22(10): 556-560.

Fujita, K., C. M. Ewing, R. H. Getzenberg, J. K. Parsons, W. B. Isaacs and C. P. Pavlovich. 2010. Monocyte Chemotactic Protein-1 (MCP-1/CCL2) Is Associated With Prostatic Growth Dysregulation and Benign Prostatic Hyperplasia. *Prostate* 70(5): 473-481.

Gatto-Menking, D. L., H. Yu, J. G. Bruno, M. T. Goode, M. Miller and A. W. Zulich. 1995. Sensitive detection of biotoxoids and bacterial spores using an immunomagnetic electrocheminescence sensor. *Biosensors and Bioelectronics* 10(6–7): 501-507.

Ganesh, N., I. D. Block, P. C. Mathias, W. Zhang, E. Chow, V. Malyarchuk and B. T. Cunningham. 2008. Leaky-mode assisted fluorescence extraction: application to fluorescence enhancement biosensors RID B-3835-2010. *Optics Express* 16(26): 21626-21640.

Geluk, A., van der Ploeg-van Schip,Jolien J., K. E. van Meijgaarden, S. Commandeur, J. W. Drijfhout, W. E. Benckhuijsen, K. L. M. C. Franken, B. Naafs and T. H. M. Ottenhoff. 2010. Enhancing Sensitivity of Detection of Immune Responses to Mycobacterium leprae Peptides in Whole-Blood Assays. *Clinical and Vaccine Immunology* 17(6): 993-1004.

Gerstein, A. S. 2001; 2002. Nucleotides, Oligonucleotides, and Polynucleotides. In *Molecular Biology Problem Solver*, 267-289. ed. Anonymous , John Wiley & Sons, Inc.

Gnedenko, O. V., Y. V. Mezentsev, A. A. Molnar, A. V. Lisitsa, A. S. Ivanov and A. I. Archakov. 2013. Highly sensitive detection of human cardiac myoglobin using a reverse sandwich immunoassay with a gold nanoparticle-enhanced surface plasmon resonance biosensor. *Analytica Chimica Acta* 759(0): 105-109.

Goletti, D., A. Raja, B. S. A. Kabeer, C. Rodrigues, A. Sodha, S. Carrara, G. Vernet, C. Longuet, G. Ippolito, S. Thangaraj, M. Leportier, E. Girardi and P. H. Lagrange. 2010. Is IP-10 an Accurate Marker for Detecting M. tuberculosis-Specific Response in HIV-Infected Persons? *Plos One* 5(9): e12577.

Goldsby, R A, Kindt, T J, Osborne, B A, Kuby, J. 2003. Enzyme-Linked Immunosorbent Assay. In *Immunology, 5th ed,* 148-150. ed. Anonymous , New York: W. H. Freeman.

Gottlieb, A., A. Luster, D. Posnett and D. Carter. 1988. Detection of a Gamma-Interferon-Induced Protein Ip-10 in Psoriatic Plaques. *Journal of Experimental Medicine* 168(3): 941-948.

Greg, H. T. 2007. Chapter 24: Preparation of Colloidal Gold-Labeled Protein. In *Bioconjugate Techniques (Second Edition),* 924-935. ed. Anonymous , New York: Academic Press.

GRIFFIN, P. and R. TAUXE. 1991. The Epidemiology of Infections Caused by *Escherichia Coli* O157-H7, Other Enterohemorrhagic *Escherichia Coli*, and the Associated Hemolytic Uremic Syndrome. *Epidemiologic reviews* 1360-98.

Gross, S. and D. Piwnica-Worms. 2005. Real-time imaging of ligand-induced IKK activation in intact cells and in living mice. *Nature Methods* 2(8): 607-614.

Guan, Z. P., Y. Jiang, F. Gao, L. Zhang, G. H. Zhou and Z. J. Guan. 2013. Rapid and simultaneous analysis of five foodborne pathogenic bacteria using multiplex PCR. *European Food Research and Technology* 237(4): 627-637.

Hall, W. P., S. N. Ngatia and R. P. Van Duyne. 2011. LSPR Biosensor Signal Enhancement Using Nanoparticle-Antibody Conjugates. *Journal of Physical Chemistry C* 115(5): 1410-1414.

Hamed, M. A. A., S. A. A. Ahmed and H. M. Khaled. 2011. Efficiency of diagnostic biomarkers among colonic schistosomiasis Egyptian patients. *Memorias do Instituto Oswaldo Cruz* 106(3): 322-329.

Hao, R., H. Song, G. Zuo, R. Yang, H. Wei, D. Wang, Z. Cui, Z. Zhang, Z. Cheng and X. Zhang. 2011. DNA probe functionalized QCM biosensor based on gold nanoparticle amplification for *Bacillus anthracis* detection. *Biosensors and Bioelectronics* 26(8): 3398-3404.

Harper, J. C., R. Polsky, D. R. Wheeler, S. M. Dirk and S. M. Brozik. 2007. Selective immobilization of DNA and antibody probes on electrode arrays: Simultaneous electrochemical detection of DNA and protein on a single platform. *Langmuir* 23(16): 8285-8287.

Haugum, K., L. T. Brandal, I. Lobersli, G. Kapperud and B. -. Lindstedt. 2011. Detection of virulent *Escherichia coli* O157 strains using multiplex PCR and single base sequencing for SNP characterization. *Journal of applied microbiology* 110(6): 1592-1600.

He, J., Y. Tian, Z. Cao, W. Zou and X. Sun. 2013. An electrochemical immunosensor based on gold nanoparticle tags for picomolar detection of c-Myc oncoprotein. *Sensors and Actuators B-Chemical* 181835-841.

Heijmans-Antonissen, C., F. Wesseldijk, R. J. M. Munnikes, F. J. P. M. Huygen, P. van der Meijden, W. C. J. Hop, H. Hooijkaas and F. J. Zijlstra. 2006. Multiplex bead array assay for detection of 25 soluble cytokines in blister fluid of patients with complex regional pain syndrome type 1. *Mediators of inflammation*28398.

Hill, H. D. and C. A. Mirkin. 2006. The bio-barcode assay for the detection of protein and nucleic acid targets using DTT-induced ligand exchange RID E-3911-2010. *Nature Protocols* 1(1): 324-336.

Hill, H. D., R. A. Vega and C. A. Mirkin. 2007. Nonenzymatic detection of bacterial genomic DNA using the bio bar code assay RID E-3911-2010. *Analytical Chemistry* 79(23): 9218-9223.

Ho, J., D. N. Rush, M. Karpinski, L. Storsley, I. W. Gibson, J. Bestland, A. Gao, W. Stefura, K. T. HayGlass and P. W. Nickerson. 2011. Validation of Urinary CXCL10 As a Marker of Borderline, Subclinical, and Clinical Tubulitis. *Transplantation* 92(8): 878-882.

Huang, R., B. Burkholder, V. S. Jones, W. Jiang, Y. Mao, Q. Chen and Z. Shi. 2012. Cytokine Antibody Arrays in Biomarker Discovery and Validation. *Current Proteomics* 9(1): 55-70.

Ibenyassine, K., R. Aitmhand, Y. Karamoko and M. Mustapha Ennaji. 2008. A simple and rapid detection by pcr of enteropathogenic *Escherichia coli* in naturally contaminated vegetables. *Journal of Rapid Methods and Automation in Microbiology* 16(2): 113-121.

Ikeguchi, M. and Y. Hirooka. 2005. Interleukin-2 gene expression is a new biological prognostic marker in hepatocellular carcinomas. *Onkologie* 28(5): 255-259.

Imashuku, S., S. Hibi, Y. Tabata, M. Sako, Y. Sekine, K. Hirayama, H. Sakazaki, N. Maeda, H. Kito, H. Shichino and H. Mugishima. 1998. Biomarker and morphological characteristics of Epstein-Barr virus-related hemophagocytic lymphohistiocytosis. *Medical and pediatric oncology* 31(3): 131-137.

Janeway, C. A. J., P. Travers, M. Walport and M. J. Shlomchik. 2001. *Immunobiology, 5th edition.* New York: Garland Science.

Jenison, R., H. La, A. Haeberli, R. Ostroff and B. Polisky. 2001. Silicon-based biosensors for rapid detection of protein or nucleic acid targets. *Clinical chemistry* 47(10): 1894-1900.

Jiang, D., F. Liu, C. Liu, L. Liu and X. Pu. 2013. An Electrochemical Sensor Based on Allosteric Molecular Beacons for DNA Detection of *Escherichia Coli* O157:H7. *International Journal of Electrochemical Science* 8(7): 9390-9398.

Jiang, X., R. Wang, Y. Wang, X. Su, Y. Ying, J. Wang and Y. Li. 2011. Evaluation of different micro/nanobeads used as amplifiers in QCM immunosensor for more sensitive detection of *E. coli* O157:H7. *Biosensors and Bioelectronics* 29(1): 23-28.

Jiao, X. X., J. R. Chen, X. Y. Zhang, H. Q. Luo and N. B. Li. 2013. A chronocoulometric aptasensor based on gold nanoparticles as a signal amplification strategy for detection of thrombin. *Analytical Biochemistry* 441(2): 95-100.

Jie, G., B. Liu, H. Pan, J. Zhu and H. Chen. 2007. CdS nanocrystal-based electrochemiluminescence biosensor for the detection of low-density lipoprotein by increasing sensitivity with gold nanoparticle amplification. *Analytical Chemistry* 79(15): 5574-5581.

Johnson, R., R. Durham, S. Johnson, L. MacDonald, S. Jeffrey and B. Butman. 1995. Detection of *Escherichia-Coli* O157-H7 in Meat by an Enzyme-Linked-Immunosorbent-Assay, Ehec-Tek. *Applied and Environmental Microbiology* 61(1): 386-388.

Joung, H., N. Lee, S. K. Lee, J. Ahn, Y. B. Shin, H. Choi, C. Lee, S. Kim and M. Kim. 2008. High sensitivity detection of 16s rRNA using peptide nucleic acid probes and a surface plasmon resonance biosensor. *Analytica Chimica Acta* 630(2): 168-173.

Kabeer, B. S. A., B. Raman, A. Thomas, V. Perumal and A. Raja. 2010. Role of QuantiFERON-TB Gold, Interferon Gamma Inducible Protein-10 and Tuberculin Skin Test in Active Tuberculosis Diagnosis. *Plos One* 5(2): e9051.

Kaplan, G., A. Luster, G. Hancock and Z. Cohn. 1987. The Expression of a Gamma-Interferon Induced Protein (Ip-10) in Delayed Immune-Responses in Human-Skin. *Journal of Experimental Medicine* 166(4): 1098-1108.

Karlsson, A. C., J. N. Martin, S. R. Younger, B. M. Bredt, L. Epling, R. Ronquillo, A. Varma, S. G. Deeks, J. M. McCune, D. F. Nixon and E. Sinclair. 2003. Comparison of the ELISPOT and cytokine flow cytometry assays for the enumeration of antigen-specific T cells. *Journal of immunological methods* 283(1–2): 141-153.

Kasprowicz, V. O., J. E. Mitchell, S. Chetty, P. Govender, K. G. Huang, H. A. Fletcher, D. P. Webster, S. Brown, A. Kasmar, K. Millington, C. L. Day, N. Mkhwanazi, C. McClurg, F. Chonco, A. Lalvani, B. D. Walker, T. Ndung'u and P. Klenerman. 2011. A Molecular Assay

for Sensitive Detection of Pathogen-Specific T-Cells RID D-1470-2011. *Plos One* 6(8): e20606.

Kato, M., H. Tsukagoshi, M. Yoshizumi, M. Saitoh, K. Kozawa, Y. Yamada, K. Maruyama, Y. Hayashi and H. Kimura. 2011. Different cytokine profile and eosinophil activation are involved in rhinovirus- and RS virus-induced acute exacerbation of childhood wheezing. *Pediatric Allergy and Immunology* 22(1): e87-e94.

Kellar, K. L., J. Gehrke, S. E. Weis, A. Mahmutovic-Mayhew, B. Davila, M. J. Zajdowicz, R. Scarborough, P. A. LoBue, A. A. Lardizabal, C. L. Daley, R. R. Reves, J. Bernardo, B. H. Campbell, W. C. Whitworth and G. H. Mazurek. 2011. Multiple Cytokines Are Released When Blood from Patients with Tuberculosis Is Stimulated with Mycobacterium tuberculosis Antigens. *Plos One* 6(11): e26545.

Kim, D., A. Reilly and D. Lawrence. 2001. Relationships between IFN gamma, IL-6, corticosterone, and Listeria monocytogenes pathogenesis in BALB/c mice. *Cellular immunology* 207(1): 13-18.

Konjevic, G., S. Radenkovic, T. Srdic, V. Jurisic, L. Stamatovic and M. Milovic. 2011. Association of decreased NK cell activity and IFN gamma expression with pSTAT dysregulation in breast cancer patients. *Journal of Buon* 16(2): 219-226.

Krasnikova, T. L., P. I. Nikitin, T. I. Ksenevich, B. G. Gorshkov, T. L. Bushueva, T. I. Arefieva, N. Y. Ruleva, M. V. Sidorova, A. A. Azmuko and Z. D. Bespalova. 2011. Inhibitor of Inflammation, Peptide Fragment (65-76) of Monocyte Chemotactic Protein-1 (MCP-1), Prevents Binding of MCP-1 to Heparin. *Biologicheskie Membrany* 28(1): 68-76.

Kudva, I., P. Hatfield and C. Hovde. 1997. Characterization of *Escherichia coli* O157:H7 and other Shiga toxin-producing *E-coli* serotypes isolated from sheep. *Journal of clinical microbiology* 35(4): 892-899.

Kumar, A., S. Grover and V. K. Batish. 2013. Application of multiplex PCR assay based on uidR and fliCH7 genes for detection of *Escherichia coli* O157:H7 in milk. *Journal of General and Applied Microbiology* 59(1): 11-19.

La Belle, J. T., K. Bhavsar, A. Fairchild, A. Das, J. Sweeney, T. L. Alford, J. Wang, V. P. Bhavanandan and L. Joshi. 2007. A cytokine immunosensor for multiple sclerosis detection based upon label-free electrochemical impedance spectroscopy. *Biosensors and Bioelectronics* 23(3): 428-431.

Laczka, O., J. Maesa, N. Godino, J. del Campo, M. Fougt-Hansen, J. P. Kutter, D. Snakenborg, F. Muñoz-Pascual and E. Baldrich. 2011. Improved bacteria detection by coupling magneto-immunocapture and amperometry at flow-channel microband electrodes. *Biosensors and Bioelectronics* 26(8): 3633-3640.

Law, H., C. Cheung, H. Ng, S. Sia, Y. Chan, W. Luk, J. Nicholls, J. Peiris and Y. Lau. 2005. Chemokine up-regulation in SARS-coronavirus-infected, monocyte-derived human dendritic cells RID C-4233-2009 RID C-4608-2009. *Blood* 106(7): 2366-2374.

Lee, E. and R. Holzman. 2002. Evolution and current use of the tuberculin test. *Clinical Infectious Diseases* 34(3): 365-370.

Li, K., Y. Lai, W. Zhang and L. Jin. 2011. Fe2O3@Au core/shell nanoparticle-based electrochemical DNA biosensor for *Escherichia coli* detection. *Talanta* 84(3): 607-613.

Li, Y., L. Fang, P. Cheng, J. Deng, L. Jiang, H. Huang and J. Zheng. 2013. An electrochemical immunosensor for sensitive detection of *Escherichia coli* O157:H7 using C60 based biocompatible platform and enzyme functionalized Pt nanochains tracing tag. *Biosensors and Bioelectronics* 49(0): 485-491.

Li, Y., P. Cheng, J. Gong, L. Fang, J. Deng, W. Liang and J. Zheng. 2012. Amperometric immunosensor for the detection of *Escherichia coli* O157:H7 in food specimens. *Analytical Biochemistry* 421(1): 227-233.

Linman, M. J., K. Sugerman and Q. Cheng. 2010. Detection of low levels of *Escherichia coli* in fresh spinach by surface plasmon resonance spectroscopy with a TMB-based enzymatic signal enhancement method. *Sensors and Actuators B: Chemical* 145(2): 613-619.

Liu, M., S. Guo and J. K. Stiles. 2011. The emerging role of CXCL10 in cancer (Review). *Oncology Letters* 2(4): 583-589.

Liu, W., H. Dan, Z. Wang, L. Jiang, Y. Zhou, M. Zhao, Q. Chen and X. Zeng. 2009. IFN-Gamma and IL-4 in Saliva of Patients with Oral Lichen Planus: A Study in an Ethnic Chinese Population. *Inflammation* 32(3): 176-181.

Liu, Y., D. Yao, H. Chang, C. Liu and C. Chen. 2008. Magnetic bead-based DNA detection with multi-layers quantum dots labeling for rapid detection of *Escherichia coli* O157:H7. *Biosensors and Bioelectronics* 24(4): 558-565.

Liu, Y., N. Tuleouva, E. Ramanculov and A. Revzin. 2010. Aptamer-Based Electrochemical Biosensor for Interferon Gamma Detection. *Analytical Chemistry* 82(19): 8131-8136.

Liu, Y., Y. Zhu, Y. Zeng and F. Xu. 2009. An Effective Amperometric Biosensor Based on Gold Nanoelectrode Arrays. *Nanoscale Research Letters* 4(3): 210-215.

Ljung, T., L. -. Axelsson, M. Herulf, J. O. Lundberg and P. M. Hellstrom. 2007. Early changes in rectal nitric oxide and mucosal inflammatory mediators in Crohn's colitis in response to infliximab treatment. *Alimentary Pharmacology & Therapeutics* 25(8): 925-932.

Locking, M., S. O'Brien, W. Reilly, E. Wright, D. Campbell, J. Coia, L. Browning and C. Ramsay. 2001. Risk factors for sporadic cases of *Escherichia coli* O157 infection: the importance of contact with animal excreta. *Epidemiology and infection* 127(2): 215-220.

Lokensgard, J., S. Hu, W. Sheng, M. vanOijen, D. Cox, M. Cheeran and P. Peterson. 2001. Robust expression of TNF-alpha, IL-1 beta, RANTES, and IP-10 by human microglial cells during nonproductive infection with herpes simplex virus RID C-2135-2009. *Journal of neurovirology* 7(3): 208-219.

Lowanitchapat, A., S. Payungporn, A. Sereemaspun, P. Ekpo, D. Phulsuksombati, Y. Poovorawan and C. Chirathaworn. 2010. Expression of TNF-α, TGF-β, IP-10 and IL-10 mRNA in kidneys of hamsters infected with pathogenic Leptospira. *Comparative immunology, microbiology and infectious diseases* 33(5): 423-434.

Luo, Y., S. Nartker, H. Miller, D. Hochhalter, M. Wiederoder, S. Wiederoder, E. Setterington, L. T. Drzal and E. C. Alocilja. 2010. Surface functionalization of electrospun nanofibers for detecting *E. coli* O157:H7 and BVDV cells in a direct-charge transfer biosensor. *Biosensors and Bioelectronics* 26(4): 1612-1617.

Luster, A. D., J. C. Unkeless and J. V. Ravetch. 1985. Gamma-interferon transcriptionally regulates an early-response gene containing homology to platelet proteins. *Nature* 315(6021): 672-676.

Ma, Y., L. Visser, H. Roelofsen, M. de Vries, A. Diepstra, G. van Imhoff, T. van der Wal, M. Luinge, G. Alvarez-Llamas, H. Vos, S. Poppema, R. Vonk and A. van den Berg. 2008. Proteomics analysis of Hodgkin lymphoma: identification of new players involved in the cross-talk between HRS cells and infiltrating lymphocytes RID D-1204-2012 RID H-1718-2011. *Blood* 111(4): 2339-2346.

Maecker, H. 2004. Cytokine Flow Cytometry. In *Flow Cytometry Protocols,* 95-107. ed. T. Hawley and Hawley, R., Totowa, NJ: Humana Press.

Maecker, H. T., J. Hassler, J. K. Payne, A. Summers, K. Comatas, M. Ghanayem, M. A. Morse, T. M. Clay, H. K. Lyerly, S. Bhatia, S. A. Ghanekar, V. C. Maino, C. delaRosa and M. L. Disis. 2008. Precision and linearity targets for validation of an IFN gamma ELISPOT, cytokine flow cytometry, and tetramer assay using CMV peptides. *Bmc Immunology* 99.

Maecker, H., A. Rinfret, P. D'Souza, J. Darden, E. Roig, C. Landry, P. Hayes, J. Birungi, O. Anzala, M. Garcia, A. Harari, I. Frank, R. Baydo, M. Baker, J. Holbrook, J. Ottinger, L. Lamoreaux, C. Epling, E. Sinclair, M. Suni, K. Punt, S. Calarota, S. El-Bahi, G. Alter, H. Maila, E. Kuta, J. Cox, C. Gray, M. Altfeld, N. Nougarede, J. Boyer, L. Tussey, T. Tobery, B. Bredt, M. Roederer, R. Koup, V. Maino, K. Weinhold, G. Pantaleo, J. Gilmour, H. Horton and R. Sekaly. 2005. Standardization of cytokine flow cytometry assays. *Bmc Immunology* 6.

Malu, S., S. Srinivasan, P. Kumar Maiti, D. Rajagopal, B. John and D. Nandi. 2003. IFN-γ bioassay: development of a sensitive method by measuring nitric oxide production by peritoneal exudate cells from C57BL/6 mice. *Journal of immunological methods* 272(1–2): 55-65.

Martha Salgado, D., J. Miguel Eltit, K. Mansfield, C. Panqueba, D. Castro, M. Rocio Vega, K. Xhaja, D. Schmidt, K. J. Martin, P. D. Allen, J. Antonio Rodriguez, J. H. Dinsmore, J. R. Lopez and I. Bosch. 2010. Heart and Skeletal Muscle Are Targets of Dengue Virus Infection. *Pediatric Infectious Disease Journal* 29(3): 238-242.

Matoba, N., Y. Yu, K. Mestan, C. Pearson, K. Ortiz, N. Porta, P. Thorsen, K. Skogstrand, D. M. Hougaard, B. Zuckerman and X. Wang. 2009. Differential Patterns of 27 Cord Blood Immune Biomarkers Across Gestational Age. *Pediatrics* 123(5): 1320-1328.

Matsunaga, K., T. Ichikawa, S. Yanagisawa, K. Akamatsu, A. Koarai, T. Hirano, H. Sugiura, Y. Minakata and M. Ichinose. 2009. Clinical Application of Exhaled Breath Condensate Analysis in Asthma: Prediction of FEV(1) Improvement by Steroid Therapy. *Respiration* 78(4): 393-398.

Mazurek, G. H., S. E. Weis, P. K. Moonan, C. L. Daley, J. Bernardo, A. A. Lardizabal, R. R. Reves, S. R. Toney, L. J. Daniels and P. A. LoBue. 2007. Prospective comparison of the tuberculin skin test and 2 whole-blood interferon-gamma release assays in persons with suspected tuberculosis. *Clinical Infectious Diseases* 45(7): 837-845.

Meager, A. 2002. Biological assays for interferons. *Journal of immunological methods* 261(1-2): 21-36.

Min, K., M. Cho, S. Han, Y. Shim, J. Ku and C. Ban. 2008. A simple and direct electrochemical detection of interferon-γ using its RNA and DNA aptamers. *Biosensors and Bioelectronics* 23(12): 1819-1824.

Miszczycha, S. D., S. Ganet, L. Duniere, C. Rozand, E. Loukiadis and D. Thevenot-Sergentet. 2012. Novel Real-Time PCR Method To Detect *Escherichia coli* O157:H7 in Raw Milk Cheese and Raw Ground Meat. *Journal of food protection* 75(8): 1373-1381.

Moganedi, K. L. M., E. M. A. Goyvaerts, S. N. Venter and M. M. Sibara. 2007. Optimisation of the PCR-invA primers for the detection of Salmonella in drinking and surface waters following a pre-cultivation step RID A-9987-2008. *Water Sa* 33(2): 195-202.

Morgan, M., C. Horstmeier, D. Deyoung and G. Roberts. 1983. Comparison of a Radiometric Method (Bactec) and Conventional Culture Media for Recovery of Mycobacteria from Smear-Negative Specimens. *Journal of clinical microbiology* 18(2): 384-388.

Moser, B. and P. Loetscher. 2001. Lymphocyte traffic control by chemokines. *Nature immunology* 2(2): 123-128.

Murphy, C. J., A. M. Gole, S. E. Hunyadi, J. W. Stone, P. N. Sisco, A. Alkilany, B. E. Kinard and P. Hankins. 2008. Chemical sensing and imaging with metallic nanorods. *Chemical Communications*(5): 544-557.

Nakai, H., Y. Kawamura, K. Sugata, H. Sugiyama, Y. Enomoto, Y. Asano, M. Ihira, M. Ohashi, T. Kato and T. Yoshikawa. 2012. Host factors associated with the kinetics of Epstein-Barr virus DNA load in patients with primary Epstein-Barr virus infection. *Microbiology and immunology* 56(2): 93-98.

Nam, J., S. Stoeva and C. Mirkin. 2004. Bio-bar-code-based DNA detection with PCR-like sensitivity. *Journal of the American Chemical Society* 126(19): 5932-5933.

Niederfuhr, A., H. Kirsche, T. Deutschle, S. Poppert, H. Riechelmann and N. Wellinghausen. 2008. Staphylococcus aureus in nasal lavage and biopsy of patients with chronic rhinosinusitis. *Allergy* 63(10): 1359-1367.

O'Connor, K. A., A. Holguin, M. K. Hansen, S. F. Maier and L. R. Watkins. 2004. A method for measuring multiple cytokines from small samples. *Brain, behavior, and immunity* 18(3): 274-280.

Ojala, J., I. Alafuzoff, S. Herukka, T. van Groen, H. Tanila and T. Pirttila. 2009. Expression of interleukin-18 is increased in the brains of Alzheimer's disease patients. *Neurobiology of aging* 30(2): 198-209.

Okamoto, M., T. Kawabe, Y. Iwasaki, T. Hara, N. Hashimoto, K. Imaizumi, Y. Hasegawa and K. Shimokata. 2005. Evaluation of interferon-γ, interferon-γ-inducing cytokines, and interferon-γ–inducible chemokines in tuberculous pleural effusions. *Journal of Laboratory and Clinical Medicine* 145(2): 88-93.

Padhye, N. and M. Doyle. 1991. Rapid Procedure for Detecting Enterohemorrhagic *Escherichia Coli* O157-H7 in Food. *Applied and Environmental Microbiology* 57(9): 2693-2698.

Pai, M., A. Zwerling and D. Menzies. 2008. Systematic review: T-cell-based assays for the diagnosis of latent tuberculosis infection: An update. *Annals of Internal Medicine* 149(3): 177-184.

Pai, M., L. W. Riley and J. M. Colford Jr. 2004. Interferon-γ assays in the immunodiagnosis of tuberculosis: a systematic review. *The Lancet Infectious Diseases* 4(12): 761-776.

Pal, S. and E. C. Alocilja. 2009. Electrically active polyaniline coated magnetic (EAPM) nanoparticle as novel transducer in biosensor for detection of Bacillus anthracis spores in food samples. *Biosensors and Bioelectronics* 24(5): 1437-1444.

Park, S., J. Min and Y. Kim. 2012. Chemiluminescent enzyme-linked immunosorbent assay on a strip to detect *Escherichia coli* O157:H7. *International journal of environmental analytical chemistry* 92(6): 655-664.

Park, S., H. Kim, S. Paek, J. W. Hong and Y. Kim. 2008. Enzyme-linked immuno-strip biosensor to detect *Escherichia coli* O157:H7. *Ultramicroscopy* 108(10): 1348-1351.

Patnaik, P. 2003. *Handbook of Inorganic Chemicals.* McGraw-Hill.

Paul, M., D. L. Van Hekken and J. D. Brewster. 2013. Detection and quantitation of *Escherichia coli* O157 in raw milk by direct qPCR. *International Dairy Journal* 32(2): 53-60.

Qari, M. H., U. Dier and S. A. Mousa. 2012. Biomarkers of Inflammation, Growth Factor, and Coagulation Activation in Patients With Sickle Cell Disease. *Clinical and Applied Thrombosis-Hemostasis* 18(2): 195-200.

Radke, S. M. and E. C. Alocilja. 2005. A high density microelectrode array biosensor for detection of *E. coli* O157:H7. *Biosensors and Bioelectronics* 20(8): 1662-1667.

Richardson, P., R. Schlossman, S. Jagannath, M. Alsina, R. Desikan, E. Blood, E. Weller, C. Mitsiades, T. Hideshima, F. Davies, D. Doss, A. Freeman, J. Bosch, J. Patin, R. Knight, J. Zeldis, W. Dalton and K. Anderson. 2004. Thalidomide for patients with relapsed multiple myeloma after high-dose chemotherapy and stem cell transplantation: Results of an open-label Multicenter phase 2 study of efficacy, toxicity, and biological activity. *Mayo Clinic proceedings* 79(7): 875-882.

Robbe-Austerman, S., J. Stabel and M. Palmer. 2006a. Evaluation of the gamma interferon ELISA in sheep subclinically infected with Mycobacterium avium subspecies paratuberculosis using a whole-cell sonicate or a johnin purified-protein derivative. *Journal of Veterinary Diagnostic Investigation* 18(2): 189-194.

Robbe-Austerman, S., A. Krull and J. Stabel. 2006b. Time delay, temperature effects and assessment of positive controls on whole blood for the gamma interferon ELISA to detect paratuberculosis. *Journal of Veterinary Medicine Series B-Infectious Diseases and Veterinary Public Health* 53(5): 213-217.

Romagnani, P. and C. Crescioli. 2012. CXCL10: A candidate biomarker in transplantation. *Clinica Chimica Acta* 413(17–18): 1364-1373.

Rosca, D., J. A. Wright, D. L. Hughes and M. Bochmann. 2013. Gold peroxide complexes and the conversion of hydroperoxides into gold hydrides by successive oxygen-transfer reactions. *Nature Communications* 42167.

Rozmus, J., K. R. Schultz, K. Wynne, A. Kariminia, P. Satyanarayana, M. Krailo, S. A. Grupp, A. L. Gilman and F. D. Goldman. 2011. Early and Late Extensive Chronic Graft-versus-Host Disease in Children Is Characterized by Different Th1/Th2 Cytoki e Profiles: Findings of the Children's Oncology Group Study ASCT0031. *Biology of Blood and Marrow Transplantation* 17(12): 1804-1813.

Rudman, S. M., M. B. Jameson, M. J. McKeage, P. Savage, D. I. Jodrell, M. Harries, G. Acton, F. Erlandsson and J. F. Spicer. 2011. A Phase 1 Study of AS1409, a Novel Antibody-Cytokine Fusion Protein, in Patients with Malignant Melanoma or Renal Cell Carcinoma. *Clinical Cancer Research* 17(7): 1998-2005.

Ruhwald, M., M. Bjerregaard-Andersen, P. Rabna, K. Kofoed, J. Eugen-Olsen and P. Ravn. 2007. CXCL10/IP-10 release is induced by incubation of whole blood from tuberculosis patients with ESAT-6, CFP10 and TB7.7. *Microbes and Infection* 9(7): 806-812.

Ruhwald, M., J. Petersen, K. Kofoed, H. Nakaoka, L. E. Cuevas, L. Lawson, S. B. Squire, J. Eugen-Olsen and P. Ravn. 2008. Improving T-Cell Assays for the Diagnosis of Latent TB Infection: Potential of a Diagnostic Test Based on IP-10. *Plos One* 3(8): e2858.

Sack, R., L. Conradi, D. Krumholz, A. Beaton, S. Sathe and C. Morris. 2005. Membrane array characterization of 80 chemokines, cytokines, and growth factors in open- and closed-eye

tears: Angiogenin and other defense system constituents. *Investigative ophthalmology & visual science* 46(4): 1228-1238.

Saetan, N., S. Honsawek, A. Tanavalee, S. Tantavisut, P. Yuktanandana and V. Parkpian. 2011. Association of plasma and synovial fluid interferon-gamma inducible protein-10 with radiographic severity in knee osteoarthritis. *Clinical biochemistry* 44(14-15): 1218-1222.

Santos Mendonça, R. C., A. M. F. Morelli, J. A. M. Pereira, M. M. de Carvalho and N. L. de Souza. 2012. Prediction of *Escherichia coli* O157:H7 adhesion and potential to form biofilm under experimental conditions. *Food Control* 23(2): 389-396.

Sanvicens, N., C. Pastells, N. Pascual and M. -. Marco. 2009. Nanoparticle-based biosensors for detection of pathogenic bacteria. *TrAC Trends in Analytical Chemistry* 28(11): 1243-1252.

Schets, F. M., M. During, R. Italiaander, L. Heijnen, S. A. Rutjes, W. K. van der Zwaluw and A. M. de Roda Husman. 2005. *Escherichia coli* O157:H7 in drinking water from private water supplies in the Netherlands. *Water research* 39(18): 4485-4493.

Schmittel, A., U. Keilholz and C. Scheibenbogen. 1997. Evaluation of the interferon-γ ELISPOT-assay for quantification of peptide specific T lymphocytes from peripheral blood. *Journal of immunological methods* 210(2): 167-174.

Schotter, J., A. Shoshi and H. Brueckl. 2009. Development of a magnetic lab-on-a-chip for point-of-care sepsis diagnosis. *Journal of Magnetism and Magnetic Materials* 321(10): 1671-1675.

Schreiber, R. D. 2001. Measurement of mouse and human interferon gamma. *Current protocols in immunology / edited by John E.Coligan ...[et al.]* Chapter 6Unit 6.8.

Schroder, K., P. Hertzog, T. Ravasi and D. Hume. 2004. Interferon-gamma: an overview of signals, mechanisms and functions. *Journal of leukocyte biology* 75(2): 163-189.

Sen, A., T. Harvey and J. Clausen. 2011. A microsystem for extraction, capture and detection of *E. Coli* O157:H7. *Biomedical Microdevices* 13(4): 705-715.

Setterington, E. B., B. C. Cloutier, J. M. Ochoa, A. K. Cloutier, P. Jain and E. C. Alocilja. 2011. Rapid, sensitive, and specific immunomagnetic separation of foodborne pathogens. *International Journal of Food Safety, Nutrition and Public Health* 4(1): 83-100.

Setterington, E. B. and E. C. Alocilja. 2011. Rapid electrochemical detection of polyaniline-labeled *Escherichia coli* O157:H7. *Biosensors and Bioelectronics* 26(5): 2208-2214.

Siawaya, J. F. D., T. Roberts, C. Babb, G. Black, H. J. Golakai, K. Stanley, N. B. Bapela, E. Hoal, S. Parida, P. van Helden and G. Walzl. 2008. An Evaluation of Commercial Fluorescent Bead-Based Luminex Cytokine Assays. *Plos One* 3(7): e2535.

Singh, R., R. Verma, G. Sumana, A. K. Srivastava, S. Sood, R. K. Gupta and B. D. Malhotra. 2012. Nanobiocomposite platform based on polyaniline-iron oxide-carbon nanotubes for bacterial detection. *Bioelectrochemistry* 86(0): 30-37.

Stewart II, W. E., ed. 1979. *The Interferon System.* Springer Vienna.

Stigter, E. C. A., G. J. d. Jong and W. P. van Bennekom. 2005. An improved coating for the isolation and quantitation of interferon-γ in spiked plasma using surface plasmon resonance (SPR). *Biosensors and Bioelectronics* 21(3): 474-482.

Strachan, N. J. C. and I. D. Ogden. 2000. A sensitive microsphere coagulation ELISA for *Escherichia coli* O157:H7 using Russell's viper venom. *FEMS microbiology letters* 186(1): 79-84.

Suen, J., C. Liu, Y. Lin, Y. Tsai, S. H. Juo and Y. Chou. 2010. Urinary chemokines/cytokines are elevated in patients with urolithiasis RID C-9545-2009. *Urological research* 38(2): 81-87.

Sumino, K. C., M. J. Walter, C. L. Mikols, S. A. Thompson, M. Gaudreault-Keener, M. Q. Arens, E. Agapov, D. Hormozdi, A. M. Gaynor, M. J. Holtzman and G. A. Storch. 2010. Detection of respiratory viruses and the associated chemokine responses in serious acute respiratory illness. *Thorax* 65(7): 639-644.

Sun, H., T. S. Choy, D. R. Zhu, W. C. Yam and Y. S. Fung. 2009. Nano-silver-modified PQC/DNA biosensor for detecting *E. coli* in environmental water. *Biosensors and Bioelectronics* 24(5): 1405-1410.

Takahata, Y., H. Takada, A. Nomura, H. Nakayama, K. Ohshima and T. Hara. 2003. Detection of interferon-gamma-inducible chemokines in human milk. *Acta Paediatrica* 92(6): 659-665.

Takahata, Y., H. Takada, A. Nomura, K. Ohshima, H. Nakayama, T. Tsuda, H. Nakano and T. Hara. 2001. Interleukin-18 in human milk. *Pediatric research* 50(2): 268-272.

Tan, F., P. H. M. Leung, Z. Liu, Y. Zhang, L. Xiao, W. Ye, X. Zhang, L. Yi and M. Yang. 2011. A PDMS microfluidic impedance immunosensor for *E. coli* O157:H7 and Staphylococcus aureus detection via antibody-immobilized nanoporous membrane. *Sensors and Actuators B-Chemical* 159(1): 328-335.

Tang, S., J. Zhao, J. J. Storhoff, P. J. Norris, R. F. Little, R. Yarchoan, S. L. Stramer, T. Patno, M. Domanus, A. Dhar, C. A. Mirkin and I. K. Hewlett. 2007. Nanoparticle-based biobarcode amplification assay (BCA) for sensitive and early detection of human immunodeficiency type 1 capsid (p24) antigen RID E-3911-2010. *Jaids-Journal of Acquired Immune Deficiency Syndromes* 46(2): 231-237.

Thaxton, C., H. Hill, D. Georganopoulou, S. Stoeva and C. Mirkin. 2005. A bio-bar-code assay based upon dithiothreitol-induced oligonucleotide release RID E-3911-2010. *Analytical Chemistry* 77(24): 8174-8178.

Thiruppathiraja, C., S. Kamatchiammal, P. Adaikkappan, D. J. Santhosh and M. Alagar. 2011. Specific detection of Mycobacterium sp. genomic DNA using dual labeled gold nanoparticle based electrochemical biosensor. *Analytical Biochemistry* 417(1): 73-79.

Tilley, P. and J. Menon. 2000. Detection of Mycobacterium-specific interferon-gamma-producing human T lymphocytes by flow cytometry. *Apmis* 108(1): 57-66.

Tinkle, S., L. Kittle, B. Schumacher and L. Newman. 1997. Beryllium induces IL-2 and IFN-gamma in berylliosis. *Journal of Immunology* 158(1): 518-526.

Tracey, K., Y. Fong, D. Hesse, K. Manogue, A. Lee, G. Kuo, S. Lowry and A. Cerami. 1987. Anti-Cachectin Tnf Monoclonal-Antibodies Prevent Septic Shock during Lethal Bacteremia. *Nature* 330(6149): 662-664.

Triroj, N., P. Jaroenapibal, H. Shi, J. I. Yeh and R. Beresford. 2011. Microfluidic chip-based nanoelectrode array as miniaturized biochemical sensing platform for prostate-specific antigen detection. *Biosensors and Bioelectronics* 26(6): 2927-2933.

Truchetet, M., N. C. Brembilla, E. Montanari, Y. Allanore and C. Chizzolini. 2011. Increased frequency of circulating Th22 in addition to Th17 and Th2 lymphocytes in systemic sclerosis: association with interstitial lung disease. *Arthritis Research & Therapy* 13(5): R166.

Tu, S., S. Reed, A. Gehring and Y. He. 2011. Simultaneous Detection of *Escherichia coli* O157:H7 and *Salmonella Typhimurium*: The Use of Magnetic Beads Conjugated with Multiple Capture Antibodies. *Food Analytical Methods* 4(3): 357-364.

Tuleuova, N. and A. Revzin. 2010. Micropatterning of Aptamer Beacons to Create Cytokine-Sensing Surfaces. *Cellular and Molecular Bioengineering* 3(4): 337-344.

Turner, A.P.F., 1996. Biosensors: Past, Present and Future. Available at: http://www.cranfield.ac.uk/health/researchareas/biosensorsdiagnostics/page18795.html. Accessed Apr 4th, 2012.

Vaidya, V. S., S. S. Waikar, M. A. Ferguson, F. B. Collings, K. Sunderland, C. Gioules, G. Bradwin, R. Matsouaka, R. A. Betensky, G. C. Curhan and J. V. Bonventre. 2008. Urinary Biomarkers for Sensitive and Specific Detection of Acute Kidney Injury in Humans. *Cts-Clinical and Translational Science* 1(3): 200-208.

Varshney, M., Y. Li, B. Srinivasan and S. Tung. 2007. A label-free, microfluidics and interdigitated array microelectrode-based impedance biosensor in combination with nanoparticles immunoseparation for detection of *Escherichia coli* O157:H7 in food samples. *Sensors and Actuators B: Chemical* 128(1): 99-107.

Vega, B., L. Martinez Munoz, B. L. Holgado, P. Lucas, J. M. Rodriguez-Frade, A. Calle, J. L. Rodriguez-Fernandez, L. M. Lechuga, J. F. Rodriguez, R. Gutierrez-Gallego and M. Mellado. 2011. Technical Advance: Surface plasmon resonance-based analysis of CXCL12 binding using immobilized lentiviral particles. *Journal of leukocyte biology* 90(2): 399-408.

Wang, C., X. Yuan, X. Liu, Q. Gao, H. Qi and C. Zhang. 2013. Signal-on impedimetric electrochemical DNA sensor using dithiothreitol modified gold nanoparticle tag for highly sensitive DNA detection. *Analytica Chimica Acta* 799(0): 36-43.

Wang, J., G. Liu and A. Merkoci. 2003. Electrochemical coding technology for simultaneous detection of multiple DNA targets RID C-6175-2011. *Journal of the American Chemical Society* 125(11): 3214-3215.

Wang, J., J. Lu, S. Hocevar, P. Farias and B. Ogorevc. 2000. Bismuth-coated carbon electrodes for anodic stripping voltammetry RID C-6175-2011. *Analytical Chemistry* 72(14): 3218-3222.

Wang, L., Q. Liu, Z. Hu, Y. Zhang, C. Wu, M. Yang and P. Wang. 2009. A novel electrochemical biosensor based on dynamic polymerase-extending hybridization for *E. coli* O157:H7 DNA detection. *Talanta* 78(3): 647-652.

Wang, Y., R. Wang, Y. Li, B. Srinivasan, S. Tung, H. Wang, M. F. Slavik and C. L. Griffis. 2010. Detection of *Escherichia coli* O157:H7 using interdigitated array microelectrode-based immunosensor. *Biological Engineering* 2(2): 49-62.

Wang, Y. and E. C. Alocilja. 2012. Sensor technologies for anti-counterfeiting. *International Journal of Comparative and Applied Criminal Justice* 36(4): 291-304.

Wang, Y. and E. C. Alocilja. In press. AuNP-labeled Biosensor for Rapid and Sensitive Detection of Bacterial Pathogens. *Medical & Biological Engineering & Computing*.

Welinder-Olsson, C. and B. Kaijser. 2005. Enterohemorrhagic *Escherichia coli* (EHEC). *Scandinavian Journal of Infectious Diseases* 37(6-7): 405-416.

Weseslindtner, L., R. Nachbagauer, M. Kundi, P. Jaksch, H. Kerschner, B. Simon, L. Hatos-Agyi, A. Scheed, J. H. Aberle, W. Klepetko and E. Puchhammer-Stoeckl. 2011. Human Cytomegalovirus Infection in Lung Transplant Recipients Triggers a CXCL-10 Response. *American Journal of Transplantation* 11(3): 542-552.

Whelan, R. J. and R. N. Zare. 2003. Single-cell immunosensors for protein detection. *Biosensors and Bioelectronics* 19(4): 331-336.

WHO, 2006. Diagnostics for tuberculosis-global demand and market potential. WHO, Switzerland.

WHO, 2011. Global tuberculosis control 2011. WHO Press, Switzerland.

Xu, M., J. Wu and G. Zhao. 2013. Direct Electrochemistry of Hemoglobin at a Graphene Gold Nanoparticle Composite Film for Nitric Oxide Biosensing. *Sensors* 13(6): 7492-7504.

Xu, C., Z. Zhang, H. Wang and Q. Ye. 2003. A novel way to synthesize lead sulfide QDs via γ-ray irradiation. *Materials Science and Engineering: B* 104(1–2): 5-8.

Yang, F., Z. Tu, Y. Fang, Y. Li, Y. Peng, T. Dong, C. Wang, S. Lin, N. Zhan, Z. Ma, Y. Feng, S. Tan and X. Lai. 2012. Monitoring of Peptide-Specific and Gamma Interferon-Productive T Cells in Patients with Active and Convalescent Tuberculosis Using an Enzyme-Linked Immunosorbent Spot Assay. *Clinical and Vaccine Immunology* 19(3): 401-410.

Yang, L., Y. Li and G. Erf. 2004. Interdigitated array microelectrode-based electrochemical impedance immunosensor for detection of *Escherichia coli* O157 : H7. *Analytical Chemistry* 76(4): 1107-1113.

Yang, Y., F. Xu, H. Xu, Z. P. Aguilar, R. Niu, Y. Yuan, J. Sun, X. You, W. Lai, Y. Xiong, C. Wan and H. Wei. 2013. Magnetic nano-beads based separation combined with propidium monoazide treatment and multiplex PCR assay for simultaneous detection of viable Salmonella Typhimurium, *Escherichia coli* O157:H7 and Listeria monocytogenes in food products. *Food Microbiology* 34(2): 418-424.

Yilmaz, N., S. Z. Aydin, N. Inanc, S. Karakurt, H. Direskeneli and S. Yavuz. 2012. Comparison of QuantiFERON-TB Gold test and tuberculin skin test for the identification of latent Mycobacterium tuberculosis infection in lupus patients. *Lupus* 21(5): 491-495.

Yoshitomi, K. J., K. C. Jinneman, R. Zapata, S. D. Weagant and W. M. Fedio. 2012. Detection and Isolation of Low Levels of *E. coli* O157:H7 in Cilantro by Real-Time PCR, Immunomagnetic Separation, and Cultural Methods with and without an Acid Treatment. *Journal of Food Science* 77(8): M481-M489.

Yurkovetsky, Z. R., J. M. Kirkwood, H. D. Edington, A. M. Marrangoni, L. Velikokhatnaya, M. T. Winans, E. Gorelik and A. E. Lokshin. 2007. Multiplex analysis of serum cytokines in melanoma patients treated with interferon-alpha 2b. *Clinical Cancer Research* 13(8): 2422-2428.

Zeremski, M., M. Markatou, Q. B. Brown, G. Dorante, S. Cunningham-Rundles and A. H. Talal. 2007. Interferon gamma-inducible protein 10 - A predictive marker of successful treatment response in hepatitis C virus/HIV-coinfected patients. *Jaids-Journal of Acquired Immune Deficiency Syndromes* 45(3): 262-268.

Zhang, D., M. C. Huarng and E. C. Alocilja. 2010. A multiplex nanoparticle-based bio-barcoded DNA sensor for the simultaneous detection of multiple pathogens. *Biosensors and Bioelectronics* 26(4): 1736-1742.

Zhang, D., D. J. Carr and E. C. Alocilja. 2009. Fluorescent bio-barcode DNA assay for the detection of Salmonella enterica serovar Enteritidis. *Biosensors and Bioelectronics* 24(5): 1377-1381.

Zhu, P., D. R. Shelton, S. Li, D. L. Adams, J. S. Karns, P. Amstutz and C. Tang. 2011. Detection of *E. coli* O157:H7 by immunomagnetic separation coupled with fluorescence immunoassay. *Biosensors and Bioelectronics* 30(1): 337-341.

Zhu, N., A. Zhang, Q. Wang, P. He and Y. Fang. 2004. Lead sulfide nanoparticle as oligonucleotides labels for electrochemical stripping detection of DNA hybridization. *Electroanalysis* 16(7): 577-582.

Zumdahl, S. S. 2002. *Chemical Principles*. 4 th ed. New York: Houghton Mifflin Co.